KNOCK-INDUCED NOISE AND VIBRATION IN I.C. ENGINES

P W Schaberg

B.Sc.(Eng), Cape Town

May 1991

Submitted to the University of Cape Town in fulfilment of the requirements for the degree of Master of Science in Engineering.

I, Paul Werner Schaberg, submit this thesis in fulfilment of the requirements for the degree of Master of Science in Engineering.

I claim that this is my original work and that it has not been submitted in this or in a similar form for a degree at any university.

Signed by candidate

.....

P W Schaberg, B.Sc.(Eng).

ABSTRACT

This thesis describes an investigation into the noise and vibration resulting from knocking combustion in automotive engines, with the focus primarily on spark ignition engines. The objective of the investigation was to determine the mechanisms by which the cylinder pressure development resulting from knock excite the engine structure into vibration.

An investigation into the noise produced by a knocking spark ignition engine showed that there is a considerable increase in noise level in the high frequency range from 6000 Hz upwards, as well as a lesser increase over the mid-frequency range between 800 and 2500 Hz. These two frequency ranges correspond respectively to the frequencies of the cylinder pressure oscillations which result from knock, and the engine structural natural frequencies of highest response, suggesting that knock has the ability to induce both transient and forced vibration of the engine structure. This was confirmed by the frequency analysis of the recorded cylinder pressure diagrams of knocking cycles, which showed increased excitation levels over the engine structure frequency range, and a number of high frequency peaks corresponding to the cylinder pressure oscillations.

The nature of the cylinder pressure oscillations was investigated in greater detail, and good correlation was found between the measured frequencies and the natural frequencies predicted by the theory for a plane-ended cylindrical cavity, thus confirming that the pressure oscillations are due to excitation of the combustion chamber cavity resonances. Analysis of cylinder pressure diagrams recorded simultaneously at two locations in the combustion chamber of a knocking engine

also confirmed the mode shapes predicted by the cavity resonance theory.

In all of the investigations described above, use was made of a computer program which was written for the purpose of computing the cylinder pressure spectra of recorded cylinder pressure diagrams. A comparison was made between the cylinder pressure developments encountered in various types of automotive engine combustion systems, and that resulting from knock in spark ignition engines. Because the true nature of the rapid pressure rise caused by knock is masked by the oscillatory response of the combustion chamber cavity, this comparison gave the false impression of more severe combustion noise potential than the worst case diesel engines. This notion was dispelled, however, by comparison of the computed cylinder pressure spectra.

Vibration measurements were made on the main bearing cap and cylinder head of a spark ignition engine under normal combustion and knocking conditions. The results show the cylinder head response to be primarily in the high frequency region, while engine structural frequencies dominate the bearing cap response. The frequencies of the cylinder pressure oscillations are clearly discernable in the bearing cap vibration spectra as well, however. Significantly, there is also a time delay between the response of the cylinder head and that of the bearing cap.

It was therefore concluded that the path of the forced vibrations is directly from the combustion chamber to the engine structure, while the transient response mechanism is as in diesel engines, with the vibrations being initiated at the main bearings. This suggestion is supported by the fact that the high frequency vibration levels recorded on the cylinder head are higher than those recorded on the bearing cap, while

the opposite occurs over the engine structure frequency range, as well as the fact that, since the theoretical pressure distribution associated with the pressure oscillations inside the combustion chamber predicts that the nett oscillating pressure on the piston crown is zero, there should consequently be no transmission of the oscillating gas force along the cranktrain.

ACKNOWLEDGEMENTS

An enormous debt of gratitude is owed to Professor T Priede for his supervision and guidance, as well as his endless enthusiasm and the wealth of knowledge that he has shared during the course of this thesis.

In addition, I wish to express my sincere thanks to:

Mr A W D Jongens of the Central Acoustics Laboratory, for his invaluable advice and the use of the noise and vibration measurement apparatus.

Mr L Watkins, Mr D Simpson, and Mr J Watts of the Energy Research Institute, for their technical assistance in the preparation and testing of the engines and in the construction of various pieces of equipment.

Finally, Professor R K Dutkiewicz and the Energy Research Institute, for the use of the test facilities and equipment.

TABLE OF CONTENTS

	Page
ABSTRACT	i
ACKNOWLEDGEMENTS	ii
TABLE OF CONTENTS	v
LIST OF FIGURES	ix
NOMENCLATURE	xii
CHAPTER 1 : INTRODUCTION	1
1.1 BACKGROUND AND OBJECTIVES	1
1.2 THESIS OUTLINE	4
CHAPTER 2: LITERATURE OVERVIEW	6
2.1 COMBUSTION-INDUCED NOISE IN I.C. ENGINES	6
2.2 KNOCK-INDUCED NOISE IN I.C. ENGINES	11
2.2.1 Spark Ignition Knock and the Autoignition Theory	11
2.2.2 Diesel Knock	13
2.2.3 Cylinder Pressure Oscillations	13
2.2.4 Engine Structure Response	15
2.2.5 Knock-induced Noise in Spark Ignition Engines	16
2.3 DISCUSSION	16
CHAPTER 3: GENERAL CONSIDERATIONS REGARDING THE MECHANISMS OF ENGINE NOISE	18
3.1 PRIMARY NOISE GENERATION MECHANISMS	18
3.1.1 Combustion-Induced Noise - Undirectional Force Excitation	20
3.1.2 Mechanically-Induced Noise - Reversible Force Excitation	21
3.2 ENGINE STRUCTURE RESPONSE AND NOISE RADIATION	23
3.3 NOISE PRODUCED BY I.C. ENGINES	24

CHAPTER 4 : DESCRIPTION OF KNOCK-INDUCED NOISE IN SPARK IGNITION ENGINES 27

4.1 ENGINE NOISE CHARACTERISTICS 27

4.1.1 Noise Characteristics with Normal Combustion 28

4.1.2 Noise Characteristics with Knocking Combustion 32

4.2 DISCUSSION OF RESULTS 36

CHAPTER 5 : CHARACTERISATION OF THE CYLINDER PRESSURE DEVELOPMENT BY MEANS OF THE CYLINDER PRESSURE SPECTRUM 39

5.1 ANALYSIS OF CYLINDER PRESSURE DIAGRAMS. 40

5.1.1 Fourier Analysis 40

5.1.2 Digitisation Effects 43

5.2 "EDAP" - ENGINE DATA ANALYSIS PROGRAM 44

5.2.1 FFT Algorithm 44

5.2.2 Data Pre-Processing 44

5.2.3 Data Post-Processing 45

5.2.4 Validation of Results 46

5.2.5 Zero-Padding versus Interpolation 46

5.3 CHARACTERISATION OF CYLINDER PRESSURE DIAGRAMS BY CYLINDER PRESSURE SPECTRA 49

5.3.1 Range of Frequency Response 50

5.3.2 Magnitude of the Combustion Pressure Rise. 53

5.3.3 Rate of Combustion Pressure Rise 53

5.3.4 Phasing of the Combustion Pressure Rise .. 55

5.3.5 Effect of Engine Speed 56

5.3.6 Cylinder Pressure Oscillations 57

5.3.7 Synthesis of a Complete Pressure Diagram . 58

CHAPTER 6 : RESPONSE OF THE COMBUSTION CHAMBER CAVITY 60

6.1 NATURE OF THE RESPONSE OF THE COMBUSTION CHAMBER CAVITY 60

6.1.1 Mechanism by which the Combustion Chamber Cavity is Excited 63

6.1.2 Theoretical analysis of the Acoustic Characteristics of Combustion Chambers ... 65

6.1.3 Application of the Theoretical Model to the Measured Response 68

6.2 DEVELOPMENT AND PROPAGATION OF PRESSURE WAVES RESULTING FROM KNOCK 72

6.3 ANALYSIS OF DIFFERENT COMBUSTION CHAMBER SHAPES 77

6.3.1 Wedge Shape (Nissan L28) 78

6.3.2 Bath Tub Shape (Volkswagen 1800) 80

6.3.3 Hemispherical Combustion Chamber (Toyota 4AF) 82

6.3.4 Bowl-in-Piston Combustion Chamber (Ford V6 engine) 84

CHAPTER 7 : THE EXCITING CHARACTERISTICS OF THE CYLINDER PRESSURE DEVELOPMENT 86

7.1 REVIEW OF THE CHARACTERISTICS OF THE CYLINDER PRESSURE DEVELOPMENT 87

7.1.1 Rates of Pressure Rise 89

7.1.2 Peak Cylinder Pressures 92

7.1.3 Cylinder Pressure Spectra 94

7.2 KNOCKING COMBUSTION IN SPARK IGNITION ENGINES .. 96

7.2.1 Rates of Pressure Rise 96

7.2.2 Peak Cylinder Pressures 97

7.2.3 Cylinder Pressure Spectra 97

7.3 DISCUSSION 101

7.3.1 Transient Excitation Levels due to the Rapid Pressure Rise 101

7.3.2 Forced Excitation Levels due to the Cylinder Pressure Oscillations 101

7.3.3 Repetition Rate 102

CHAPTER 8 : ENGINE STRUCTURE RESPONSE 103

8.1 STRUCTURE RESPONSE TO KNOCK IN S.I. ENGINES 103

8.1.1 Time Domain Response 104

8.1.2 Frequency Domain Response 108

8.2 EFFECT OF KNOCK INTENSITY AND ENGINE SPEED 109

8.2.1 Transient Response 110

8.2.2 Forced Response 114

8.3 DISCUSSION 117

CHAPTER 9 : CONCLUSIONS 119

9.1 ENGINE NOISE CHARACTERISTICS 119
9.2 CYLINDER PRESSURE DEVELOPMENT 119
9.3 ENGINE STRUCTURE RESPONSE 120

REFERENCES 121

APPENDICES

APPENDIX A - DETAILS OF TEST ENGINES ..... A 1
APPENDIX B - ENGINE INSTRUMENTATION ..... B 1
APPENDIX C - RESULTS OF ENGINE NOISE TESTS ..... C 1
APPENDIX D - FOURIER SERIES EXPANSION OF A TRIANGULAR SAWTOOTH WAVEFORM ..... D 1
APPENDIX E - FOURIER SERIES EXPANSION OF AN EXPONENTIALLY DECAYING SINE WAVE ..... E 1
APPENDIX F - NISSAN L28 ENGINE TEST RESULTS ..... F 1
APPENDIX G - VOLKSWAGEN 1800 ENGINE TEST RESULTS ..... G 1

LIST OF FIGURES

		Page
Figure 2.1	Relation between the form of the cylinder pressure development and noise in diesel engines [2].	8
Figure 2.2	Average Structure Response Function [10].	9
Figure 3.1	Cross-section of an automotive diesel engine and the equivalent system [27]. ..	19
Figure 4.1	Third octave band noise spectra recorded over the speed range with normal combustion.	29
Figure 4.2	Third octave noise spectra recorded over a range of spark advance settings at 3500 rpm and with normal combustion.	29
Figure 4.3	Noise/speed relationships with normal combustion and various spark advance settings.	30
Figure 4.4	Averaged third octave noise levels between 800 and 3150 Hz, and 6300 and 20000 Hz, over the speed range.	31
Figure 4.5	Third octave noise spectra recorded over the speed range with knocking combustion.	32
Figure 4.6	Third octave noise spectra recorded at 1500 and 4000 rpm with various degrees of knock intensity.	34
Figure 4.7	Overall A-weighted noise levels over the speed range and with various degrees of knock intensity.	35
Figure 4.8	Maximum third octave band noise levels between 6300 and 20000 Hz with various degrees of knock intensity.	36
Figure 4.9	Maximum third octave band noise levels between 800 and 3150 Hz with various degrees of knock intensity.	37
Figure 5.1	Triangular sawtooth waveform and its spectrum.	47
Figure 5.2	Three elements of a cylinder pressure diagram and their spectra.	51
Figure 5.3	Pressure diagram assembled from the three elements in Figure 5.2a, and its spectrum.	52
Figure 5.4	Effect of a finite rate of pressure rise on the cylinder pressure spectrum.	54

Figure 5.5	Effect of a late pressure rise on the cylinder pressure spectrum.	56
Figure 5.6	Effect of engine speed on the cylinder pressure spectrum.	57
Figure 5.7	A complete synthesised diesel pressure diagram and its spectrum.	59
Figure 6.1	Cylinder pressure diagram showing heavy knock, and its cylinder pressure spectrum.	62
Figure 6.2	Cylinder pressure diagram showing impulse type excitation of the combustion chamber cavity.	64
Figure 6.3	Schematic diagram showing the mode shapes associated with the first five transverse modes of a plane ended cylinder.	67
Figure 6.4	Sketch of the Toyota 21R combustion chamber, showing the location of the two pressure transducers, and the recorded cylinder pressure diagrams.	73
Figure 6.5	Cylinder pressure spectra of simultaneously recorded cylinder pressure diagrams.	74
Figure 6.6	Cylinder pressure diagram recorded in the Nissan L28 engine, and its cylinder pressure spectrum.	79
Figure 6.7	Cylinder pressure diagram recorded in the Volkswagen 1800 engine, and its cylinder pressure spectrum.	81
Figure 6.8	Cylinder pressure diagram recorded in the Toyota 4AF engine, and its cylinder pressure spectrum.	83
Figure 6.9	Cylinder pressure diagram recorded in the Ford V6 engine, and its cylinder pressure spectrum.	85
Figure 7.1	Different forms of cylinder pressure development found in automotive engines.	88
Figure 7.2	Typical maximum rates of pressure rise for the pressure diagrams shown in Figure 7.1.	91
Figure 7.3	Typical peak cylinder pressures for the pressure diagrams shown in Figure 7.1. ..	93
Figure 7.4	Typical cylinder pressure spectra for the pressure diagrams shown in Figure 7.1. ..	95
Figure 7.5	Range of peak knock pressures for the Nissan L28 engine.	98

Figure 7.6 Spectra recorded over the speed range with knocking combustion in the Nissan L28 engine. 99

Figure 7.7 Range of spectral levels associated with the cylinder pressure oscillations for the Nissan L28 engine. 100

Figure 8.1 Cylinder pressure diagram and spectrum with knocking combustion, as well as bearing cap and cylinder head vibration oscillograms 105

Figure 8.2 Bearing cap and cylinder head vibration spectra. 106

Figure 8.3 Average bearing cap vibration levels between 1000 and 4000 Hz with varying degrees of knock intensity. 111

Figure 8.4 Average cylinder head vibration levels between 1000 and 4000 Hz with varying degrees of knock intensity. 112

Figure 8.5 Average bearing cap vibration levels between 6000 and 20000 Hz with varying degrees of knock intensity. 115

Figure 8.6 Average cylinder head vibration levels between 6000 and 20000 Hz with varying degrees of knock intensity. 116

NOMENCLATURE

Symbols

A	Amplitude
$\alpha_{m,n}$	Non-dimensional co-efficient
B	Bore diameter
c	Speed of sound
F,f	Frequency
f_R	Resonant frequency
J_m	Bessel function of order m
g(t)	Function of time
G(f)	Function of frequency
k	Harmonic number, modulus of decay
L	Axial length
m	Circumferential mode number
n	Data point number, radial mode number
N	Number of data points
p	Axial mode numbers
t	Time
T	Period

Subscripts

m,n,p	Circumferential, radial, and axial mode numbers

Abbreviations

BDC	Bottom dead center
BTDC	Before top dead center
C.F.R.	Co-operative Fuel Research
dB(A)	A-weighted decibel scale
DFT	Discrete Fourier Transform
D.I.	Direct injection

FFT	Fast Fourier Transform
I.C.	Internal combustion
I.D.I.	Indirect injection
I.S.V.R.	Institute of Sound and Vibration Research, University of Southampton
N.A.	Naturally aspirated, or normally aspirated
RON	Research Octane Number
S.I.	Spark ignition
SPL	Sound Pressure Level
TDC	Top dead center

CHAPTER 1

INTRODUCTION

1.1 BACKGROUND AND OBJECTIVES

It is difficult to imagine the world as we know it without the automobile, and since the reciprocating internal combustion engine has had the overall monopoly in road transportation for some time, the two have become inextricably linked. Few will disagree that, without the automobile, the technological development attained since the beginning of the twentieth century would not have been possible, and seen in this light, it would seem to be one of the more praiseworthy products of mankind's inventiveness.

On the other hand, the emergence of an ever-increasing environmental consciousness has highlighted the automobile as one of the biggest culprits responsible for the pollution of the atmosphere. While some forms of this pollution, for example gaseous exhaust emissions, only show visible effects in areas with a very dense automobile population, one form only requires the presence of a single vehicle to become apparent, namely, the noise emitted by its engine. Engineers realised at a very early stage that the inherent noisiness of the internal combustion engine was a factor which could severely limit its acceptability in many applications. As a result, attempts to understand and control the phenomenon have progressed in parallel with engine development since the earliest days.

Today, only two distinct combustion systems are in use in automotive applications, namely, the spark ignition engine and the compression ignition, or diesel engine. Initially, the

spark ignition engine covered a wide range of size and power, but it was gradually displaced in many applications by the more efficient diesel engine. It has, however, found its place as the unchallenged power unit for passenger cars. The diesel engine, apart from its use in stationary plants and for powering ships, locomotives, and construction equipment, is used almost exclusively for commercial road transportation.

In recent years, increased emphasis has been placed on controlling the objectionable qualities of engine noise, in addition to reducing the absolute noise levels. When compared to the spark ignition engine, the diesel engine is disadvantaged in meeting both of these criteria. Not only is it generally noisier, but it also has a distinctive impulsive noise characteristic known as "diesel knock", which is absent in spark ignition engines. As a result, the diesel engine has been the subject of the majority of noise investigations, and the impulsive noise characteristic has been shown to be due to a rapid pressure rise occurring in the combustion chamber due to the combustion of the pre-mixed portion of the fuel/air charge [1,2]. This rapid pressure rise induces transient vibration of the engine structure at its natural frequencies.

A rapid pressure rise can also be made to occur in spark ignition engines, resulting in a distinctive noise known as "spark knock", which, although also of an impulsive nature, has very different characteristics to "diesel knock". The rates and magnitudes of pressure rise which occur are often far more severe than those occurring in a diesel engine, and large amplitude, high frequency pressure oscillations are induced in the combustion chamber. As opposed to the diesel engine, it is the high frequency noise resulting from these pressure oscillations which dominates the noise emitted by a knocking spark ignition engine [3].

While the mechanism of the transient engine structure vibration resulting from the rapid pressure rise has been thoroughly researched and is fairly well understood, the same cannot be said for the mechanism by which the cylinder pressure oscillations induce vibration in the engine structure. The lack of research in this field is understandable, as spark ignition engine knock is an unwanted phenomenon which often results in severe engine damage or failure, and is consequently usually avoided at all costs. There are two reasons why an investigation into the mechanism by which noise and vibration is generated in a knocking spark ignition engine can be beneficial, however.

The first is simply to further our general understanding of the mechanisms by which engine noise is generated, and therefore represents primarily academic interests. The phenomenon of knock in spark ignition engines presents an interesting platform from which combustion-induced noise in general, as well as the hitherto poorly understood primary noise generation mechanism in small, high speed engines, may be studied.

The second reason has a more commercial nature and concerns the field of knock detection. As motor manufacturers strive to increase engine efficiency by increasing compression ratios, so the possibility of running into knock and the associated risks increases. Modern electronic engine management systems allow for operation as close as possible to the knock limit by employing knock detection devices to warn of the occurrence of knock. While most of these devices usually consist of a vibration sensor mounted on the engine structure, a number of acoustic methods have also been suggested. Consequently, a better understanding of the noise and vibration resulting from knock may aid in the development of more sensitive knock detection devices, which could result in gains in engine

efficiency, by allowing operation at conditions closer to the knock limit.

1.2 THESIS OUTLINE

The first chapter of this thesis contains a literature survey which covers the subjects of combustion-induced noise, knock in spark ignition and diesel engines, and the pressure oscillations which result from knock. This is followed by a brief overview of general considerations regarding the mechanisms of engine noise. This was deemed necessary to provide a background against which the study of the mechanism of knock-induced noise could take place. Chapter 4 contains a description of the noise produced by a spark ignition engine under normal combustion and knocking conditions, showing the effects of engine speed and varying knock intensity levels.

In order to quantify the excitation levels to which the engine structure is subjected as a result of the cylinder pressure development, a computer program was written to perform frequency analyses of cylinder pressure diagrams. This program is described in Chapter 5, along with a description of the relationship between the cylinder pressure diagram and its spectrum. When knock occurs, the cylinder pressure diagram is influenced considerably by the response of the combustion chamber cavity, and an investigation of this phenomenon is presented in Chapter 6. Chapter 7 presents a comparison between the cylinder pressure developments which occur in various different combustion systems, as well as their tendency to excite the engine structure into vibration, with that resulting from knock in spark ignition engines.

An investigation into the nature of the engine structure response to this gas force excitation, as well as the mechanism by which it occurs, is described in Chapter 8. Finally,

conclusions which can be drawn as a result of this investigation into knock-induced noise, are presented in Chapter 9.

CHAPTER 2

LITERATURE OVERVIEW

This chapter provides a literature overview of the topics pertinent to the subject matter of this thesis. These necessarily include the widely researched fields of combustion-induced noise and spark ignition engine knock. However, as the consequences of knock in terms of the excitation of the engine structure, rather than the knock event itself, are of interest for the sake of this thesis, the discussion of the mechanism of knock will be limited to a very brief overview.

2.1 COMBUSTION-INDUCED NOISE IN I.C. ENGINES

Early combustion noise investigations were focussed primarily on the search for a suitable criterion by which the noise-generation propensity of the various forms of cylinder pressure diagram could be judged. Some of the criteria which were considered were the peak cylinder pressure, the rate of pressure rise (first derivative of cylinder pressure with respect to time), and the acceleration of the pressure rise (second derivative of cylinder pressure with respect to time).

Janeway [4] was the first to show, by means of a theoretical analysis, that the form of the cylinder pressure development determines the dynamic stresses in engine parts, and proposed that the acceleration of the cylinder pressure with respect to time was the predominant factor. Other researchers supported him in this conclusion [1], while others found a better correlation with the rate of pressure rise. Hinze [5] made an important contribution, by showing fundamentally that the form of a rapidly increasing excitation force only has an influence if the period over which the rapid increase occurs is greater than a quarter of the period of the natural vibratory response

of a system. This showed, amongst other things, that, as the engine speed was increased, the minimum frequency affected by the form of the cylinder pressure development also increased.

It was recognised that a frequency domain representation of the cylinder pressure development would be a very useful tool for quantifying the exciting properties of the gas force in a way which was universally independent of the engine structure. This was only achieved, however, after considerable advances were made in the fields of dynamic pressure measurement and signal processing technology, and the first reliable results were obtained by Priede and Austen at Lucas CAV Ltd. in the early 1950's [6].

The relationship between the cylinder pressure development, its frequency spectrum, and the emitted engine noise, was subsequently investigated extensively in diesel engines, and Figure 2.1a shows the cylinder pressure spectra measured over the speed range for an indirect injection diesel engine, as well as the corresponding noise spectra. Priede investigated the relationship between the form of the cylinder pressure development and the cylinder pressure spectrum, by analysing various forms of diesel cylinder pressure diagrams, as well as motored compression curves and electrically generated sawtooth waveforms [2]. He concluded that the form of the cylinder pressure spectrum was controlled by the peak cylinder pressure in the low frequency part (up to 150 Hz), and by the rate of pressure rise at the higher frequencies.

By determining the frequency spectrum of the cylinder pressure diagram, it also became possible to characterise the acoustical properties of the engine structure by means of a "structure attenuation" curve, i.e. the decibel difference between each

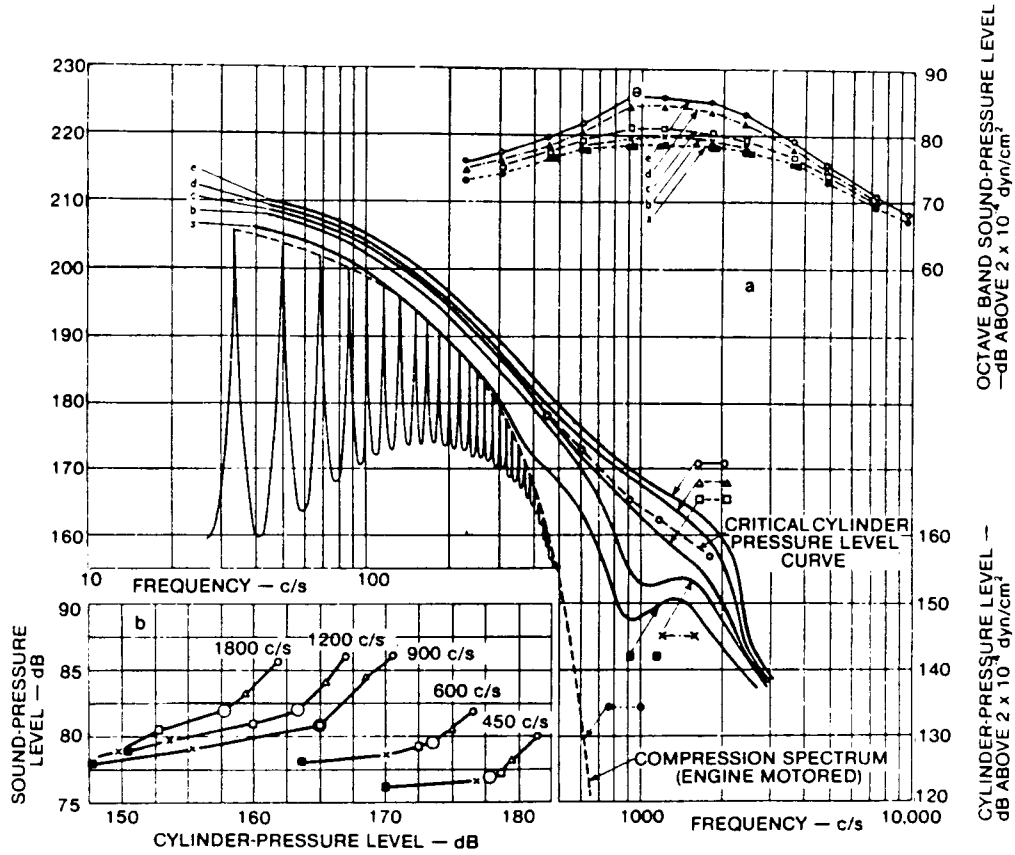

Figure 2.1 Relation between the form of the cylinder pressure development and noise in diesel engines [2].

frequency component of cylinder pressure and the corresponding noise component measured at a distance of 1 meter from the engine [7]. This is the decibel equivalent of the reciprocal of the modulus of the transfer function between the cylinder pressure and the noise 1 meter away from the engine. The attenuation curve is independent of the engine operating conditions, namely speed and load, and has the important property of showing over which part of the frequency range the cylinder pressure levels are likely to influence noise levels the most. The usefulness of this property is greatly enhanced by the fact that the overall shape of the attenuation curve is similar for most engines [8,9], and this has led to the

introduction of an average response function, which allows easy comparison of the influence of different combustion systems, fuels, and fuel injection equipment, on combustion noise [10]. An example of such a structure response curve is shown in Figure 2.2.

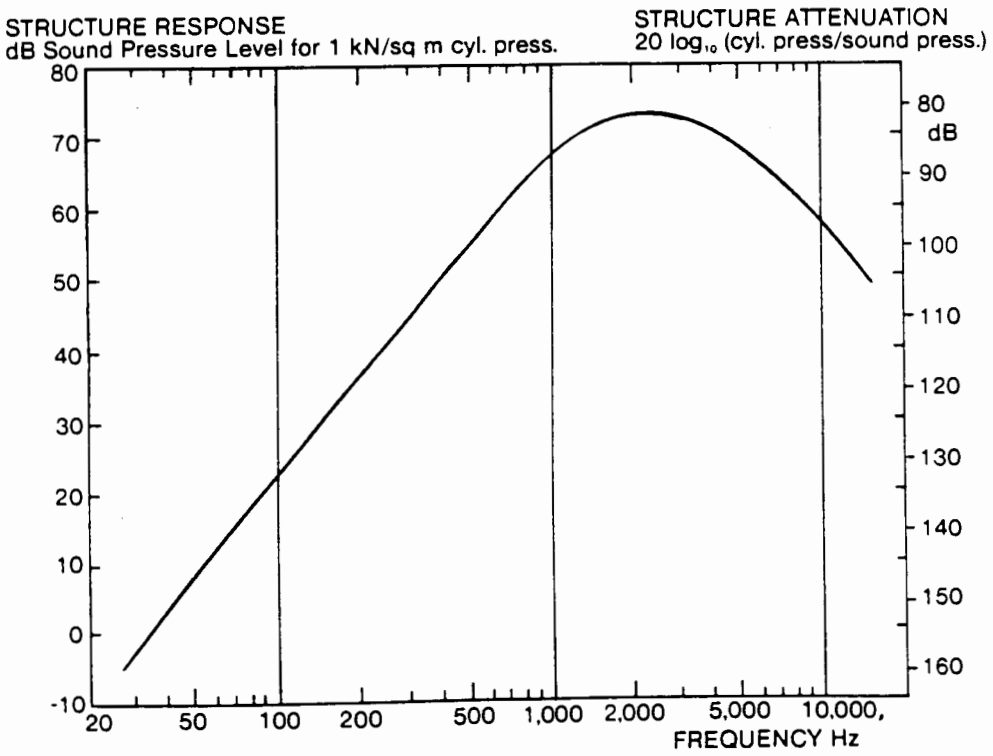

Figure 2.2 Average Structure Response Function [10].

The shape of this average curve shows that the attenuation increases from a maximum at low frequencies to reach the minimum level over the frequency range between 1000 and 5000 Hz, beyond which it increases again. For this curve to be valid, however, it is essential that the emitted engine noise be combustion controlled, and this was borne out by subsequent investigations where attempts to extend the method to engines

with smooth cylinder pressure developments showed considerable discrepancies.

These investigations led to another very important result, however, namely, the definition of a "critical cylinder pressure spectrum level" [2], at which the level of combustion-induced noise of an engine was equal to the mechanical noise. This level is determined by plotting the sound pressure level against the cylinder pressure level, at the frequency points of interest, as shown in Figure 2.1b. There is a gradual increase in SPL as the cylinder pressure level is increased until the critical level is reached, beyond which the SPL increases at a rate which is approximately directly proportional to the increase in cylinder pressure level. The transition points are then plotted as a function of frequency, indicating the critical cylinder pressure level. At cylinder pressure levels below this limit any changes to the form of the cylinder pressure development will have little affect on engine noise, whereas, on the linear part of the curve beyond this point, noise will be predominantly combustion controlled. By ensuring that cylinder pressure levels are above this limit, it was possible to investigate the effects of various operating parameters such as engine speed, load, the injection characteristics, and the fuel properties, without interference from mechanical noise sources. It was found, however, that mechanical noise from certain sources, such as piston slap and timing gear impacts, could increase with increasing gas loads, and was therefore not independent of the combustion-induced noise. This effect could, however, be eliminated by keeping peak cylinder pressures constant over the speed range, and varying only the form of the cylinder pressure development, or by more extreme methods aimed at eliminating mechanical noise altogether [11].

In summary, it may therefore be said that the relationship between the cylinder pressure development and the emitted noise of an engine may be defined by the cylinder pressure spectrum, in conjunction with the critical cylinder pressure level, and the engine structure attenuation (or response) curve. More importantly, the structure attenuation characteristic determines that the rate of pressure rise is the parameter most likely to affect combustion noise, as its frequency response range coincides with the frequency range over which the minimum structural attenuation occurs.

2.2 KNOCK-INDUCED NOISE IN I.C. ENGINES

The term "knock" refers to the audible impulsive noise which results from a rapid pressure rise in the combustion chamber of an internal combustion engine. During the First World War Sir Harry Ricardo [1] recognised the relation between the rapidity of combustion and noise in gasoline engines, and likened the effect of such a rapid pressure rise to "striking the walls of the cylinder with a hammer blow".

The cause of the rapid pressure rise is the essentially spontaneous combustion of a significant volume of the fuel-air mixture, which produces an almost instantaneous pressure rise locally in the combustion chamber. Whilst the term "knock" is applicable to both diesel and spark ignition combustion systems, the mechanism responsible for the rapid pressure rise in each case is different. In both cases, however, it is an undesirable phenomenon, and requires control.

2.2.1 Spark Ignition Knock and the Autoignition Theory

Despite many years of research, a large degree of uncertainty still surrounds the fundamental mechanisms causing and controlling knock in spark ignition engines. Knock has variously been associated with end gas autoignition,

detonation, acceleration of the "normal" flame front, rapid combustion of partially oxidised gases behind the flame front, and a range of combinations of these effects [12]. Of these, the first two theories, namely end gas autoignition and detonation, have, historically, been the most popular. Recently, however, the autoignition theory has gained the majority of support and a very brief description of this theory will be given here. More exhaustive reviews of the knock phenomenon may be found in the mass of literature the abounds regarding the subject, not the least of which are the classic works such as that of Ricardo [1], as well as the recent textbook by Heywood [13].

According to the autoignition theory, knock is the result of the spontaneous combustion of the unburned mixture in the end-gas, near the combustion chamber wall, before the arrival of the turbulent flame front. With normal combustion, the flame front propagates uniformly outwards from the point of initiation at the spark plug, and the mixture of fuel, air and residual gas ahead of the advancing flame front is subjected to increasing temperature and pressure by the expanding burnt gases. Knock occurs when a critical condition is reached in the temperature and pressure history of the unburned mixture, resulting in the fuel oxidation process - starting with the pre-flame reactions and ending with the rapid energy release - occurring spontaneously. The balance of the end-gas fuel's chemical energy is released, resulting in a substantial local increase in the gas pressure and temperature, and photographic studies [14] have shown this pressure discontinuity to result in the propagation of shock waves with velocity exceeding that of sound, across the combustion chamber. Numerous autoignition sites may be established in the end-gas zone [15,16], usually within close vicinity of one another, and the complete autoignition of the end-gas completes the combustion process.

2.2.2 Diesel Knock

As opposed to the spark ignition engine, spontaneous ignition is a required phenomenon for the operation of the diesel combustion system, and occurs as soon as a combustible mixture of the fuel and surrounding high temperature air is established. It was shown by Austen and Lyn [17] that it is inevitable that, however small, there is always a finite volume of the pre-mixed fuel which detonates during the start of combustion. As the bulk of the remaining charge is not pre-mixed and homogeneous, as in the case of the spark ignition engine, this spontaneous ignition will not necessarily result in the instantaneous combustion of all of the remaining charge, and subsequent combustion will be controlled by the injector spray characteristics and the rate at which the fuel is injected into the combustion chamber. These two parameters have been manipulated extensively in efforts to obtain smooth pressure developments by eliminating the abrupt pressure rise corresponding to the initial spontaneous ignition phase. A notable result is the M.A.N. "M System" for direct-injection engines, in which a single fuel spray is directed onto the wall of the combustion chamber, thus reducing the air-distributed charge for the purpose of ignition. Pilot-injection schemes have also been investigated recently in attempts to reduce the pre-mixed portion of the fuel/air mixture before the start of combustion [18].

2.2.3 Cylinder Pressure Oscillations

If the rate of pressure rise resulting from combustion is of sufficient magnitude, severe pressure oscillations may be induced in the combustion chamber. These are particularly evident in knocking spark ignition engines, and a rigorous explanation for their existence was first offered by Draper in 1938 [19], who showed them to due to the excitation of the acoustical resonances of the combustion chamber cavity. He compared the frequencies of cylinder pressure oscillations

measured in a C.F.R. engine to those predicted by the acoustical theory for a plane-ended cylindrical cavity, and found good correlation.

This work was re-visited some 40 years later by Hickling and his colleagues [20,21], who correlated the high frequency peaks recorded on cylinder pressure spectra to the various natural modes of the combustion chamber cavity in both spark ignition and open chamber diesel engines. In addition, by mounting four pressure transducers in a C.F.R. engine, it was possible to determine the mode shapes associated with each of the resonant peaks. Combustion chamber shapes which differed from the plane-ended cylinder were also investigated with the natural frequencies and mode shapes being predicted by finite element models of the combustion chambers. As an extension of the work, Hickling was also able to calculate estimates of the bulk gas temperature in the cylinder as a function of crankangle on the expansion stroke, from the modulation of the measured frequencies of the pressure oscillations.

Fundamental studies attempting to investigate the effects of various combustion chamber shapes were performed at the University of Cape Town [22]. Mode shapes in plastic models of combustion chambers excited at discrete frequencies by a small vibrating piston were determined by measuring the sound pressure level at various points inside the cavity by means of a probe microphone. Although actual combustion chambers were used for moulding the plastic models, good correlation was still found with the theory for a plane-ended cylinder, in terms of the natural frequencies of the cavities as well as the associated mode shapes. The mode shapes determine that the pressure oscillations with the highest amplitudes occur at the periphery of the combustion chamber, and, whilst not proven, this is supported by observed engine damage caused by knock, as

this damage often manifests itself as erosion of the piston at its periphery and cylinder head gasket failure [13].

Whilst it is possible to determine the amplitudes of the pressure oscillations theoretically for a given forcing function, Priede [3] suggested that the response of the combustion chamber cavity could be modelled by the a simple oscillator subjected to a step excitation force. Thus the amplitude of the oscillations will be equal to the magnitude of the step rise in pressure, and the maximum rate of pressure rise will be determined by highest mode of vibration that is excited.

2.2.4 Engine Structure Response

It has been established that the transient exciting properties of the gas force are transmitted to the main load-carrying structure of the engine, namely the cylinder block and crankcase, at the main bearings [23]. This has been verified in running engines where strong correlation has been found between the axial vibration of the bearing cap and the emitted noise [24], as well as in experiments on non-running engines [25,26]. These experiments, which were conducted at I.S.V.R., University of Southampton, included the use of a so-called "banger rig" in which a propane/air/oxygen charge is ignited in a pre-chamber adjoining the combustion chamber of the engine, the crankshaft of which had been fixed. This single event excitation by a rapid pressure rise in the combustion chamber allowed the force transmission paths and structural wave propagation to be studied, and provided conclusive evidence that the transmission of the gas force to the outer engine structure is via the cranktrain.

2.2.5 Knock-induced Noise in Spark Ignition Engines

Priede and Dutkiewicz [3] quantified the effect of varying degrees of knock on spark ignition engine noise, and postulated the following regarding the mechanism for knock-induced noise:

> "The rapid pressure rise produced by knock excites the natural frequencies of the engine structure in the frequency range between 1000 and 3000 Hz in the same way as in diesel engines.", and
>
> "The rapid pressure rise excites the combustion chamber cavity at its natural frequencies, producing large amplitude pressure oscillations. This oscillating gas force produces forced vibrations of the engine structure resulting in emitted noise."

These investigations showed maximum increases in the measured noise level of approximately 12 dB over the frequency range between 1000 and 3000 Hz, and significantly larger increases of up to 20 dB in the high frequency range above 6000 Hz, in an engine running under heavy knock which was induced by considerably advancing the spark timing and using low octane fuel. The corresponding cylinder pressure diagrams showed peak knock pressures greater than 90 bar, which represents an increase of about 30 bar over the normal peak combustion pressure. It was concluded that the amplitude of the pressure oscillations and the emitted noise are directly related to the magnitude of the knock pressure rise. It must be noted, however, that this conclusion did not differentiate between the noise contribution of the high frequencies due to the pressure oscillations, and the lower frequencies due to the resonant vibration of the engine structure.

2.3 DISCUSSION

A number of interesting factors emerge from the literature survey presented in this chapter. Since combustion-induced noise is rarely predominant in spark ignition engines, the

majority of research on the subject has been done on diesel engines. Consequently the "diesel knock" phenomenon is well understood, and the presence of a rapid pressure rise which excites the engine structure at its natural frequencies, has been identified as the source of the impulsive noise which is emitted. Knock in spark ignition engines would, however, appear to represent a far more severe case in terms of the cylinder pressure development, in that the rates and magnitudes of pressure rise often exceed those encountered in diesel engines. The predominant noise levels lie in the frequency range of the cylinder pressure oscillations, but the increase in the noise level over the engine structure natural frequency range is not of the magnitude that one would expect, considering the severity of the perceived combustion excitation.

This observation gives rise to speculation about the presence of a different structural excitation mechanism, or, more likely, that the transient exciting properties of the gas force are not as severe as perceived from the cylinder pressure diagram. Consequently, this thesis will address two areas, namely, a quantitative analysis of the exciting characteristics of the cylinder pressure development arising out of knock in spark ignition engines, and an investigation into the way in which such a cylinder pressure development excites the engine structure.

CHAPTER 3

GENERAL CONSIDERATIONS REGARDING THE MECHANISMS OF ENGINE NOISE

This chapter provides a brief description of the fundamental noise generation mechanisms present in reciprocating internal combustion engines, in order to provide a background against which the influence of combustion noise, and in particular, knock-induced noise, can be studied.

3.1 PRIMARY NOISE GENERATION MECHANISMS

Two primary noise generation mechanisms may be identified in internal combustion engines, namely combustion-induced noise, and mechanically-induced noise. The contribution of ancillary equipment such as the valve gear, injection system, and water and lubricating oil pumps, to engine noise, is not of interest in this study, and disregarding these elements allows the engine to be regarded as consisting of two basic structural elements [27]:

> An internal load-carrying structure, consisting of the piston-connecting rod-crankshaft system, and
>
> An outer load-carrying structure, consisting of the cylinder block structure.

This equivalent system is illustrated in Figure 3.1. The two structural elements are mechanically separated by running clearances, and are subjected to two different types of forces which are ultimately responsible for the engine structure vibration and emitted noise. These are unidirectional forces arising out of the combustion process, and reversible forces

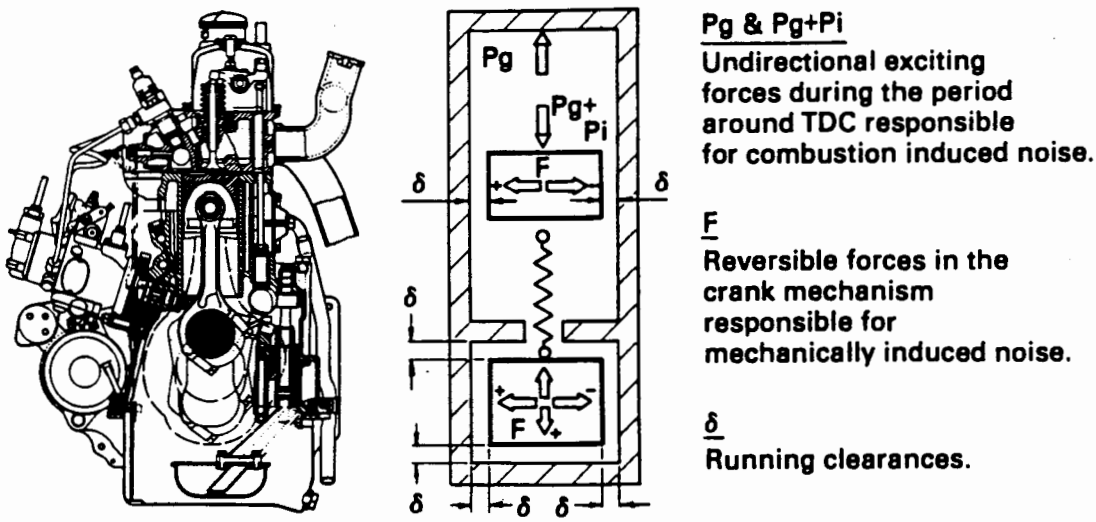

Figure 3.1 Cross-section of an automotive diesel engine and the equivalent system [27].

arising out of the mechanical inertia of the reciprocating and rotating crank-train elements.

With normal combustion, the frequency range over which an engine emits the highest noise levels corresponds to the engine structure natural frequencies of highest response. These usually lie in the range between 800 to 2500 Hz for automotive engines. In order to excite the engine structure in this frequency range, the level of the corresponding frequency components of the excitation force must be of sufficient magnitude.

An additional parameter which provides further insight into the nature of the dominant excitation mechanism, is an engine's noise/speed relationship. Since the excitation mechanisms in

question are periodic with crankshaft rotation, the rate of decay of harmonics of the excitation force responsible for the emitted noise will determine the increase in noise level with engine rotational speed.

3.1.1 Combustion-Induced Noise - Undirectional Force Excitation

The compression and combustion of the fuel-air mixture within the combustion chamber and the resulting pressure rise due to heat release, exerts a unidirectional gas force on the piston. This force acts on the compression and expansion strokes and is significant only over a comparatively small part of the engine cycle near TDC. Some deformation of the engine structure occurs due to the force exerted by a smooth pressure rise such as that due to compression. However, since the gas force does not undergo any change in direction, the only mechanism by which appreciable transient excitation of the engine structure can be induced, is by a rapid change in the magnitude of the force. The rapid pressure rise occurring at the onset of combustion in naturally-aspirated direct-injection diesel engines is an example of this mechanism. Thus the rate of pressure rise is an important parameter in assessing combustion-induced noise, and also categorises the nature of gas force excitation as transient and cyclic.

The effects of such a rapid pressure rise and other combustion phenomena are illustrated very clearly by means of cylinder pressure spectra, and are described in detail in Chapter 5, in which the relationship between the cylinder pressure diagram and the cylinder pressure spectrum is described.

The gas force acts on the piston and is transmitted to the outer load-carrying structure at the main bearings, via the connecting rod and crankshaft. The mechanical inertia of these

reciprocating and rotating elements constitutes and additional, reversible force which also acts on the main bearings.

3.1.2 Mechanically-Induced Noise - Reversible Force Excitation

The inertia forces acting on the main bearings display rates of change which are too small to induce appreciable vibration amplitudes in the comparatively stiff outer engine structure. The reversible nature of these forces, however, results in the acceleration of various elements of the internal load-carrying structure across the clearances between them, thereby causing impacts which effectively induce engine structure vibrations. On impact, kinetic energy is imparted to the engine structure in the form of an instantaneous step load, whilst continuing application of the changing force after the impact produces further excitation of the engine structure.

Since a pure impact will excite all frequencies equally, there should be no increase in noise level with repetition rate (i.e. engine speed). All engines display an increase in noise with speed, and it may thus be concluded that the impacts alone are not responsible for the noise. The inertia forces on the other hand display a high rate of decay of harmonics resulting in excitation levels over the frequency range of importance which are too low to be of significance.

The combined gas and inertia force loads can result in the crankshaft deflecting between its support points at the main bearings, and the rotation of the deformed crankshaft in its bearings has been found to be a source of transient mechanical excitation. Raff and Grover [28] found that the movement of the crankshaft journals in their bearings produces impulsive hydraulic loads in the lubricating oil film in the clearances between the components, and that the frequency characteristic of these hydraulic loads is such as to provide significant

levels of excitation in the frequency range between 1000 Hz and 3000 Hz. They concluded that this was the primary mode of generation of mechanically-induced noise in small high-speed engines.

This excitation mechanism has an interesting property for which no rigorous explanation has been offered as yet, in that it displays a dual slope force/speed characteristic. The rate at which the force level increases with speed, increases dramatically after a certain transition speed has been reached.

It should be noted that the inertia forces acting on the crankshaft increase with the square of the engine speed, indicating that, at high engine speeds, the magnitude of the gas force may become small compared to the inertia forces. The shape of the gas force component, however, remains unaltered.

In diesel engines, particularly towards the top end of the automotive size range, piston slap is often a predominant source of mechanical noise. The combined gas and inertia force on the piston, which acts along the vertical cylinder axis, is reacted by the connecting rod, which, in general, is not vertical. This results in a reversible sideways force component which accelerates the piston across any clearance which may exist and impacts it against the liner, resulting in high frequency excitation of the engine structure. Lalor [29] proposed a simple model based on the energy transfer during impact, which is dependent on the rate of change of side-force which in turn is strongly influenced by the peak cylinder pressures. Consequently, engines with very high peak cylinder pressures, such as turbocharged diesel engines, are particularly susceptible to this form of mechanical excitation.

A large amount of time and effort has been expended in investigating piston slap, resulting in computer models and

advanced experimental techniques which have enabled engineers to reduce piston slap noise to levels where it is seldom a problem in modern engines.

3.2 ENGINE STRUCTURE RESPONSE AND NOISE RADIATION

The forces applied to the engine structure by the combustion process and mechanical impacts may cause vibration of the external structure by two means, namely periodic (forced) vibration, or resonant (damped natural) vibration which occurs in a large number of normal modes. The forces due to combustion are transmitted to the load-carrying structure of the engine at the main bearings via the piston-connecting rod-crankshaft assembly, resonances of which may also be excited to the extent of making a significant contribution to the structure response [30].

The extent to which the external noise radiating surfaces are excited depends on the coupling between the crankshaft and the dominant noise generating modes of these surfaces. The two most important structural deflection modes for in-line engines are bending vibration of the whole engine in the horizontal plane, and panel type vibrations of the thin-walled parts of the crankcase casting, while the primary mode of vibration in V-engines has been identified as a cylinder bank-to-bank mode similar to the prongs of a tuning fork [31]. This distortion of the cylinder block excites forced and resonant vibration in the oil pan and valve gear covers, and these unstressed covers have been found to be a predominant source of automotive engine noise.

Studies have shown transient characteristics of the crank-train forces, such as those caused by an abrupt pressure rise and bearing impacts, to result in engine surface vibrations which are transient and localised, and that the major source of

vibration is initiated from the exciting forces at the main bearings [23]. It has been found that the fundamental crankcase panel mode is particularly sensitive to the cylinder pressure development. The crankpin forces, of which the gas force may form a major part, exert moments on the main bearing bulkheads, causing them to deflect axially outwards in both directions, which in turn causes a sympathetic inward deflection of the adjacent crankcase panel.

The way in which the engine structure radiates noise may be described as follows [32]. Many of the normal modes of surface vibration involve motion at right angles to the plane of the surface, which forces the air particles in contact with them to move. At low frequencies the air moves without significant pressure variations being generated, resulting in little energy being imparted to it. At higher frequencies, where the half-wavelength of sound is similar to the dimensions of the radiating surfaces, sufficient pressure may be built up by the vibration to radiate a large amount of sound power. At higher frequencies still, the surface of the structure vibrates in a very large number of normal modes, each making a contribution to the total sound power radiated by the engine.

3.3 NOISE PRODUCED BY I.C. ENGINES

The relative magnitudes and excitation properties of the combustion and mechanical noise generation mechanisms described earlier in this chapter, will determine which one is dominant in a particular engine. Since most engines are essentially similar from a mechanical point of view, the factor which has the greatest influence in this regard is the combustion system of the engine, or more specifically, the cylinder pressure development. Experience has shown that, if the cylinder pressure development of an engine displays a rapid pressure rise of sufficient magnitude, then combustion-induced noise

will dominate that engine's noise characteristic. If the cylinder pressure development is smooth, on the other hand, the mechanically-induced noise will dominate.

The reasoning presented above allows engines to be classified, from a noise point of view, according to their combustion systems. It also implies that an engine with a smooth cylinder pressure development and a level of mechanical noise which is not abnormally high, will be inherently quieter than a mechanically similar engine with a significantly abrupt cylinder pressure development. The four most common combustion systems, namely the naturally-aspirated direct-injection (N.A. D.I.) diesel engine, the turbocharged direct-injection (TC D.I.) diesel engine, the indirect-injection (I.D.I.) diesel engine, and the spark ignition (S.I.) engine, each have distinctly different cylinder pressure developments, with correspondingly different noise characteristics.

Comparison of the overall noise levels at full load of some 44 different engines, measured at the I.S.V.R. at the University of Southampton [27], shows spark ignition engines to have the lowest noise levels, followed by I.D.I. diesel engines, with turbocharged and N.A. D.I. engines being the noisiest.

Spark ignition engines and high-speed I.D.I. diesel engines display the dual slope noise-speed relationship characteristic of the primary mechanically-induced noise generation mechanism, namely that of impulsive hydraulic loads in the main bearings. This, in conjunction with the smooth cylinder pressure developments displayed by these engines, would indicate this mechanism as being the predominant source of noise.

The D.I. diesel engines' noise-speed relationships have a single slope. This may, however, be as a result of the rated speed of the engine being below the transition speed at which the change in slope would occur, as these engines operate at

significantly lower speeds than S.I. and I.D.I. diesel engines. Correlation has, however, been found between the slopes of the cylinder pressure spectrum and the slope of the noise/speed relationship of N.A. D.I. diesel engines [33], indicating that the noise is combustion controlled. The high noise levels of turbocharged diesel engines may be ascribed to the fact that turbocharging only results in a smooth cylinder pressure development at rated speed, and at low speeds the form of the cylinder pressure development reverts to the abrupt nature of a naturally-aspirated engine. In addition, the high peak cylinder pressures encountered in turbocharged engines result in increased susceptibility to piston slap.

In summary, it can be said that the generation of engine noise is the product of the complex interaction of multiple noise generation mechanisms, and that the characteristics of these mechanisms at a particular operating point will determine the noise characteristic of the engine, at that point.

CHAPTER 4

DESCRIPTION OF KNOCK-INDUCED NOISE IN SPARK IGNITION ENGINES

Knock may be induced in varying degrees in spark ignition engines by the choice of a suitable fuel and sufficient ignition advance. Priede and Dutkiewicz [3] quantified the effect of varying degrees of knock on spark ignition engine noise, and postulated that the rapid pressure rise produced by knock excites the engine structural frequencies whilst the pressure oscillations which are induced in the combustion chamber cavity impart a forced vibration on the engine structure.

These postulates are supported by the results yielded by noise measurements made on a Nissan L28 engine (see Appendices A and B for the engine and instrumentation details). The engine was found to knock readily when running on 93 RON gasoline, and showed a strong susceptibility to high speed knock, in the region of 4000 to 4500 rpm. Different levels of knock intensity were obtained by altering the spark timing, and investigations were made over the range of 5° to 20° before TDC, in 5° increments.

4.1 ENGINE NOISE CHARACTERISTICS

The noise characteristics of the engine with normal combustion will be described first in order to provide a basis for comparison for the noise characteristics with varying degrees of knock, a description of which will follow. The complete results of the noise measurements are presented for reference in Appendix C.

4.1.1 Noise Characteristics with Normal Combustion

Advancing the spark timing has a considerable effect on the form of the cylinder pressure diagram, with the peak cylinder pressure occurring earlier in the cycle and increasing in magnitude, as the spark advance is increased. Since it is reasonable to presume that these differences will have an effect on the emitted engine noise, a knock-free datum was established at each spark timing, using high octane aviation fuel (AvGas), or 98 RON gasoline at the lesser amounts of spark advance.

Figure 4.1 shows the third octave noise spectra over the speed range, with 20° of spark advance and aviation fuel. The spectra retain approximately the same shape as the engine speed is increased, indicating that the frequency response is determined by the engine structure natural frequencies. The natural frequencies of maximum response may be seen to lie in the region of 1000 to 3000 Hz.

The effect of spark timing on the third octave noise spectra with normal combustion is shown in Figure 4.2. The engine speed was 3500 rpm, and it can be seen that, while the spectra retain the same shape as the spark advance is increased, there is a difference of approximately 8 dB in sound pressure level between 5° and 25° before TDC. This increase in noise level is also evident on the noise/speed curves, as shown in Figure 4.3. It can be seen that the curves retain the dual slope characteristic which is typical of high speed gasoline engines, with an almost uniform increase of approximately 1 dBA per 5° of spark advance. Over the low speed range of between 1500 rpm and 3000 rpm, the noise level increases at a rate of 24 dB/decade, while above 3000 rpm the rate of increase is 45 dB/decade.

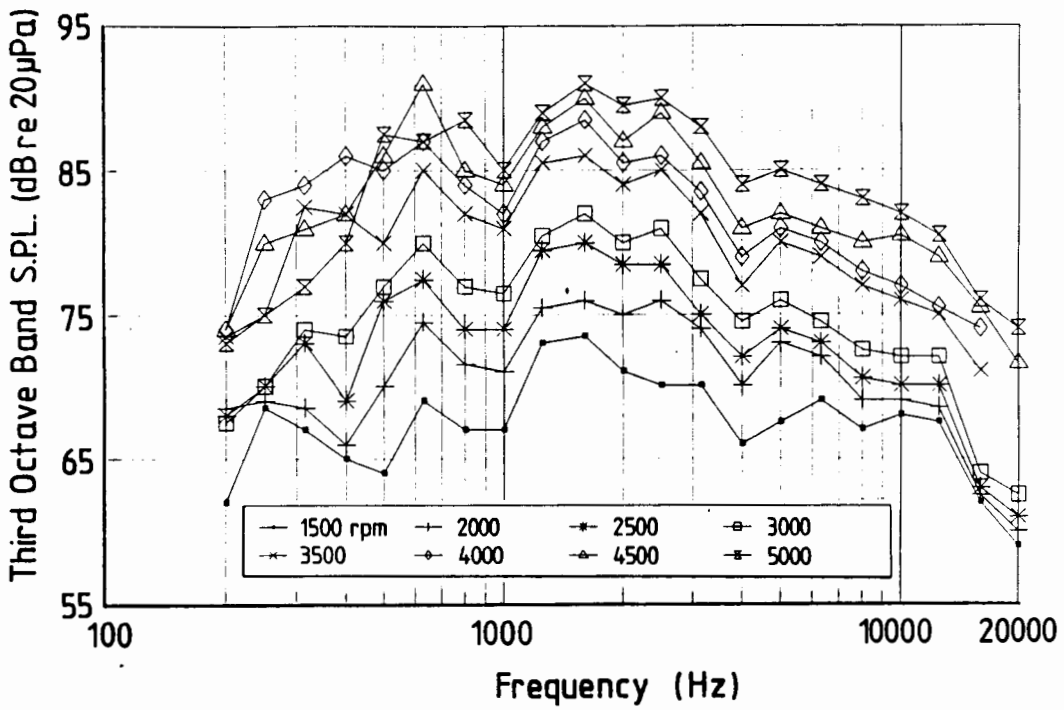

Figure 4.1 Third octave band noise spectra recorded over the speed range with normal combustion.

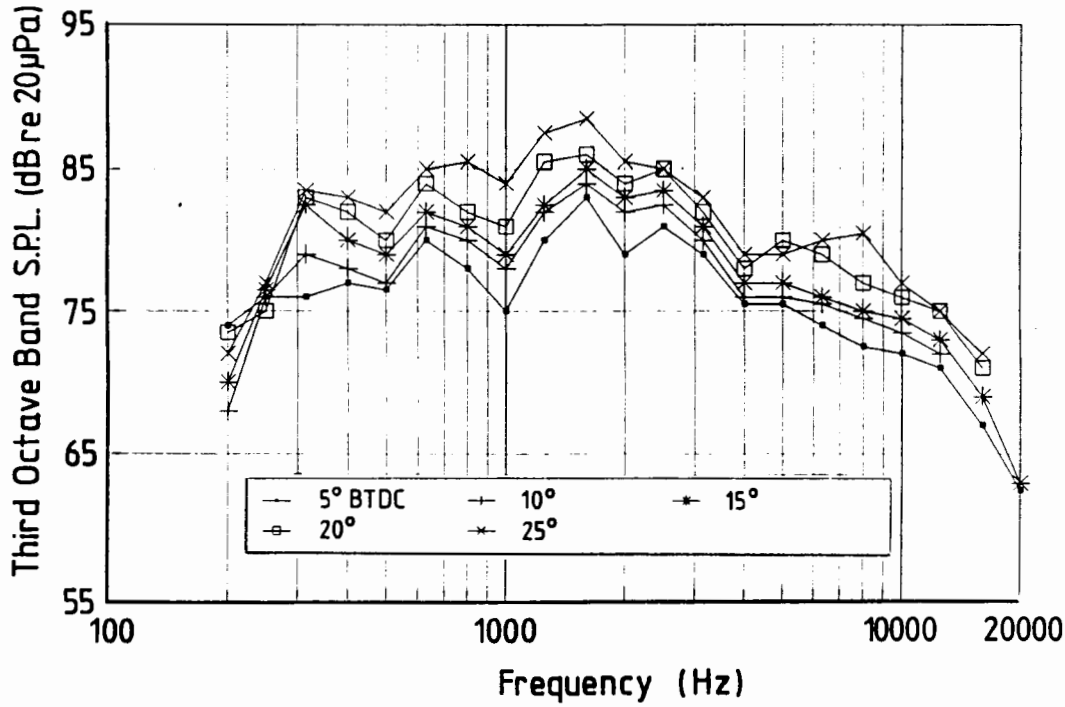

Figure 4.2 Third octave noise spectra recorded over a range of spark advance settings at 3500 rpm and with normal combustion.

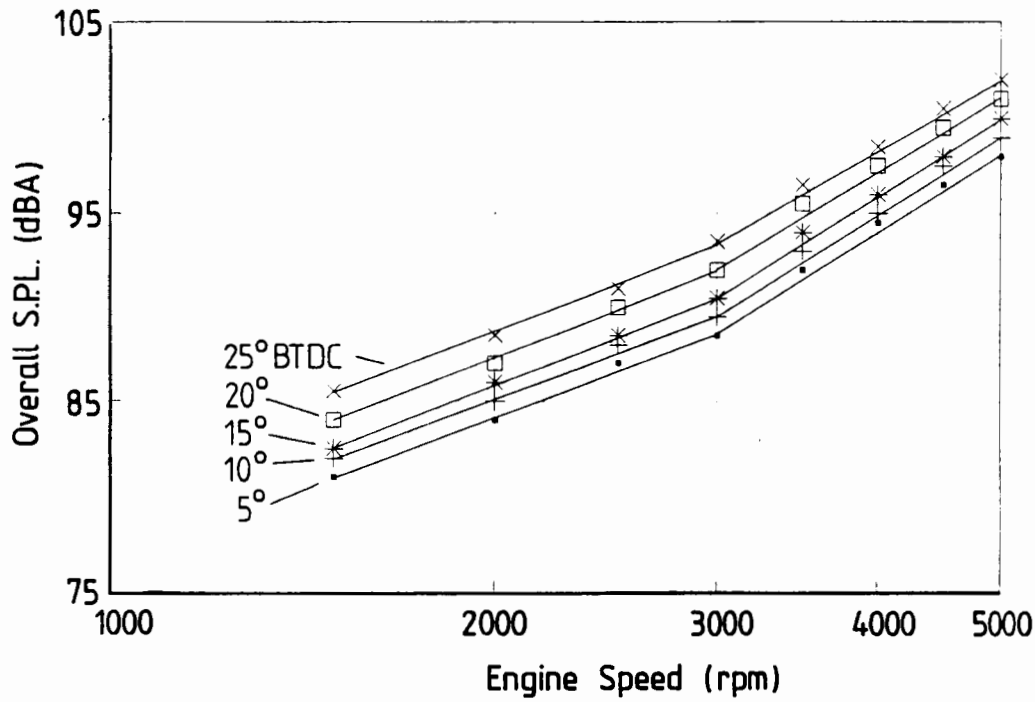

Figure 4.3 Noise/speed relationships with normal combustion and various spark advance settings.

Separating the frequency spectra into middle and high frequency parts gives some insight into the primary noise generation mechanism of the engine. The averaged SPL values of the frequency ranges from 800 to 3150 Hz and from 6300 to 20000 Hz are shown in Figure 4.4, as a function of speed. It can be seen that the averaged high frequency noise values display a far more prominent two slope characteristic than the low frequency noise values. In the middle frequencies the noise level increases at a rate of approximately 17.5 dB/decade up to 3000 rpm, and at approximately 38 dB/decade between 3000 and

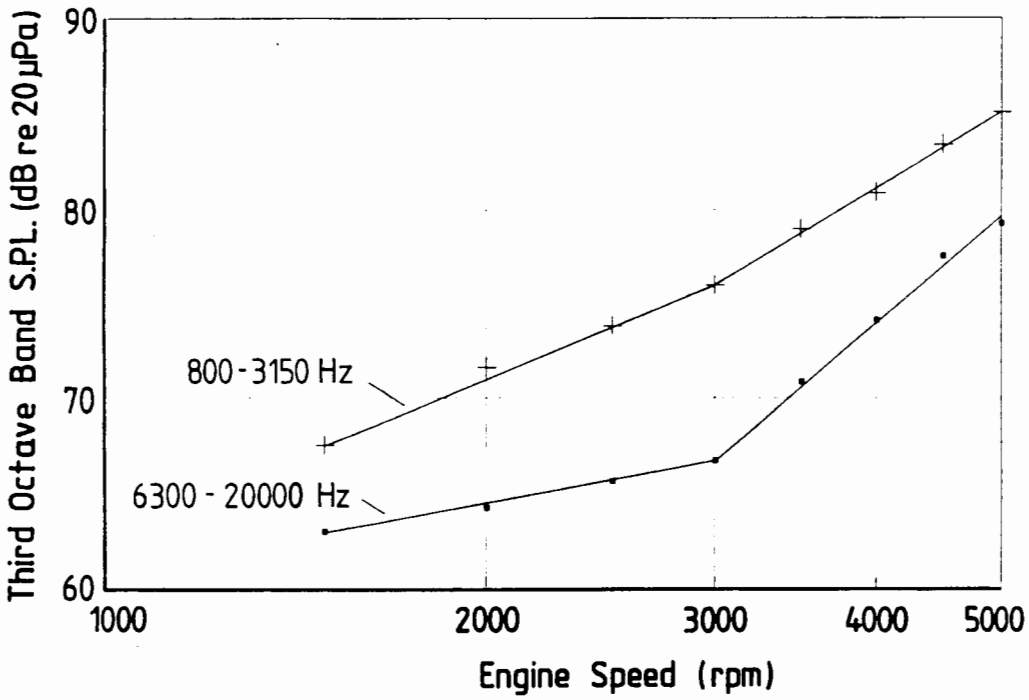

Figure 4.4 Averaged third octave noise levels between 800 and 3150 Hz, and 6300 and 20000 Hz, over the speed range.

5000 rpm. The corresponding values for the high frequency part of the spectrum are 5.5 dB/decade and 45 dB/decade respectively, although the noise level over the speed range for the middle frequencies is between 5 and 10 dB higher than in the high frequency region.

This observation is in agreement with the primary noise generation mechanism for gasoline engines proposed by Raff and

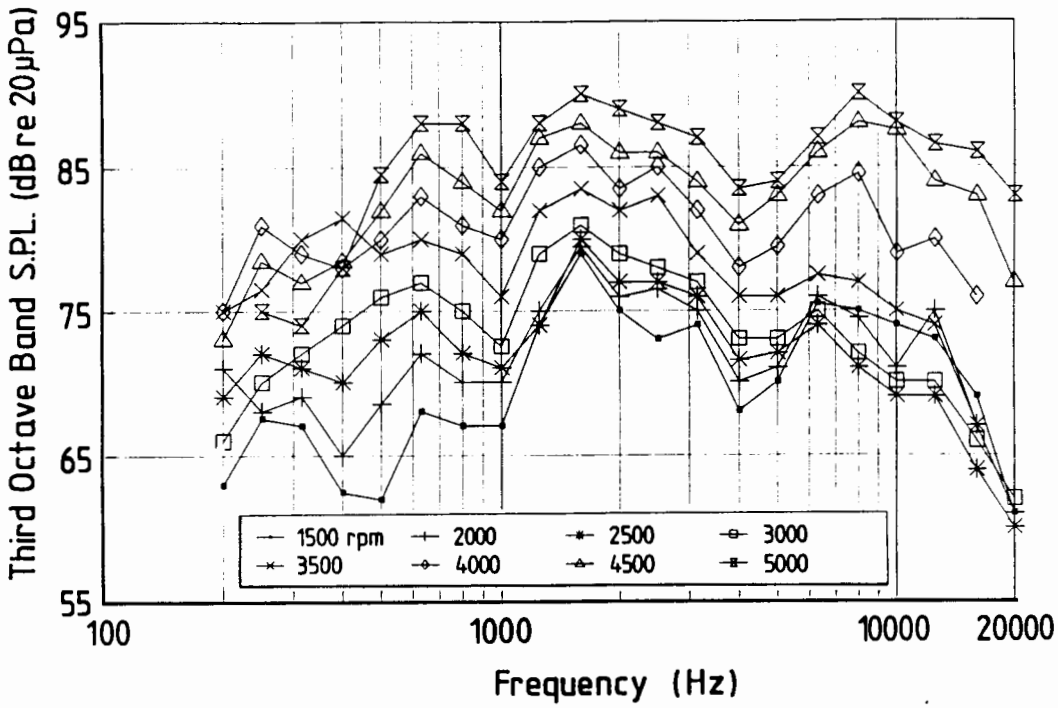

Figure 4.5 Third octave noise spectra recorded over the speed range with knocking combustion.

Grover [28], as described in the Chapter 3, in that the impulsive nature of the hydraulic forces in the main bearings will result in increased excitation of the higher modes of the engine structure.

4.1.2 Noise Characteristics with Knocking Combustion

The effect of knock on the engine noise characteristics is particularly evident in the third octave noise spectra recorded with the engine running on 93 RON gasoline and with 20° of spark advance, as shown in Figure 4.5. Two differences are immediately noticeable when compared to the spectra in Figure

4.1. The most prominent difference is in the high frequency region above 5000 Hz, where noise levels have increased by up to 20 dB in the 8000 Hz third octave band. The second difference is in the frequency region between 1000 and 3000 Hz, where noise levels have increased by up to 10 dB at low engine speeds. This increase appears to diminish as engine speed is increased, however.

Figures 4.6a and b show the third octave noise spectra recorded over a range of spark advance settings at 1500 and 4000 rpm respectively. The fuel is 93 RON pump gas, and the effect of the severity of the knock on the emitted noise is clearly visible. At 1500 rpm the increase in noise level in the 8000 Hz third octave band is approximately 20 dB between 5° and 20° of spark advance, while there is an average increase in noise level between 1800 Hz and 3150 Hz of 10 dB over the same range. At 4000 rpm the increase in this frequency range is small (of the order of 3 dB) compared to the 14 dB increase in the 8000 Hz third octave band. In addition to the two major differences mentioned above, there is also a noticeable noise level increase in the frequency range between 4000 and 5000 Hz, although this is only evident at 1500 rpm.

The knock-induced noise is also clearly evident on the noise/speed characteristic of the engine. The A-weighted overall noise levels measured at different spark advance settings and with 93 RON pump gasoline are shown in Figure 4.7. At 1500 rpm there is an increase of 13 dBA between the normal combustion noise level with 5° spark advance, and the noise level at 20° spark advance. The influence of the severity of the knock as indicated by the amount of spark advance, is clearly evident over the speed range. The difference between the knock-free and knocking noise levels at all the spark advance settings investigated, shows a decreasing trend up to 3000 rpm, beyond which there is an increasing trend

a)

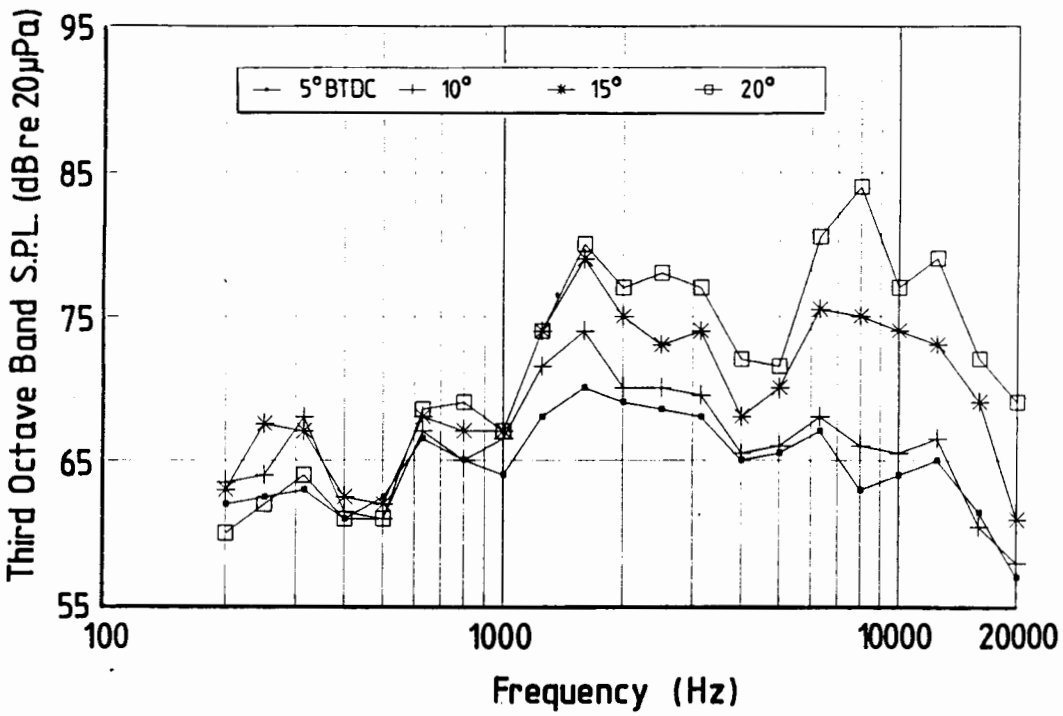

b)

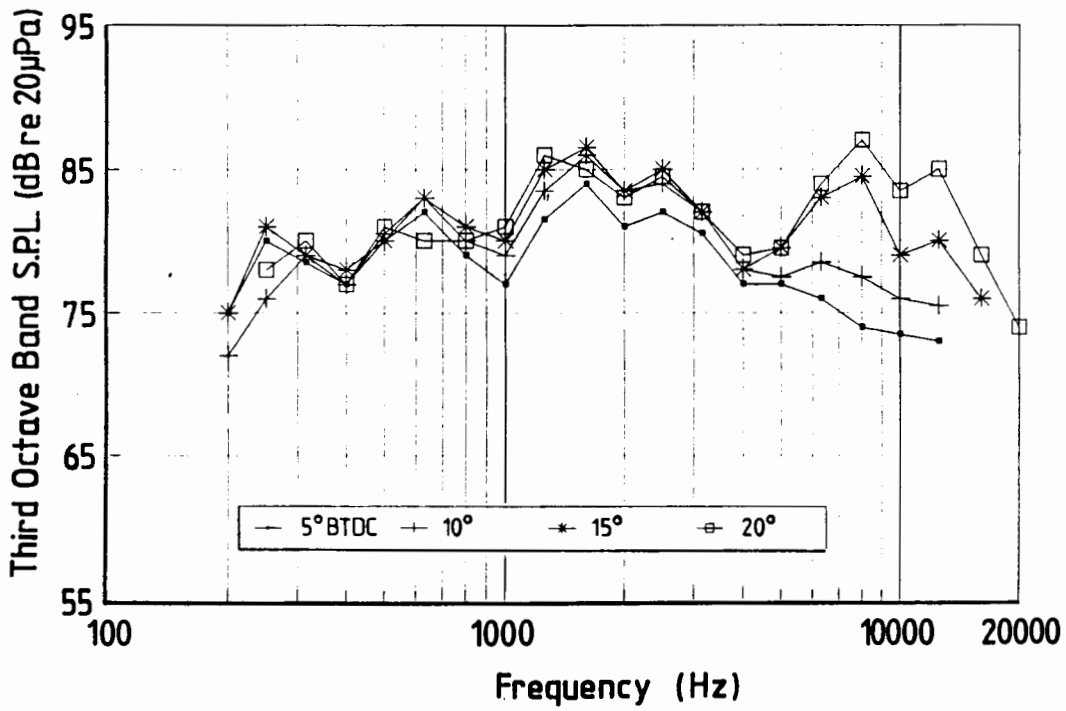

Figure 4.6 Third octave noise spectra recorded at 1500 and 4000 rpm with various degrees of knock intensity.

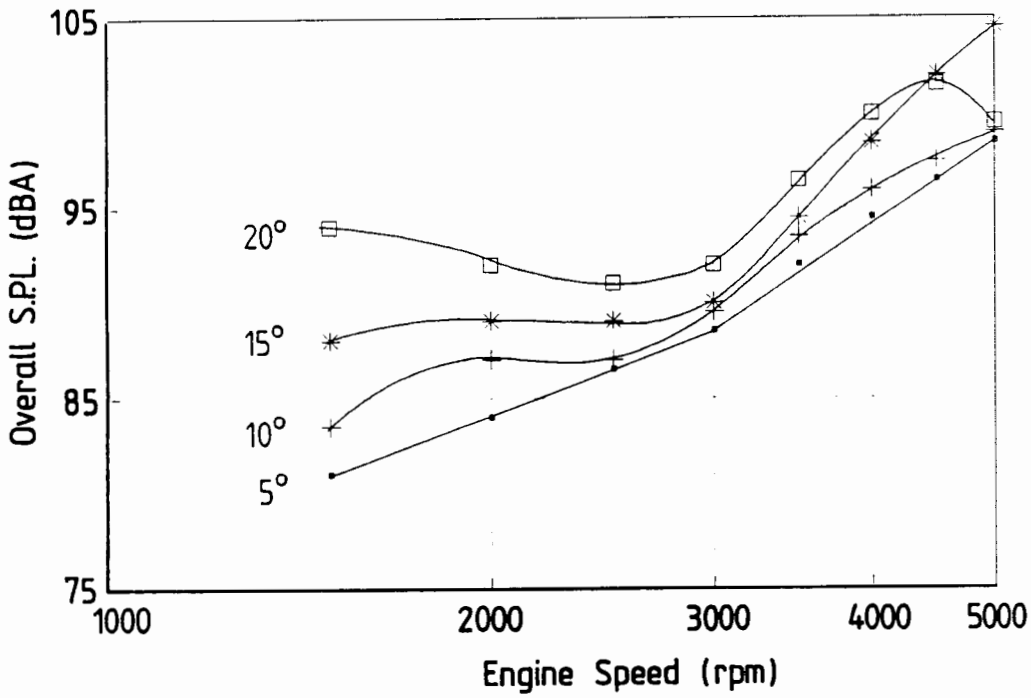

Figure 4.7 Overall A-weighted noise levels over the speed range and with various degrees of knock intensity.

again. An interesting exception to this trend occurs beyond 4000 rpm, where the knock intensity at 20° of spark advance decreases, while the general increasing trend is still strongly evident at 15° of spark advance.

A more distinct measure of the knock-induced noise is obtained by recording the peak third octave band noise level above 6000 Hz. The results of this analysis are plotted against speed, in Figure 4.8. The same trends are evident as in the A-weighted noise levels, but are far more distinct. These results give a clear indication of the engine's propensity to knock over the

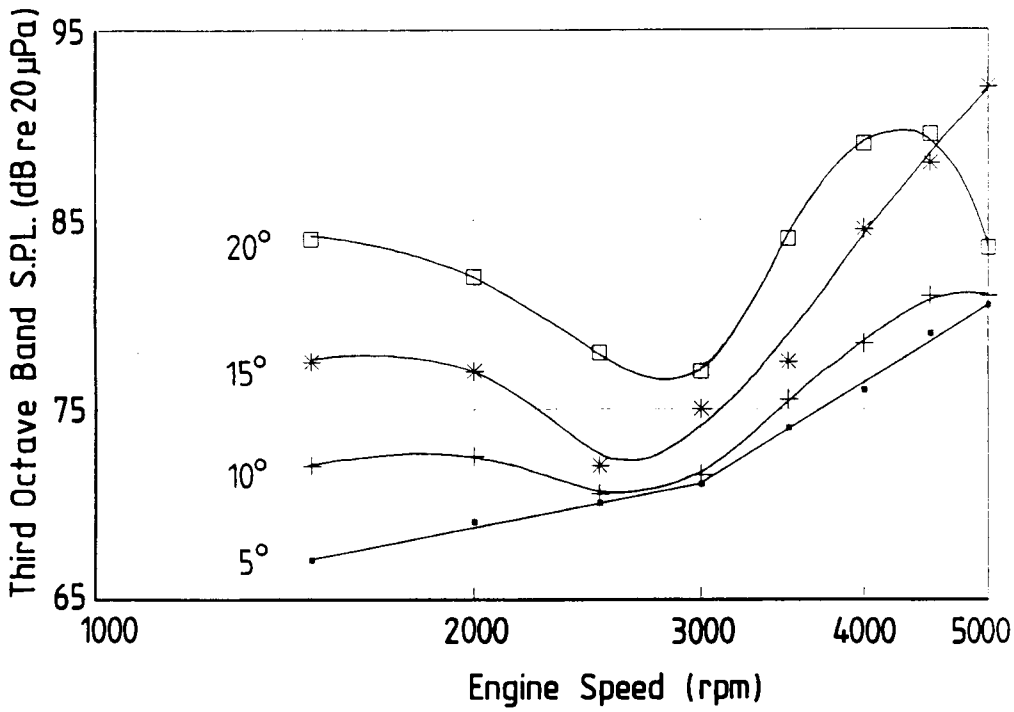

Figure 4.8 Maximum third octave band noise levels between 6300 and 20000 Hz with various degrees of knock intensity.

speed range. As expected, the most severe knock occurs at low speed, but the extraordinary susceptibility to high speed knock of this particular engine is also clearly evident.

4.2 DISCUSSION OF RESULTS

A number of observations may be made regarding the engine noise characteristics which have been described above. The two knock-induced noise generation mechanisms proposed by Priede are strongly evident, with the emitted noise being dominated by

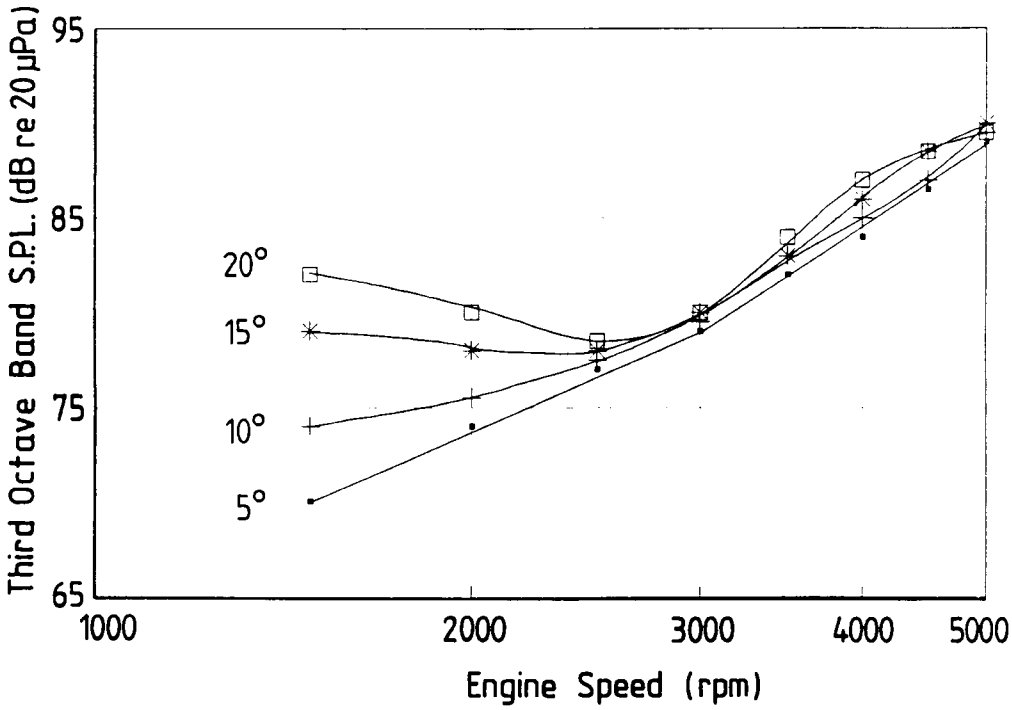

Figure 4.9 Maximum third octave band noise levels between 800 and 3150 Hz with various degrees of knock intensity.

the high frequency component (above 6000 Hz) which corresponds to the frequencies of oscillation of the combustion gases following the knock event. The second mechanism, namely the excitation of the engine structural natural frequencies by the initial rapid pressure rise, is also evident, but only at the lower engine speeds, up to 3000 rpm. This may be illustrated by plotting the peak third octave band noise levels recorded between 800 and 3150 Hz, over the speed range, as shown in Figure 4.9. It can be seen that an appreciable increase in the excitation of the structural modes occurs only up to 3000 rpm. Recorded cylinder pressure diagrams indicate that instantaneous

pressure rises of the same and greater magnitudes as those occurring at the lower speeds, occurred at 4000 and 4500 rpm. It would thus appear that the primary noise generation mechanism which is present at speeds beyond 3000 rpm, is dominant enough to mask the effect of instantaneous combustion pressure rises, even of the rates and magnitudes encountered during knock.

CHAPTER 5

CHARACTERISATION OF THE CYLINDER PRESSURE DEVELOPMENT BY MEANS OF THE CYLINDER PRESSURE SPECTRUM

The concept of the cylinder pressure spectrum was introduced in Chapter 2 of this thesis, but as combustion noise is usually dominant only in diesel engines, the cylinder pressure spectrum has not found much application in spark ignition engines. The rapid pressure rise and the large amplitude pressure oscillations which result from knock can, however, increase combustion noise levels considerably, and the effects of these phenomena on the exciting properties of the cylinder pressure development can be identified most easily in the frequency domain. The cylinder pressure spectrum is thus an invaluable tool in any investigation into knock-induced noise.

Unlike their compression ignition siblings, spark ignition engines display, at best, significant cycle-to-cycle variations in their cylinder pressure diagrams, a situation which is worsened considerably by the introduction of an essentially uncontrolled phenomenon such as knock. In order to perform a quantitative analysis of knocking cylinder pressure developments, it is therefore necessary to examine individual pressure diagrams and their spectra. Consequently, the averaged cylinder pressure spectra which are usually obtained from electronic frequency analysers are of little use, because the period over which these analyses are done spans several cycles. This has necessitated the development of a means of deriving the frequency spectrum of individual cycles from cylinder pressure records which have been digitised. A computer program which performs this task was developed as part of this thesis, and is described in this chapter.

5.1 ANALYSIS OF CYLINDER PRESSURE DIAGRAMS.

The analysis program makes use of a Fast Fourier Transform (FFT) algorithm to compute the spectrum, and the application of this technique of spectral estimation to the computation of cylinder pressure spectra will first be discussed, as a pretext to the description of the program itself. In addition, some of the problems associated with the digitisation of waveforms will also be mentioned.

5.1.1 Fourier Analysis

The mathematical basis of frequency analysis is the Fourier Transform which is the subject of a large number of texts [34,35,36] and will not be described rigorously here. In order to highlight some of the problems inherent in its application to the analysis of cylinder pressure diagrams, however, it is necessary to give a brief description of the fundamentals.

The Fourier Transform takes on different forms depending on the nature of the waveform being analysed, the most general case being the Integral Transform of which the forward transform has the following form (37):

$$G(f) = \int_{-\infty}^{\infty} g(t)e^{-2\pi ft}\,dt \qquad (5.1)$$

In this case the waveform is an infinite and continuous function in both the time and frequency domains, and the transform may be applied to functions which are not necessarily periodic because the limits of integration tend to infinity. This transform may be adapted to practical (finite) waveforms by assuming that the input function is periodic over some period T, and the result is the well known Fourier Series

expansion, whereby the input waveform is represented as a sum of sinusoidal components at equally spaced frequencies kf_1, where f_1 is the reciprocal of the periodic time (=1/T). The kth component is obtained from the integral

$$G(f_k) = \frac{1}{T}\int_{-\frac{T}{2}}^{\frac{T}{2}} g(t)e^{-2\pi f_k t}\,dt \qquad (5.2)$$

where $f_k = kf_1$ (i.e. the k^{th} harmonic of f_1)

In this case the waveform is a continuous periodic function in the time domain, but becomes a discrete function in the frequency domain.

The final adaptation is to functions which are sampled in the time domain, resulting in the Discrete Fourier Transform (DFT):

$$G(f_k) = \frac{1}{N}\sum_{n=0}^{N-1} g(t_n)e^{\frac{-j2\pi nk}{N}} \qquad (5.3)$$

The result is a function which is discrete and periodic in both the time and frequency domains, and it can be seen that this adaptation of the Fourier Transform is well suited to the analysis of digitised waveforms by means of a digital computer.

It can also be seen, however, that obtaining N frequency components from N time samples requires N^2 complex multiplications. This can be overcome by making use of one of the variations of the Fast Fourier Transform (FFT) algorithm, which reduces the number of complex multiplications down to the order of $N\log_2 N$, and is thus computationally much more efficient than the DFT, while obtaining the identical result. A detailed description of the FFT will not be given here, as

the subject is covered extensively in a large number of publications and texts [38,39,40,41].

The advent of the FFT has made the analysis of time sampled waveforms comprising many thousands of data points by means of low cost personal computers a practical reality, and this was the approach adopted for the frequency analysis of cylinder pressure diagrams. The DFT implementation of the Fourier Transform, as described above, carries with it a number of implicit pre-conditions and assumptions, however, and these will be addressed in the following section.

The first assumption is that of periodicity, and as it turns out this is conveniently satisfied by performing the analysis over a complete 720° engine cycle, so that the repetition frequency is equal to the engine speed. As a result, the frequency spectra carry the assumption that the waveform is repetitive, and the levels of the frequency components are scaled accordingly.

The second condition relates to the nature of the signal to be analysed. Combustion in spark ignition and diesel engines can essentially be regarded as a transient phenomenon occurring at a fixed repetition rate. As such the cylinder pressure diagram of a complete 720° cycle has a finite total energy content which must be maintained in the frequency domain representation. This can be achieved if the input waveform tends to zero at the limits of integration, a condition which can be met by analysing the cylinder pressure signal over the 720° period between two successive TDC(exhaust) points. Besides minimising so-called "leakage" effects, this also eliminates the need for any data windowing functions, such as the popular Hanning, Hamming, Blackman, Parzen, Welch, or Gaussian windows.

An associated concern is that of the scaling of the results. Those forms of the Fourier Transform which result in spectra which are continuous functions have units of "spectral density". For example, an amplitude squared spectrum of this type may have units of energy per unit frequency, and must be integrated over a finite bandwidth to give a finite energy. This occurs implicitly when normalising by the period of integration (T), as in equation (5.2), which amounts to the same as multiplying by the "bin-width" of each discrete spectral line.

5.1.2 Digitisation Effects

If the rudimentary requirements of digital data acquisition are complied with, such that the resolution, dynamic range, sampling frequency, and data record length are sufficient to accurately represent the analogue signal over the required frequency range, then the foremost problem accompanying digitisation is that of "aliasing". Since a minimum of two data points are required to represent one period of a waveform, the maximum frequency which can be represented by a digitised waveform is equal to half the sampling frequency (called the Nyquist frequency). Aliasing refers to a process whereby frequencies which are higher than the Nyquist frequency, and are therefore too high to be accurately represented due to the limited sampling frequency, falsely contribute to the spectrum. The most effective way of eliminating aliasing is to low-pass filter the signal at or below the Nyquist frequency. Unfortunately, this option was not available, and also has problems associated with phase shifts which are introduced by the filter. The effects of aliasing may, however, also be reduced by using a sufficiently high sampling frequency, and a sampling rate of 125 kHz was used in the hope that adverse effects over the frequency range of interest, namely up to 20 kHz, would be negligible.

5.2 "EDAP" - ENGINE DATA ANALYSIS PROGRAM

The program was written in Turbo Pascal for an IBM PC or equivalent computer (ideally equipped with a math co-processor). Besides processing by the FFT algorithm, the data are also subjected to pre- and post-processing stages, their respective functions being to condition the signal for processing and to extract the power spectrum from the output.

5.2.1 FFT Algorithm

The FFT algorithm used is a variation of the classic Cooley-Tukey radix 2 algorithm, which requires the number of complex input data points to be a power of 2. The input of N complex data points is transformed into a N/2 point complex spectrum covering the frequency range from 0 Hz (dc) to half of the sampling frequency (the Nyquist frequency).

A feature of the complex FFT algorithm is that, if the input data is real, then twice the number of points may be analysed. This is done by passing every alternate real data point to the algorithm as a complex point, and then reconstructing the real spectrum from the resulting transform.

5.2.2 Data Pre-Processing

The digitised data is read from magnetic disk and the waveform plotted on the computer screen. The chosen 720° engine cycle demarcated by the captured TDC(exhaust) pulses is extracted from the displayed waveform and converted to pressure units (Pa). The fixed digitisation rate dictates that the number of data points is a function of engine speed, and thus requires conversion to the required base 2 number. This is achieved by means of either zero-padding or interpolation, depending on the application, and these are discussed in greater detail later in

this chapter. Since the FFT algorithm sees the incoming data set as representing a repetitive waveform, it is imperative that there be no sharp discontinuity between the start and end points. In the case of cylinder pressure diagrams, any small linear trend between these points (which should not exist as both are at TDC on the exhaust stroke, but which may arise due to thermal shock induced drift in the pressure transducer) is thus removed. The N real data points are then mapped onto N/2 complex data points for processing by the FFT algorithm. The maximum number of complex data points that can be analysed by the FFT algorithm is 8192, thus allowing the analysis of 16384 real data points.

5.2.3 Data Post-Processing

The raw transformed data is complex, has units of energy spectral density, and extends between the positive and negative Nyquist frequencies. (The concept of negative frequencies is a mathematical abstraction indicating frequencies with phase shifts measured in the negative direction.) The Fourier coefficients at each discrete frequency are calculated by adding the corresponding positive and negative frequency components and normalising the result by the period of the input waveform. The magnitude and phase of each frequency component are then extracted from its complex value, and stored in separate data channels. The RMS power spectrum is then computed in units of dB (re 2×10^{-5} Pa for cylinder pressure spectra) and plotted, optionally on a logarithmic frequency axis. The raw data has a resolution of 12 bits, giving a dynamic range of 72 dB, which should be maintained during the subsequent processing which was done using 6 byte real numbers.

5.2.4 Validation of Results

The accuracy of the computation may be checked against a synthesised input signal for which the Fourier Series expansion may be determined analytically by means of equation (5.3). For this purpose the sawtooth waveform used by Priede [2] was chosen, and an example of such an input waveform and the resulting spectrum are shown in Figure 5.1a and b. The levels of the harmonics can be verified by solving for the Fourier Series coefficients analytically and comparing the levels computed from the two techniques. The derivation is presented in Appendix D and the solution takes the form:

$$|G(f_k)| = 20 \log \left\{ \frac{\sqrt{2}\,A}{2 \times 10^{-5}\, \pi f_k T} \right\} \qquad (5.4)$$

The inverse relationship between the levels of the harmonics and their frequencies results in their decay at a rate of 20 dB/decade increase in frequency, and it can be seen that this feature is accurately reproduced in the computed spectrum. It can easily be verified that the numerically computed levels agree with those calculated analytically. In particular, the sawtooth waveform in Figure 5.1a has a period of 20 msec and an amplitude of 1, which translate to a fundamental with a frequency of 50 Hz and a RMS power magnitude of 87.05 dB (re 2×10^{-5}). It can be seen that these parameters are accurately predicted by the FFT.

5.2.5 Zero-Padding versus Interpolation

A problem arises in the method used for converting the arbitrary number of data points to a base 2 number suitable for processing by the FFT algorithm.

a)

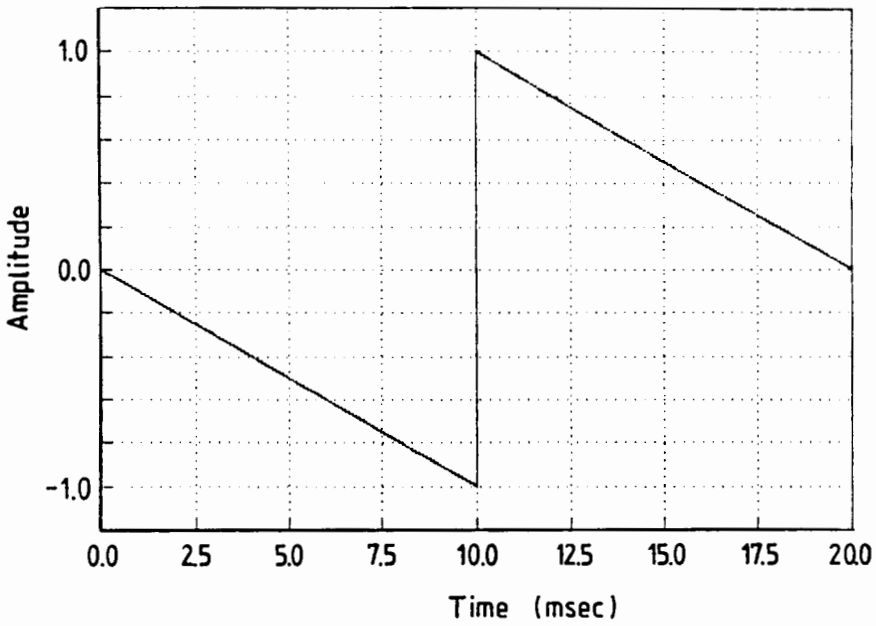

b)

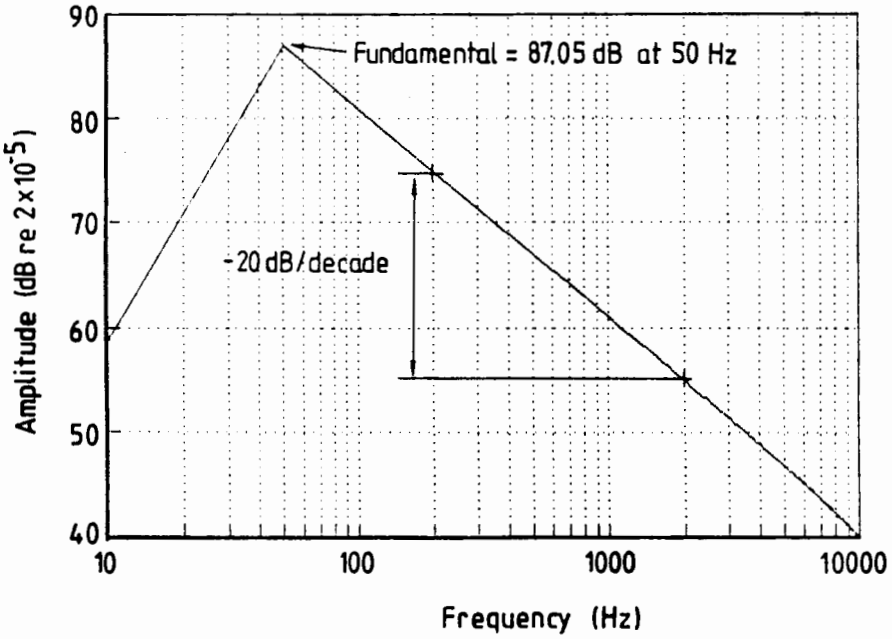

Figure 5.1 Triangular sawtooth waveform and its spectrum.

From a mathematical point of view, zero-padding (adding zeros to the end of the waveform to increase the number of data points to the required number) has a number of advantages. The resolution of the spectrum is increased as there are more data points covering the same frequency range, so-called "end effects" are diminished, and it is computationally efficient. Care must be taken to scale the transform output according to the original period, and not the period of the input waveform (which has increased due to the addition of the zeroes). There is one disadvantage, however, in that the discrete frequencies comprising the output of the transformed waveform are now harmonics of the fundamental frequency of the padded waveform, and thus the amplitude of the original fundamental is not accurately portrayed. The curve joining the levels of the higher harmonics does, however, give an accurate indication of the levels at frequencies which fall between the data points, and the higher (original) harmonics are thus accurately represented.

The other alternative is interpolation of the original data record at the sampling interval required for a suitable record length. This method preserves the period of the waveform, but has the disadvantages that interpolation to a smaller number of points effectively decreases the sampling rate, and that it requires more computation time. In addition, the accuracy with which the features of the original waveform, particularly sharp peaks, are reproduced in the interpolated waveform may be questionable.

Since the level of the fundamental is not of interest in this study (cylinder pressure spectra are usually evaluated between 100 Hz and 20 kHz), and it is of vital importance to maintain the (already limited by digitisation) accuracy of the original cylinder pressure trace during the analysis, zero-padding was chosen as the preferred method of obtaining the correct number

of input data points. Interpolation was maintained as an option, however, for use in applications where the level of the fundamental was of interest.

5.3 CHARACTERISATION OF CYLINDER PRESSURE DIAGRAMS BY CYLINDER PRESSURE SPECTRA

In order to appreciate the contribution of knock to the cylinder pressure spectrum, it is necessary to define the frequency domain response of the various features of the cylinder pressure diagram, as well as the effect of the various operating parameters on these responses. The computation of cylinder pressure spectra from a digitised waveform allows the analysis of mathematically defined computer-generated waveforms, and this procedure will be used in the following section of this chapter, in order to develop an understanding of the relationship between the various features of a typical cylinder pressure diagram and its spectrum.

In order to categorise the relationship between the cylinder pressure diagram and its spectrum, the former may be described as comprising three elements:

a) the pressure rise due to compression,
b) the pressure rise due to combustion which may be rapid or relatively gentle, depending on the combustion characteristics, and
c) any pressure oscillations which may be induced by disturbances such as a rapid pressure rise.

For the sake of computer analysis, these three elements have been modelled by a mathematically computed compression curve, a triangular sawtooth waveform, and an exponentially decaying sinusoidal waveform, respectively. The complete synthesised diagram is constructed by summing these separate components,

and since the FFT is a linear function, the spectrum of the sum of the parts may also be computed by summing the spectra of the individual parts.

Figures 5.2a and b show the computer generated versions of the three elements and their respective spectra, and the complete synthesised pressure diagram and its spectrum are shown in Figures 5.3a and b respectively. The compression curve is computed for an engine speed of 2000 rpm, and reaches a maximum pressure of 42.5 bar, while the contribution due to combustion consists of an instantaneous pressure rise of 10 bar and occurs at TDC. The exponentially decaying pressure oscillations have a frequency of 6000 Hz and initial amplitude of 5 bar. The simplest case has been chosen for the sake of illustration, and more realistic variations of these waveforms will be presented in the next section of this chapter, where the response range of the individual elements, as well as the effects of various variables such as the rate, magnitude, and phasing of the combustion pressure rise, and the effect of engine speed, will be illustrated.

5.3.1 Range of Frequency Response

As it so happens, the three components used to construct the pressure diagram have their most profound influences over different parts of the frequency range. The compression curve has the highest levels and dominates the low frequency part of the combined spectrum, where the level at the frequency of the fundamental is 208.15 dB. Unless the frequency analysis is done with a very high frequency resolution, the spectra cannot distinguish between individual harmonics and a continuous line representing the decreasing levels of the harmonics is depicted. The contribution of the combustion pressure to the level of the fundamental is small, in the region of 1.6 dB, and up to about 300 Hz (the 18^{th} harmonic), the form of the

a)

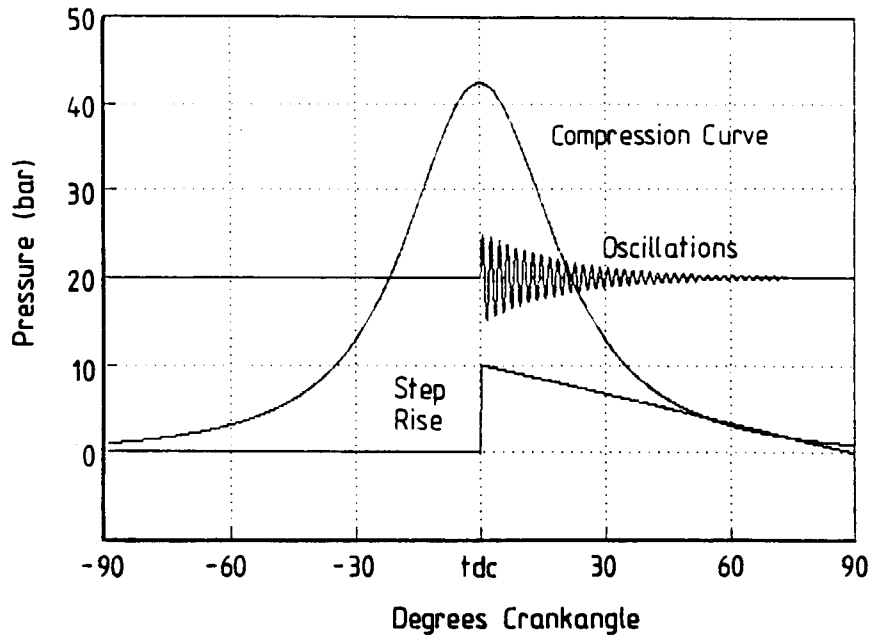

b)

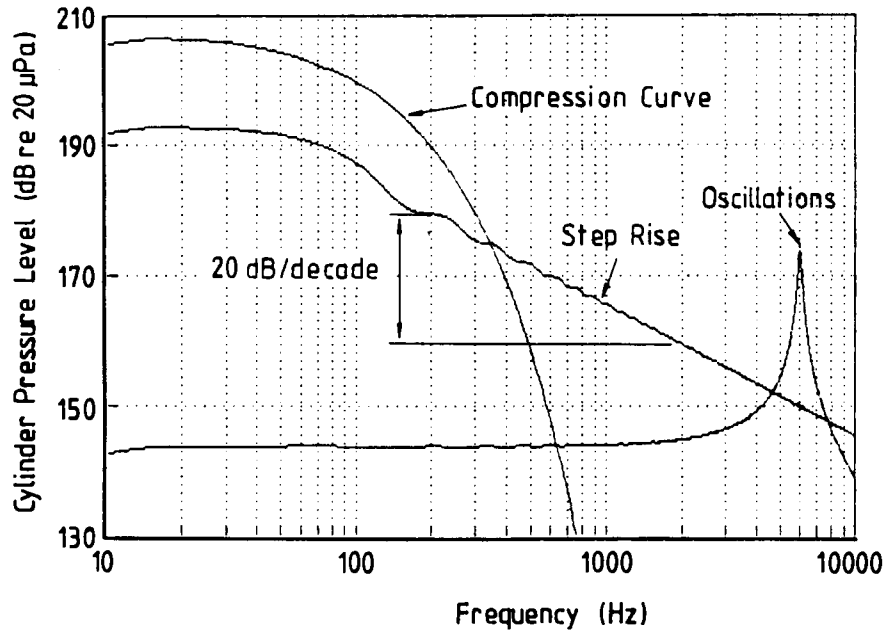

Figure 5.2 Three elements of a cylinder pressure diagram and their spectra.

a)

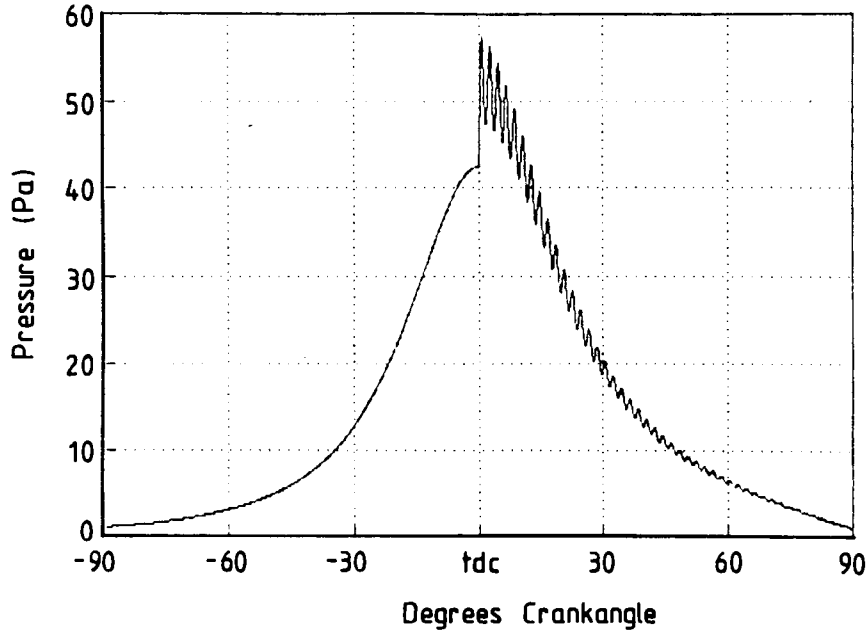

b)

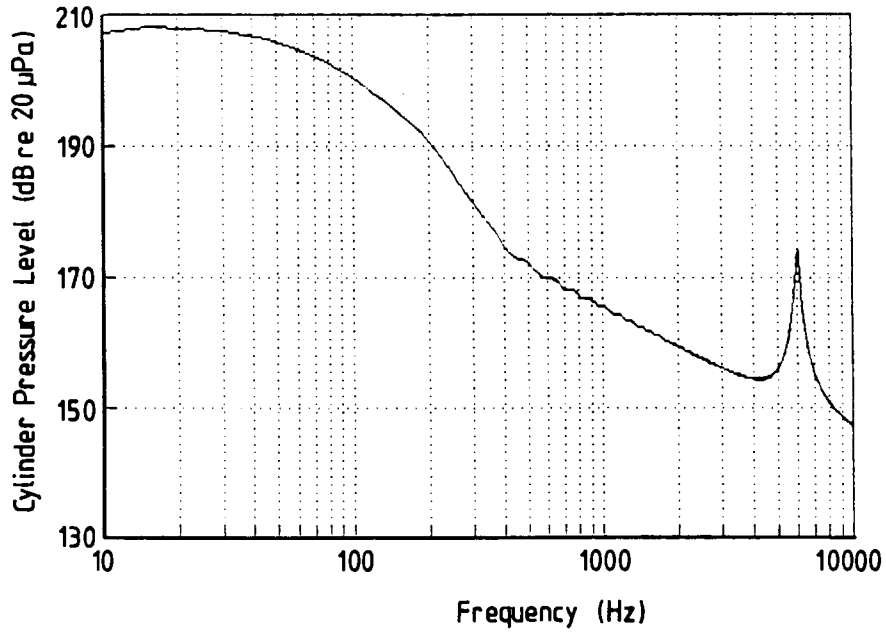

Figure 5.3 Pressure diagram assembled from the three elements in Figure 5.2a, and its spectrum.

spectrum follows that of the compression curve. In the mid-frequency range, namely from 300 Hz up to about 4000 Hz, the distinct -20 dB/decade slope of the instantaneous combustion pressure rise is dominant, with a level of 165.5 dB at 1000 Hz. The peak associated with the pressure oscillation emerges from this slope and reaches a level of 174.3 dB at 6000 Hz.

5.3.2 Magnitude of the Combustion Pressure Rise.

The magnitude of the instantaneous pressure rise due to combustion determines the level of the -20 db/decade slope over the frequency range, and may be calculated using equation (5.4), with the amplitude A equal to half the magnitude of the rapid pressure rise. This relationship is of great significance in that it allows the magnitude of the actual pressure rise resulting from knock to be determined if a distinct -20 dB/decade slope is distinguishable on the cylinder pressure spectrum, a technique which will be used extensively in this thesis.

5.3.3 Rate of Combustion Pressure Rise

The slope of the spectrum of the rapid pressure rise is dependent on the rate of pressure rise, and attains the minimum rate of decay of 20 dB/decade only for an instantaneous pressure rise. The effect of a finite rate of pressure rise is illustrated in Figures 5.4a and b, which show a sawtooth waveform with a 10 bar pressure rise, but with a rate of pressure rise of 2 bar/degree crankangle (24 bar/msec), and its spectrum. The fundamental reaches the same level as that for the instantaneous pressure rise shown in Figure 5.2a, and the form of the spectrum is the same up to about 600 Hz (i.e. it has the same -20 dB/decade slope), after which the level falls away rapidly. A local minima is reached at 2400 Hz, this frequency being determined by the period of the pressure rise,

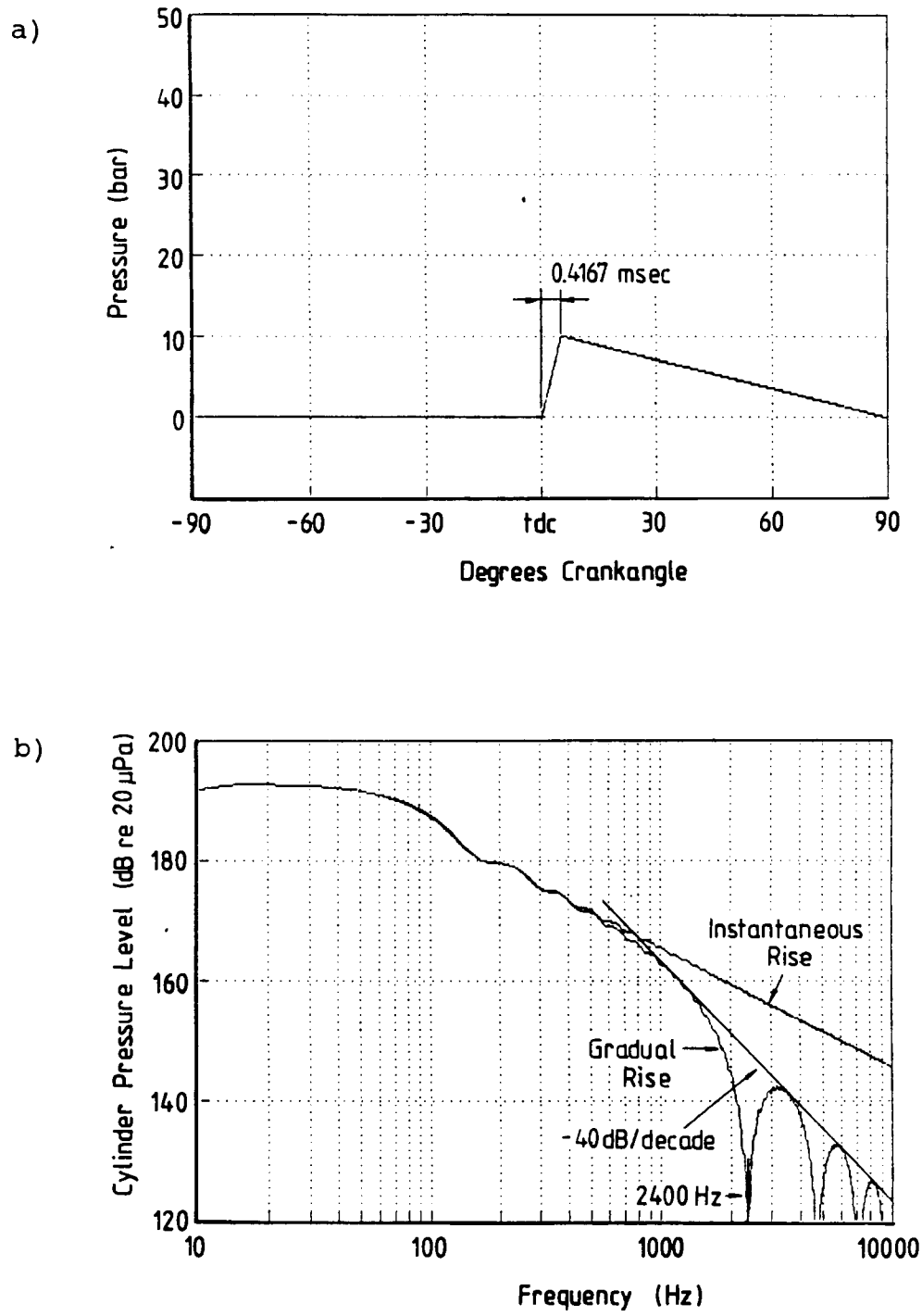

Figure 5.4 Effect of a finite rate of pressure rise on the cylinder pressure spectrum.

namely 0.4167 msec. As the frequency increases from this point, the level of the frequency components traces out a series of lobes occurring at 2400 Hz intervals and with peak levels which decay at a rate of 40 dB/decade.

5.3.4 Phasing of the Combustion Pressure Rise

Figure 5.5 shows the effect of delaying the point at which the instantaneous pressure rise occurs by 10 degrees. While the form of the spectrum is not altered by the shifted pressure rise, the spectrum of the combined combustion and compression curves, as shown in Figure 5.5, changes significantly. The shape of the spectrum is unaltered up to approximately 100 Hz, after which it decays at an increased rate until a local minimum is reached at 350 Hz. The level rises rapidly again as the frequency is increased up to approximately 600 Hz, beyond which the level assumes the normal -20 dB/decade slope at the level determined by the magnitude of the pressure rise.

The reason for discontinuity between the compression and combustion pressure components is that the harmonics of the combustion pressure curve have undergone a phase shift relative to the harmonics of the compression pressure. The resulting phase differences between the two spectra are apparently large enough to cause the harmonics to cancel one another over parts of the frequency range. This phenomenon appears to occur between 100 Hz and 600 Hz, resulting in the sharp drop in spectral level up to a frequency of 350 Hz, where the contribution from the compression curve is equal to that of the combustion curve. Beyond this frequency the spectrum of the combustion curve begins to dominate, and the spectral level rises again until the contribution from the compression curve is negligible.

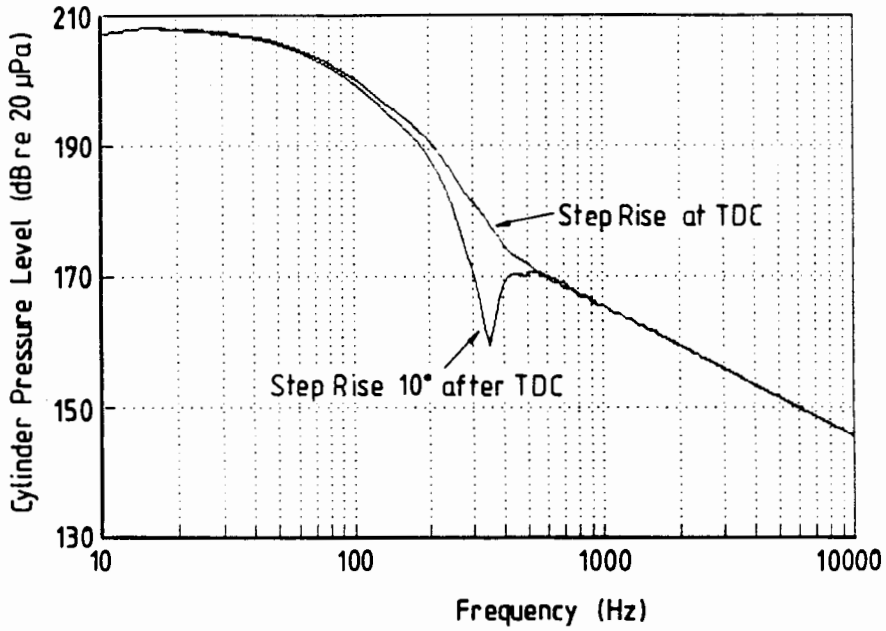

Figure 5.5 Effect of a late pressure rise on the cylinder pressure spectrum.

The frequency at which the trough on the spectrum occurs is thus determined by the point where the spectral level of the two components is equal, and is not dependent on the phase shift of the combustion pressure rise.

5.3.5 Effect of Engine Speed

The effect of engine speed on the cylinder pressure spectra is intuitively obvious. As the engine speed is increased, the frequency of the fundamental is increased. The shape of the spectrum remains unchanged, and the harmonics therefore experience the same shift in the direction of increasing frequency. There is thus an increase in the spectral level at frequencies above the fundamental, the magnitude of which is dependent on the slope of the spectrum. This is illustrated in

Figure 5.6 which shows the spectra of identical cylinder pressure developments synthesized at speeds of 2000, 3000, 4000, and 5000 rpm. It can easily be verified that the rate of increase of the cylinder pressure level with speed is equal to the slope of the spectrum.

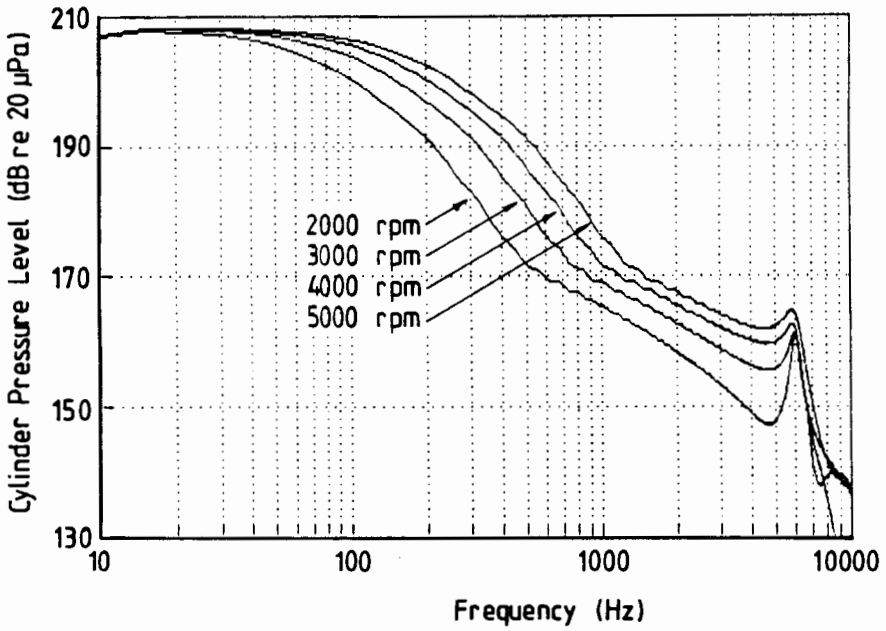

Figure 5.6 Effect of engine speed on the cylinder pressure spectrum.

5.3.6 Cylinder Pressure Oscillations

As with the rapid pressure rise, the level of the high frequency peak associated with the simulated pressure oscillation, may also be calculated from an analytically derived formula. The derivation of this formula is presented in Appendix E, and the solution at the frequency of the oscillations is given by equation (5.5).

$$|G(F)| \simeq 20 \log \left\{ \frac{\sqrt{2}\, Ak}{4 \times 10^{-5}\, T} \right\} \qquad (5.5)$$

It can be seen that the level of the frequency component corresponding to the frequency of the oscillations is dependent on the product of the initial amplitude and the modulus of decay, as well as the repetition rate. This dependence on repetition rate may be annulled to a certain extent, however, if the modulus of decay is a more or less constant fraction of the total cycle period. This is not improbable, as the physical dimensions of the combustion chamber cavity are a direct function of crankangle (due to piston movement), and must be assumed to play a strong role in the damping characteristics of cavity.

5.3.7 Synthesis of a Complete Pressure Diagram

Figure 5.7a shows the result of the combination of the features discussed above. The synthesized pressure diagram has a pressure rise due to combustion occurring at 10° before TDC with a magnitude of 10 bar and a rate of pressure rise of 2 bar/degree. The synthesized pressure oscillations have a frequency of 6000 Hz and an amplitude of 2 bar. The cylinder pressure spectrum of this pressure diagram is shown in Figure 5.7b.

a)

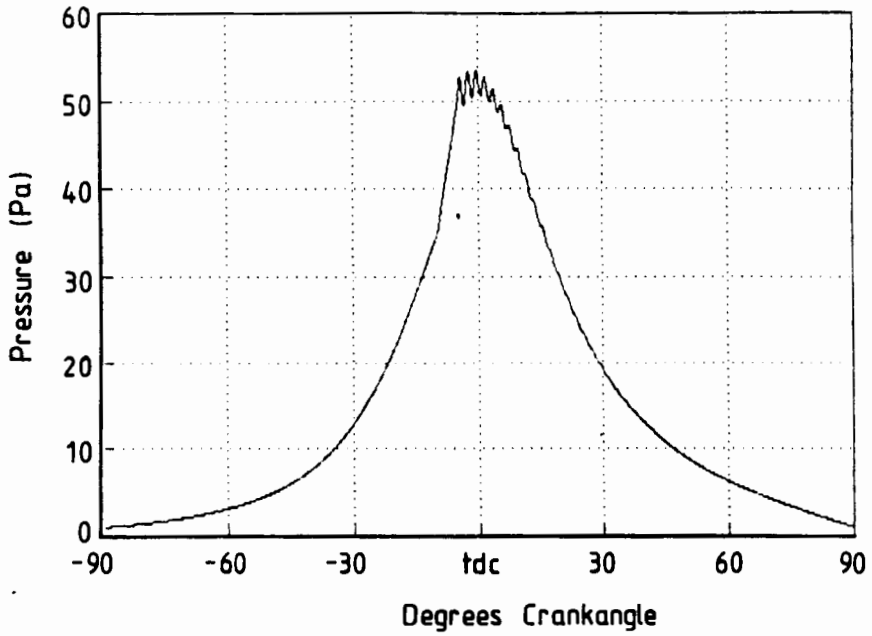

b)

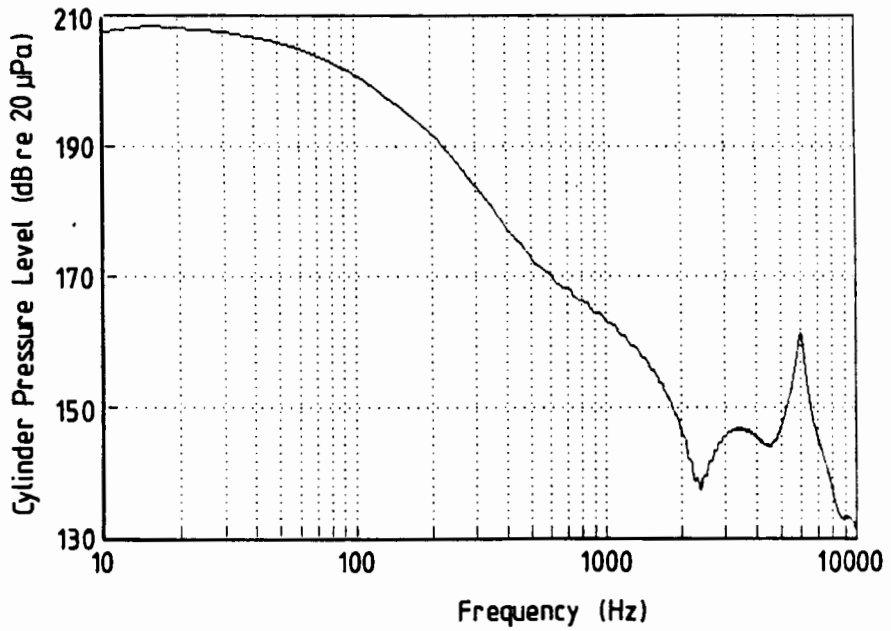

Figure 5.7 A complete synthesised diesel pressure diagram and its spectrum.

CHAPTER 6

RESPONSE OF THE COMBUSTION CHAMBER CAVITY

The combustion chamber cavity is the first elastic element of the engine to which the gas pressures arising out of the combustion event are applied. It is well known that, if the pressure rise due to combustion is very rapid, as is the case when knock occurs, pressure oscillations are induced inside the combustion chamber. These pressure oscillations modify the gas force acting on the engine structure, and have been identified as the cause of the high frequency noise associated with knock in spark ignition engines. In order to determine the mechanism by which the engine structure is excited by these pressure oscillations, it is thus necessary to investigate their origins and nature thoroughly. These will be a function of both the knock event itself, as well as the acoustic characteristics of the combustion chamber, and an investigation of these two entities is presented in this chapter.

6.1 NATURE OF THE RESPONSE OF THE COMBUSTION CHAMBER CAVITY

Knock in spark ignition engines is often illustrated by means of cylinder pressure diagrams. It is important to stress, however, that the cylinder pressure development, as measured in the combustion chamber of a running engine by a pressure transducer, is a record of the response of the combustion chamber cavity to the knock event, rather than of the knock event itself. Thus, the knock event, or more specifically, the rapid pressure rise due to knock, represents the excitation force to which the combustion chamber cavity is subjected, and the recorded cylinder pressure development of which the pressure oscillations represent the predominant feature,

indicates the response of the dynamic system (the combustion chamber cavity) to this excitation force.

It is therefore essential, in investigating either the knock event or the acoustic characteristics the combustion chamber by means of cylinder pressure diagrams, that the contributions of the excitation force and the system response be isolated, and it has been shown in Chapter 5 which deals with the relationship between the cylinder pressure diagram and its spectrum, that this may be achieved with relative ease by means of the cylinder pressure spectrum.

A typical cylinder pressure development for a knocking engine cycle recorded at 1500 rpm in a Nissan L28 engine, is depicted in Figure 6.1a, accompanied by the corresponding cylinder pressure spectrum in Figure 6.1b. The cylinder pressure diagram has been magnified for greater detail, and shows an initial pressure rise with a magnitude of approximately 30 bar, followed by large amplitude oscillations which persist for some 90 degrees of the expansion stroke.

The cylinder pressure spectrum shows a distinct -20 dB/decade slope between 600 and 4000 Hz which is due to the initial rapid pressure rise, and a number of high frequency peaks are evident, which correspond to the frequency content of the resulting pressure oscillations. The actual magnitude of the pressure rise resulting from autoignition is not immediately evident from the pressure diagram as it has been magnified by the oscillatory response of the combustion chamber cavity, but may be determined from the level of the -20 dB/decade slope of the cylinder pressure spectrum. This slope attains a level of 164.7 dB at a frequency of 1000 Hz, which corresponds to an instantaneous pressure rise of 12.2 bar.

a)

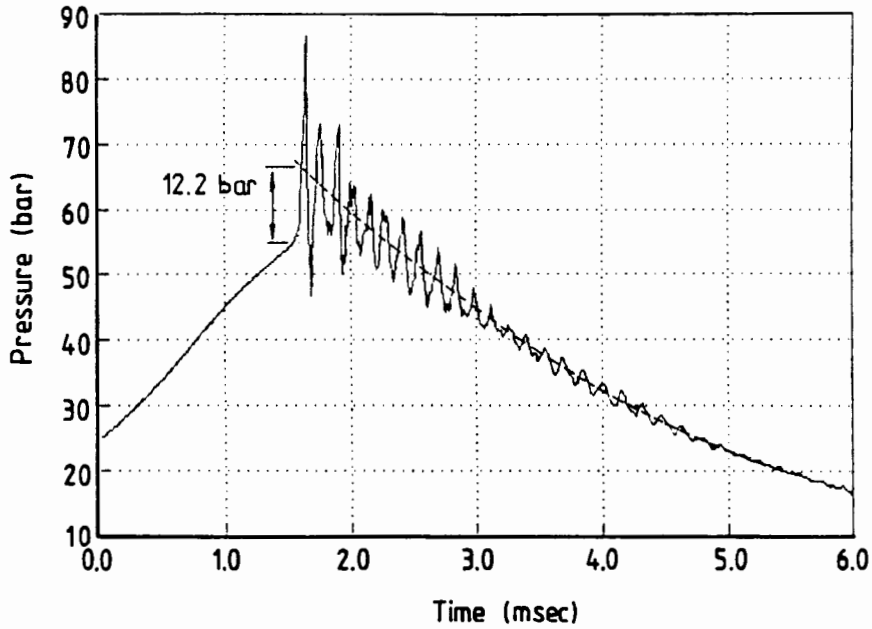

b)

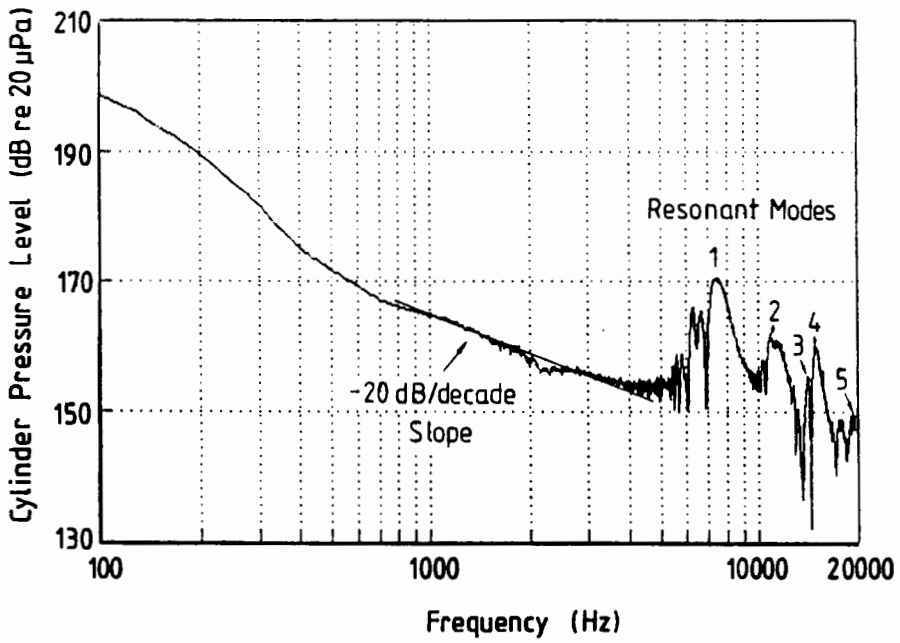

Figure 6.1 Cylinder pressure diagram showing heavy knock, and its cylinder pressure spectrum.

6.1.1 Mechanism by which the Combustion Chamber Cavity is Excited

It can be seen from the cylinder pressure diagram that the amplitude of the undamped pressure oscillations is approximately 20 bar for the first cycle, after which it is approximately equal to the calculated magnitude of the initial pressure rise, namely 12 bar. This would suggest that the proposal by Priede [3], namely that the response of the combustion chamber may be approximated by the response of a simple oscillator to a rectangular step excitation force, is valid to some extent. The response of such a system without damping is equal to that of the static deflection due to the applied force, with the initial displacement being equal to twice the static deflection.

The rate of displacement of a simple oscillator after being subjected to a step exciting force will be limited by its natural frequency. A combustion chamber cavity, however, has many degrees of freedom, and high rates of pressure rise will indicate the presence of higher modes of excitation. If the combustion chamber did not have elastic properties, the pressure trace after the initial rapid pressure rise would follow the path of the mean of the oscillations, as indicated in Figure 6.1a.

Analysis of a large number of knocking cycles, as presented in Appendices F and G, has shown that considerable variations from the proposed theory do exist, however, suggesting that some modification to this theory may be necessary. Specifically, the amplitude of the oscillations is usually considerably greater than that predicted, to the extent that there sometimes appears to be very little net increase in the mean cylinder pressure, despite large amplitude oscillations which would suggest the contrary. This situation is illustrated in Figure

6.2, which shows a cylinder pressure diagram recorded in the same Nissan L28 engine at 5000 rpm. The initial amplitude of

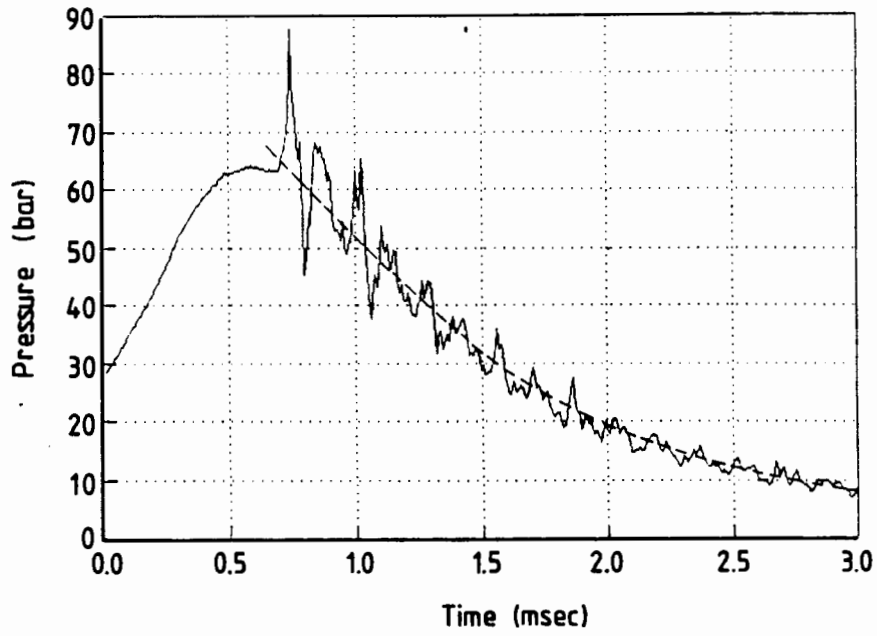

Figure 6.2 Cylinder pressure diagram showing impulse type excitation of the combustion chamber cavity.

the pressure oscillations is approximately 20 bar, but if the mean path of the oscillations is traced to the point of initiation, it would almost appear to be a continuation of the normal combustion curve. In this case it would seem that the initial oscillatory response approximates that of a simple oscillator to an impulse, rather than to a step forcing function. It is conceivable that such a situation can arise if the initial rapid pressure rise is very localised, for example if the autoignition occurs in a constrained volume such as in a squish zone. While the initial local pressure may be very

high, the resultant pressure increase acting over the whole combustion chamber surface is much smaller.

It is therefore suggested that, unless the pressure transducer is located precisely at the autoignition site, the initial high localised pressure increase is not recorded, rather the resultant pressure increase after dissipation over the whole combustion chamber volume. Consequently, a direct relationship between the magnitude of the initial pressure rise and the amplitude of the pressure oscillations is difficult to establish.

All of the above explanations assume that the pressure transducer signal is a true representation of the actual dynamic pressure. It is also possible, however, that the initial pressure rise causes excitation of the pressure transducer at its natural frequency which is specified as being 100 kHz, and this may result in recorded pressure peaks which are greater in magnitude than the actual pressures. This phenomenon was observed by Hayashi et al [14], who used the same AVL 8QP pressure transducers in their rapid compression machine experiments and made use of a digital filtering technique to remove these effects.

6.1.2 Theoretical analysis of the Acoustic Characteristics of Combustion Chambers

In the reviewed literature, and from experience, good correlations have been achieved by applying the acoustic theory for a cylindrical cavity to real combustion chambers, and this theory is reviewed briefly in the following section.

To a first approximation, a combustion chamber may be regarded as a plane ended cylinder, and this configuration may easily be analysed using classical acoustic theory. The acoustical natural frequencies of a homogeneous gas in a rigid-walled

cylindrical cavity with plane ends are given by equation (6.1)[42].

$$f_R = c \left[\left\{ \frac{\alpha_{m,n}}{B} \right\}^2 + \left\{ \frac{P}{2L} \right\}^2 \right]^{\frac{1}{2}} \qquad (6.1)$$

where B = cavity diameter
L = cavity axial length
f_R = possible resonant frequencies
m,n,p = integers denoting the circumferential, radial, and axial mode numbers respectively
$\alpha_{m,n}$ = a non-dimensional number
c = speed of sound in the gas

The $\alpha_{m,n}$ are found by solving for the n^{th} root of the derivative of the Bessel function of order m, and then dividing by π. i.e., by solving the equation:

$$J_m'(\pi\alpha_{m,n}) = 0 \qquad (6.2)$$

where J_m = the Bessel function of order m.

Only that portion of the engine cycle near top-dead-center is under consideration. Thus the axial dimension is small compared to the transverse dimension, and only the latter modes will be considered. The equation may therefore be simplified to:

$$f_R = \frac{c}{B} \alpha_{m,n} \qquad (6.3)$$

Thus the natural frequencies are proportional to the speed of sound in the chamber and the inverse of the bore diameter.

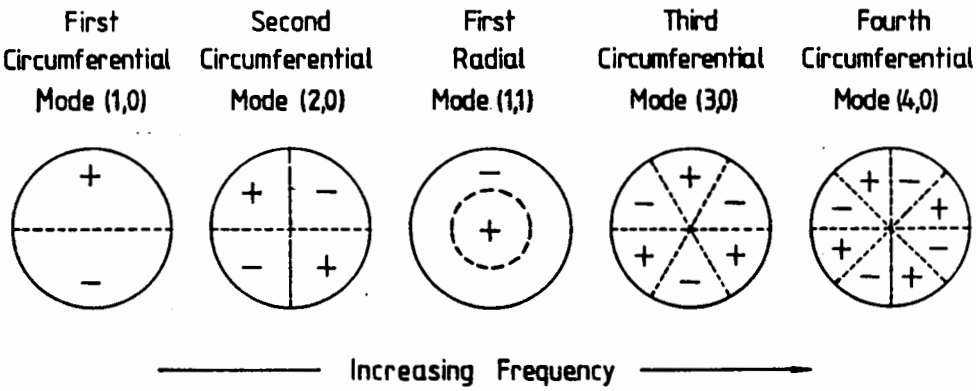

Figure 6.3 Schematic diagram showing the mode shapes associated with the first five transverse modes of a plane ended cylinder.

Figure 6.3 is a diagrammatic representation of the first four transverse mode shapes, showing the orientation of the nodal lines. An important observation is that, at any instant in time, each region of positive pressure acting on the end of the cavity is balanced by a symmetrical region of negative pressure (i.e. of opposite phase), resulting in the total pressure acting on the axial ends of the cavity summing to zero. The significance of this observation will be seen in Chapter 8 which describes the engine structure response.

A number of shortcomings are immediately evident in the application of this theoretical approach to the practical situation inside the combustion chamber of a running engine. These are listed below, and will be discussed in greater detail as this chapter progresses.

(1) Real combustion chambers do not have usually have plane ends, and the cylindrical part of the combustion chamber may constitute only a small part of the total combustion chamber volume at TDC.

(2) The piston is not stationary over the period of duration of the pressure oscillations, and the cavity shape is thus changing.

(3) The speed of sound is dependent on the temperature of the gas which is not known a priori and is decreasing over the expansion stroke.

(4) The amplitude of the pressure oscillations is large by acoustical standards and shock waves with velocities in excess of the speed of sound have been detected in knocking engines. Thus the applicability of linear acoustic theory to such a situation is questionable.

(5) The burned gas temperature and composition are not homogeneous throughout the combustion chamber volume, although the magnitudes of these changes are not known and may be small enough to be negligible.

6.1.3 Application of the Theoretical Model to the Measured Response

The frequencies of the gas vibration in a knocking engine may be determined from the cylinder pressure spectrum, and in order to facilitate comparison between the calculated and measured frequencies, it is necessary to eliminate the effect of the differences in the speed of sound. This is done by comparing the ratios of the frequencies for the higher modes to that of the first mode, to the ratios predicted by the theory, rather than comparing the frequencies themselves. These ratios may be calculated by dividing the $\alpha_{m,n}$ by $\alpha_{1,0}$, and are tabulated in Table 6.1, in ascending order up to the 10^{th} mode.

Table 6.1. List of values of $\alpha_{m,n}/\alpha_{1,0}$.

Mode No.	(m,n)	$\alpha_{m,n}$	$\alpha_{m,n}/\alpha_{1,0}$
1	(1,0)	0.586	1.000
2	(2,0)	0.971	1.659
3	(0,1)	1.219	2.081
4	(3,0)	1.337	2.282
5	(4,0)	1.692	2.888
6	(1,1)	1.697	2.895
7	(5,0)	2.042	3.484
8	(2,1)	2.136	3.642
9	(0,2)	2.235	3,810
10	(6.0)	2.387	4.074

The deviation of the combustion chamber shape from a plane ended cylinder will manifest itself as a deviation in the value of the $\alpha_{m,n}$, and the extent to which these values differ from those listed above has been studied by measuring the frequency response of a plastic model of the combustion chamber of the Volkswagen engine, which was used extensively in the engine tests done [43]. It was found that the differences between the experimentally and theoretically determined ratios were generally less than 3 percent, thus making the theoretically derived values suitable for use in identifying the various modes of vibration from the cylinder pressure spectrum.

The position of the nodal diameter for each circumferential mode will be determined by symmetries in the combustion chamber shape. In practice, however, combustion chambers do not often have distinct features which are symmetrical about some axis, and it would appear that the most accurate way of determining the nodal lines is by the finite element modelling technique used by Hickling [20,21].

An important result of Hickling's work was the discovery that one of the effects of combustion chamber asymmetries was the degeneration of the first few circumferential modes, in that the modes are split into two components each with a distinct nodal diameter, and with the frequencies of these components differing by a small amount. This may be seen to be the case in the cylinder pressure spectrum shown in Figure 6.1b, where the dominant fundamental peak at 7460 Hz is immediately preceded by two peaks of smaller magnitude. For the purpose of calculating the ratio of the frequencies in order to identify the higher modes, the average frequency of the three peaks is used.

The frequencies and modal indices of the various modes evident on the cylinder pressure spectrum in Figure 6.1b are tabulated in Table 6.2 below.

Table 6.2. Modes of Gas Vibration identified from a Cylinder Pressure Spectrum

Mode no.	Frequency (Hz)	Amplitude (dB)	Ratio $f_{m,n}/f_{1,0}$	Indices (m,n,p)
1	6795	170.9	1.000	(1,0)
2	11405	161.4	1.678	(2,0)
3	14061	154.1	2.069	(0,1)
4	14921	159.7	2.196	(3,0)
5	19655	149.9	2.893	(4,0)

It can be seen that the first four circumferential modes as well as the first radial mode can be readily identified. In this case the level of the fundamental circumferential mode is considerably higher (of the order of 8.5 dB) than the higher circumferential modes, while the (4,0) circumferential mode has the lowest level.

The effect of the movement of the piston on the gas vibration may be assumed to be negligible, because the Mach number of the piston relative to the speed of sound in the gas is generally quite low (in the order of 1/20). The effect of the change in cavity shape due to the piston movement, as reflected in the change in the values of the $\alpha_{m,n}$, can, however, be significant. Intuitively, as the piston to cylinder head clearance increases, a greater proportion of the cavity volume is contained in the cylinder bore, and the values of the $\alpha_{m,n}$ will tend towards those of a plane ended cylinder. This was confirmed by Hickling who used the finite element technique to compute the $\alpha_{m,n}$ for the first four modes as a function of piston-to-cylinder head clearance, for various D.I. diesel engine combustion chambers. The combustion chambers with the greatest volume proportion enclosed in a non-conforming cavity were found to show the largest changes in the ratio of $\alpha_{m,n}/\alpha_{1,0}$, of the order of 15 percent over the range of piston position over which the pressure oscillations occur. This effect is naturally highly dependent on the combustion chamber shape, and would appear to be less significant for the engines tested in this study, in that the modes may be readily identified from the cylinder pressure spectra.

The effect of the decrease in gas temperature over the expansion stroke is to reduce the frequency of the oscillations. This sometimes results in prominent side lobes on the low frequency side of the spectral peaks associated with each mode of vibration. Combustion models have predicted maximum burned gas temperatures of between 2500 to 3000 K occurring near TDC [13]. The decrease in temperature over the next 60 degrees crankangle does not amount to more than about 10% however, and this, in conjunction with the fact that the frequency is dependent on the square root of the gas temperature, results in the frequency shift with crankangle not being large enough to render the spectral peaks indistinguishable.

6.2 DEVELOPMENT AND PROPAGATION OF PRESSURE WAVES RESULTING FROM KNOCK

The combustion chamber of a Toyota 21R engine was instrumented with two pressure transducers, allowing the simultaneous recording of the cylinder pressure histories at opposing sides of the combustion chamber. The combustion chamber is of a high swirl design and has a hemispherical shape, and the positions of the two transducers, labelled A and B, are illustrated in Figure 6.4a. The cylinder pressure diagrams recorded at these positions for a knocking cycle at 2000 rpm are shown in Figure 6.4b, while the corresponding cylinder pressure spectra, are shown in Figures 6.5a, and b.

The rapid pressure rise due to autoignition is first registered by the transducer at position A, which is situated in the vicinity of the spark plug. Thus the autoignition did not occur at a point furthest away from the spark plug as is expected, and this may be explained by the high level of charge motion due to swirl, which will result in the flame front not moving uniformly outwards from the spark plug.

The development of the initial pressure wave is influenced by a large number of factors, including the possibility that multiple autoignition sites exist. Autoignition usually takes place near the combustion chamber wall, and the sudden energy release results in an increase in the local temperatures and pressures. The large pressure discontinuity that results causes a pressure wave to propagate across to the opposite end of the combustion chamber, and an expansion wave to propagate into the high pressure region.

a)

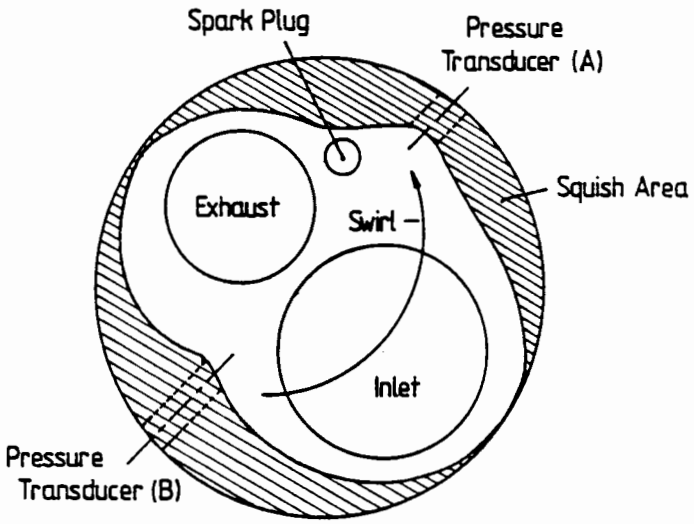

b)

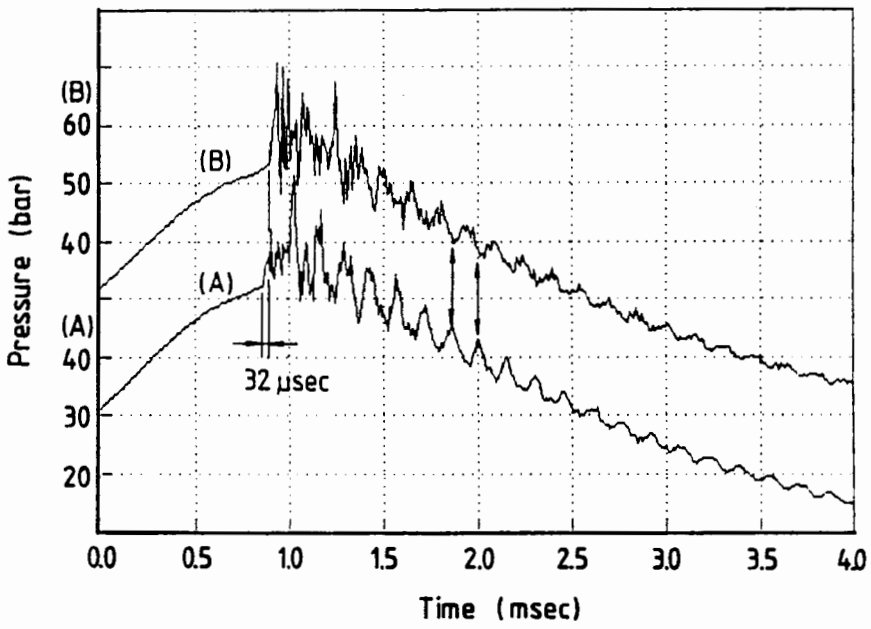

Figure 6.4 Sketch of the Toyota 21R combustion chamber, showing the location of the two pressure transducers, and the recorded cylinder pressure diagrams.

a)

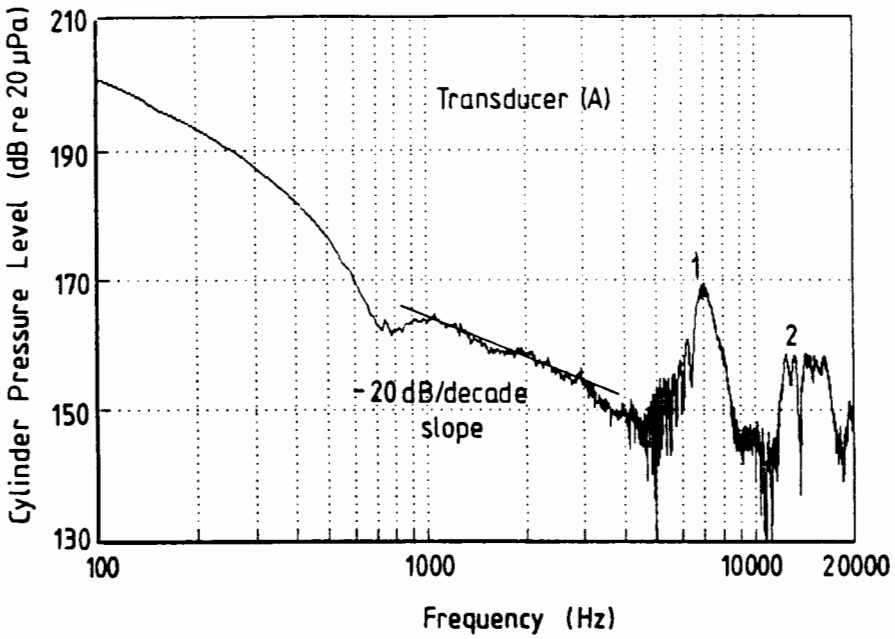

b)

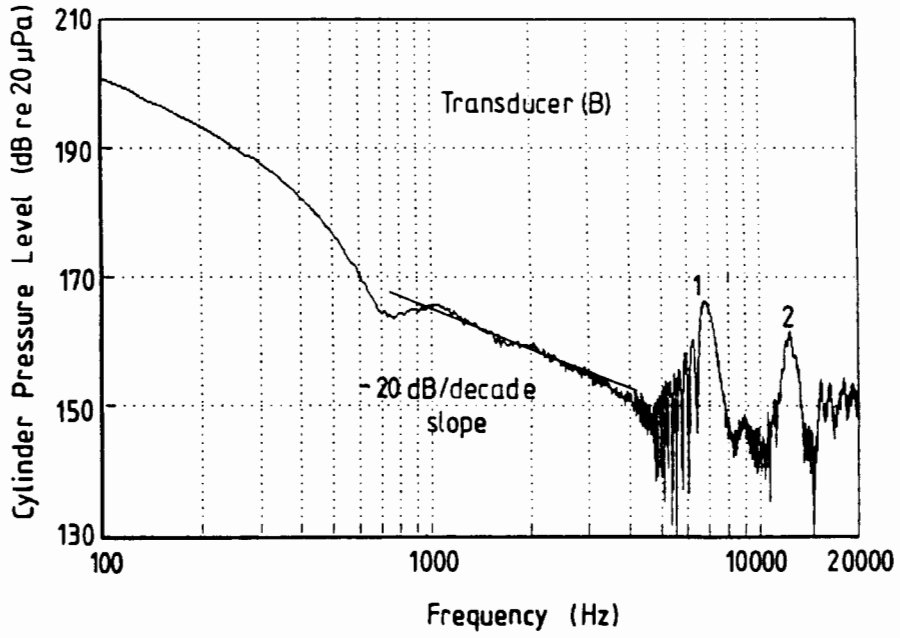

Figure 6.5 Cylinder pressure spectra of simultaneously recorded cylinder pressure diagrams.

Whilst it is not possible to calculate the speed of propagation from the two measured pressure traces since the position of the autoignition site is not known, it may be safely assumed that the pressure wave propagates as a shock wave initially. The speed of sound in the burnt gas as calculated from the frequency of the pressure oscillations (using the theoretical value of 0.586 for $\alpha_{1,0}$) is approximately 975 m/s, and the initial propagation speed will be considerably higher than this: experimental observations [14,44] and theoretical models [45] have shown speeds in excess of 1500 m/s.

The burnt gases ahead of the shock wave are at a lower temperature than the gases behind it, and the difference in the speed of sound may result in the wave front steepening as it travels across the chamber. This is evident in the two recorded pressure traces, where it can be seen that the initial pressure rise at transducer B is greater than that at transducer A. This phenomenon was also observed by Hayashi et al in their rapid compression machine experiments. The shock and expansion waves reflect off the combustion chamber walls and interact, while at the same time the speed of the pressure wave reduces to sonic speed in the burnt gases. The interaction of the reflected waves results in the standing wave mode shapes associated with each of the excited modes of gas vibration. It is important to note, however, that the initial speed of propagation is sufficient that it may be assumed that the rapid pressure rise acts over the whole piston area. This is confirmed by examining the magnitude of the initial pressure rise recorded at each transducer from the respective cylinder pressure spectra. Similar -20 dB/decade slopes are evident on both spectra, each attaining a level of 165 dB at 1000 Hz. Thus the pressure rise registered at each transducer is of the same magnitude, and may be calculated to be approximately 9.5 bar.

Both pressure traces exhibit pressure oscillations with a strong fundamental component, as well as higher frequency components which are damped out soon after the initial pressure rise. This is confirmed by the cylinder pressure spectra which show a dominant fundamental at approximately 6800 Hz. The pressure oscillations at this frequency can be seen to be almost 180 degrees out of phase, indicating that they are associated with a circumferential mode with an odd-numbered index (see Figure 6.3), and the mode can thus confidently be identified as the fundamental circumferential mode. The amplitude of the oscillations in this mode, as determined from the spectra, is slightly higher at position A than at position B (169 vs 167 dB), and this may be explained by the fact that the pressure transducer at position A is located closer to the periphery of the chamber, where, according to the theoretical mode shape, the highest amplitude oscillations will occur. It is conceivable that, had the transducers been mounted equidistant from the cylinder bore axis, the oscillations would have been exactly 180 degrees out of phase and of the same magnitude.

From the spectra it is also evident that the second mode of vibration is more pronounced at position B than at position A (this is also evident on the pressure traces themselves), indicating that the nodal line associated with this mode lies closer to position A.

All of the observations described above support the theoretical predictions of the frequencies and mode shapes describing the response of the combustion chamber cavity. In particular, they lend credibility to the theoretical prediction that the vector sum of all the pressures acting on the piston face due to the pressure oscillations at any instant in time, is zero.

6.3 ANALYSIS OF DIFFERENT COMBUSTION CHAMBER SHAPES

In all, cylinder pressure diagrams were recorded in six different spark ignition engines, representing four different combustion chamber shapes, namely the wedge shape, the bath tub shape, the hemispherical shape, and the bowl-in-piston chamber. Technical details of the engines are presented in Appendix A. Naturally, the knock characteristics of the engines vary considerably, and it is not practically possible to compare the responses of their combustion chamber cavities to the same forcing function. (It is possible to determine the transfer function between the response of the cavity and the rapid pressure rise from the recorded pressure trace, but the position and number of autoignition sites is not known, and must be assumed to have a significant effect.) Distinct differences in the nature of the pressure oscillations are, however, discernable between the different chamber shapes, as is illustrated in Figures 6.6 to 6.9 which show cylinder pressure diagrams and spectra recorded at 2500 rpm and with moderate knock, for each of the four shapes. These will now be described separately, and where possible, the modes of gas vibration will be identified and tabulated.

In some of the engines the presence of the degenerate, or "split" modes described by Hickling has been identified. For the purpose of identifying higher modes, the frequency associated with these modes is taken to be the average frequency of the multiple peaks present, and the amplitude listed will be the maximum present. For the sake of clarity, frequency values which represent split modes will be identified by a superscripted asterisk (*) in the following sections.

6.3.1 Wedge Shape (Nissan L28)

Of all the chambers investigated, this one gave the results most consistent with the theoretical analysis described earlier in this chapter. The cylinder pressure diagram and its spectrum are shown in Figures 6.6a and b respectively. It can be seen that the pressure oscillations are almost completely damped out after a relatively short period (about 40 degrees crankangle), and show a strong fundamental component with some contribution from higher frequencies. The frequencies present in the oscillations, as determined from the cylinder pressure spectrum, are tabulated in Table 6.3 below.

Table 6.3. Modes of Gas Vibration for the Wedge Shape Combustion Chamber.

Mode no.	Frequency (Hz)	Amplitude (dB)	Ratio $f_{m,n}/f_{1,0}$	Indices (m,n)
1	7072*	165.6	1.0	(1,0)
2	11497	158.0	1.626	(2,0)
3	15456	160.7	2.186	(3,0)
4	19500	151.3	2.758	(4,0)

It can be seen that there are two peaks present in the region of the first circumferential mode, thus suggesting that this is a degenerate or split mode, and the frequency has been listed as such. A large number of pressure diagrams and spectra recorded from this engine are presented in Appendix F, and the split fundamental circumferential mode can be seen to occur frequently and would thus appear to be a feature of this combustion chamber. Three higher circumferential modes of smaller amplitude are present, and no radial modes may be identified in this case.

a)

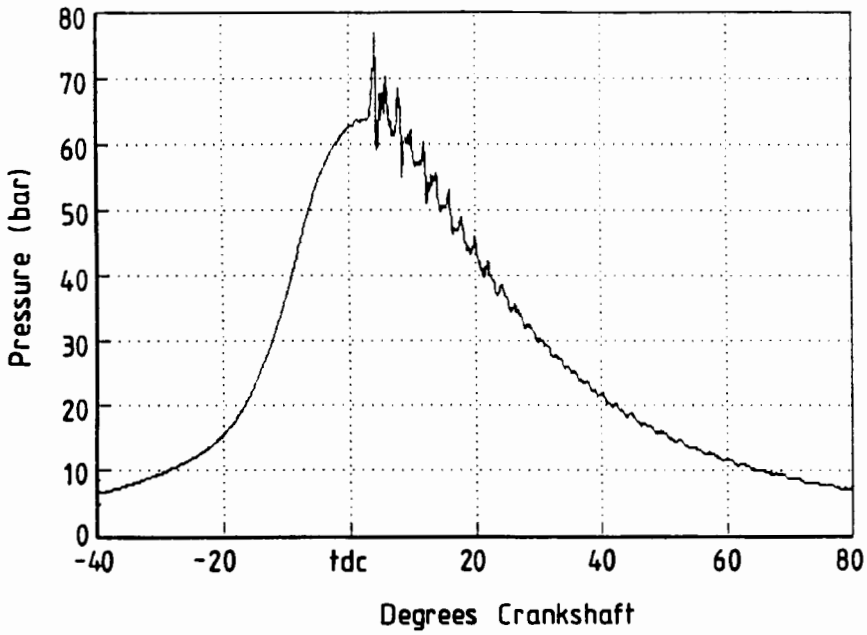

b)

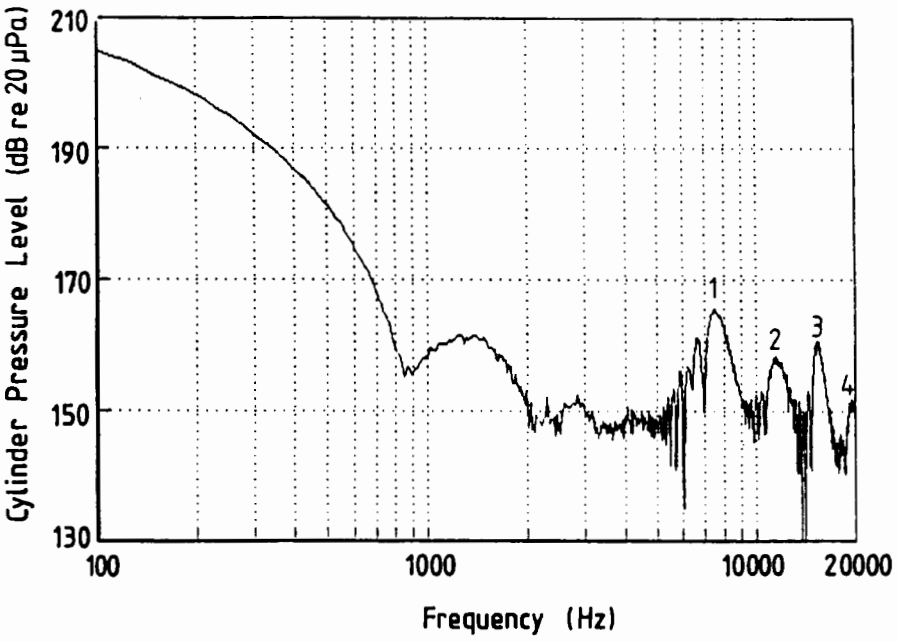

Figure 6.6 Cylinder pressure diagram recorded in the Nissan L28 engine, and its cylinder pressure spectrum.

6.3.2 Bath Tub Shape (Volkswagen 1800)

The cylinder pressure diagram and its spectrum for this combustion chamber are shown in Figures 6.7a and b, and the pressure trace shows oscillations which are present over practically the whole expansion stroke. The presence of strong higher modes is also evident on the pressure trace and this is confirmed by the cylinder pressure spectrum from which four distinct modes can be identified. These are tabulated in Table 6.4 below.

Table 6.4. Modes of Gas Vibration for the Bath Tub Shape Combustion Chamber.

Mode no.	Frequency (Hz)	Amplitude (dB)	Ratio $f_{m,n}/f_{1,0}$	Indices (m,n)
1	7344	166.9	1.0	(1,0)
2	12773	164.7	1.739	(2,0)
3	17031	161.3	2.319	(3,0)
4	20224	162.9	2.751	(4,0)

The amplitude difference between the fundamental and the three higher circumferential modes identified is less than 6 dB in this case. It is interesting to note that the level of the (4,0) mode is higher than that of the (3,0) mode. From Table 6.1 it can be seen that the frequency ratios associated with this mode and the (1,1) mode lie very close together, and it may be that the peak at 20224 Hz represents the contribution of both of these modes.

a)

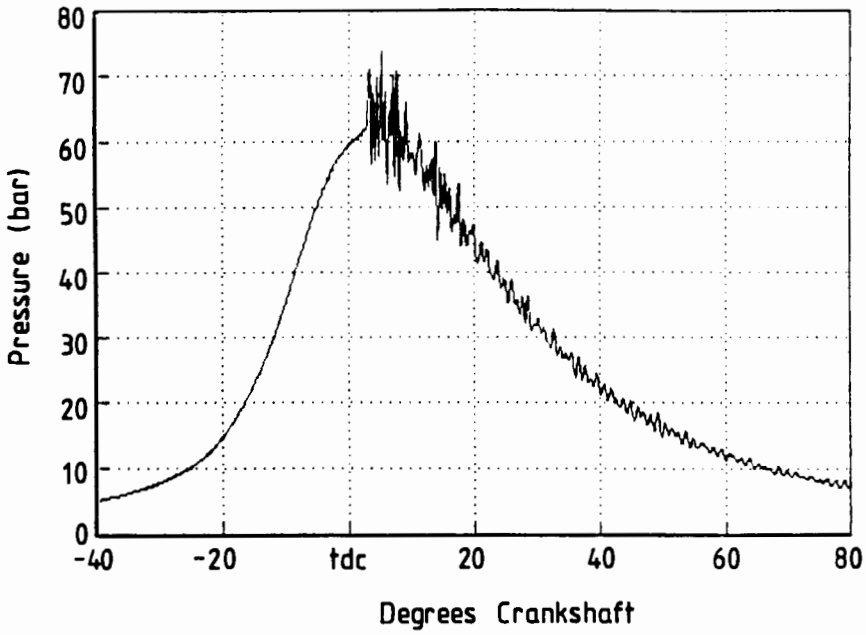

b)

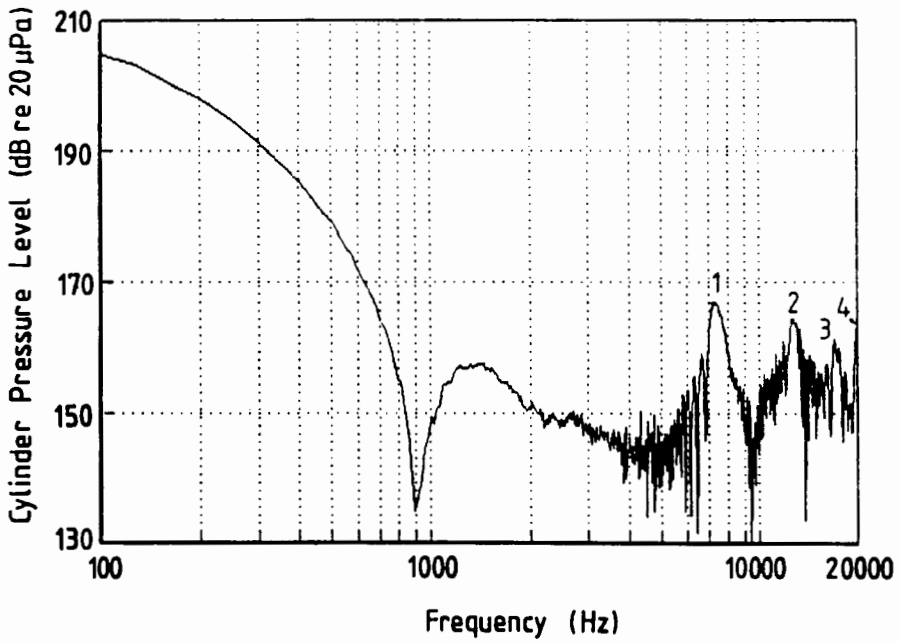

Figure 6.7 Cylinder pressure diagram recorded in the Volkswagen 1800 engine, and its cylinder pressure spectrum.

6.3.3 Hemispherical Combustion Chamber (Toyota 4AF)

The cylinder pressure diagram for the hemispherical combustion chamber shape and its spectrum are shown in Figures 6.8a and b respectively. The identification of the various modes of gas vibration present in this combustion chamber has been found to be the most problematic, with the pressure oscillations usually being represented by a broad high frequency peak extending from 4000 up to 20000 Hz. A number of high frequency peaks may, however, be identified, and these are listed in Table 6.5 below.

Table 6.5. Modes of Gas Vibration for the Hemispherical Shape Combustion Chamber.

Mode no.	Frequency (Hz)	Amplitude (dB)	Ratio $f_{m,n}/f_{1,0}$	Indices (m,n)
1	7025*	165.4	1.0	(1,0)
2	11369	161.5	1.618	(2,0)
3	14061	155.4	2.002	(0,1)
4	16237	158.5	2.311	(3,0)

The first circumferential mode would appear to be degenerate, and two peaks, namely at 9498 Hz and 12533 Hz cannot be identified. It is possible that the second circumferential mode is also degenerate and includes one or both of these spurious frequencies, but the usual "split peak" shape is not evident in this case. Besides the three circumferential modes identified in this case, the first radial mode also appears to be present, with a frequency of about 14000 Hz. At 155.4 dB, this mode has a significantly lower level than the circumferential modes, whose levels differ by less than 6 dB.

a)

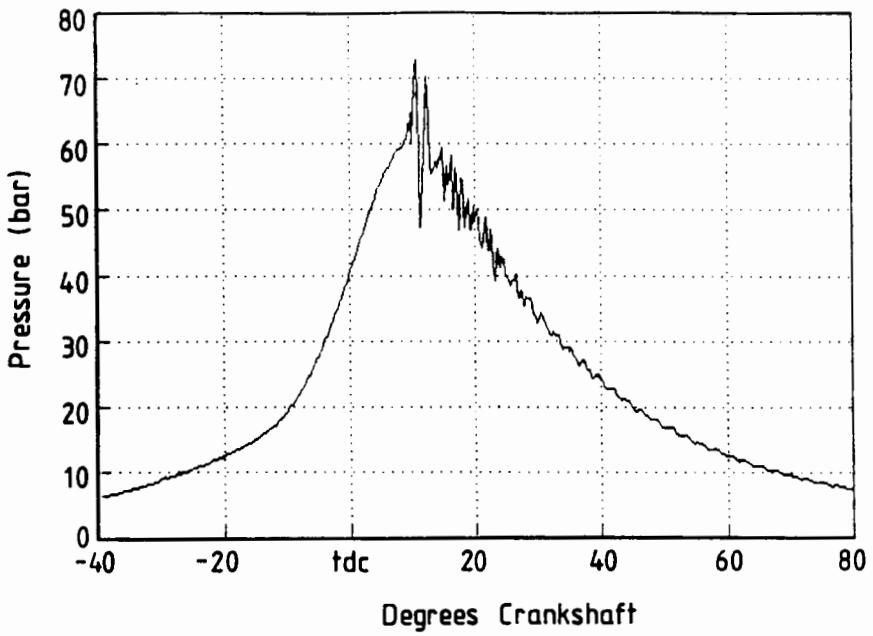

b)

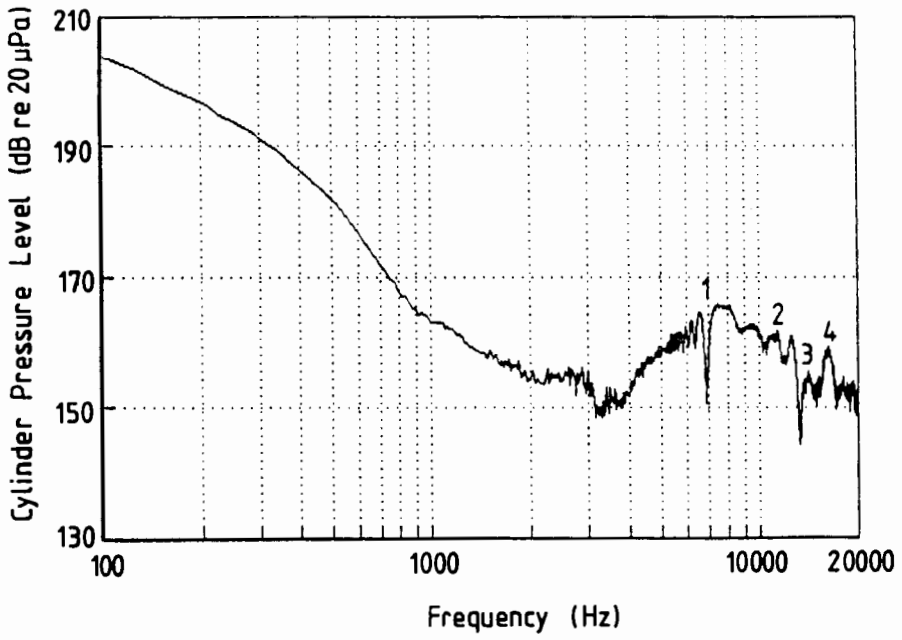

Figure 6.8 Cylinder pressure diagram recorded in the Toyota 4AF engine, and its cylinder pressure spectrum.

6.3.4 Bowl-in-Piston Combustion Chamber (Ford V6 engine)

Figures 6.9a and b show the pressure diagram and spectrum recorded in the bowl-in-piston combustion chamber of the Ford V6 engine. The spectrum shows a prominent peak at approximately 7500 Hz, followed by a series of closely spaced peaks up to 20000 Hz. These are listed in Table 6.6 below, and it can be seen that reasonable correlation is obtained if the second circumferential mode is assumed to be degenerate.

Table 6.6. Modes of Gas Vibration for the Bowl-in-Piston Combustion Chamber.

Mode no.	Frequency (Hz)	Amplitude (dB)	Ratio $f_{m,n}/f_{1,0}$	Indices (m,n)
1	7538	167.0	1.0	(1,0)
2	11662*	163.9	1.547	(2,0)
3	14764	166.8	1.959	(0,1)
4	17395	161.5	2.308	(3,0)
5	19674	152.8	2.610	(4,0)

The first radial mode can be seen to present in this case, with an amplitude of 188.8 dB which is practically equal to that of the fundamental circumferential mode.

a)

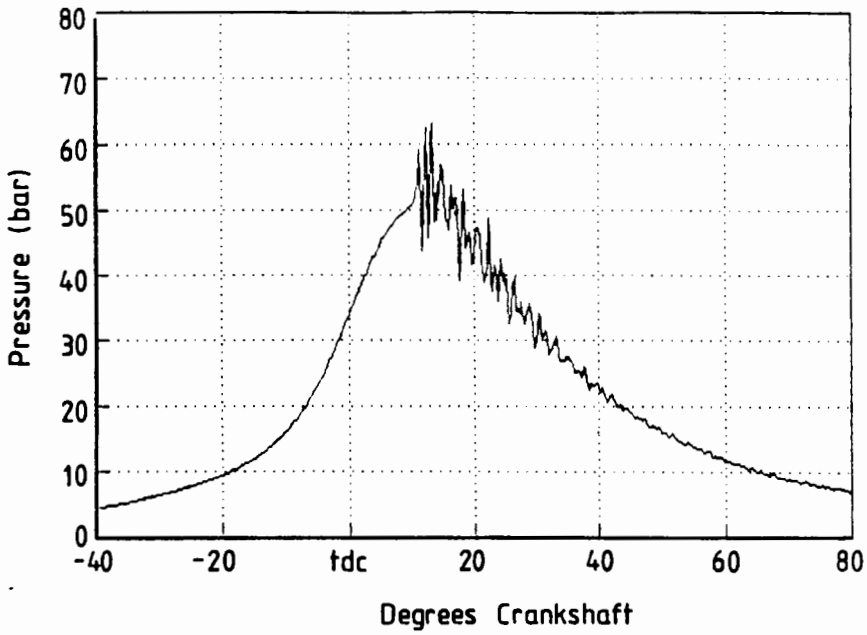

b)

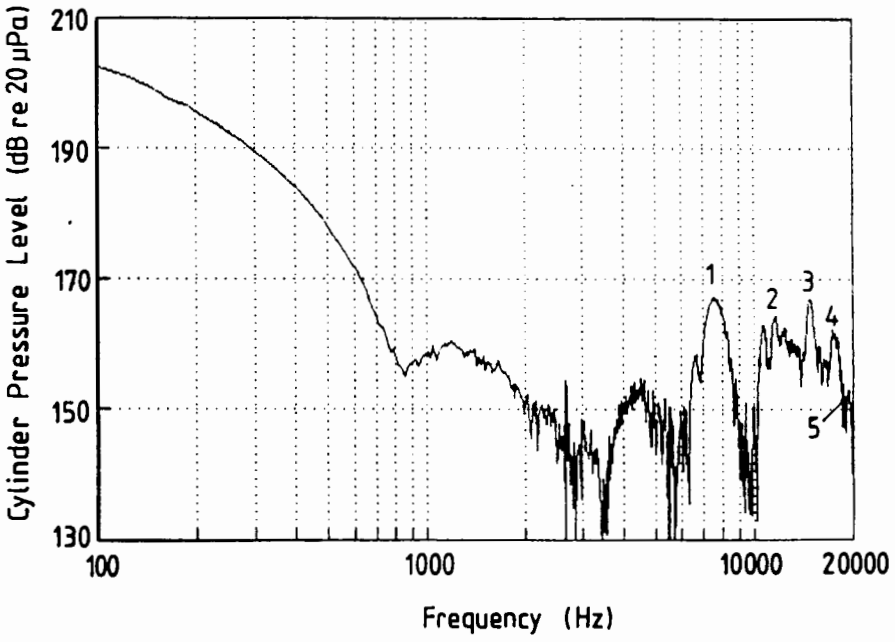

Figure 6.9 Cylinder pressure diagram recorded in the Ford V6 engine, and its cylinder pressure spectrum.

CHAPTER 7

THE EXCITING CHARACTERISTICS OF THE CYLINDER PRESSURE DEVELOPMENT

The noise emitted by an engine is the result of a multitude of noise generation mechanisms. The nature of the mechanism itself determines the character of its noise contribution and is the most helpful clue for identifying the sources of individual noise components. Since knock is a combustion phenomenon, it follows that knock-induced noise is, by definition, a combustion related phenomenon initiated by the cylinder pressure development. The magnitude and nature of exciting properties of the cylinder pressure development will determine the character of the resulting noise as well as the extent to which it is discernable above the noise generated by other mechanisms.

In Chapter 5 which describes the characterisation of the cylinder pressure development by means of the cylinder pressure spectrum, the frequency ranges over which the various features of a knocking cylinder pressure development are likely to excite the engine structure are demonstrated, and mathematical relationships between the magnitude of the rapid pressure rise and the initial amplitude of the pressure oscillations are presented. This chapter presents the results of the analysis of a large number of knocking cylinder pressure developments, and discusses the ensuing possibilities for engine structure excitation.

The first section of the chapter presents a broad description of the various types of cylinder pressure developments encountered in internal combustion engines. These have been categorised according to their noise generating potential, and

are described in terms of the rates of pressure rise, peak pressures, and cylinder pressure spectra. It should be noted that the diagrams chosen represent generalised cases, and specific engines may differ considerably in some or all respects. The second section of the chapter focuses on the cylinder pressure development resulting from knocking combustion in spark ignition engines.

7.1 REVIEW OF THE CHARACTERISTICS OF THE CYLINDER PRESSURE DEVELOPMENT

When dealing with the exciting propensities of the cylinder pressure development, a number of distinct forms of pressure development may be recognised, and these are illustrated for comparison in Figure 7.1. In spark ignition engines, the shape of the pressure diagrams does not vary considerably, and is shown in Figure 7.1a. There is a very gradual pressure rise from the onset of ignition, followed by an almost linear rapid pressure rise until the completion of combustion. The pressure reaches a maximum at about 10 to 15 degrees after TDC.

In diesel engines there is, by contrast, a great variety of cylinder pressure developments. Figure 7.1b shows the typical normally-aspirated direct-injection diesel pressure diagram with a small but rapid pressure rise at about 10 to 15 degrees before TDC, the rate of which then decreases more or less exponentially. Peak cylinder pressures occur at some 5 to 10 degrees after TDC. Another form of naturally-aspirated engines is illustrated in Figure 7.1c. These have an almost linear pressure rise (of smaller magnitude than in diagram b) at around TDC, with peak pressures occurring at 10 to 15 degrees after TDC.

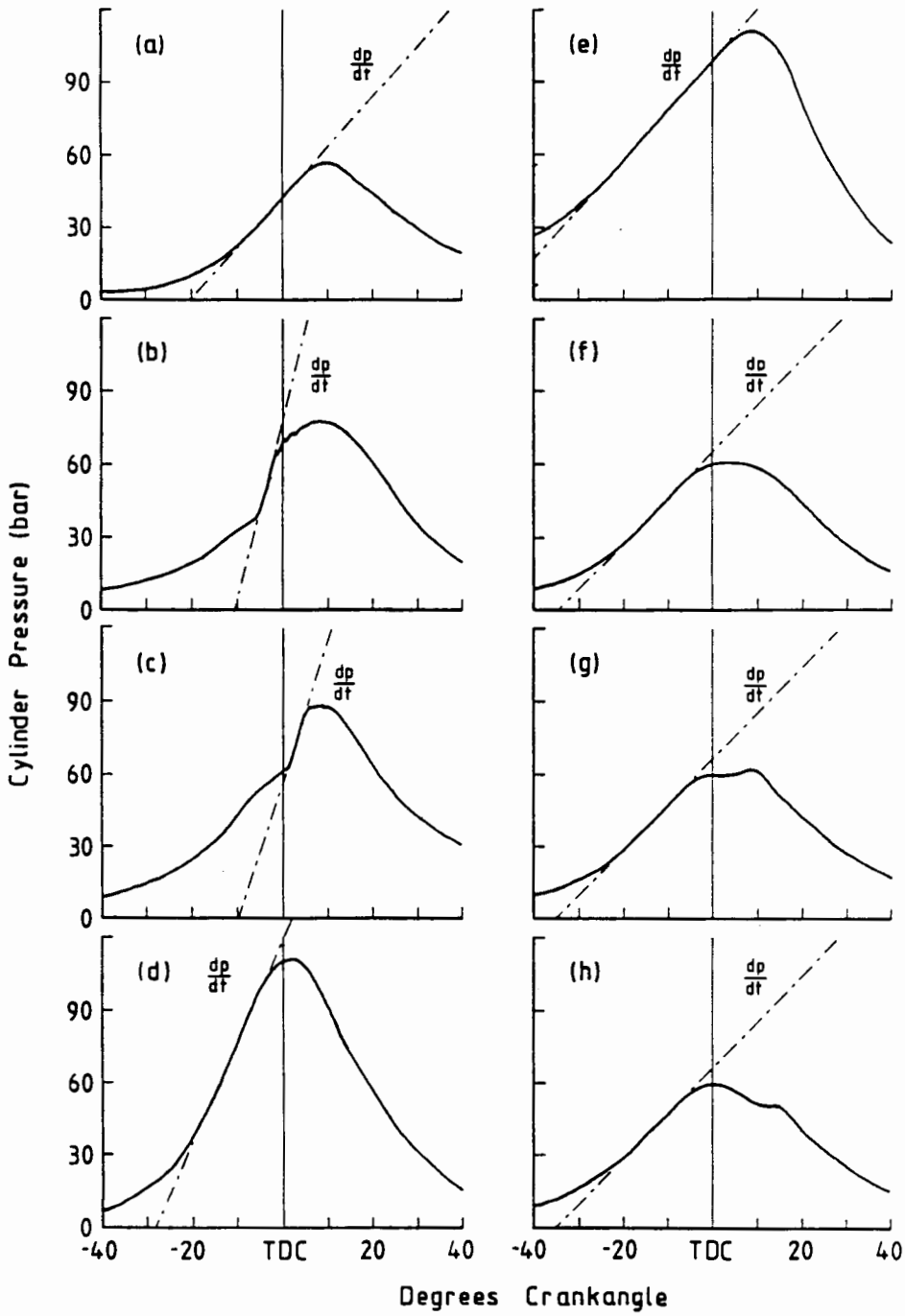

Figure 7.1 Different forms of cylinder pressure development found in automotive engines.

Turbocharging provides significant smoothing of the cylinder pressure development, particularly when operating close to rated engine conditions, and two forms of cylinder pressure development occurring in turbocharged diesel engines are shown. Diagram d of Figure 7.1 shows a reasonably smooth blending of the pressure rise with the compression curve, but with a considerable rate of pressure rise, while in Figure 7.1e the rate of pressure rise due to combustion does not exceed that due to compression. Peak pressures occur at around TDC in both these cases. At low engine speeds and light loads the pressure diagrams of the turbocharged engines change to a form with a more abrupt nature, similar to diagrams b and c, however.

The Ricardo indirect-injection swirl chamber combustion system is widely used in small car diesel engines, and reasonably smooth cylinder pressure developments have been achieved using high compression ratios (in the region of 20 to 23.5 : 1), and careful matching of the injection characteristics. Typical forms of the cylinder pressure developments are shown in Figure 7.1f, g, and h. In the case of diagram f the pressure rise due to combustion does not exceed that due to compression, resulting in a flat top characteristic. In the case of diagram g the pressure rise, although small, is some 5 to 10 degrees after TDC, while in the case of diagram h the pressure rise due to combustion takes place on the expansion stroke.

7.1.1 Rates of Pressure Rise

The rate of pressure rise is an indicator of the severity of combustion, and its significance from a noise point of view, as demonstrated in the previous chapters of this thesis, arises out of the fact that it has a strong influence in determining the levels of the cylinder pressure spectrum over the engine structure natural frequency range. Figure 7.2 shows the typical maximum rates of pressure rise measured in the various

types of engines for which the pressure diagrams have been considered. (The portion of the pressure development over which this maximum rate of pressure rise occurs, has been indicated in Figure 7.1.) The data are plotted on the basis of bar/msec, which can conveniently be converted to a bar/degree scale by a grid of constant bar/degree lines.

Data plotted for spark ignition engines represent values for a typical high performance engine with normal combustion. Whilst there is a considerable amount of scatter which is due to cycle-to-cycle variations typical of spark ignition pressure developments, the rate of pressure rise generally increases with engine speed from about 1 bar/degree at 1500 rpm to some 3 bar/degree at 5000 rpm.

The typically noisy normally-aspirated direct-injection diesel engine represented by pressure diagram type b shows rates of pressure rise which are between 8 to 10 bar/degree and remain almost constant over the engine speed range. The normally-aspirated direct-injection diesel engine represented by pressure diagram type c shows rates of pressure rise which are lower in magnitude by some 6 to 7 bar/degree. Turbocharged engines operating at rated conditions exhibit rates of about 4 bar/degree, increasing to 5 to 6 bar/degree at low engine speeds.

The maximum rate encountered in car indirect-injection diesel engines is due to the compression pressure development which is roughly constant at 2 bar/degree, but with the pressure diagram of type h the rate of pressure rise can increase to about 2.5 to 3 bar/degree.

From practical considerations it is generally accepted that a reasonably quiet engine is obtained if the rate of pressure rise does not exceed 4 bar/degree. This criterion is generally

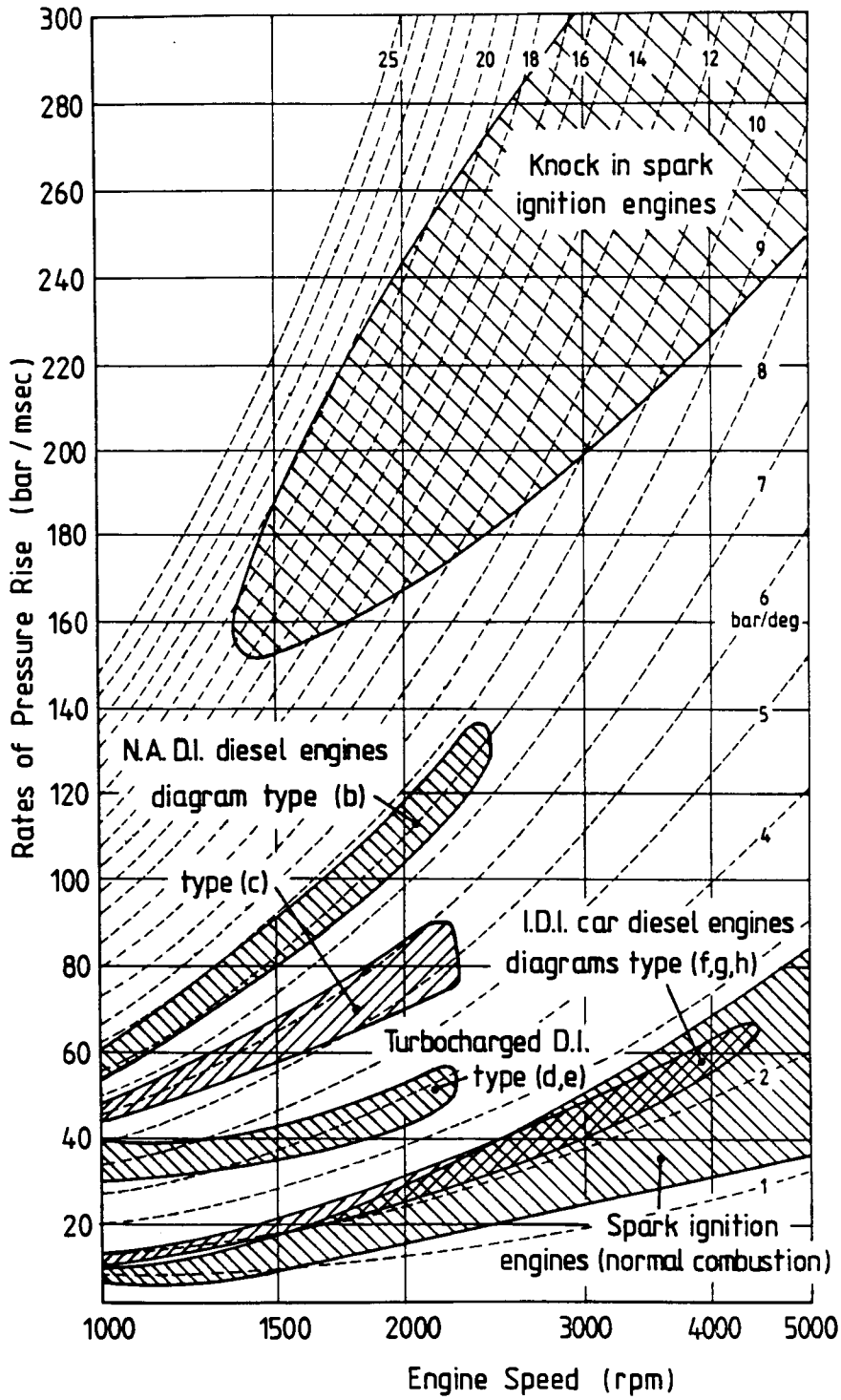

Figure 7.2 Typical maximum rates of pressure rise for the pressure diagrams shown in Figure 7.1.

very difficult to achieve in N.A. D.I. diesel engines, whilst in turbocharged engines it is only achieved near rated operating conditions. It is also important to note that rates of pressure rise which remain more or less constant over the speed range when measured against crankshaft rotation, increase with speed when measured against time.

7.1.2 Peak Cylinder Pressures

The peak cylinder pressure also has a strong influence on engine noise, but the mechanism by which the vibration is generated is entirely different from that of a rapid pressure rise. Higher peak cylinder pressures cause larger deflections of the crankshaft, resulting in higher levels of mechanical excitation arising from the rotation of the deformed crankshaft in its bearings.

The ranges of full load peak cylinder pressures for the various engine categories are shown in Figure 7.3. Spark ignition engines operating at low engine speeds generally have low peak pressures, of the order of 20 to 30 bar at 1000 rpm. The peak pressures rise rapidly with engine speed, however, and can reach magnitudes of about 65 bar at speeds of 3000 rpm and above, in higher performance engines. For moderate performance engines, the maximum pressures are around 45 bar.

For an indirect-injection car diesel engine of comparative size, the peak cylinder pressures are constant at about 60 to 70 bar over the whole speed range of the engine. It can be seen that there is a large difference in peak pressure between the spark ignition and car diesel engines over the low speed range, up to 2000 rpm.

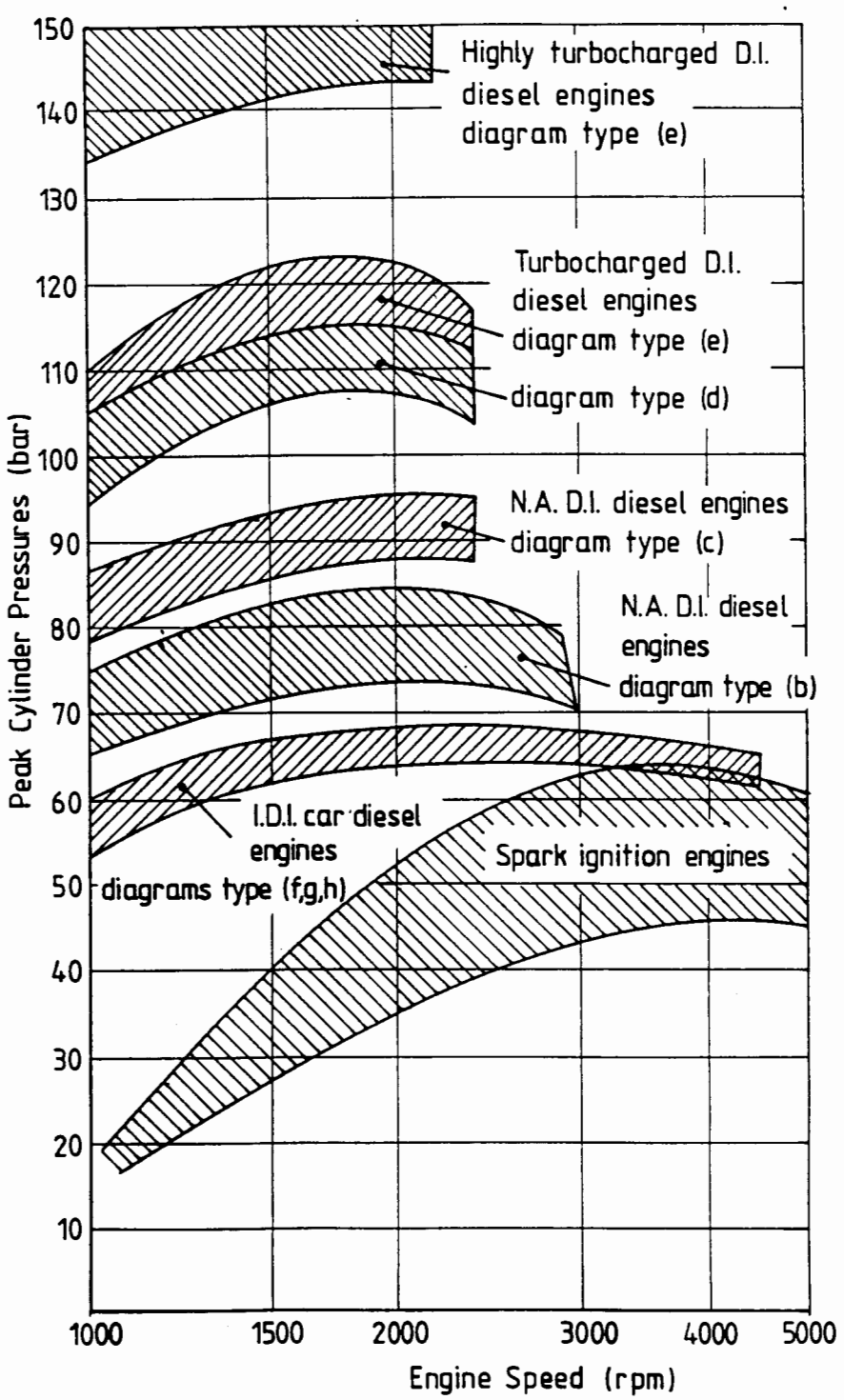

Figure 7.3 Typical peak cylinder pressures for the pressure diagrams shown in Figure 7.1.

The peak cylinder pressures of the larger normally-aspirated truck diesel engines are generally considerably higher than those of indirect-injection car diesel engines. Depending on the combustion and injection systems used, they may range between 75 to 95 bar.

Turbocharging, in general, increases the peak pressures substantially. The majority of turbocharged truck engines have peak cylinder pressures between 100 and 120 bar, while highly turbocharged, high output engines now reach peak pressures in excess of 140 bar.

7.1.3 Cylinder Pressure Spectra

The usefulness of the cylinder pressure spectrum for describing the characteristics of the cylinder pressure development was described in Chapter 5. From the engine noise point of view, the levels of the harmonics in the frequency range from 800 to 2500 Hz i.e. the frequency range where most of the predominant engine noise lies, are important. The levels over this range will generally only be significant if a rapid pressure rise occurs over some region of the cylinder pressure development, with the magnitude of the rapid pressure rise controlling the spectral level.

Figure 7.4 shows the spectra at 2000 rpm for the selected types of pressure diagrams shown in Figure 7.1. For the turbocharged engines (diagrams d and e) the high peak cylinder pressures produce high levels of harmonics only in the low frequency range, which generally contribute little to the overall noise of the engine. In the higher frequency range from 800 Hz upwards the levels are low.

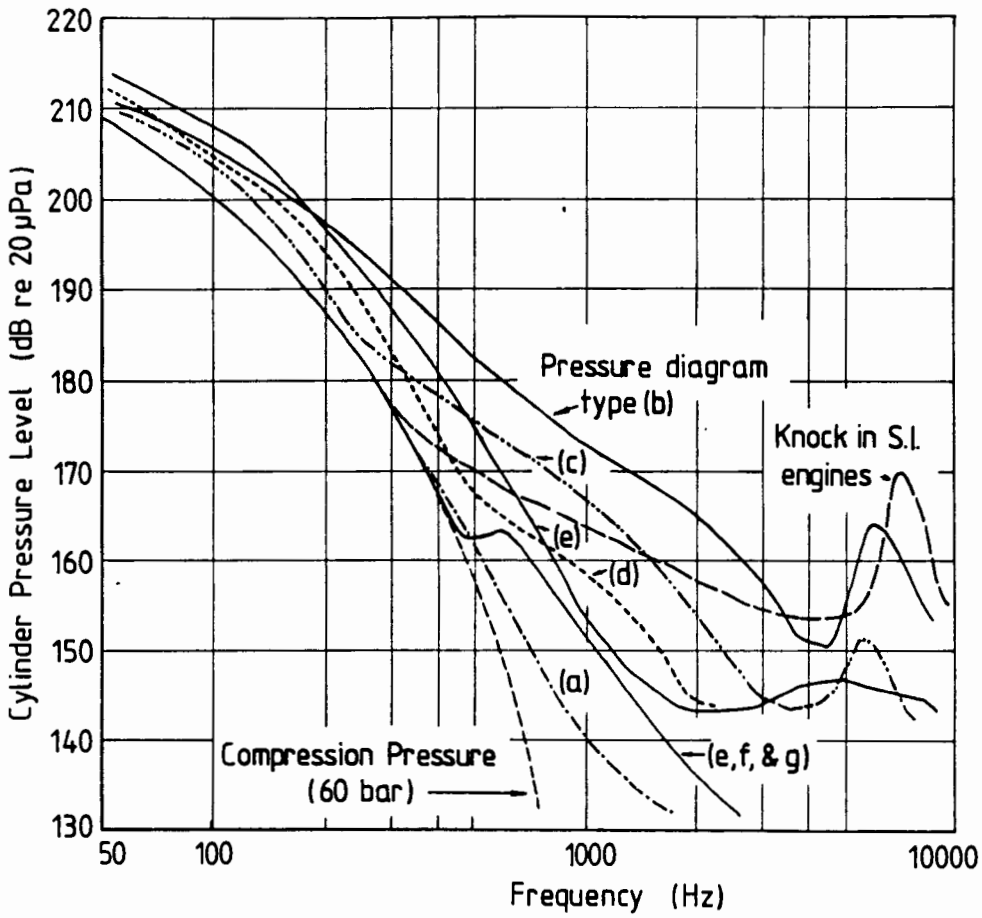

Figure 7.4 Typical cylinder pressure spectra for the pressure diagrams shown in Figure 7.1.

For indirect-injection engines (diagram f) the levels are low in both the low frequency regions (due to lower peak pressures) and high frequency range, except for a slight hump in the spectrum around 600 to 700 Hz which is due to the "flat top" or "double hump" pressure diagram. Even lower, however, are the levels for a spark ignition engine (diagram a) and a pure compression curve.

Normally-aspirated direct-injection engines (diagram b and c) produce the highest levels in the predominant frequency range. Depending on the rate and magnitude of the pressure rise, the levels are generally higher by 10 to 15 dB above those of smooth pressure developments. It is usually only in these engines where a linear relationship between cylinder pressure level and emitted noise is obtained.

It must be kept in mind that the level of the cylinder pressure spectrum is only an important factor from a noise point of view, if the so-called "critical level" is exceeded over the frequency range of interest. Consequently there is no point in expending effort on smoothing the cylinder pressure development if levels are already below this limit.

7.2 KNOCKING COMBUSTION IN SPARK IGNITION ENGINES

In the case of knock in spark ignition engines, the cylinder pressure diagram is modified considerably by the acoustical response of the combustion chamber cavity, and the gas force to which the engine structure is then subjected is comprised of the resultant cylinder pressure. (The response of the combustion chamber cavity is described in detail in Chapter 6.) A large number of cylinder pressure diagrams of knocking cycles recorded in the Nissan L28 and Volkswagen 1800 engines were analysed, and the diagrams and their spectra are presented in Appendices F and G. The parameters investigated in the previous section for normal combustion were also evaluated for the purpose of comparison, and are presented below.

7.2.1 Rates of Pressure Rise

The typical rates of pressure rise resulting from knock in the spark ignition engines investigated, are also shown in Figure

7.2. Values range from 150 bar/msec upwards to over 300 bar/msec, and are therefore considerably higher than any of the rates encountered in engines running under normal combustion conditions.

7.2.2 Peak Cylinder Pressures

The range of peak cylinder pressures recorded in the Nissan L28 engine at 6°, 15°, and 20° spark timing, and with knocking and normal combustion, are plotted in Figure 7.5 over the speed range. It can be seen that pressures in excess of 90 bar are encountered in the case of heavy knock.

It is interesting to note the relationship between knock intensity and engine speed in this particular engine: a very strong high speed knock tendency is evident. The tendency to knock decreases dramatically between 1500 rpm and 2500 rpm, and then increases again after 3000 rpm. At 20° spark timing the cylinder pressures with normal combustion increase steadily up to a speed of 4000 rpm, after which they decrease again. This decrease is not evident at 15° timing, however, indicating that at 20°, the timing may become over-advanced at high speeds. The dependence of knock on peak cylinder pressure is demonstrated, as higher knock pressures are recorded at 5000 rpm with 15° spark timing than with 20° timing.

7.2.3 Cylinder Pressure Spectra

A cylinder pressure spectrum for a knocking cycle is included in Figure 7.4 for the purposes of comparison. In addition, cylinder pressure spectra determined over the speed range for the Nissan L28 engine are shown in Figure 7.6. The effect of speed is clearly visible in the low frequency range, where the spectrum reflects the levels of the harmonics not affected by

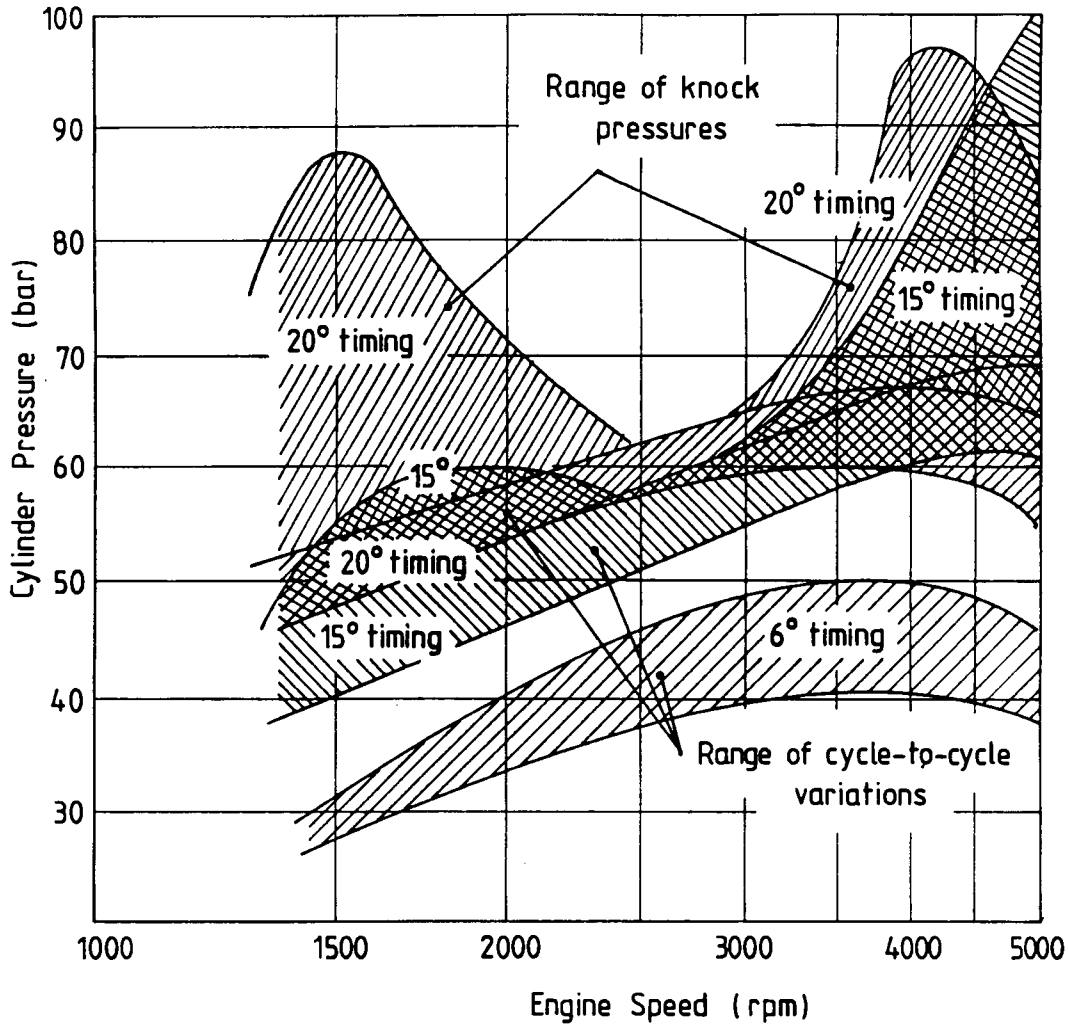

Figure 7.5 Range of peak knock pressures for the Nissan L28 engine.

the rapid pressure rise and pressure oscillations. The effect of the rapid pressure rise is clearly visible, in that the levels of the harmonics between 800 and 5000 Hz lie between 150 and 165 dB, which, when compared to the spectra shown in Figure 7.4, shows that the excitation levels are higher than those encountered in all of the forms of cylinder pressure development investigated, except the worst case normally-

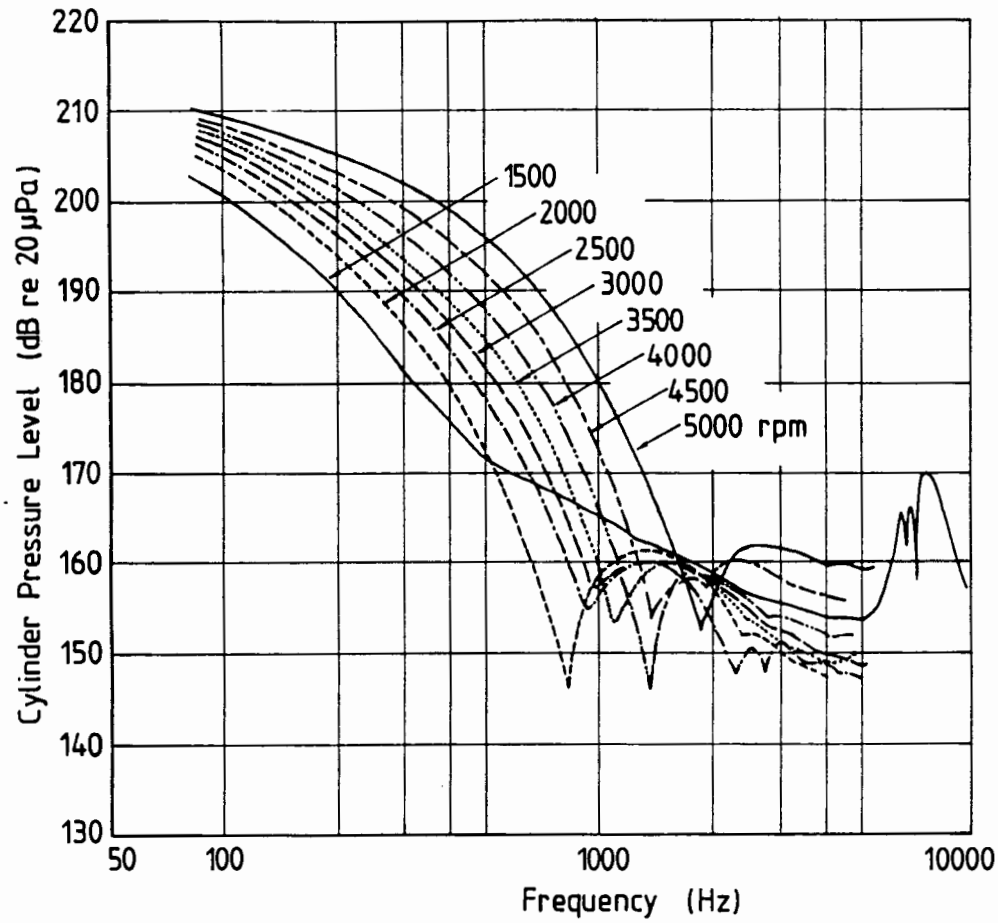

Figure 7.6 Spectra recorded over the speed range with knocking combustion in the Nissan L28 engine.

aspirated direct-injection diesel engine. Calculation of the magnitudes of the rapid pressure rise associated with these levels (as described in Chapter 5) yields values of up to 15 bar, which is approximately the same as those encountered in this type of diesel engine.

In order to maintain clarity, the high frequency peaks associated with the cylinder pressure oscillations are not

shown in Figure 7.6, but the range of levels for the highest peak, measured over the engine speed range and at 10° and 20° spark timing, are shown in Figure 7.7. It can be seen that levels of up to 180 dB have been recorded, with the highest levels occurring at the higher engine speeds of 4000 rpm and above. As is to be expected, the levels follow a similar trend with speed, as the peak knock pressures shown in Figure 7.5. At 20° spark timing the pressure levels range between 160 and 180 dB, which is up to 20 dB higher than the spectral levels recorded over the mid-frequency range between 1000 and 5000 Hz (as indicated in Figure 7.6).

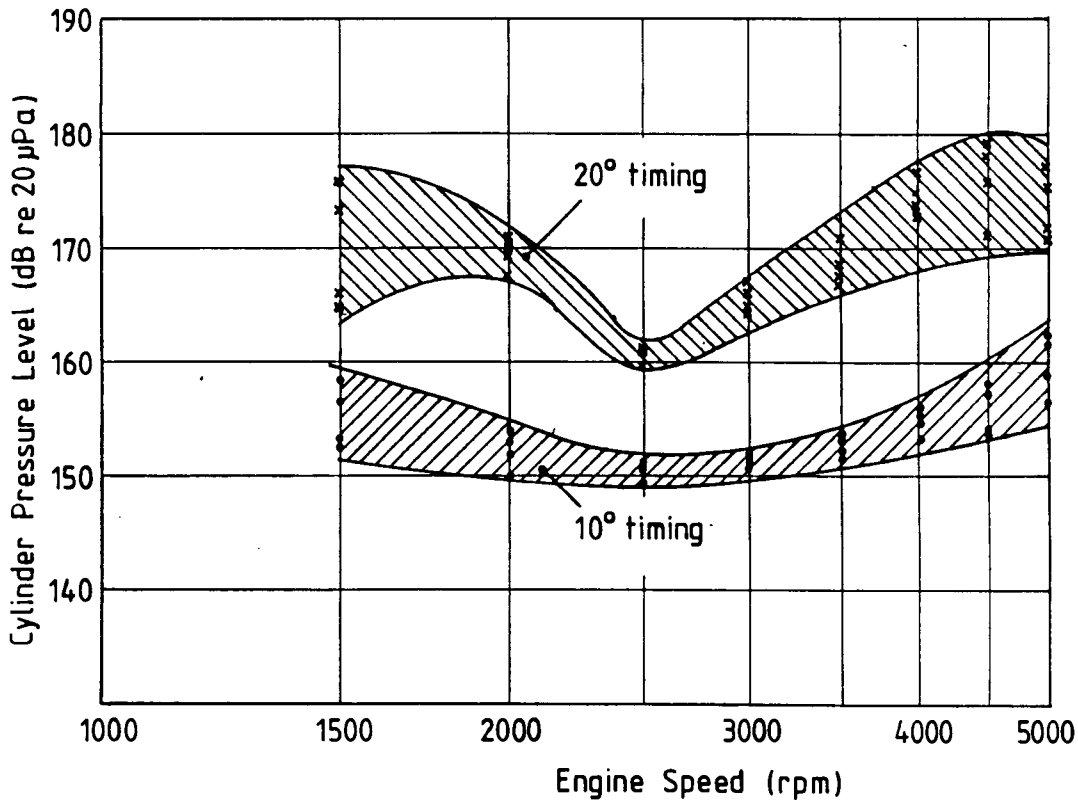

Figure 7.7 Range of spectral levels associated with the cylinder pressure oscillations for the Nissan L28 engine.

7.3 DISCUSSION

At a first glance it would appear that the cylinder pressure development for a knocking cycle in a spark ignition engine represents a very severe case from an engine noise point of view. This is not necessarily so, however, for a number of reasons which are discussed below.

7.3.1 Transient Excitation Levels due to the Rapid Pressure Rise

The high rates of pressure rise measured from knocking cycles are deceiving, in that the magnitude of the actual mean pressure rise occurring at this rate (i.e. the rapid pressure rise resulting from knock) is masked by the large amplitude pressure oscillations, and generally does not exceed 10 bar, although magnitudes of up to 15 bar may be reached in extreme cases. Thus the level of transient excitation over the engine structure natural frequency range, while increasing considerably over the normal combustion level (by 30 dB or more), does not reach the same levels experienced in the worst case diesel engines.

It was shown in Chapter 6 that the rapid pressure rise resulting from knock can be assumed to act over the whole piston area, and it is therefore reasonable to assume that it will be transmitted to the main bearings via the cranktrain, resulting in transient vibration of the engine structure by the same mechanism usually associated with diesel knock.

7.3.2 Forced Excitation Levels due to the Cylinder Pressure Oscillations

The fact that the predominant frequency of the noise emitted by a knocking spark ignition engine corresponds to the frequency

of the cylinder pressure oscillations indicates that a forced excitation of the engine structure occurs. In order to determine how this occurs, however, it is necessary to determine how the pressure oscillations interact with the engine structure. It was pointed out in Chapter 6 that the mode shapes associated with each of the modes of gas vibration in the combustion chamber cavity determines that the nett pressure acting on the piston face at any instant in time is zero, however, and therefore no forced vibration of the piston and cranktrain should occur. The transmission path of the vibrations is therefore unclear, and this aspect will be discussed in greater detail in the following chapter.

7.3.3 Repetition Rate

The Fourier analysis of the cylinder pressure diagrams assumes periodicity, and the levels of the harmonics shown are therefore representative of the level of excitation which would be encountered should that particular pressure diagram be repeated at the cyclic frequency of the engine. This does not occur in practice, however, as the cycles with heavy knock are interspersed by cycles with less severe and even no knock, and the engine structure will therefore be subjected to the excitation levels which will generally be lower than those depicted in the spectra chosen. The unpredictable nature of knock makes it very difficult to predict realistic values, or even a suitable "attenuation factor" by which a single cycle analysis can be scaled in order to make the levels more representative.

CHAPTER 8

ENGINE STRUCTURE RESPONSE

It has been established in the previous chapters of this thesis that the gas force resulting from a knocking engine cycle has the ability of inducing both transient and forced vibration of the engine structure, these being respectively associated with the rapid pressure rise and pressure oscillations. It has also been mentioned that, whilst the nature of the transient structure response mechanism has been established as a result of the extensive research done in the field of diesel engine noise, it would appear that little or no research has been done to establish the mechanism by which the engine structure responds to the high frequency pressure oscillations resulting from knock.

It must be kept in mind that the knock-induced vibration of the engine structure occurs against the background of the inherent mechanically-induced vibration, whose presence and interaction with the other excitation sources cannot be disregarded. This is particularly so at higher engine speeds, when mechanical excitation is at its maximum and may mask any other sources of vibration. For the purposes of investigation, however, it is fortunate that spark ignition engines have a greater propensity to knock at low engine speeds, when mechanically-induced vibration is at a minimum, and minimal masking of the knock-induced vibration thus takes place.

8.1 STRUCTURE RESPONSE TO KNOCK IN S.I. ENGINES

Vibration measurements were carried out in two locations on the Volkswagen 1800 engine. An accelerometer was mounted vertically on the cylinder head, next to the cylinder which was

fitted with the pressure transducer, and another was mounted vertically on the main bearing cap adjacent to the same cylinder. The vibration oscillograms were recorded digitally, as described in Appendix B, and spectra were obtained by Fourier analysis of the digitised oscillograms, using the same procedure as for the cylinder pressure spectrum, and are scaled in units of dB re 1g.

Oscillograms were recorded over the speed range and at spark advance settings of 6° (standard timing), 16°, and 26° BTDC, and their frequency spectra computed. The complete results of these analyses are presented in Appendix G for reference. Figure 8.1a shows a cylinder pressure diagram, as well as the two vibration oscillograms, recorded at 1500 rpm. The spark timing was 16° BTDC and 93 RON gasoline was used, resulting in fairly heavy knock, as can be seen from the cylinder pressure diagram. Figures 8.1b, and 8.2a and b show the cylinder pressure spectrum, and the bearing cap and cylinder head vibration spectra, respectively.

8.1.1 Time Domain Response

Both vibration oscillograms only show very small acceleration amplitudes before the onset of the rapid cylinder pressure rise due to knock. In the case of the bearing cap, a small amplitude vibration can be seen to be initiated at TDC, this being due to the crankpin force reversal taking place at that point. At the onset of knock which takes place about 8° after TDC, there is a considerable increase in the vibration amplitudes recorded by both accelerometers. Whilst the response of the cylinder head to the rapid pressure rise occurs instantaneously, there is a time delay of approximately 0.144 msec before the bearing cap responds. In comparing the two vibration oscillograms, it can be seen that the acceleration

a)

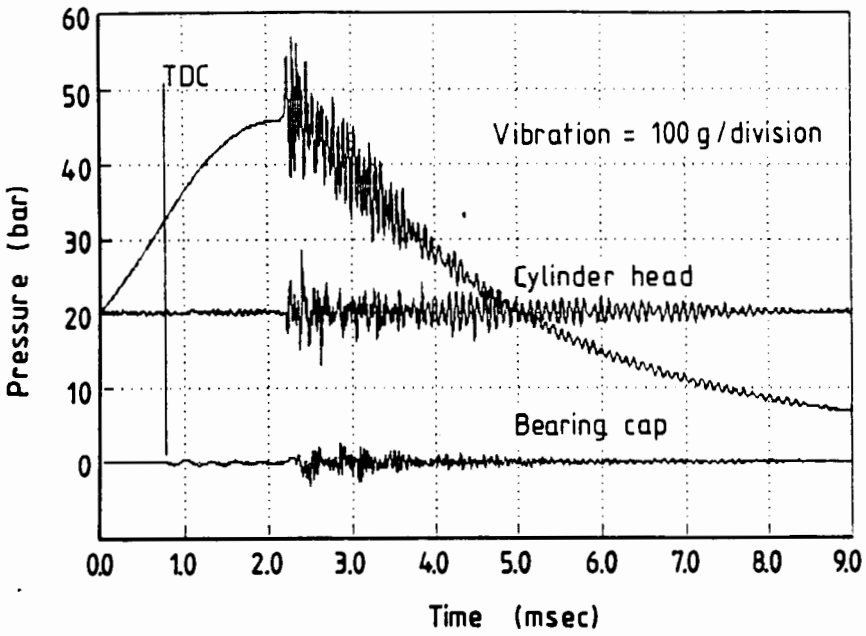

b)

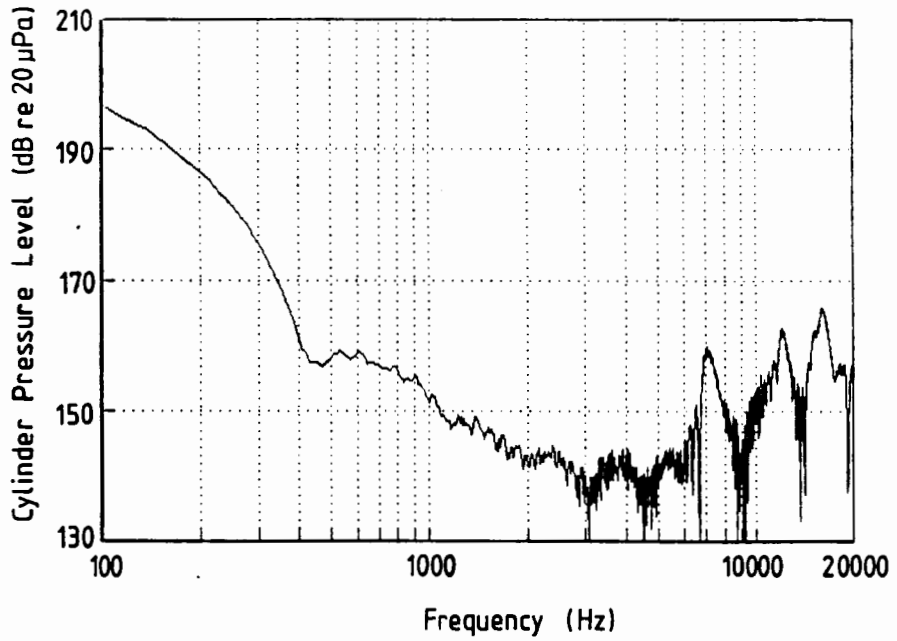

Figure 8.1 Cylinder pressure diagram and spectrum with knocking combustion. Bearing cap and cylinder head vibration oscillograms are superimposed on the pressure diagram.

a)

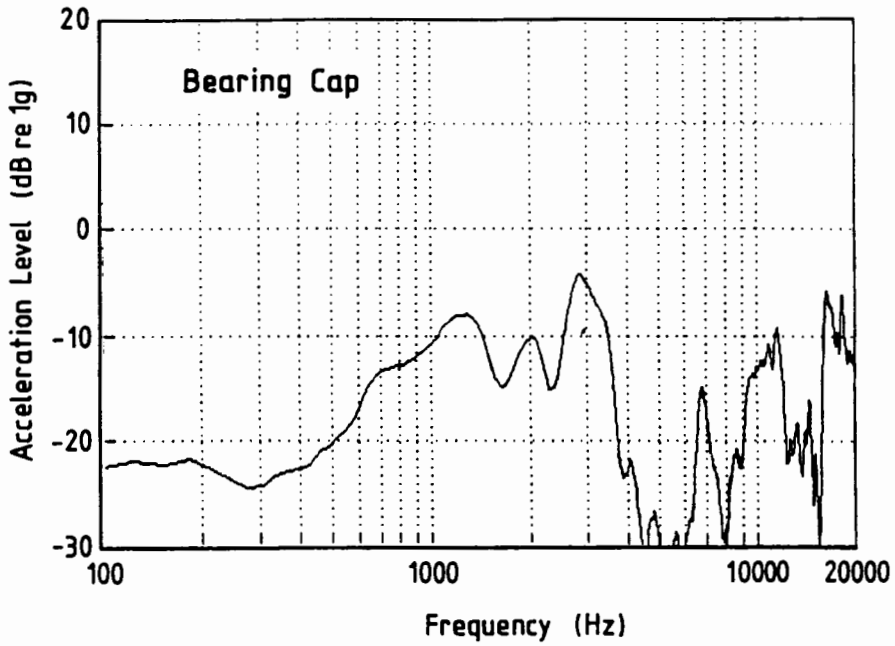

b)

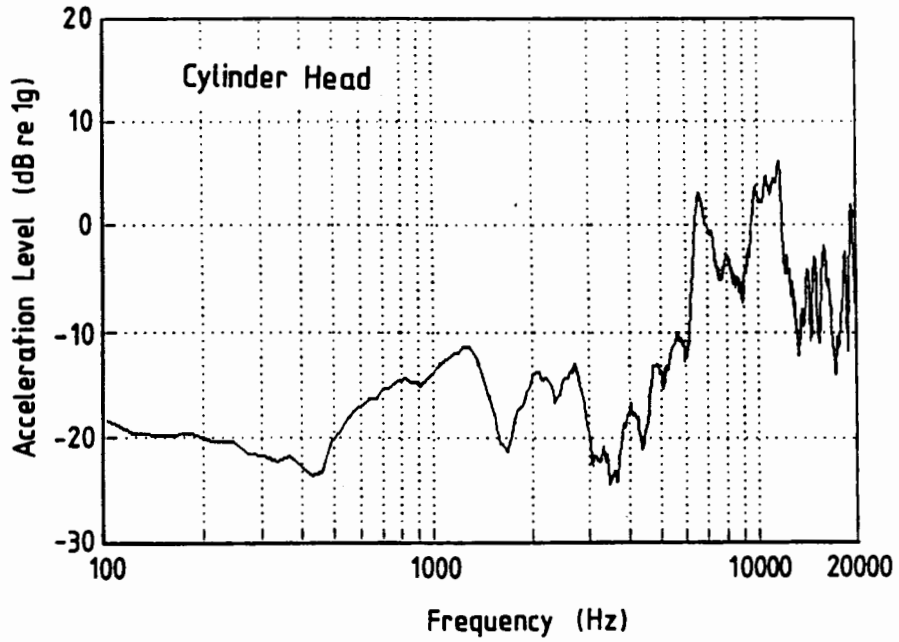

Figure 8.2 Bearing cap and cylinder head vibration spectra.

amplitudes measured on the cylinder head are greater than those at the bearing cap, with the latter also being damped out quicker. Close examination of the cylinder head vibration oscillogram shows that its frequency content follows that of the cylinder pressure oscillations closely, with the presence of highly damped high frequencies immediately after initiation, giving way to a steady oscillation with the same duration as the cylinder pressure oscillation.

There are a number of observations which may be made regarding the time domain response of the cylinder head and bearing cap. The vibration oscillogram recorded on the bearing cap shows the typical transient response characteristic. The time delay between the response of the cylinder head and the bearing cap indicates that the cylinder head responds before the bearing cap, however. This, in conjunction with the fact that the vibration amplitudes on the cylinder head are significantly larger than those on the bearing cap, suggests that the cylinder head is excited directly by the gas force, rather than by the forces transmitted to the outer engine structure at the main bearings. The cylinder head generally represents a stiffer element than the cranktrain, and one would therefore expect transient vibrations to be damped out considerably quicker in the former. This is clearly not the case, as the vibrations continue for as long as the pressure oscillations are present, thus suggesting that the vibration of the cylinder head is forced, rather than transient. The implication is thus that the cylinder head response constitutes a forced vibration at the frequency of the pressure oscillations, while the bearing cap response represents the expected transient response to the abrupt rise in the gas force. The latter is transmitted along the cranktrain, and results in an increase in the vibration levels over the engine structure natural frequency range.

This suggestion is also supported by the observation in Chapter 6, that the net oscillating gas pressure acting on the piston crown should be zero, according to the predicted mode shapes associated with the resonant frequencies of the combustion chamber cavity. Thus the bearing cap should theoretically not respond to the gas force oscillations, requiring them to be transmitted by an alternative path. Further light may be shed on the matter by examining the frequency spectra of the recorded oscillograms.

8.1.2 Frequency Domain Response

The cylinder pressure spectrum shows a distinct peak at 7020 Hz, corresponding to the fundamental mode of gas vibration, followed by peaks at 12035 and 16085 Hz representing the (2,0) and (3,0) modes respectively. The (3,0) mode has the highest level, at 166.4 dB, followed by the (2,0) mode and the (1,0) mode. The influence of the cylinder pressure oscillations on the engine structure response is very noticeable on the vibration spectra. The bearing cap vibration spectrum (Figure 8.2a) shows its dominant response to lie in the frequency band between 600 and 3500 Hz, with an average level of about -10 dB and a peak level of -4.5 dB at 2800 Hz. It also shows three distinct peaks, however, at frequencies very similar to those of the cylinder pressure oscillations. The levels of the three high frequency peaks range from -15 dB for the lowest frequency to -5.5 dB for the highest frequency peak.

The cylinder head vibration spectrum shows considerably lower levels than the bearing cap over the frequency range between 600 and 3500 Hz, with an average level of approximately -15 dB. The high frequencies above 6000 Hz dominate, however, with two peaks with similar frequencies to the (1,0) and (2,0) gas vibration modes reaching levels of 3 and 6 dB respectively.

Unlike the bearing cap, the levels of the frequencies corresponding to the (3,0) mode, are considerably lower.

The two vibration spectra show conclusively that the dominant response at the bearing cap is over the frequency range corresponding to the natural frequencies of the engine structure, whilst the dominant response of the cylinder head is over the frequency range corresponding to the frequencies of the cylinder pressure oscillations. This supports the proposal that the response of the cylinder head is forced and that of the bearing cap is transient. Contrary to expectation, however, significant vibration levels at the frequencies of the pressure oscillations are also registered on the bearing cap. Since the cylinder liner, and consequently the engine block, will be subjected to the same pressure oscillations as the cylinder head, it is not unfeasible that the forced vibrations are transmitted from the outer engine structure to the bearing cap. No tests were performed to prove or disprove this, or to show conclusively that there is no transmission of the cylinder pressure oscillations along the cranktrain, however, and such proposals thus remain purely speculative. Some further analysis of the computed vibration spectra was performed, however, the results of which are presented in the next section.

8.2 EFFECT OF KNOCK INTENSITY AND ENGINE SPEED

In order to examine the engine structure response over the two frequency ranges of interest, namely the structure natural frequency range and the cylinder pressure oscillation frequency range, the average levels of the harmonics between 1000 and 4000 Hz, and 6000 and 20000 Hz, were calculated from the vibration spectra for both the cylinder head and the bearing cap. These calculations were done over the speed range and at the three spark advance settings at which tests were performed,

and the results are presented in Figures 8.3 to 8.6, as plots of averaged vibration level against speed. At 16° and 26° spark advance settings, the recorded cycles showing the heaviest knock were analysed, and the levels are presented as bands containing measured levels, because of the expected scatter associated with knock. Thus, they are indicative of trends, rather than absolute levels, and where actual levels are quoted, these represent average values.

In the following section the transient response in the 1000 to 4000 Hz frequency range will be described first, followed by the forced response in the high frequency range.

8.2.1 Transient Response

Figure 8.3 and 8.4 show the vibration levels averaged between 1000 and 4000 Hz, for the bearing cap and cylinder head respectively. Except for the numerical levels, both graphs show very similar characteristics. In both cases a distinct two-slope characteristic is evident in both the knock-free baseline (6° spark timing), as well as the knocking vibration levels. The slopes are similar at the two measurement positions: at knock-free conditions the vibration level increases by some 44 dB/decade increase in speed, up to a speed of 3000 rpm, after which the rate of increase is 62 dB/decade. The high speed slopes at the knocking conditions (16° and 26° spark timing) are similar to those at the knock-free conditions, but deviate over the low speed range. At 16° spark timing the slope is 31 dB/decade up to 3000 rpm, while at 26° spark timing this decreases to -3 dB/decade.

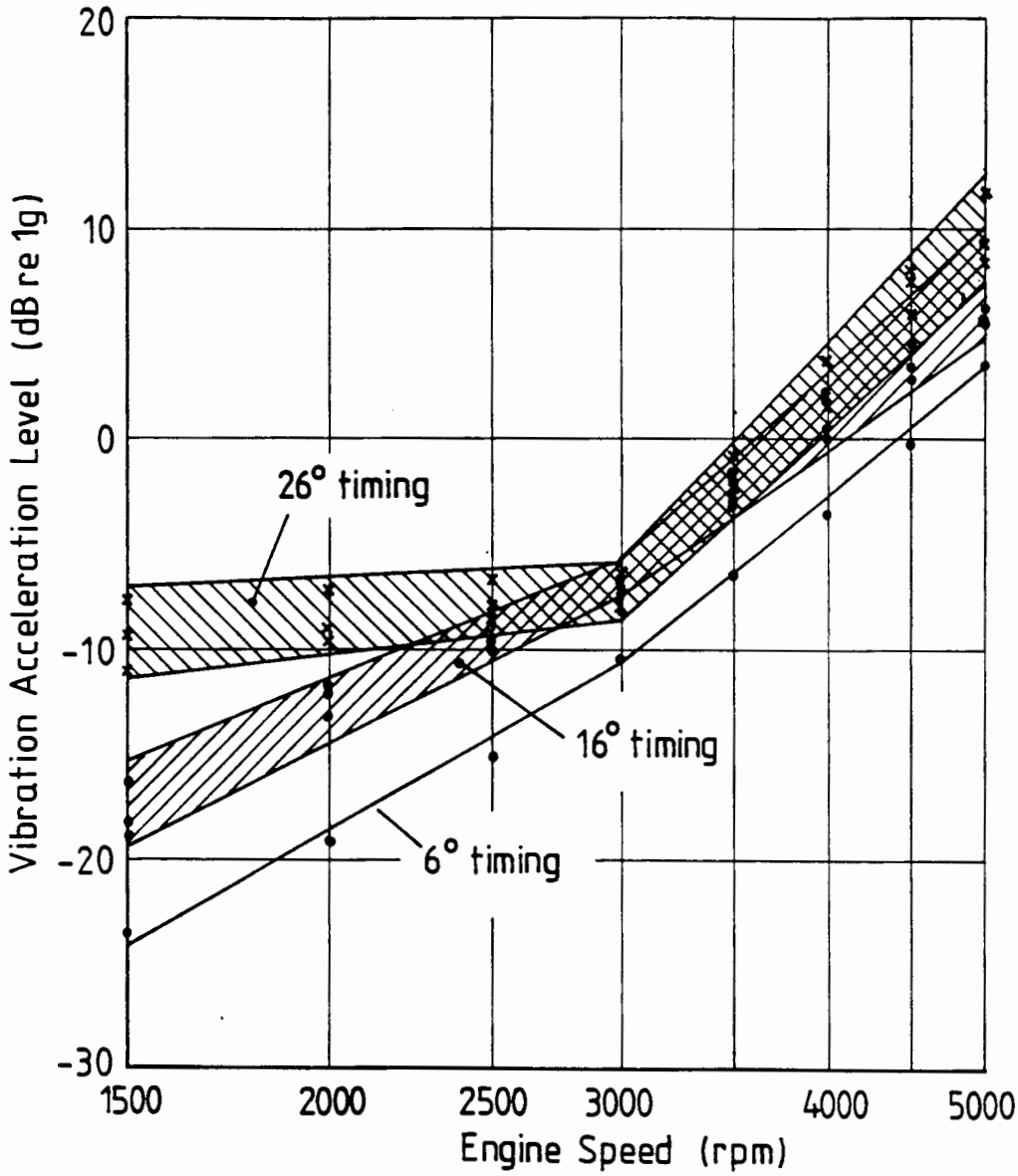

Figure 8.3 Average bearing cap vibration levels between 1000 and 4000 Hz with varying degrees of knock intensity.

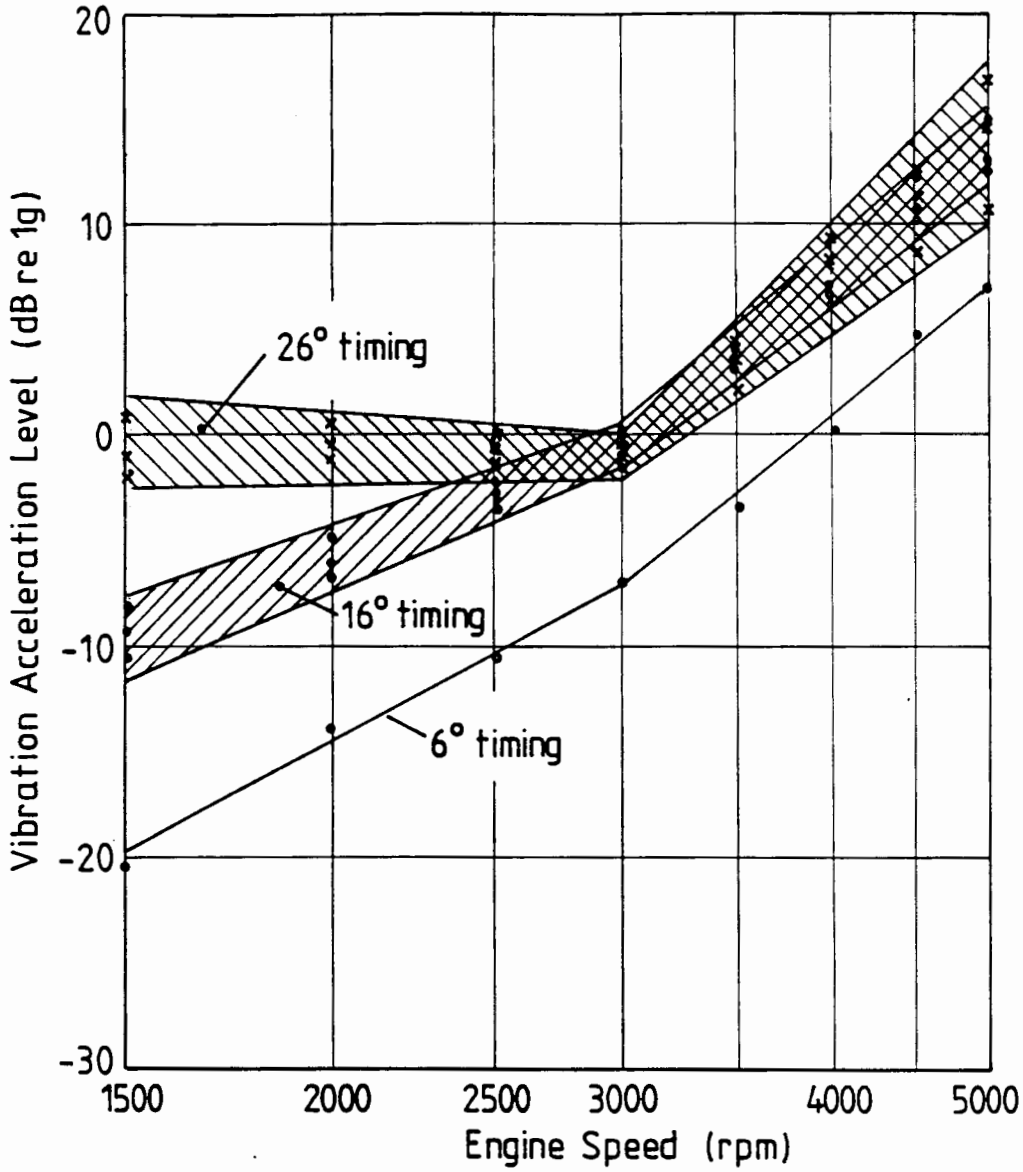

Figure 8.4 Average cylinder head vibration levels between 1000 and 4000 Hz with varying degrees of knock intensity.

The dual slope characteristic is evidence of the influence of the impulsive hydraulic forces which develop in the main bearing lubricating oil film. This is thought to be the dominant excitation mechanism under normal running conditions, but clearly has an influence in the presence of knock as well.

The fundamental difference between the averaged levels recorded on the bearing cap and cylinder head is that levels on the bearing cap are significantly higher. The knock-free level is some 3.5 db higher over the speed range, whilst the difference between this and the knocking levels is also greater on the bearing cap. This is to be expected, as the transient excitation of the engine structure originates at the main bearings. In both cases the knock severity (as indicated by the degrees of spark advance) has the greatest effect at low speeds, with the level at 26° spark timing being approximately 10 dB higher than those at 16° spark timing at 1500 rpm. This difference decreases with engine speed up to 3000 rpm, at which point the two bands converge and follow approximately the same path over the higher speed range. The higher levels over the low speed range are likely to be due to the greater knock intensity levels occurring at low speeds. The convergence of the two bands after 3000 rpm with a slope identical to that of the knock-free condition would appear to indicate an increased influence of the primary excitation mechanism, probably due to the decreased knock levels. Levels are still considerably higher than the knock-free condition, however.

The similar slopes displayed at the bearing cap and cylinder head indicate that excitation is due to the same mechanism, thus confirming that the source of transient excitation is at the bearing caps, and is then transmitted to the outer engine structure.

8.2.2 Forced Response

Figure 8.5 and 8.6 show the vibration levels averaged between 6000 and 20000 Hz, for the bearing cap and cylinder head respectively. Again the overall characteristics of the two plots are similar, except that in this case the situation is reversed in that the levels recorded on the cylinder head are considerably higher than on the bearing cap. The two-slope characteristic is also clearly evident: on the bearing cap the slope up to 3000 rpm for the knock-free curve is 32 dB/decade increase in speed, while above 3000 rpm this increases to some 55.5 dB/decade. On the cylinder head the slope over the high speed range is the same, while at speeds below 3000 rpm, it is some 5 dB/decade lower.

On the cylinder head (Figure 8.6) the vibration levels at 16° spark timing remain more or less constant with engine speed up to 3000 rpm, beyond which the slope is similar to that at the standard 6° spark timing. In this high speed region the levels at 16° and 26° spark timing can be seen to coincide at a level approximately 10 dB above that of the 6° spark timing vibration level. Below 3000 rpm, the 26° spark timing band decreases from a level approximately 24 dB above that of the knock-free level, at a rate of 16.5 dB/decade increase in engine speed. The level of the 16° band at 1500 rpm is some 6.5 dB below that of the 26° spark timing band. The negative slopes over the low speed region clearly indicate the effect of the decreasing knock intensity levels (and hence decreasing pressure oscillation amplitudes) with speed.

On the bearing cap (Figure 8.5), the knock-free vibration levels are between 10 and 11 dB lower than those on the cylinder head over this frequency range (6000 to 20000 Hz). This supports the proposal that the forced vibrations are transmitted directly to the engine structure, and not via the main bearings as is the case with the transient vibrations.

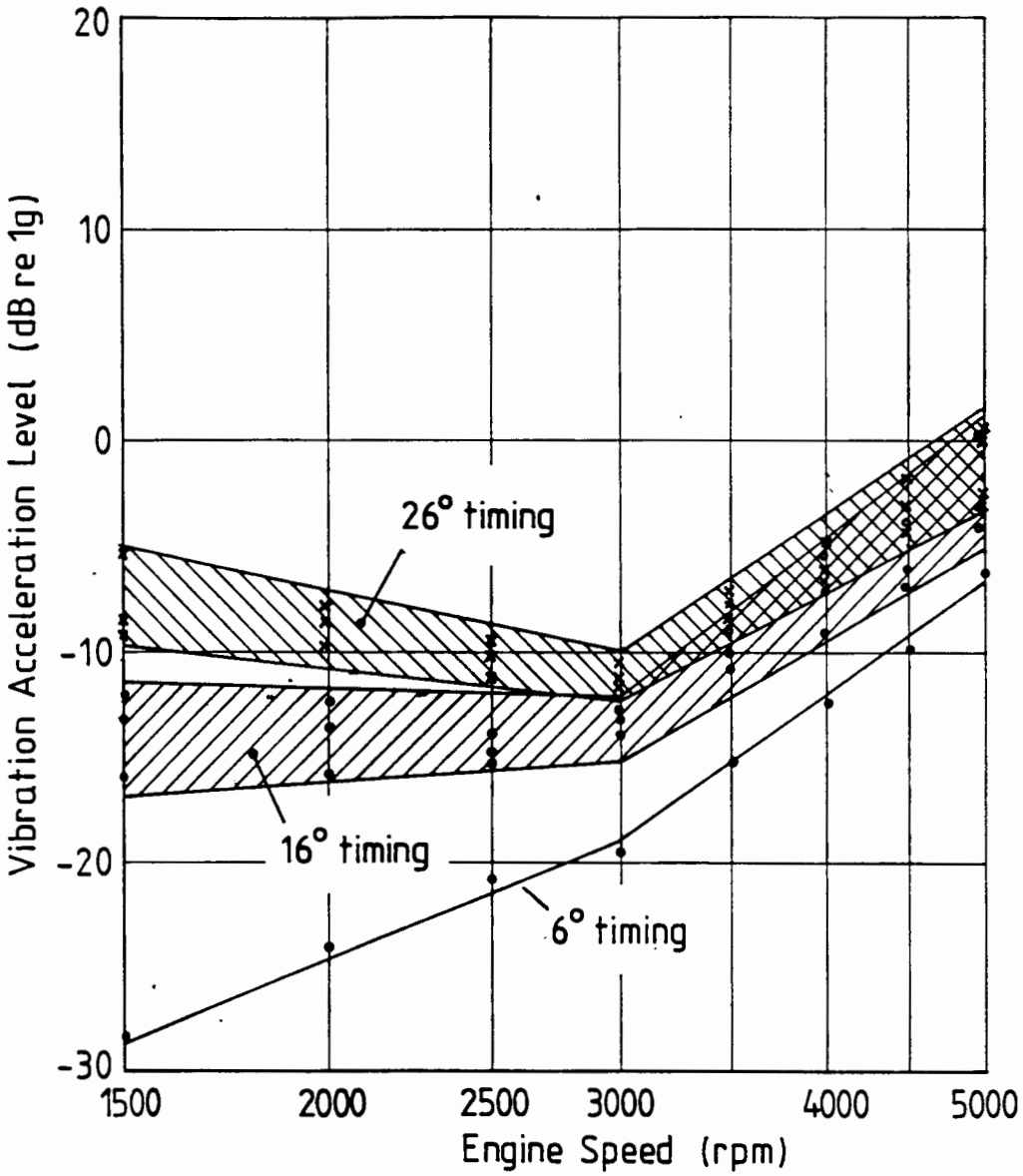

Figure 8.5 Average bearing cap vibration levels between 6000 and 20000 Hz with varying degrees of knock intensity.

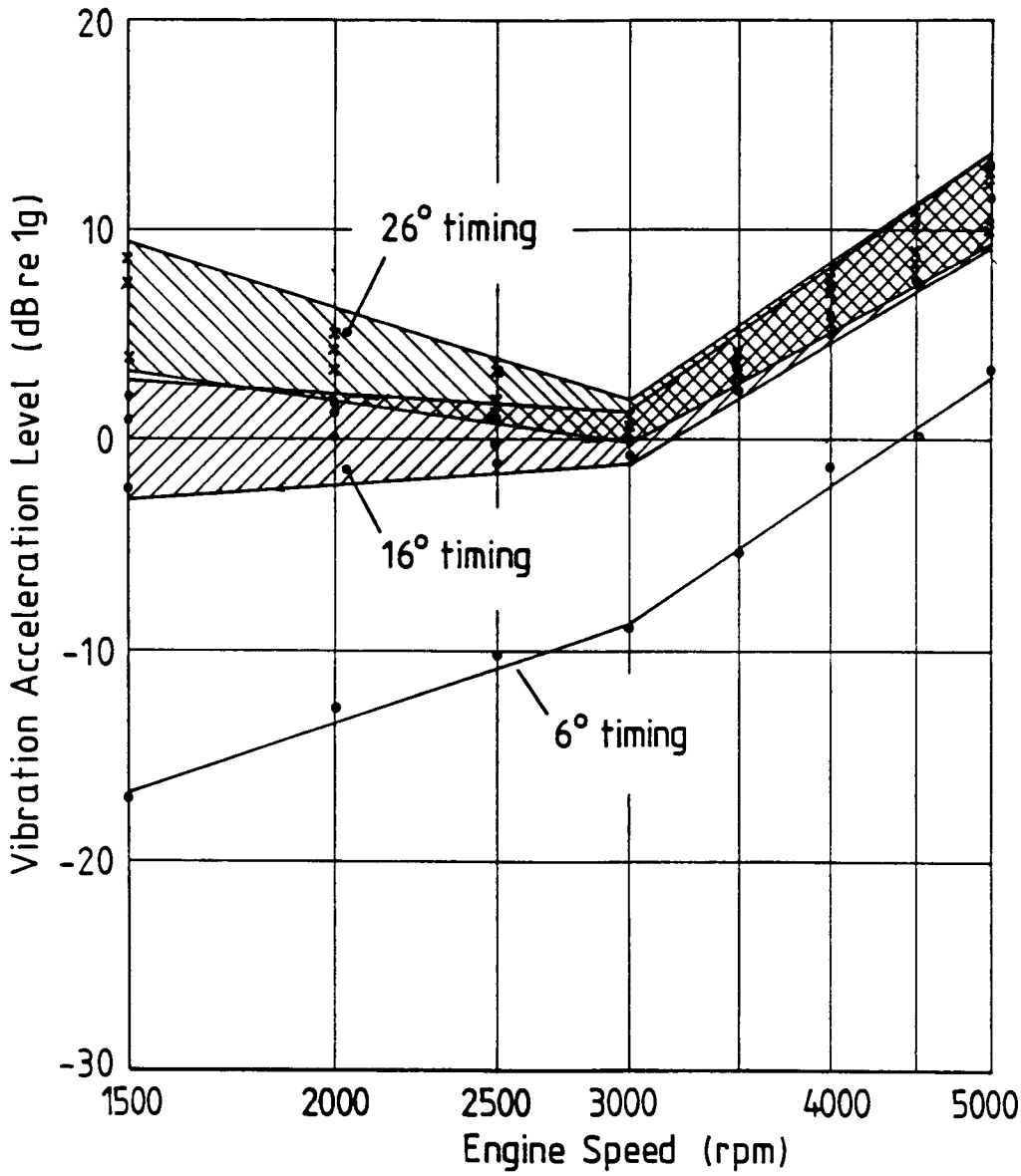

Figure 8.6 Average cylinder head vibration levels between 6000 and 20000 Hz with varying degrees of knock intensity.

The bearing cap vibration levels at 16° spark timing show the same rate of increase with speed over both the low and high speed ranges, as those measured on the cylinder head, but are on average 14 dB lower in magnitude. As opposed to the cylinder head, however, the vibration levels at 16° and 26° spark timing do not coincide over the high speed range to the same extent. The 26° band has a slope of approximately -3.5 dB/decade up to 3000 rpm, beyond which there is an increase of some 48.5 dB/decade increase in engine speed. At 1500 rpm, the differences between the average levels at 16° and 26° spark timing, and that of the knock-free level at 6° spark timing, are 22 and 15 dB respectively. These differences decrease to 8 and 5.5 dB at 3000 rpm, and 6 and 5 dB at 4500 rpm.

8.3 DISCUSSION

The analysis of the engine structure response presented in this chapter can in no way be regarded as being exhaustive. Trends can, however, be identified, which confirm that the engine structure responds to both forced excitation by the cylinder pressure oscillations, as well as transient excitation by the rapid pressure rise. Moreover, there is evidence which suggests that the transmission paths of these two excitation mechanisms differ, with transient vibrations being initiated at the bearing cap while the forced vibrations are transmitted directly to the engine structure by the gas force oscillations.

As yet the significant levels of bearing cap vibration at the frequencies of the cylinder pressure oscillations cannot be adequately explained, as well as the interaction between the exciting forces due to knock and the exciting forces which are present during normal combustion. This interaction would appear to be significant, as indicated by the presence of the dual slope characteristic of the vibration levels over the

speed range, on both the cylinder head and bearing cap, and over both of the frequency ranges investigated.

In addition, it is possible that the impulsive gas force excites transient vibrations in the cranktrain components, such as the connecting rod. Since the end conditions of the connecting rod are not known exactly, it is not a simple matter to calculate its transverse natural frequencies. It can be assumed, however, that the natural frequencies lie somewhere between those for a bar clamped at both ends, and a cantilever type system. For the connecting rod in question, which has a length of 145 cm, these conditions yield natural frequencies in the region of 18 and 9 kHz respectively. It is thus feasible that some of the high frequency vibrations measured on the bearing cap are due to transient vibration of the connecting rod.

CHAPTER 9

CONCLUSIONS

The work described in this thesis has provided some insight into the mechanisms by which noise is generated by combustion knock in automotive engines, and particularly in spark ignition engines. Investigations were carried in three areas relating to knock in spark ignition engines: the emitted noise, the cylinder pressure development, and the engine structure response. The conclusions which can be drawn from the findings of these investigations, are listed below.

9.1 ENGINE NOISE CHARACTERISTICS

Engine noise tests confirmed that knocking combustion in spark ignition engines results in increased noise levels over both the engine structural natural frequency range between 800 and 2500 Hz, as well as in the high frequency range from 6000 Hz upwards, which corresponds to the frequencies of the cylinder pressure oscillations which result from knock. The former indicate increased transient excitation of the engine structure, while the latter indicate the presence of forced vibrations due to the cylinder pressure oscillations.

9.2 CYLINDER PRESSURE DEVELOPMENT

The cylinder pressure development arising from knocking combustion in spark ignition engines shows significantly increased cylinder pressure levels over both the engine structural natural frequency range, as well as the high frequency range from 6000 Hz upwards. The latter take the form of discrete peaks which can be identified as the natural

frequencies of the combustion chamber cavity, while the former are the result of the very rapid pressure rise resulting from autoignition, which causes increased spectral levels over the mid-frequency range. Thus both the increased transient excitation levels and the forced excitation levels indicated by the engine noise measurements are confirmed, as well as the presence of the combustion chamber cavity resonances. Furthermore, the mode shapes associated with these cavity resonances predict that the nett oscillating gas force on the piston crown is zero.

9.3 ENGINE STRUCTURE RESPONSE

Vibration measurements with knocking combustion in both the time and frequency domains show increased transient and forced responses on both the cylinder head and the main bearing cap, the onset of which correspond exactly with the knock event. The relative vibration magnitudes, as well as measured response times and the predicted absence of an oscillating gas force on the piston crown, indicate that the transmission path for the forced vibrations is directly from the combustion chamber to the outer engine structure, while the transient excitation is initiated at the main bearings in the same way as in diesel engines.

REFERENCES

(1) Ricardo, H.R. The High Speed Internal Combustion Engine. First Edition, Blackie and Sons Ltd., Glasgow, 1931.

(2) Priede, T. "Relation between Form of Cylinder Pressure Diagram and Noise in Diesel Engines". Proc. Instn. Mech. Engrs. (A.D.). No.1, pp.63-77, 1960-61.

(3) Priede, T. and Dutkiewicz, R.K. "The Effect of Normal Combustion and Knock on Gasoline Engine Noise". S.A.E. Paper 891126, 1989.

(4) Janeway R W. "Combustion Control by Cylinder Head Design". S.A.E. Journal, No. 24, p.498, 1929.

(5) Hinze J O. "Effect of Cylinder Pressure Rise on Engine Vibrations". A.S.M.E. Paper 49-OG P-3, April 1949.

(6) Priede T. "In Search of Origins of Engine Noise - an Historical Review". S.A.E. Paper 800534, 1980.

(7) Austen A E W, and Priede T. "Origins of Diesel Engine Noise". Symposium on Engine Noise and Noise Suppression. Instn. Mech. Engrs., London, 1958.

(8) Russell M F. "Diesel Engine Noise: Control at Source". S.A.E. Paper 820238, 1982.

(9) Herbert A J, and Russell M F. "Measurement of Combustion Noise in Diesel Engines". Mechanical Engineering Technology, (Instn. Mech. Engrs), pp.34-39, April 1982.

(10) Russell M F, and Young C D. "Measurement of Diesel Combustion Noise". Autotech 85 Congress, Instn. Mech. Engrs., 1985.

(11) Priede T, and Grover E C. "Application of Acoustic Diagnostics to Internal Combustion Engines and Associated Machines". The Inst. Mech. Engrs. Conference on Acoustics as a Diagnostic Tool, October 1970.

(12) Miller C D. "Roles of Detonation Waves and Autoignition in SI Engine knock as shown by photographs taken at 40,000 and 200,000 frames per second". S.A.E. Quarterly Transaction, Vol.1, p.98, 1947.

(13) Heywood J B. Internal Combustion Engine Fundamentals. McGraw Hill, 1988.

(14) Tadajuni Hayashi, Masahiro Taki, Shiji Kojima, and Teruki Kondo. "Photographic Observation of Knock with a Rapid Compression and Expansion Machine". S.A.E. Paper 841336, 1984.

(15) Spicher U, and Kollmeier H P. "Detection of Flame Propagation During Knocking Combustion by Optical Fibre Diagnostics". S.A.E. Paper 861532, 1986.

(16) Konig G, and Sheppard C G W. "End Gas Autoignition and Knock in a Spark Ignition Engine". S.A.E. Paper 902135, 1990.

(17) Austen A E W, and Lyn W T. "Relation between Fuel Injection and Heat Release in a Direct Injection Engine and the Nature of the Combustion Process". Proc. Instn. Mech. Engrs. (A.D.), p.47, 1960-61.

(18) Russell M F, Young C D, and Nicol S W. "Modulation of Injection Rate to Improve Direct Injection Diesel Engine Noise. S.A.E. Paper 900349, 1990.

(18) Draper C S. "Pressure Waves Accompanying Detonation in the Internal Combustion Engine". Journal of The Aeronautical Sciences, Vol. 5, No. 6, (April 1938), pp. 219-226.

(20) Hickling R, Feldmaier D A, and Sung S H. "Knock-induced Cavity Resonances in Open Chamber Diesel Engines." Journal of the Acoustical Society of America, Vol. 65, No. 6, (June 1979), pp. 1474-1479.

(21) Hickling R, Chen F H K, and Feldmaier D A. "Pressure Pulsations in Engine Cylinders". Engine Noise: Excitation, Vibration and Radiation. General Motors Symposium 1982, Plenum Press, pp. 1-37.

(22) Schaberg P W. "Acoustic Characteristics of Petrol Engine Combustion Chambers". B.Sc.(Eng.) Thesis, Department of Mechanical Engineering, University of Cape Town, 1988.

(23) Priede T, Baker J M, Grover E C, and Ghazy R. "Characteristics of Exciting Forces and Structural Response of Turbocharged Diesel Engines". S.A.E. Paper 850972, 1985.

(24) Schaberg P W, Priede T, and Dutkiewicz R K. "Effects of a Rapid Pressure Rise on Engine Vibration and Noise". S.A.E. Paper 900013, 1990.

(25) Priede T, Dixon J, Grover E C, and Saleh N A. "Experimental Techniques Leading to a Better Understanding of the Origins of Automotive Engine Noise". Instn. Mech. Engrs. Paper C151/84, 1984.

(26) Saleh N A. "Investigation of Reciprocating Internal Combustion Engine Structure Response and Vibration Transmission using a Hydraulic Simulation Technique". Ph.D. Thesis, University of Southampton, 1987.

(27) Anderton D, and Priede T. "Applications of Engine Noise Control Research". Engine Noise : Excitation, Vibration and Radiation. General Motors Symposium, 1982, Plenum Press, pp. 1-37.

(28) Raff J A, and Grover E C. "A Primary Noise Generation Mechanism in Petrol Engines". Instn. Mech. Engrs. Conference on Passenger Car Engines, Paper C.320, 1973.

(29) Lalor N, Grover E C, and Priede T. "Engine Noise Due to Mechanical Impacts at Pistons and Bearings." S.A.E. Paper 800402, 1980.

(30) Russell M F. "Automotive Diesel Engine Noise and its Control". S.A.E. Paper 730243, 1973.

(31) Priede T, Grover E C, and Lalor N. "Relation between Noise and Basic Structural Vibration of Diesel Engines". S.A.E. Paper 690450, 1969.

(32) Russell M F. "Combustive noise in automotive diesel engines". Design and Applications in Diesel Engineering, edited by Haddad, S. and Watson, N. Ellis Horwood Limited, Chichester, 1984, pp 203-252.

(33) Priede T. "Noise and Engineering Design". Philosophical Transactions of the Royal Society of London, A.Vol. 263, 1968, p.461.

(34) Champeney D C. Fourier Transforms and their Physical Applications. Academic Press, London, New York, 1973.

(35) Sneddon I N. Fourier Transforms. McGraw-Hill, New York, Toronto, London, 1951.

(36) Papoulis A. The Fourier Integral and its Applications. McGraw-Hill, New York, San Francisco, London, Toronto, 1962.

(37) Randall R B. The Application of B & K Equipment to Frequency Analysis. Bruel & Kjaer, Naerum (Denmark), Second Edition, pp. 5-48, September 1977.

(38) Cooley J W, and Tukey J W. "An Algorithm for the Machine Calculation of Complex Fourier Series". Math. of Comp., Vol. 19, No. 90, pp 297-301, April 1965.

(39) Oppenheim A V, and Schafer R W. Digital Signal Processing. Prentice-Hall, N.J., 1975.

(40) Rabiner L R, and Gold B. Theory and Application of Digital Signal Processing. Prentice-Hall, N.J., 1975.

(41) Bergland G D. "A Guided Tour of the Fast Fourier transform". IEEE Spectrum, Vol. 6, pp 41-52, July 1969.

(42) Skudrzyk E. The Foundations of Acoustics. Springer-Verlag, New York, Wien, 1971, pp. 423-454.

(43) Schaberg P W, Priede T, and Jongens A W D, "Knock Induced Noise and Vibrations in I.C. Engines". Journal of the South African Acoustics Institute, Vol.4, pp. 1-18, 1990.

(44) Pischinger F, Kollmeier H P, and Spicher U, "Das Klopfen im Ottomotor - Ein altes Problem aus neuerer Sicht". Der Arbeitsprozess des Verbrennungsmotors, April 1987.

(45) Konig G, Maly R R, Bradley D, Lau A K C, and Sheppard C G W, "Role of Exothermic Centers on Knock Initiation and Knock Damage". S.A.E. Paper 902136, 1990.

APPENDIX A

DETAILS OF TEST ENGINES

NISSAN L18

Configuration	:	in-line 4 cylinder
Valve gear	:	Single overhead camshaft, 2 valves per cylinder
Fuel management	:	Twin carburetors
Swept Volume	:	1770 cm^3
Bore	:	85.0 mm
Stroke	:	78.0 mm
Compression Ratio	:	9.3 : 1
Standard Spark Timing	:	10° BTDC @ 750 rpm
Combustion Chamber	:	Wedge shape
Maximum Power	:	67 kW at 5500 rpm
Maximum Torque	:	129 Nm at 4000 rpm

VOLKSWAGEN 1800

Configuration	:	in-line 4 cylinder
Valve gear	:	Single overhead camshaft, 2 valves per cylinder
Fuel management	:	Single carburetor
Swept Volume	:	1781 cm^3
Bore	:	81.0 mm
Stroke	:	86.4 mm
Compression Ratio	:	10 : 1
Standard Spark Timing	:	6° BTDC @ 850 rpm
Combustion Chamber	:	Bath tub shape
Maximum Power	:	70 kW at 5200 rpm
Maximum Torque	:	150 Nm at 3500 rpm

TOYOTA 4AF 16V

Configuration	:	in-line 4 cylinder
Valve gear	:	Twin overhead camshafts, 4 valves per cylinder
Fuel management	:	Single carburetor
Swept Volume	:	1587 cm^3
Bore	:	81.0 mm
Stroke	:	77.0 mm
Compression Ratio	:	9.5 : 1
Standard Spark Timing	:	10° BTDC @ 900 rpm
Combustion Chamber	:	Hemispherical shape
Maximum Power	:	70 kW at 6000 rpm
Maximum Torque	:	135 Nm at 3600 rpm

FORD ESSEX V6

Configuration	:	6 cylinder, 60 deg. V
Valve gear	:	Pushrods, 2 valves per cylinder
Fuel management	:	Single carburetor
Swept Volume	:	2993 cm^3
Bore	:	93.67 mm
Stroke	:	72.42 mm
Compression Ratio	:	9.5 : 1
Standard Spark Timing	:	12° BTDC @ 750 rpm
Combustion Chamber	:	Bowl-in-piston
Maximum Power	:	114 kW at 5500 rpm
Maximum Torque	:	220 Nm at 4000 rpm

NISSAN L28

Configuration	:	6 cylinder, in-line
Valve gear	:	Single overhead camshaft, 2 valves per cylinder
Fuel management	:	Single carburetor
Swept Volume	:	2753 cm^3
Bore	:	86.0 mm
Stroke	:	79.0 mm
Compression Ratio	:	8.6 : 1
Standard Spark Timing	:	6° BTDC @ 700 rpm
Combustion Chamber	:	Wedge shape
Maximum Power	:	105 kW at 5000 rpm
Maximum Torque	:	209 Nm at 3000 rpm

TOYOTA 21R

Configuration	:	4 cylinder, in-line
Valve gear	:	Single overhead camshaft, 2 valves per cylinder
Fuel management	:	Single carburetor
Swept Volume	:	1972 cm^3
Bore	:	84.0 mm
Stroke	:	89.0 mm
Compression Ratio	:	9.0 : 1
Standard Spark Timing	:	8° BTDC @ 750 rpm
Combustion Chamber	:	Hemispherical shape
Maximum Power	:	72 kW at 5000 rpm
Maximum Torque	:	160 Nm at 4000 rpm

APPENDIX B

ENGINE INSTRUMENTATION

B.1 ENGINE TEST BEDS

Engine tests were conducted at the two Energy Research Institute engine test cells which are equipped with Heenan and Froude Mk.1 and Mk.2 eddy current brake dynamometers, of 150 bhp and 300 bhp capacity respectively. Engine speed and torque, as well as cooling water and oil temperatures, are indicated and recorded for each test.

B.2 CYLINDER PRESSURE MEASUREMENT

B.2.1 Pressure Transducers

Cylinder pressure measurements were made using AVL type 8QP500c watercooled piezoelectric pressure transducers, flush mounted with the combustion chamber wall. The transducers have a sensitivity of approximately 12 pC/bar and can measure pressures of up to 100 bar. The piezoelectric crystal has a natural frequency of 100 kHz.

The optimum techniques for installing cylinder pressure transducers have been researched [1,2], but these are not always amenable to the particular application, and the engine in question usually dictates the method of installation. Wherever possible, the transducer was mounted as far away from the spark plug, and as close to the exhaust valve, as possible (i.e. in the region where autoignition is most likely to occur), and care was taken to avoid a passage between the combustion chamber and the transducer face.

While it was assumed that the installation of the pressure transducer would not influence the combustion process at all, it is acknowledged that in the case of knock, the transducer may exert an influence on local surface temperatures and heat transfer.

B.2.2 Amplification

A PCB type F462A charge amplifier was used to convert the transducer signal to a voltage suitable for recording.

Because no detailed combustion analyses were to be performed, no measure of the absolute cylinder pressure was made, and an arbitrary zero level of 0 bar was used in the processing of the data.

B.3 CRANKANGLE AND TDC INDICATION

An AVL type 360C optical TDC and crank angle degree marker was used to provide electronic pulses at TDC, as well as at a selectable crankangle interval. In most cases this interval was set at 10 degrees. The TDC mark was set statically, and subsequently calibrated against the pressure signal from a motored cycle. Allowing for the effects of heat transfer, peak motoring pressure was assumed to occur at approximately 0.5 degrees before TDC.

B.4 SPARK TIMING

An inductive pickup on the spark plug HT lead was used in conjunction with an electronic triggering device to provide an electronic pulse at spark plug discharge.

B.5 VIBRATION MEASUREMENT

For vibration measurements, instrumentation varied from engine to engine. A selection of accelerometers and charge amplifiers was used, depending on availability and the application.

B.5.1 Accelerometers

The following accelerometers were used:

1) Bruel and Kjaer type 4367 (sensitivity = 22.0 pC/g)
2) Bruel and Kjaer type 8301 (sensitivity = 9.93 pC/g)
3) Endevco type 213E (sensitivity = 59.6 pC/g)

B.5.2 Amplification

The accelerometer signals were amplified by one of the following charge amplifiers:

1) PCB type F462A charge amplifier
2) Kistler type 5001 charge amplifier
3) Kistler type 503 dual mode amplifier
4) Bruel and Kjaer type 2650 precision conditioning amplifier

B.6 NOISE MEASUREMENTS

Noise measurements were made using a Bruel and Kjaer type 4165 0.5 inch condenser microphone, which has a flat frequency response (within 2 dB) up to a frequency of 20 kHz. The microphone was positioned at a distance of 1.0 m from the side of the engine, in accordance with the SAE standard J1074 for engine noise measurement. Amplification was provided by the Bruel and Kjaer type 2112 Audio Frequency Spectrometer which has an integrated amplifier.

B.7 ELECTRONIC FREQUENCY ANALYSIS

Frequency analysis of the various signals was achieved by three means, namely:

1) A switching 1/3 octave filter set.
2) A real time FFT signal analyser.
3) Fourier analysis of the stored, digitised data.

The first two options are discussed in greater detail below, while the third option is discussed in detail in Chapter 5, which describes the computer program which was written to perform the analysis.

B.7.1 1/3 Octave Filter

On-line noise and vibration spectra were obtained by means of a Bruel and Kjaer type 2112 Audio Frequency Spectrometer in conjunction with a Bruel and Kjaer type 2305 Level Recorder. The spectrometer includes an input amplifier and has 33 analogue third octave band filters with center frequencies ranging from 25 Hz to 40 kHz, as well as "A", "B", and "C" weighting networks. The frequency spectrum is obtained by sequentially switching through the filter set by means of a mechanical switching unit which is synchronised with the level recorder. A 50 dB logarithmic range potentiometer was used in the level recorder to provide noise levels in units of dB re 2 x 10^{-5} Pa.

B.7.2 FFT Frequency Analyser

Averaged cylinder pressure spectra were obtained from the cylinder pressure signal using a Rion SA-71 FFT Signal Analyser. The analyser has a frequency range of 20 kHz and the 12 bit resolution provides a dynamic range of 60 dB or more. The analyser has sufficient memory to store two spectra, and also has a built-in thermal printer, from which printouts of the spectra can be obtained after each analysis.

The sampling period of the analyser is the source of a problem however. Because the cylinder pressure oscillations associated with knock lie at relatively high frequencies (viz. 6 kHz and higher), it is necessary to utilise the whole 20 kHz bandwidth available from the instrument. At this setting, 512 points are sampled at 51.2 kHz, resulting in a data capture period of only 10 milliseconds, which, at the lowest engine speed of 1500 rpm, only covers 90 degrees crankangle. There is thus a chance that the part of the engine cycle over which knock occurs will be missed, unless the data acquisition is triggered accurately. At any rate, it is not possible to capture the whole 720 degree cycle, unless the sampling frequency is reduced. The problem can be overcome to a certain extent, however, by taking a large number of samples and averaging them. Another solution is to take one spectrum, triggered near TDC on the power stroke, at the maximum sampling rate, in order to investigate the knocking frequencies, and to take another at a sampling rate low enough to capture the whole 720 degree cycle accurately.

The Rion analyser also offers third octave spectrum analysis for noise and vibration signals, but without the option of a selectable trigger point. As each third octave analysis uses three sets of data captured at different sampling rates to synthesise the spectrum, the time required for the procedure is, however, too long for a large number of averages to be made. It was therefore decided that this was not a suitable option for obtaining noise and vibration spectra.

B.8 DATA ACQUISITION

The cylinder pressure traces, vibration oscillograms, and spark, TDC and crankangle signals were all recorded simultaneously using an ISC-16 Computerscope data acquisition system supplied by RC Electronics. The system comprises a hardware card which is installed in one of the expansion slots

of an IBM PC-XT computer, as well as driver software. Up to 16 input channels may be multiplexed to a 12 bit analogue to digital converter capable of sampling at a maximum rate of 1 MHz. An input range of -10 to +10 volts is allowed and the card has a 64 kB on-board memory buffer, allowing up to 65536 samples to be captured and saved on magnetic disk for subsequent analysis.

The spark and TDC signals were superimposed and the signal recorded on one channel of the A/D system. The pressure and acceleration signals were each recorded on separate channels, and for most of the tests done, the digitisation rate for each channel was set at 125 kHz. The 12 bit digital resolution gives a dynamic range of approximately 72 dB. The data are temporarily stored on the host computer's hard disk while the tests are in progress, and are subsequently transferred to floppy diskettes for permanent storage and later analysis.

B.9 REFERENCES

(1) Randolph A L, "Cylinder-Pressure-Transducer Mounting Techniques to Maximise Data Accuracy". S.A.E. Paper 900171.

(1) Randolph A L, "Methods of Processing Cylinder-Pressure Transducer Signals to Maximise Data Accuracy". S.A.E. Paper 900170.

APPENDIX C

RESULTS OF ENGINE NOISE TESTS

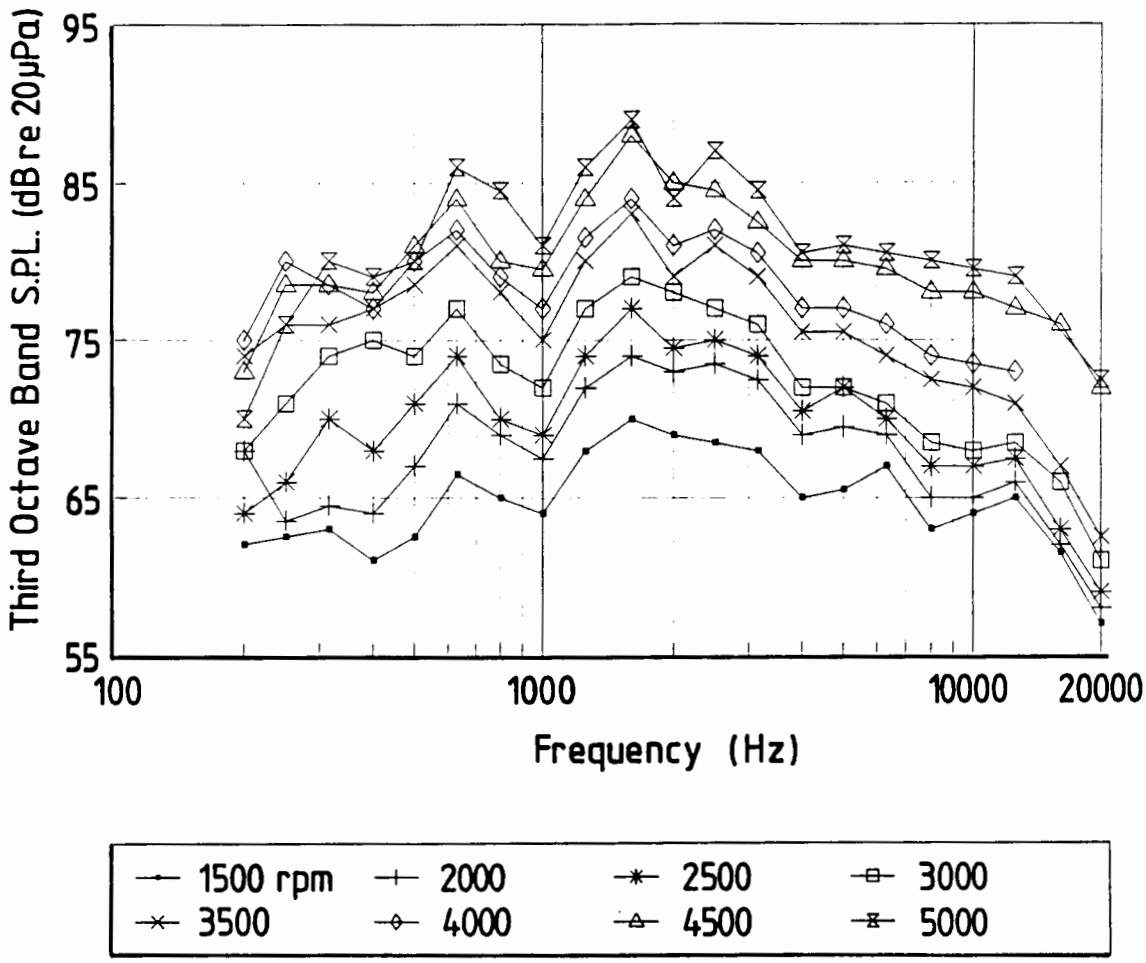

Figure C.1 Noise spectra recorded over the speed range.

Engine : Nissan L28
Spark Timing : 5° BTDC
Fuel : 93 RON gasoline

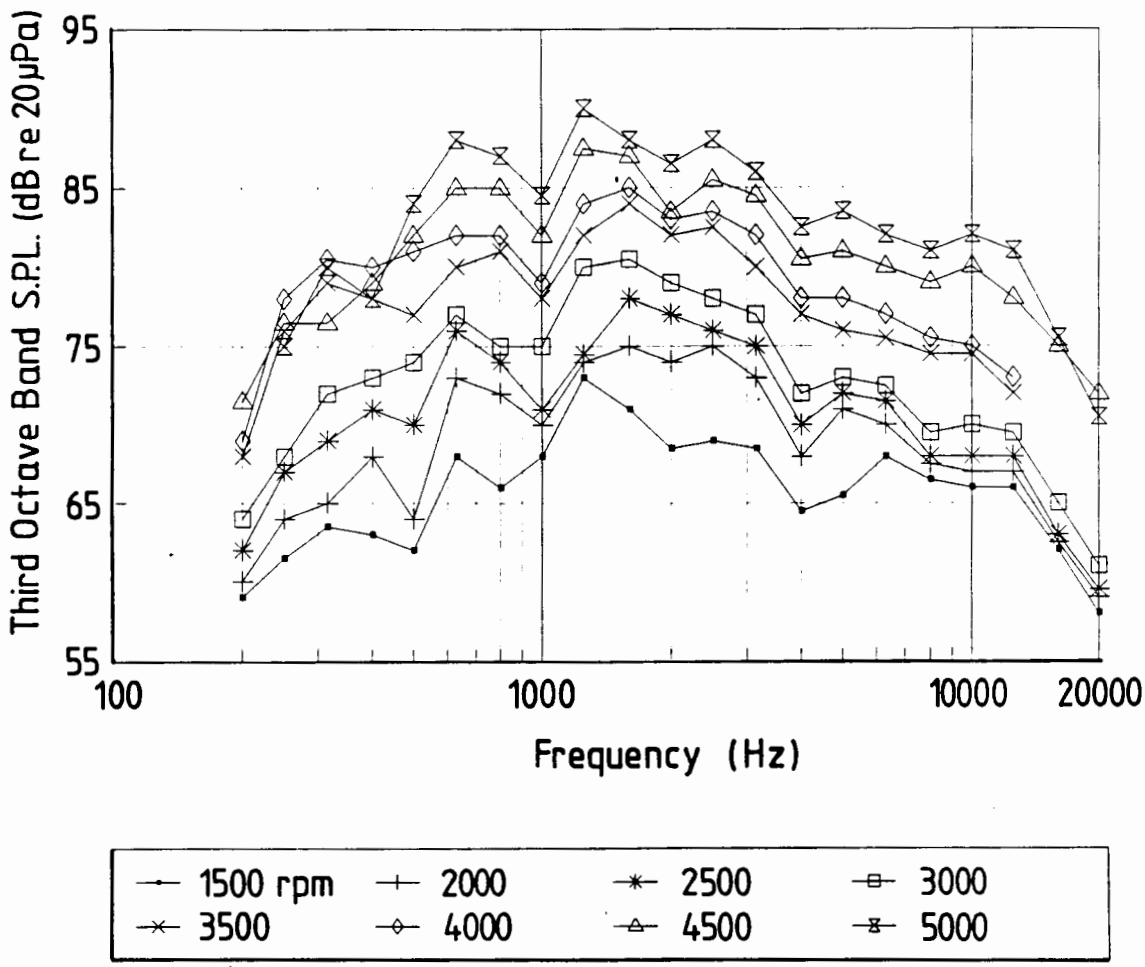

Figure C.2 Noise spectra recorded over the speed range.

Engine : Nissan L28
Spark Timing : 10° BTDC
Fuel : 98 RON gasoline

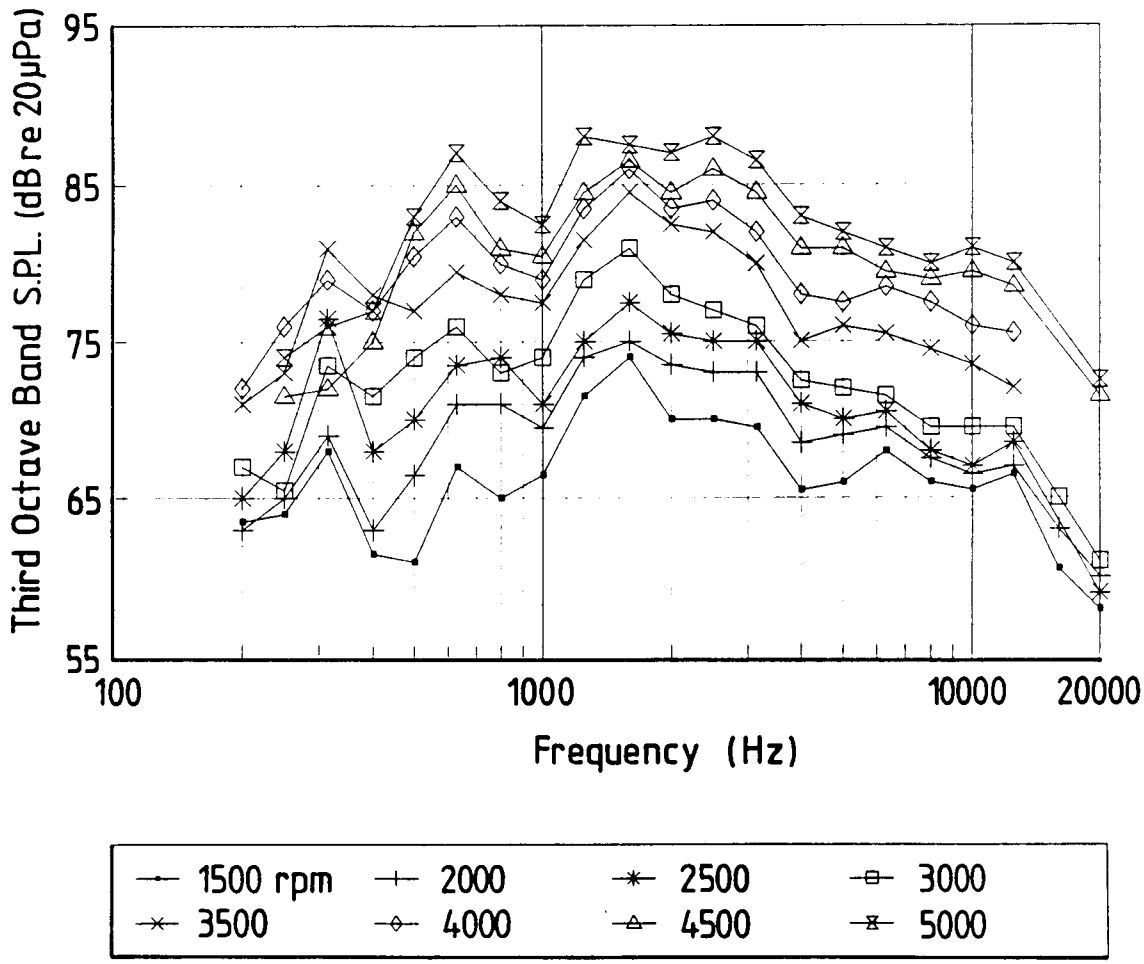

Figure C.3 Noise spectra recorded over the speed range.

Engine : Nissan L28
Spark Timing : 10° BTDC
Fuel : 93 RON gasoline

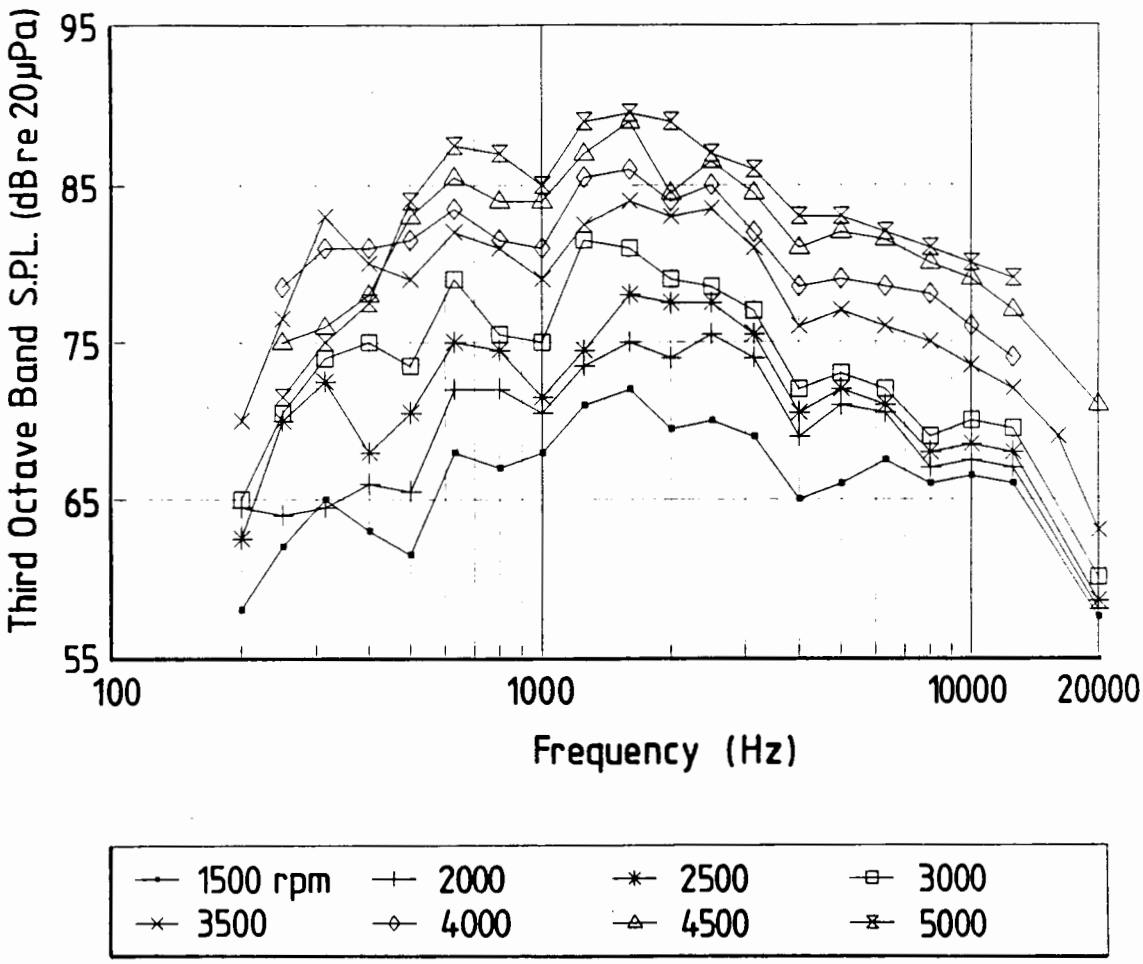

Figure C.4 Noise spectra recorded over the speed range.

Engine : Nissan L28
Spark Timing : 15° BTDC
Fuel : 98 RON gasoline

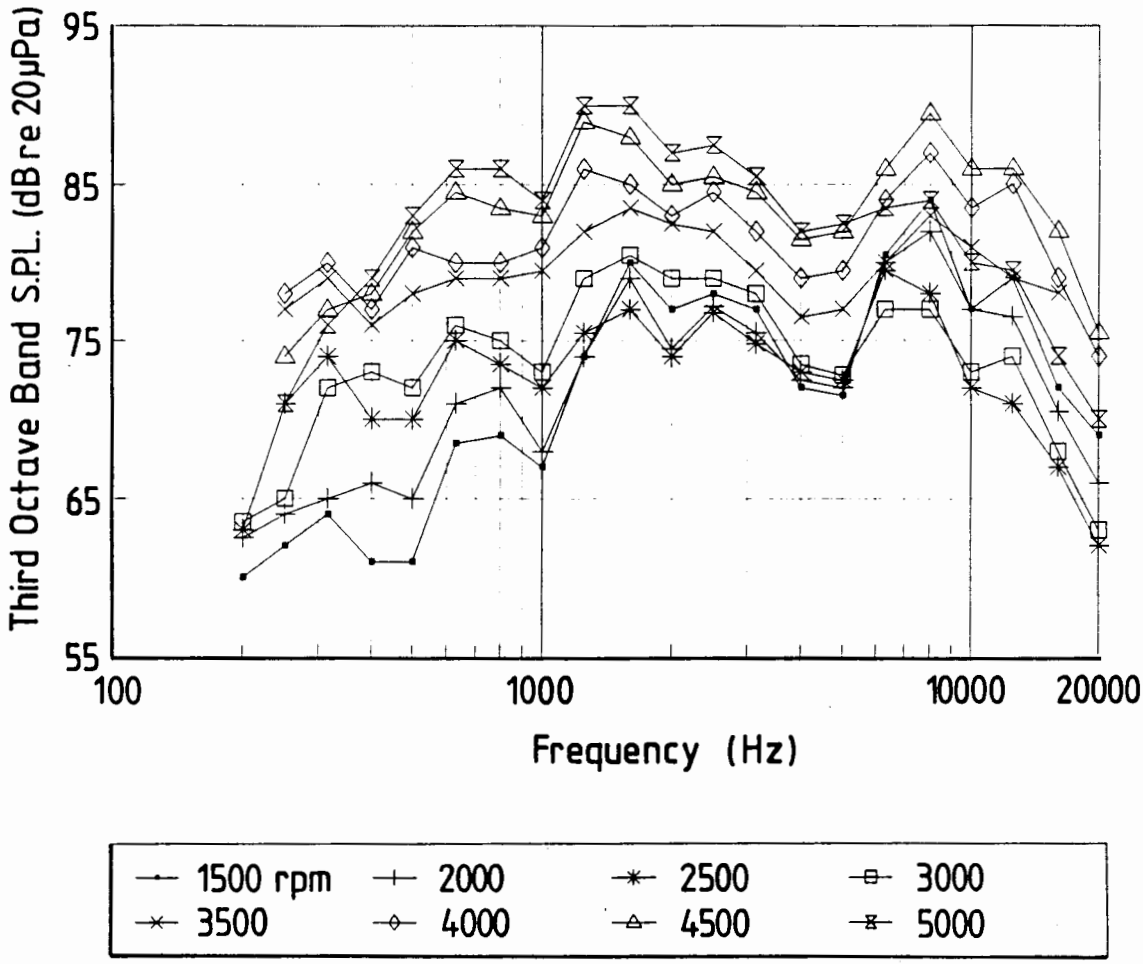

Figure C.5 Noise spectra recorded over the speed range.

Engine : Nissan L28
Spark Timing : 15° BTDC
Fuel : 93 RON gasoline

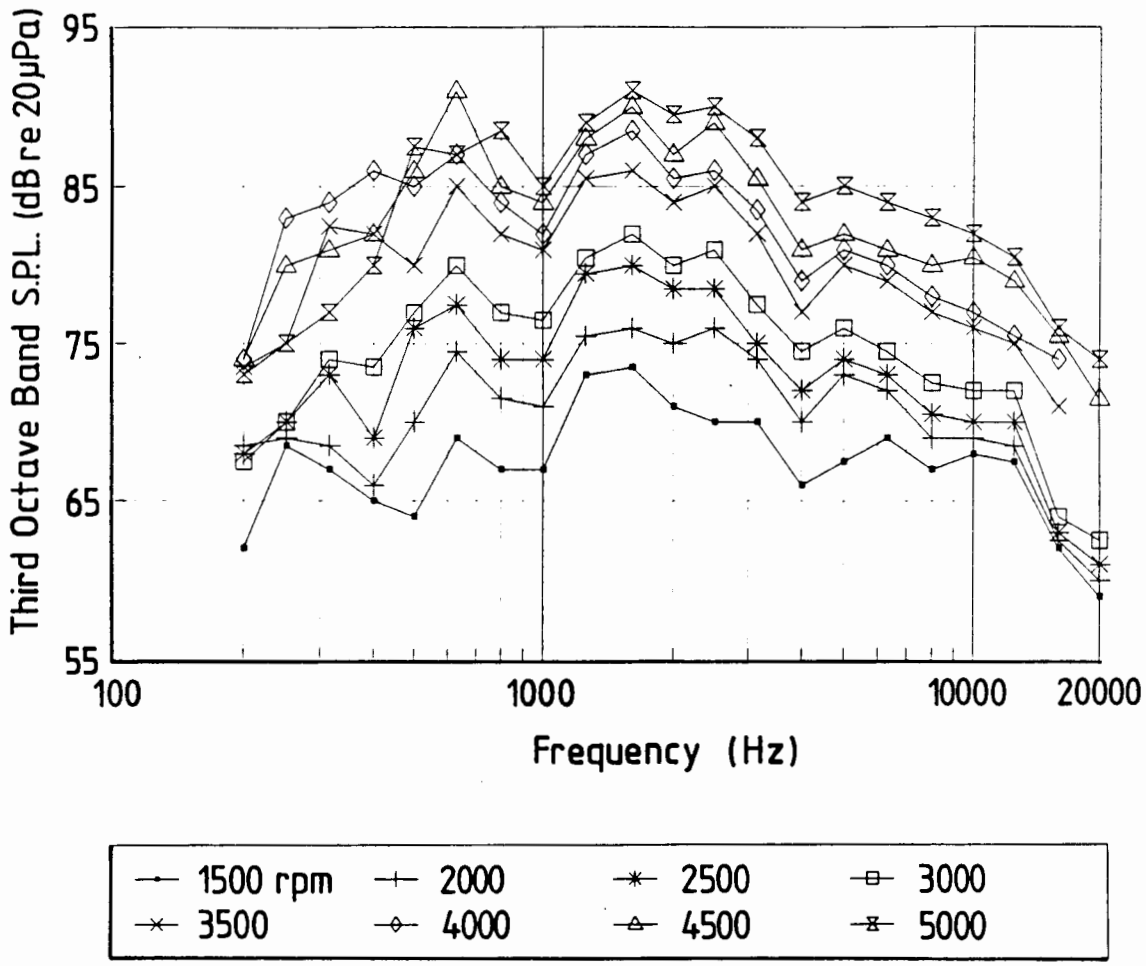

Figure C.6 Noise spectra recorded over the speed range.

Engine : Nissan L28
Spark Timing : 20° BTDC
Fuel : Aviation gasoline (AvGas)

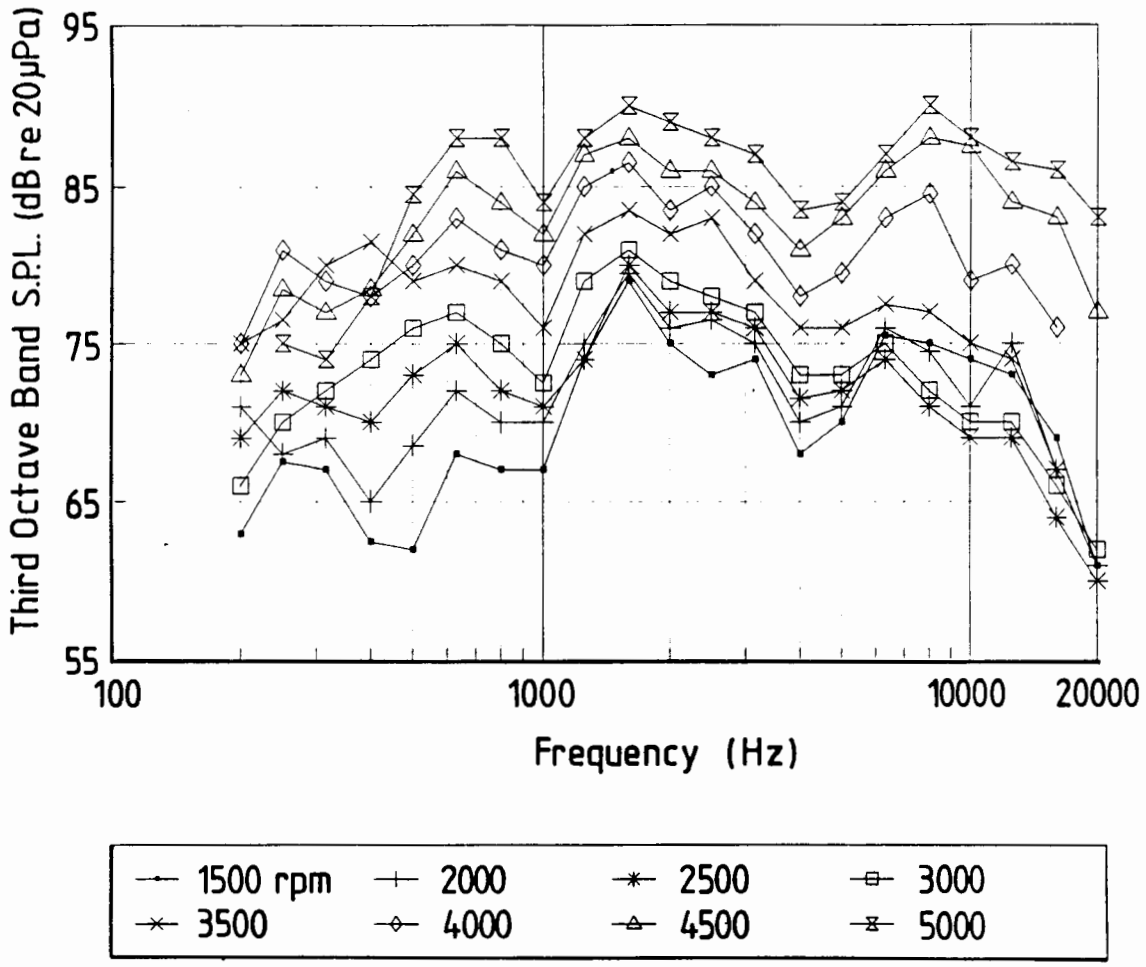

Figure C.7 Noise spectra recorded over the speed range.

Engine : Nissan L28
Spark Timing : 20° BTDC
Fuel : 93 RON gasoline

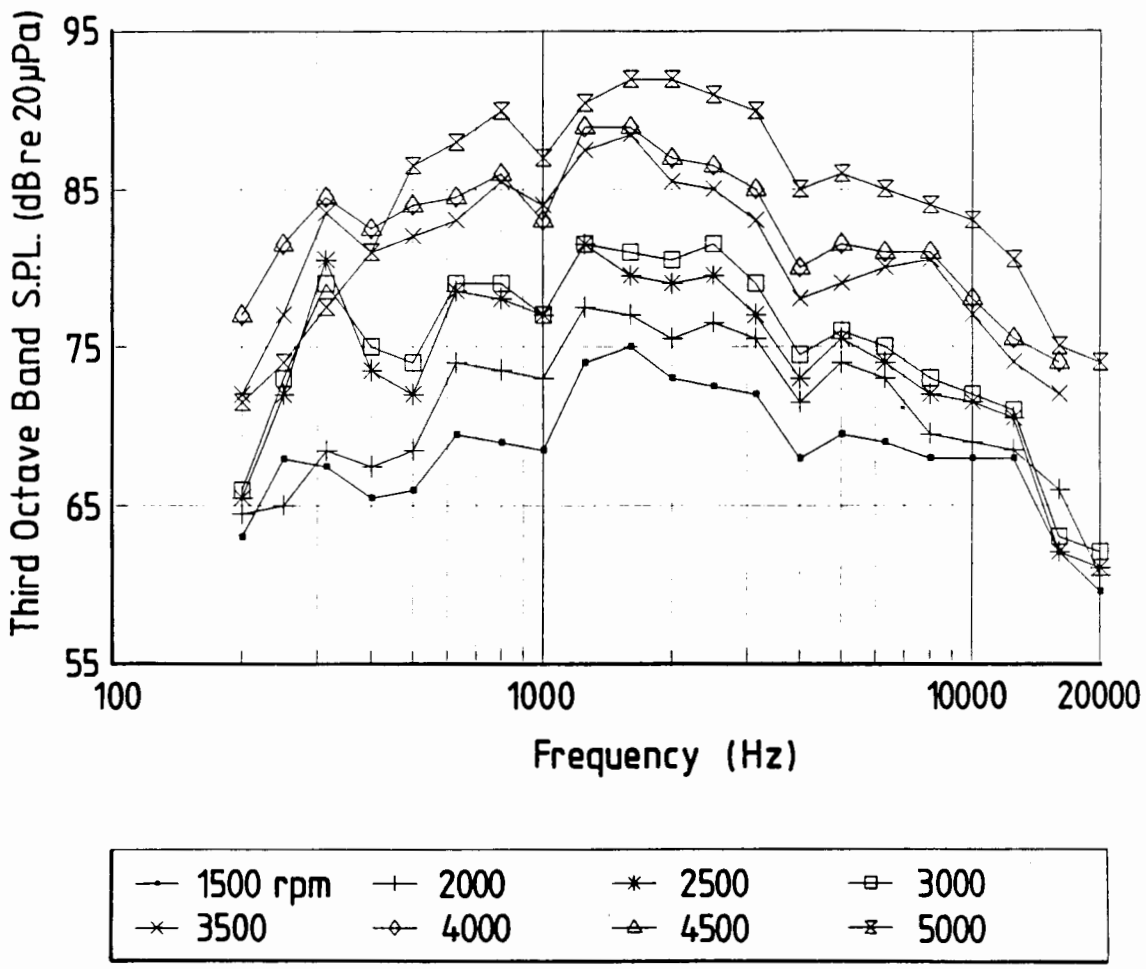

Figure C.8 Noise spectra recorded over the speed range.

Engine : Nissan L28
Spark Timing : 25° BTDC
Fuel : Aviation gasoline (AvGas)

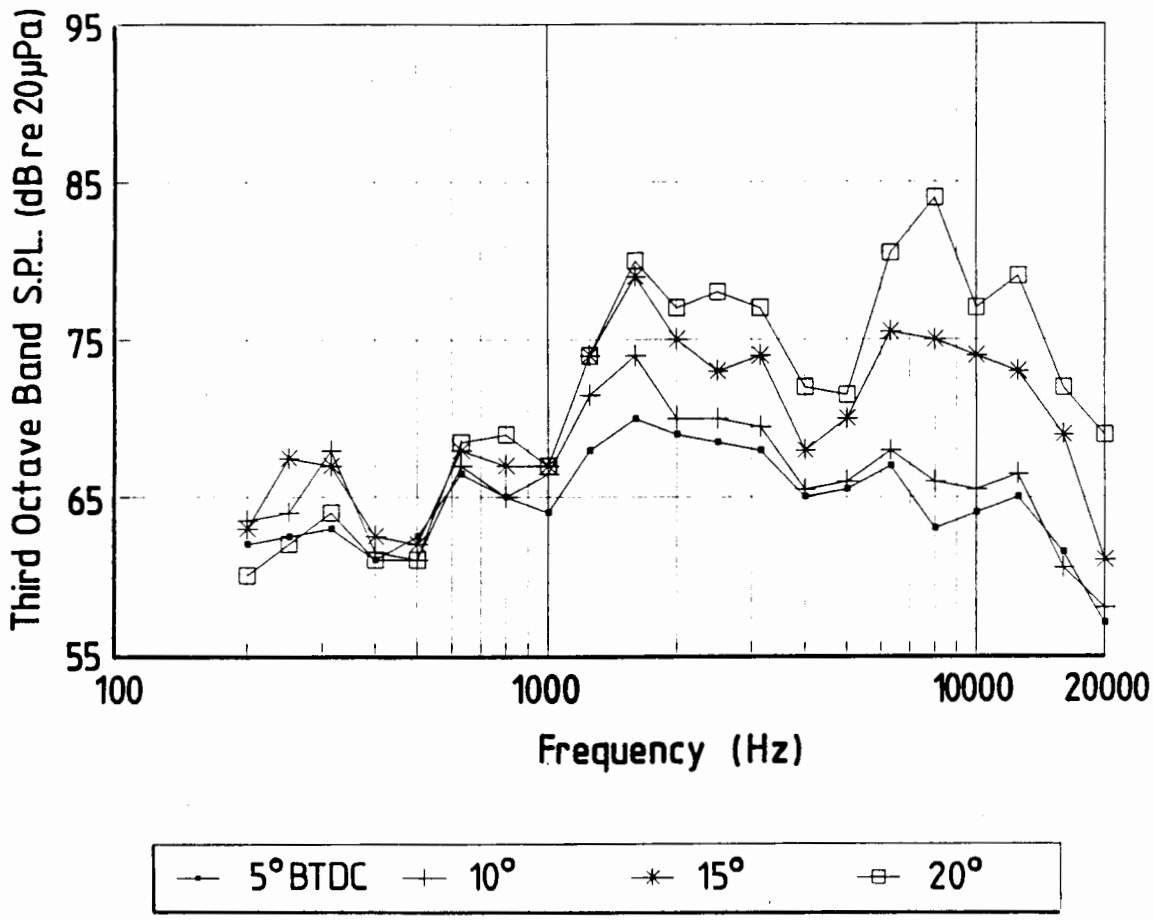

Figure C.9 Noise spectra recorded over a range of spark advance settings.

Engine : Nissan L28
Engine Speed : 1500 rpm
Fuel : 93 RON gasoline

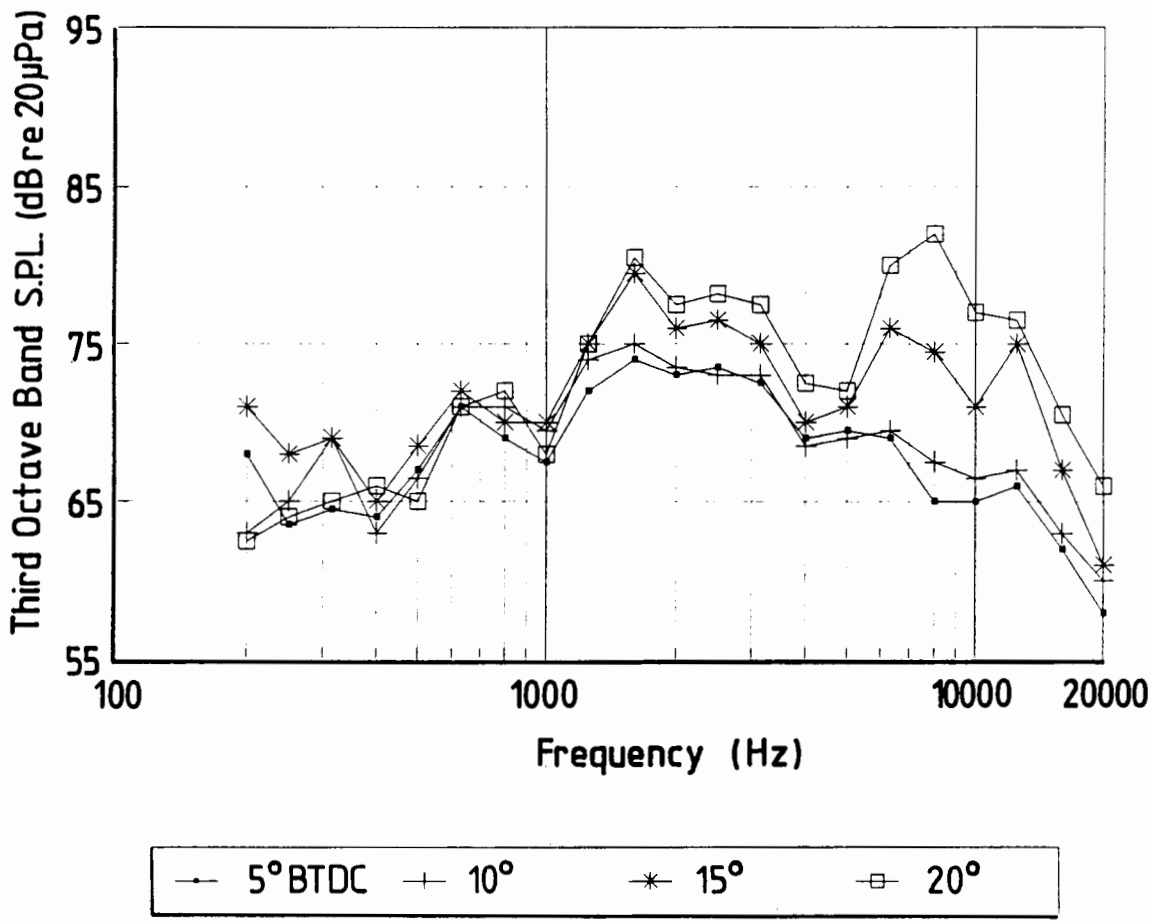

Figure C.10 Noise spectra recorded over a range of spark advance settings.

Engine : Nissan L28
Engine Speed : 2000 rpm
Fuel : 93 RON gasoline

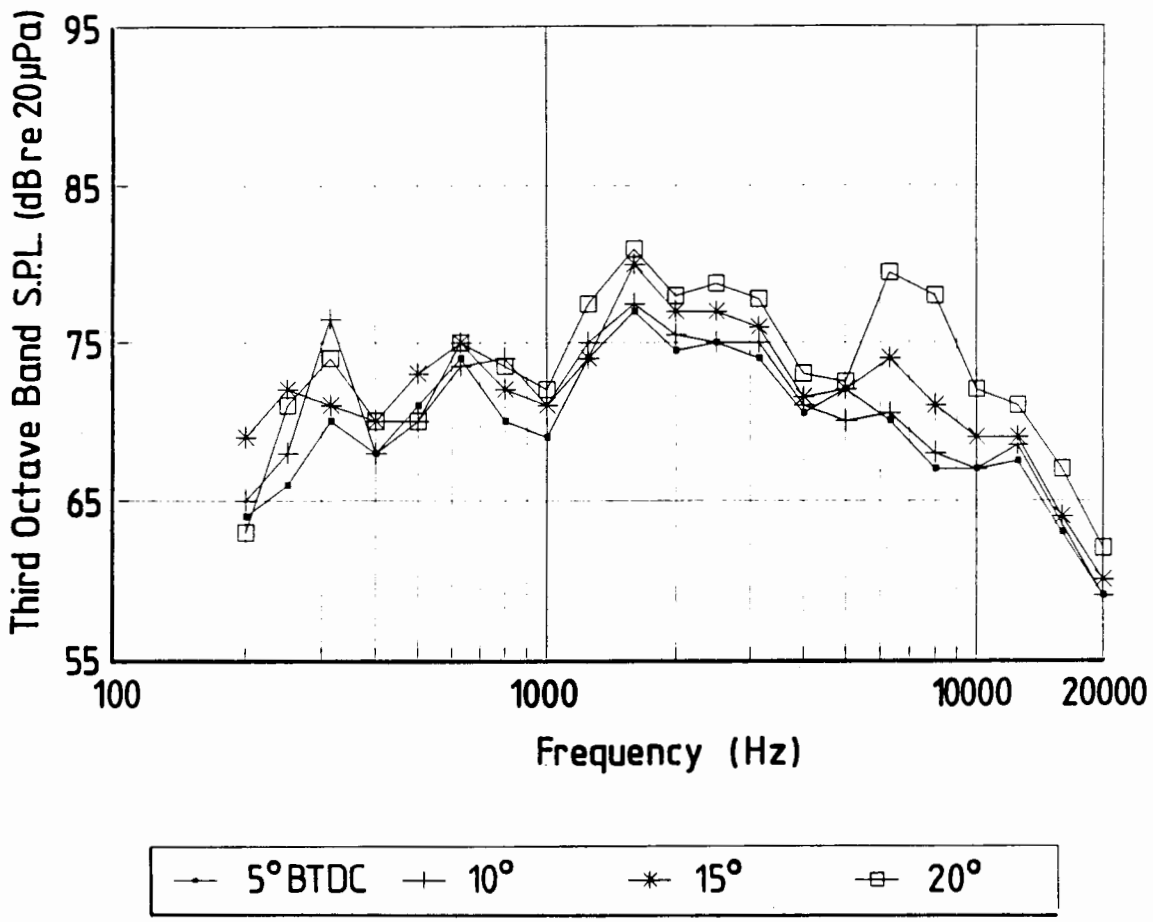

Figure C.11 Noise spectra recorded over a range of spark advance settings.

Engine : Nissan L28
Engine Speed : 2500 rpm
Fuel : 93 RON gasoline

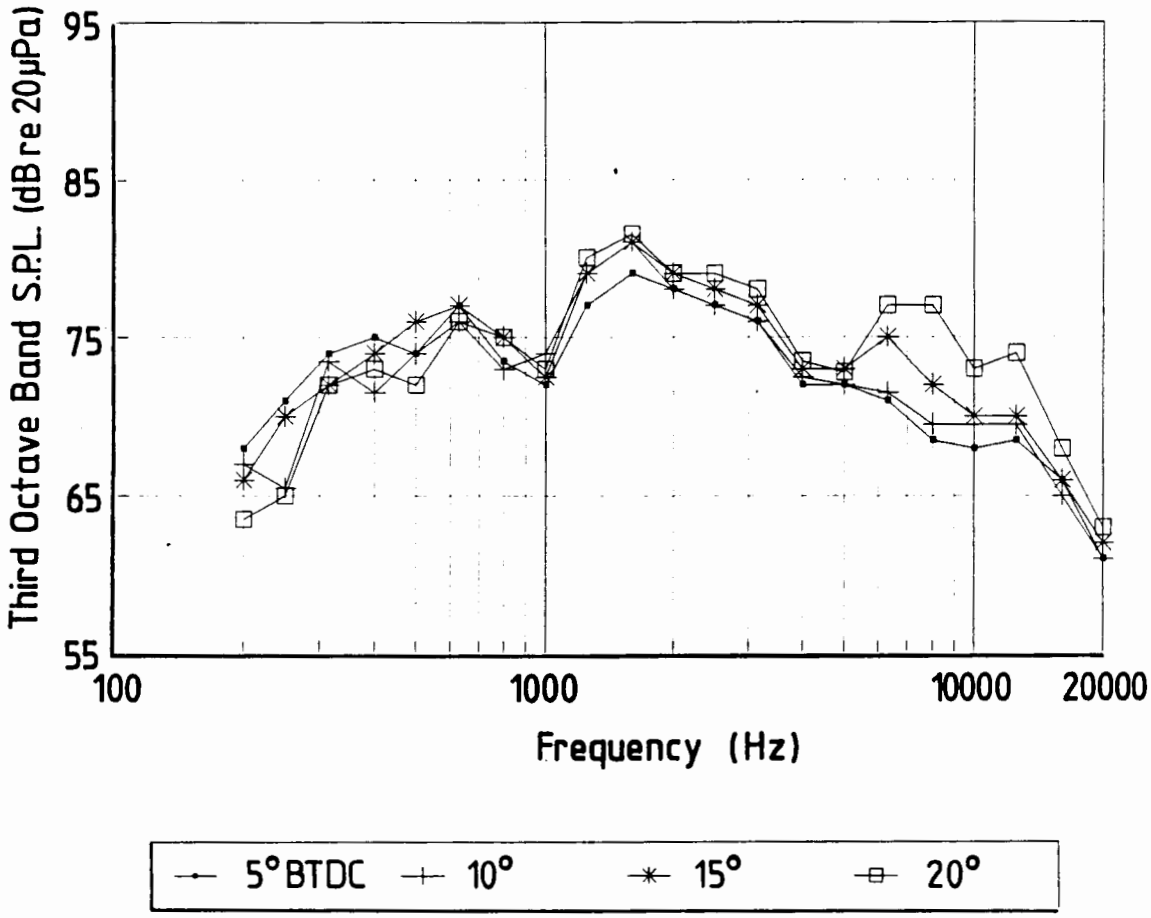

Figure C.12 Noise spectra recorded over a range of spark advance settings.

Engine : Nissan L28
Engine Speed : 3000 rpm
Fuel : 93 RON gasoline

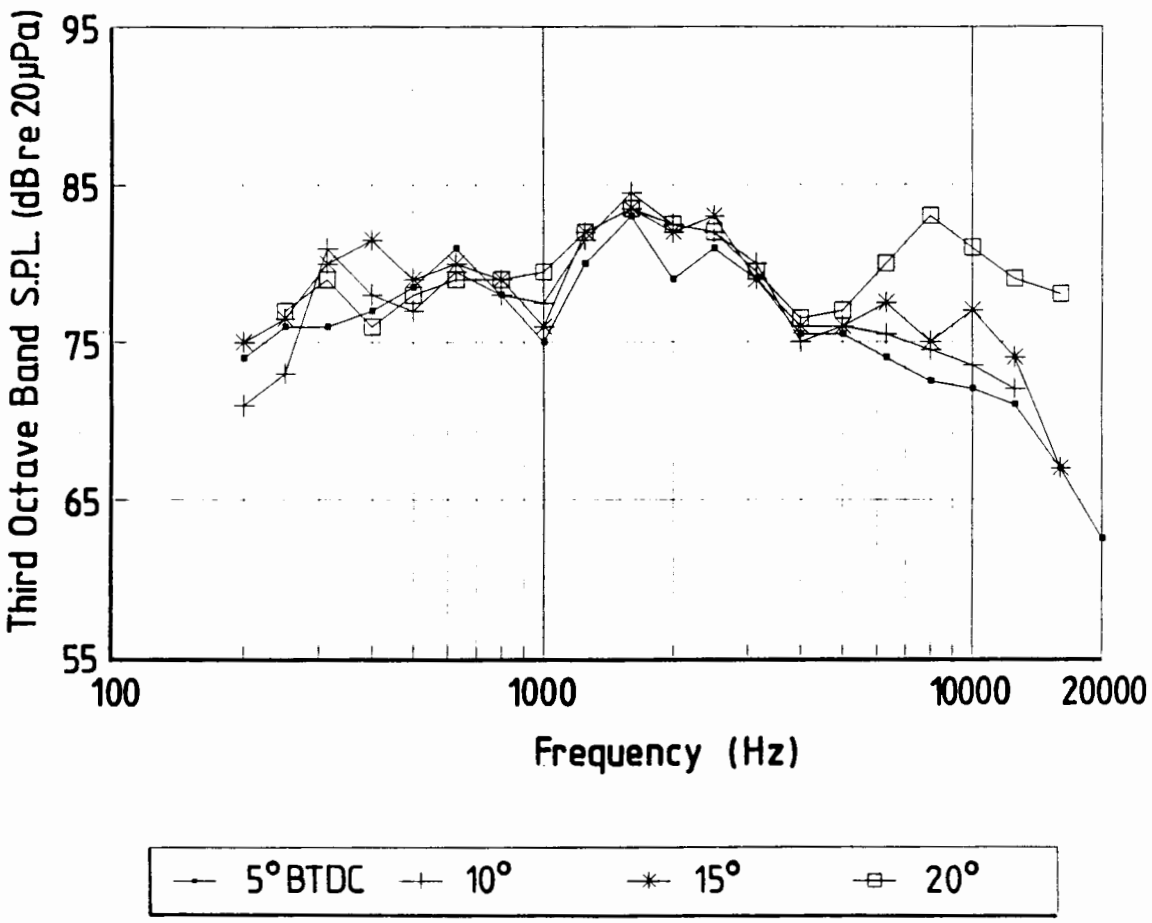

Figure C.13 Noise spectra recorded over a range of spark advance settings.

Engine : Nissan L28
Engine Speed : 3500 rpm
Fuel : 93 RON gasoline

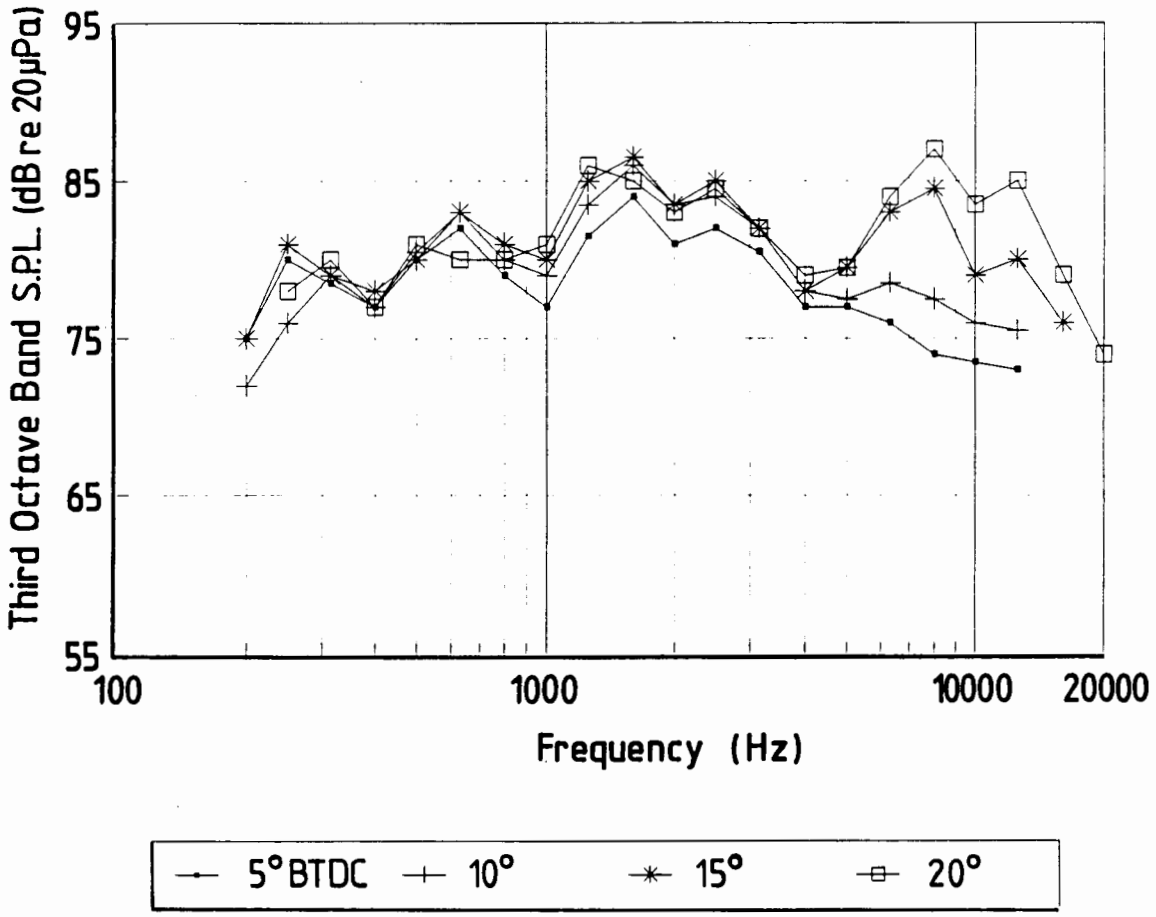

Figure C.14 Noise spectra recorded over a range of spark advance settings.

Engine : Nissan L28
Engine Speed : 4000 rpm
Fuel : 93 RON gasoline

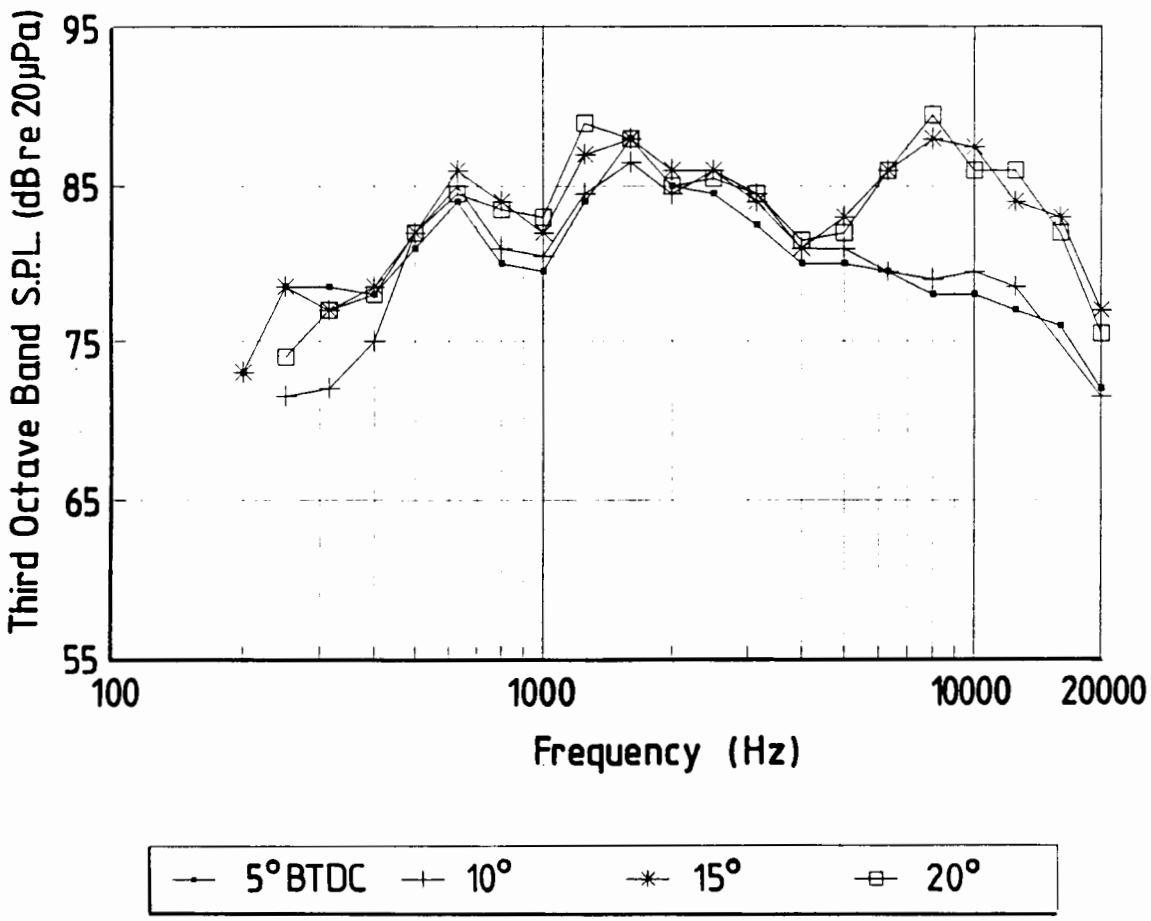

Figure C.15 Noise spectra recorded over a range of spark advance settings.

Engine : Nissan L28
Engine Speed : 4500 rpm
Fuel : 93 RON gasoline

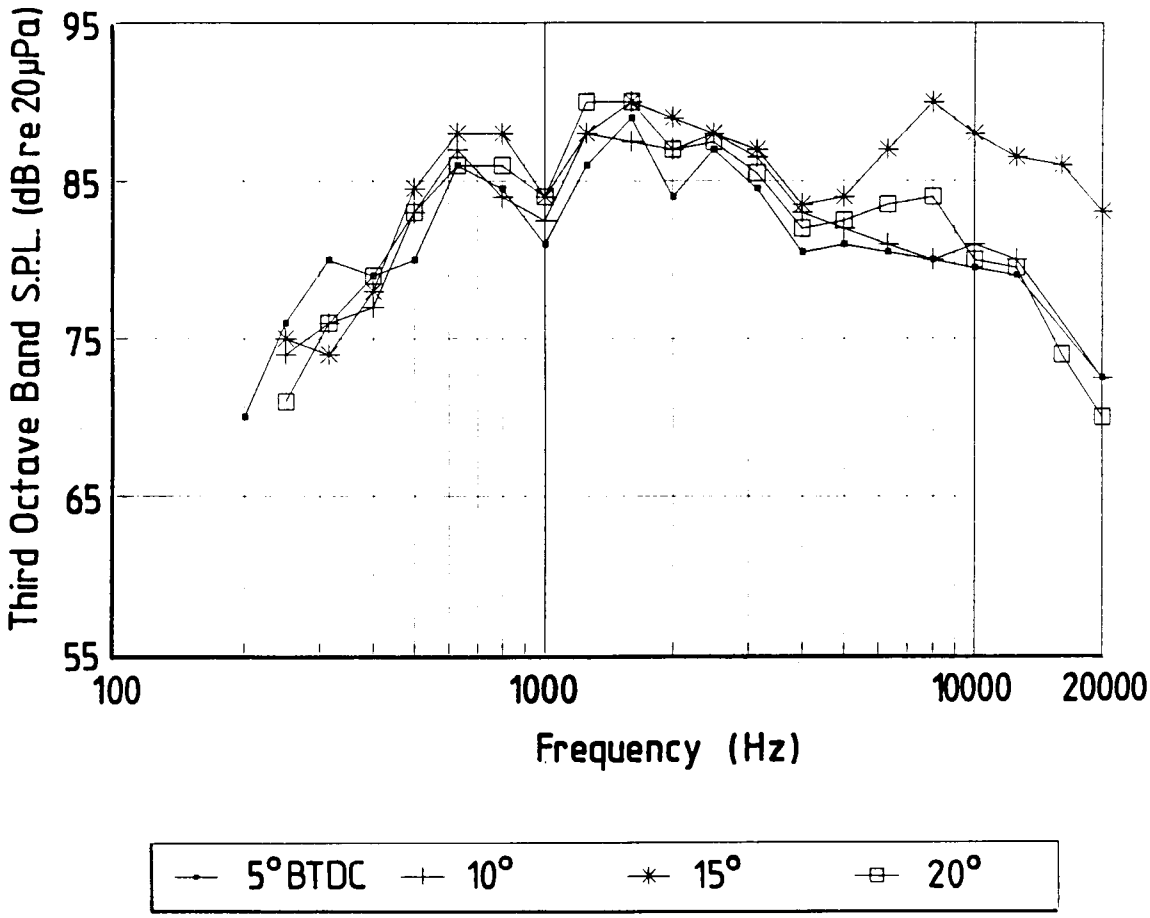

Figure C.16 Noise spectra recorded over a range of spark advance settings.

Engine : Nissan L28
Engine Speed : 5000 rpm
Fuel : 93 RON gasoline

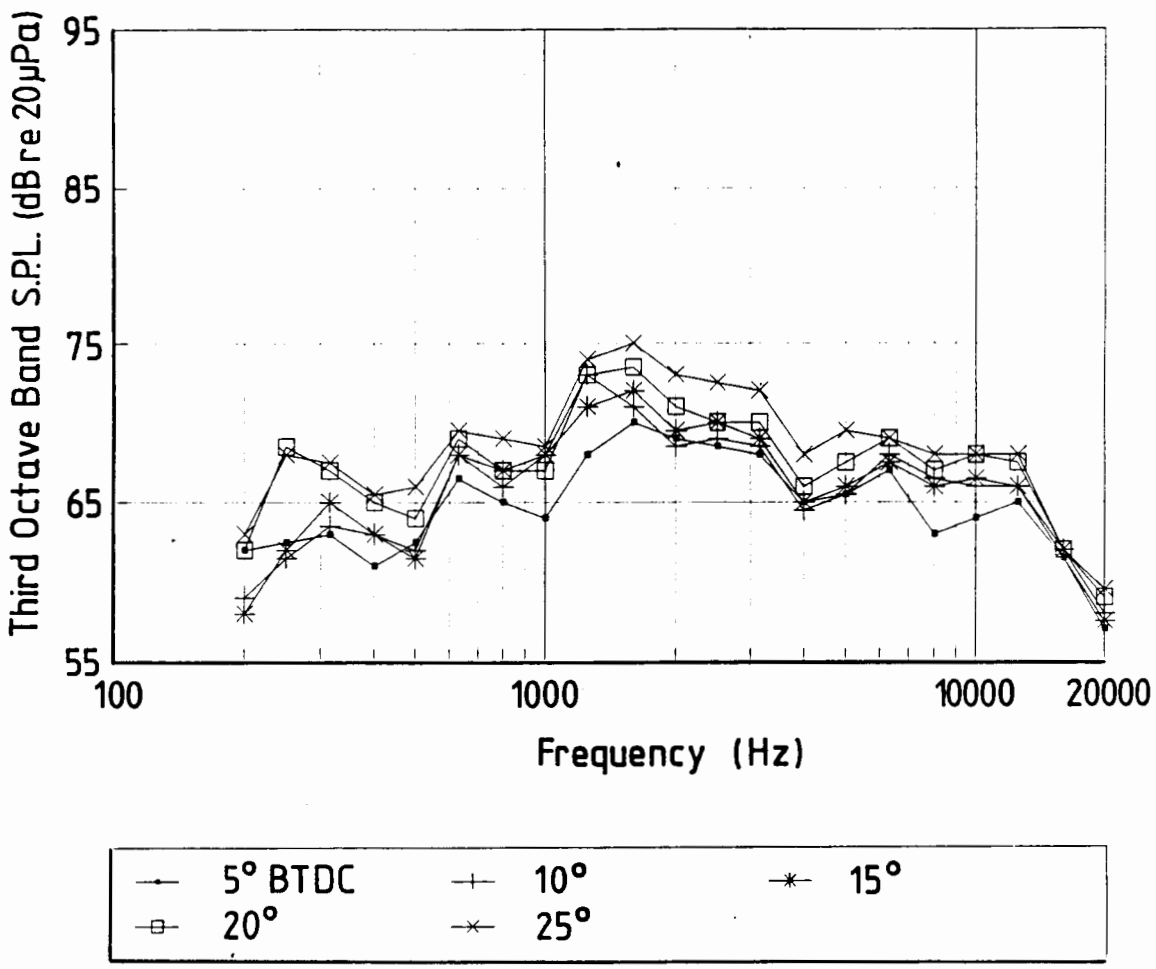

Figure C.17 Noise spectra recorded over a range of spark advance settings.

Engine : Nissan L28
Engine Speed : 1500 rpm
Fuel : 98 RON gasoline or AvGas

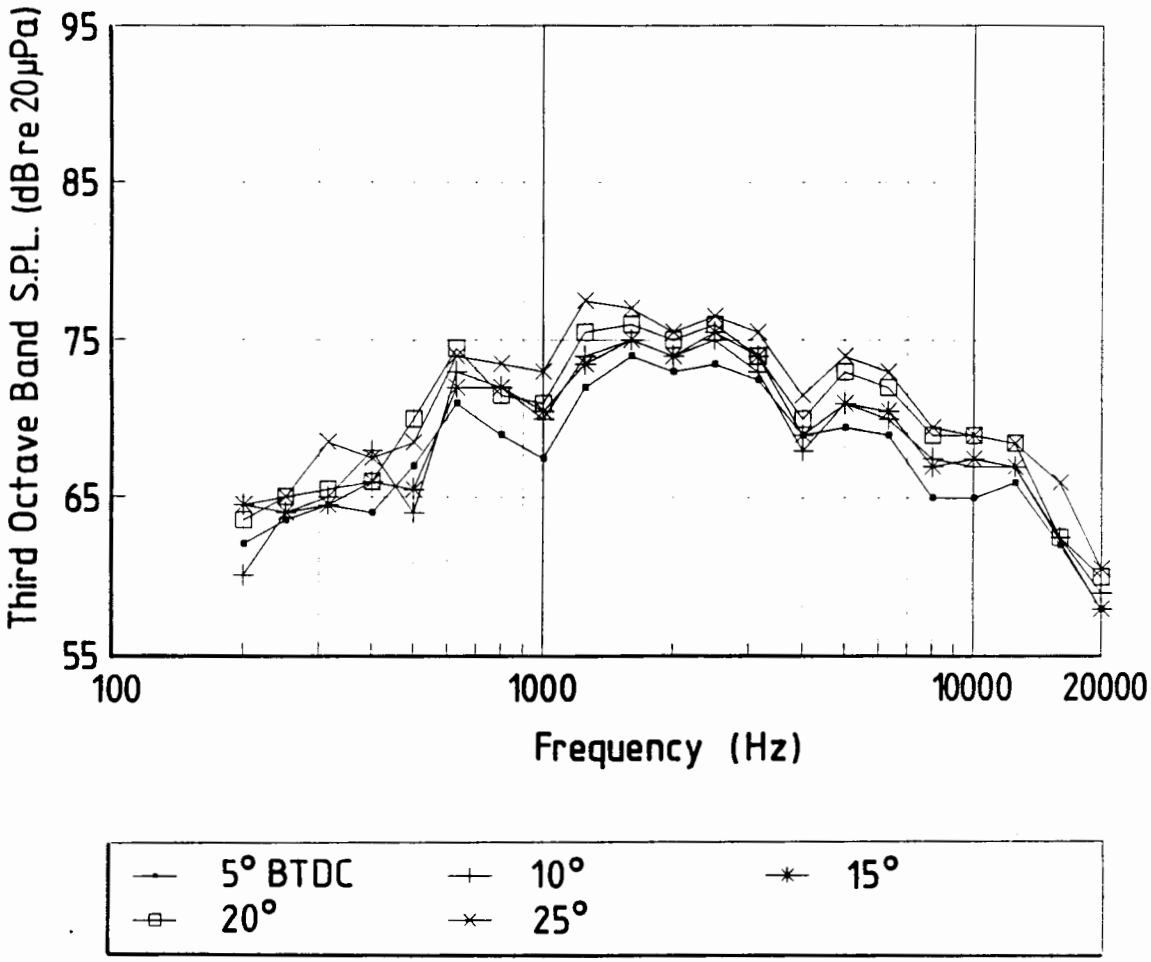

Figure C.18 Noise spectra recorded over a range of spark advance settings.

Engine : Nissan L28
Engine Speed : 2000 rpm
Fuel : 98 RON gasoline or AvGas

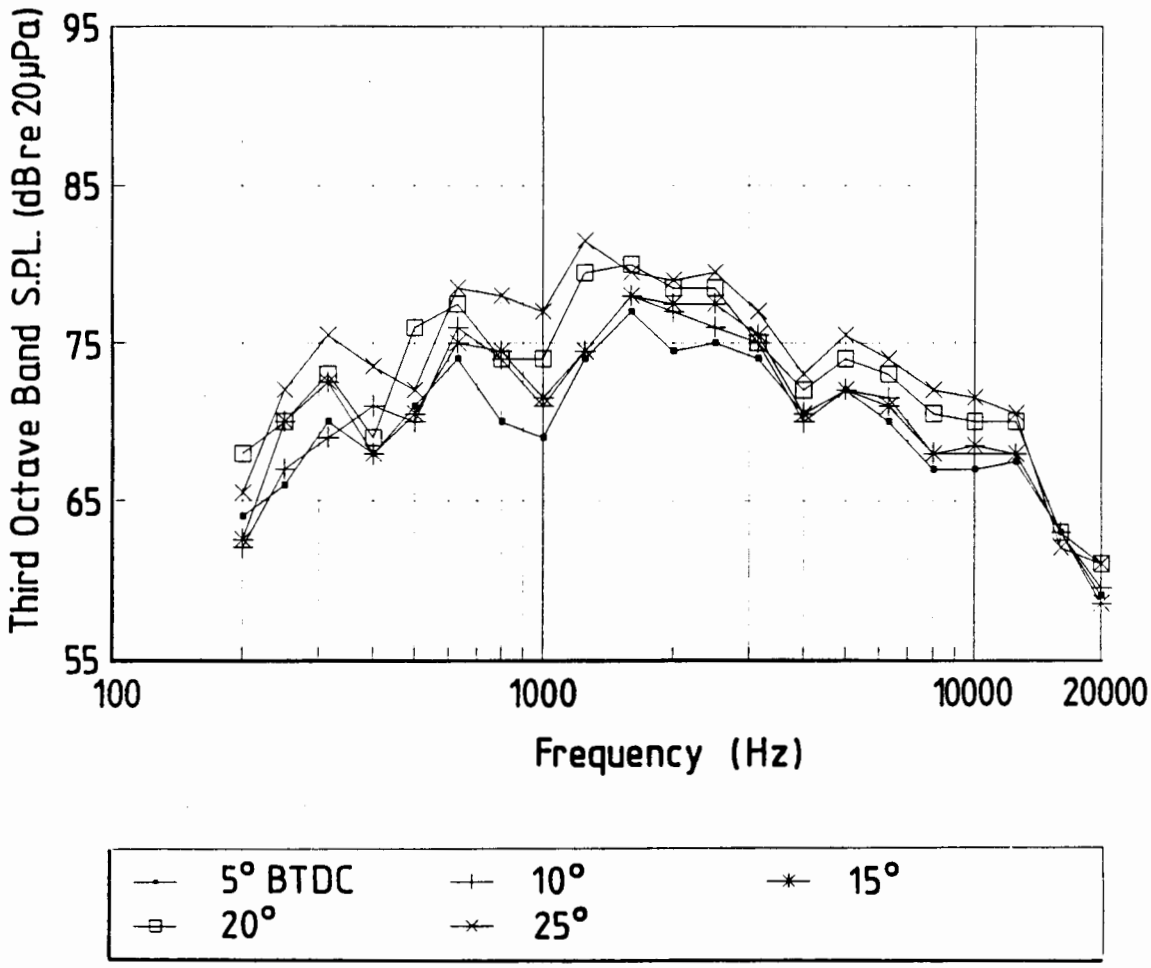

Figure C.19 Noise spectra recorded over a range of spark advance settings.

Engine : Nissan L28
Engine Speed : 2500 rpm
Fuel : 98 RON gasoline or AvGas

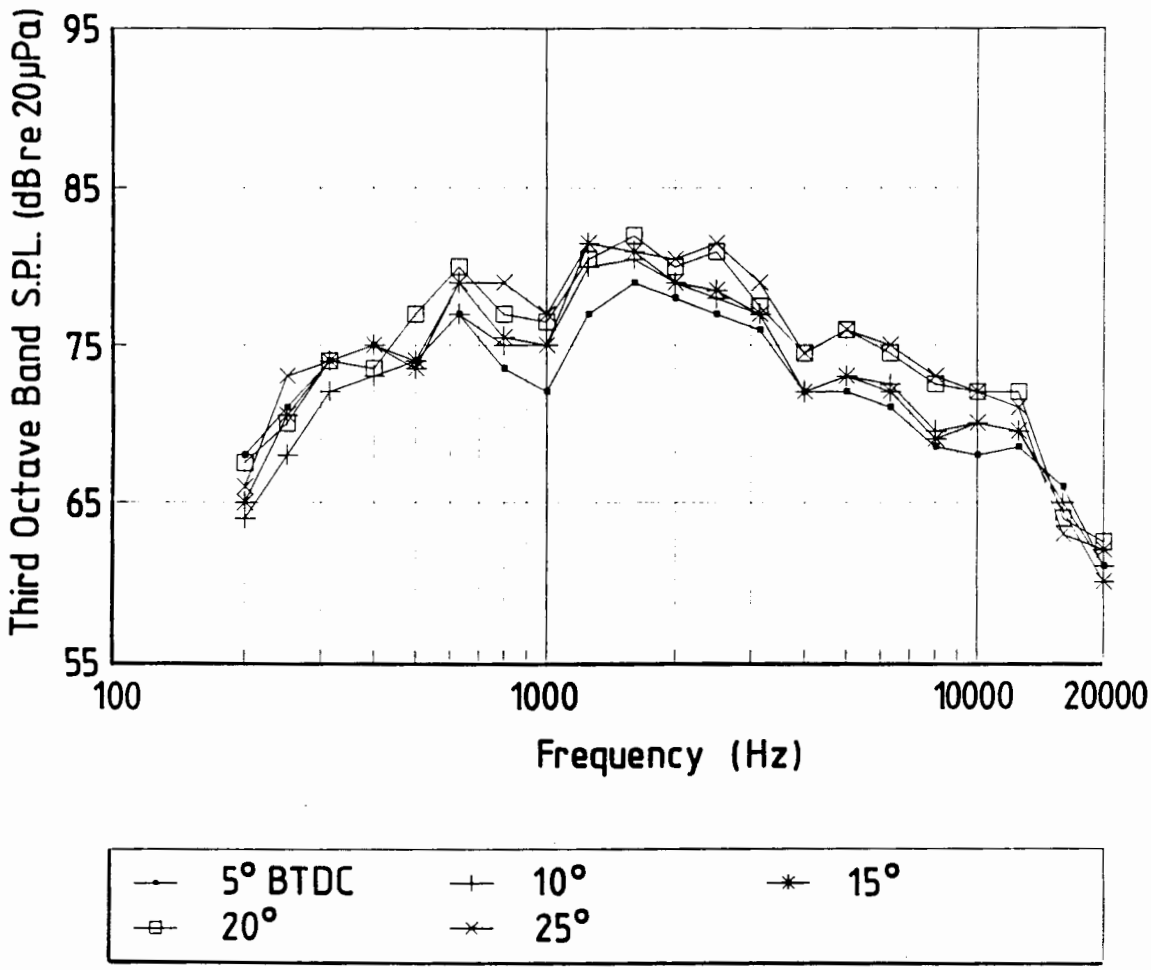

Figure C.20 Noise spectra recorded over a range of spark advance settings.

Engine : Nissan L28
Engine Speed : 3000 rpm
Fuel : 98 RON gasoline or AvGas

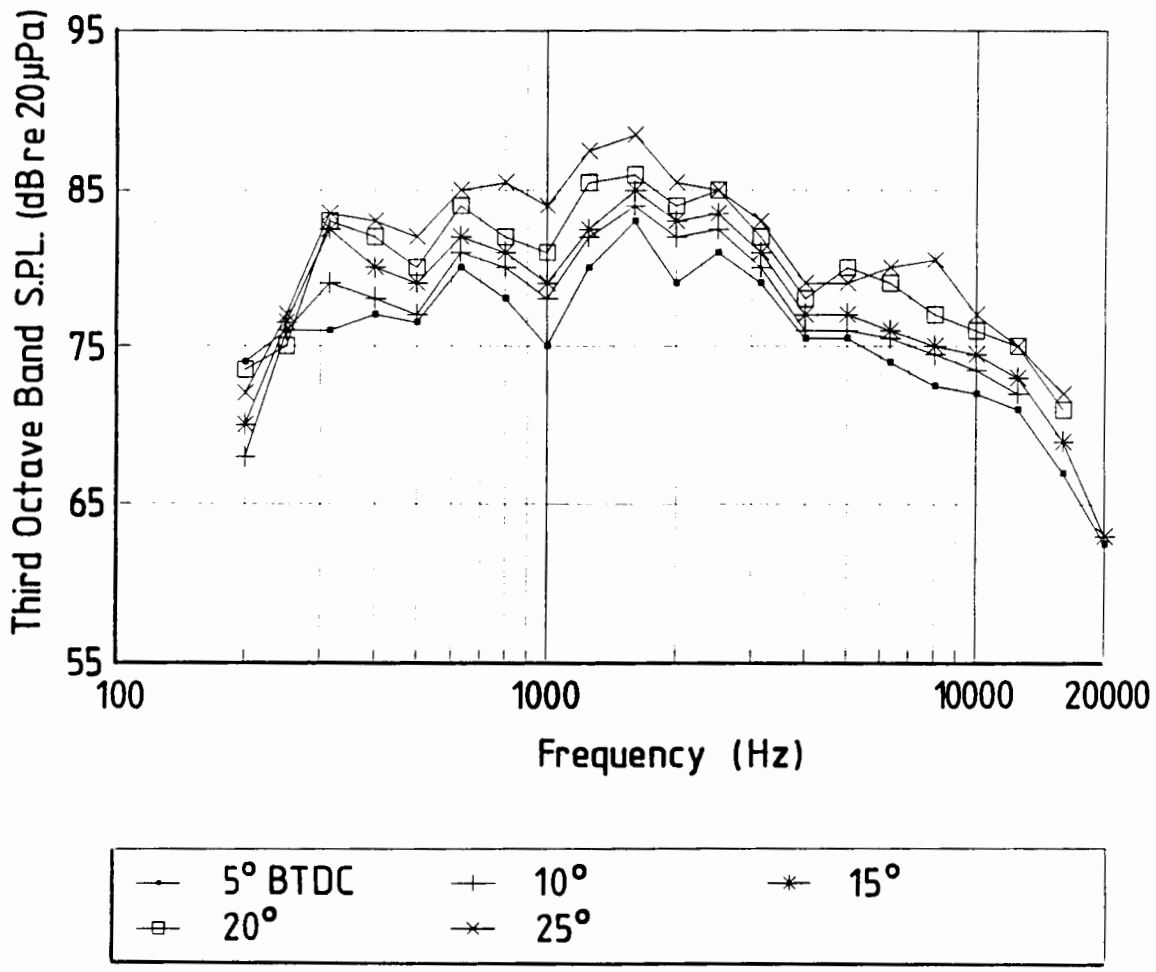

Figure C.21 Noise spectra recorded over a range of spark advance settings.

Engine : Nissan L28
Engine Speed : 3500 rpm
Fuel : 98 RON gasoline or AvGas

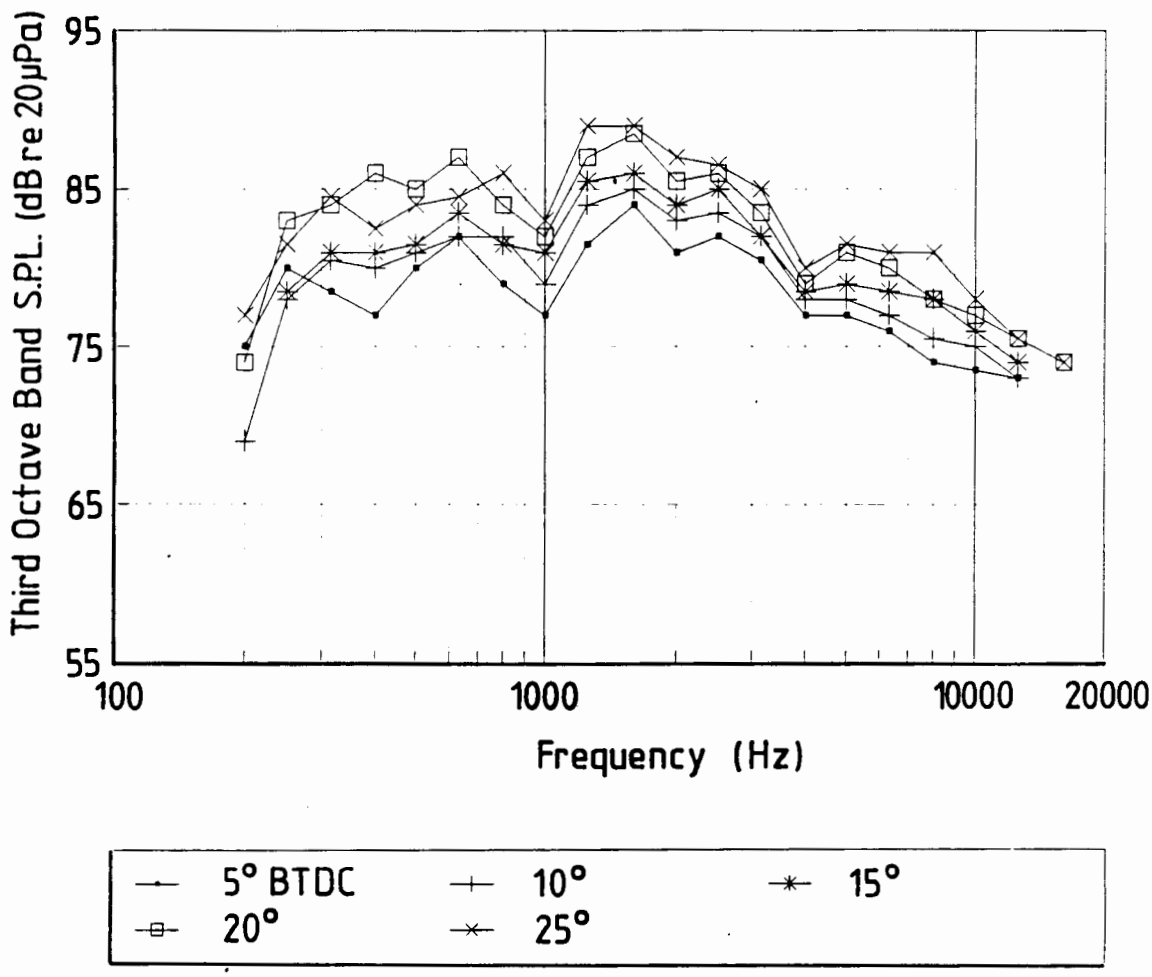

Figure C.22 Noise spectra recorded over a range of spark advance settings.

Engine : Nissan L28
Engine Speed : 4000 rpm
Fuel : 98 RON gasoline or AvGas

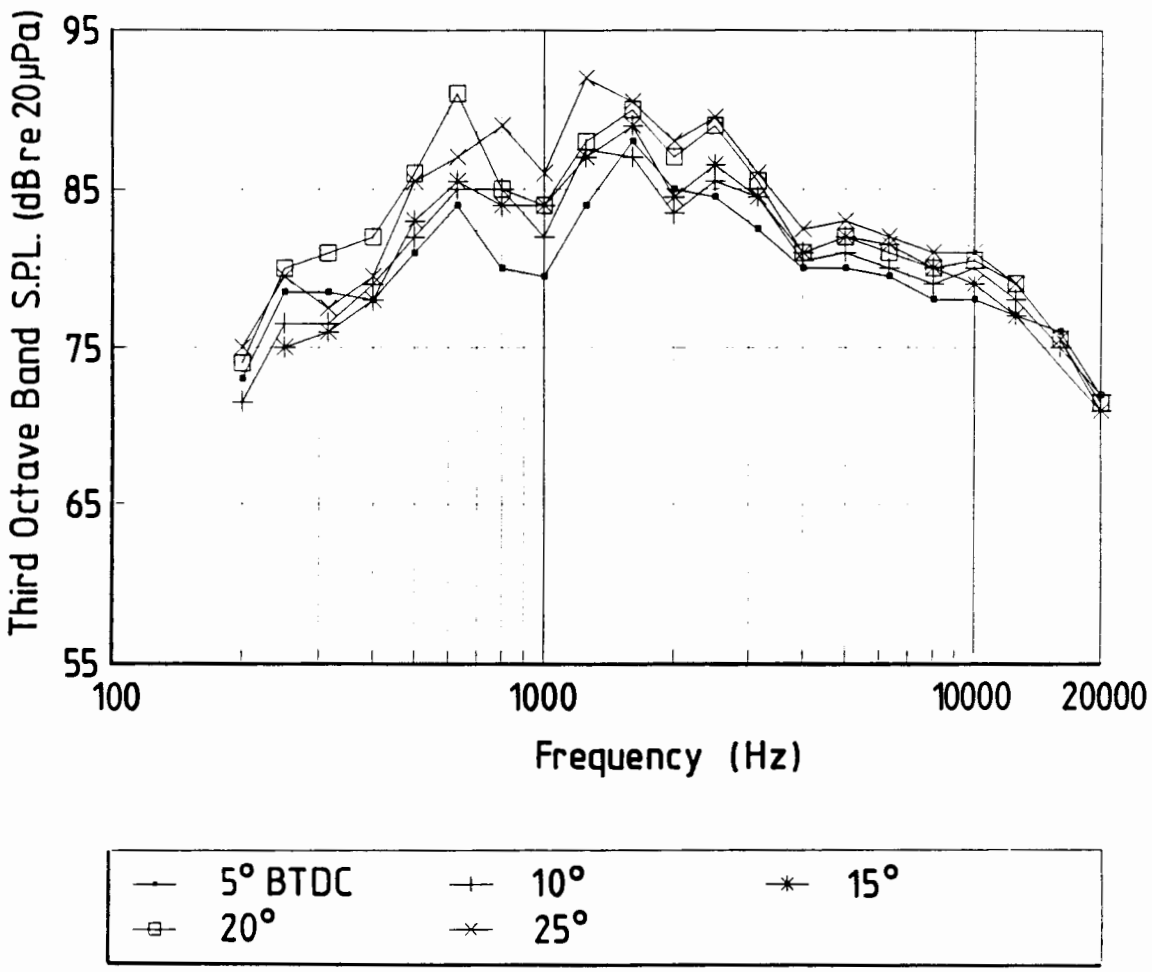

Figure C.23 Noise spectra recorded over a range of spark advance settings.

Engine : Nissan L28
Engine Speed : 4500 rpm
Fuel : 98 RON gasoline or AvGas

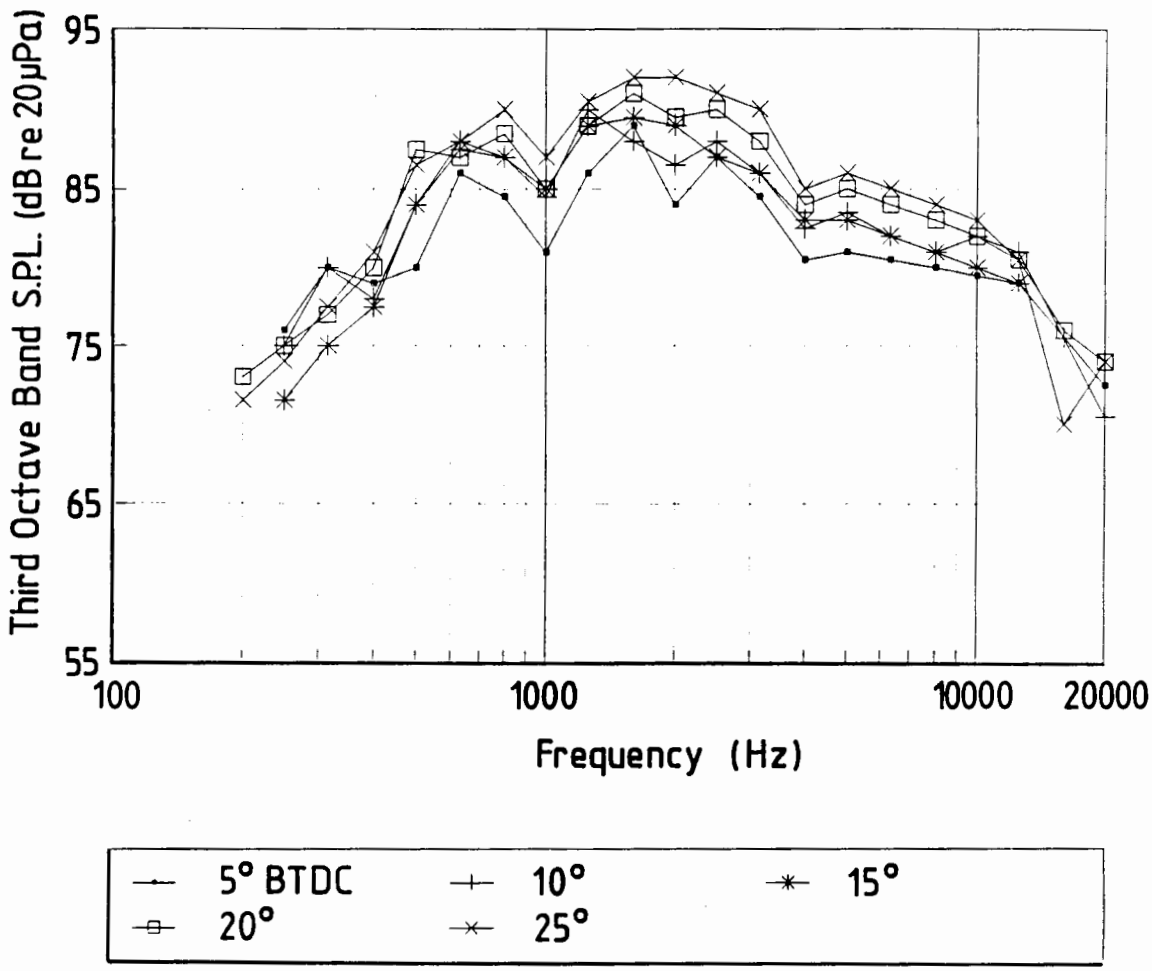

Figure C.24 Noise spectra recorded over a range of spark advance settings.

Engine : Nissan L28
Engine Speed : 5000 rpm
Fuel : 98 RON gasoline or AvGas

APPENDIX D

FOURIER SERIES EXPANSION OF A TRIANGULAR SAWTOOTH WAVEFORM

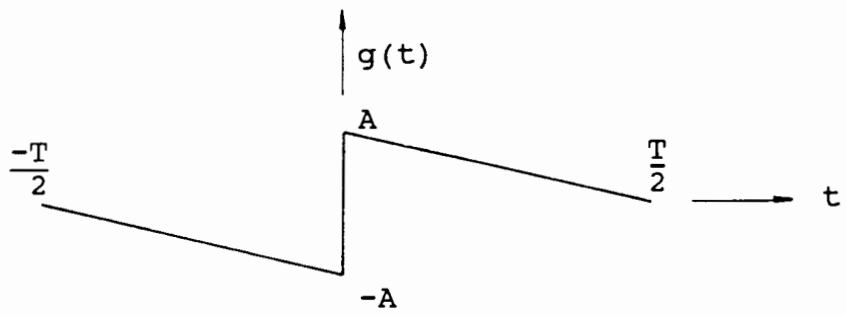

$$g(t) = \begin{cases} \frac{-2A}{T}t - A & : \quad \frac{-T}{2} \leq t < 0 \\ \frac{-2A}{T}t + A & : \quad 0 \leq t \leq \frac{-T}{2} \end{cases}$$

The expression for the Fourier Integral Transform is:

$$G(f) = \int_{\frac{T}{2}}^{0} \left\{ \frac{-2A}{T}t - A \right\} e^{-j2\pi ft} dt + \int_{0}^{\frac{T}{2}} \left\{ \frac{-2A}{T}t + A \right\} e^{-j2\pi ft} dt$$

$$= \frac{-2A}{T} \int_{\frac{T}{2}}^{\frac{T}{2}} te^{-j2\pi ft} dt - A \int_{\frac{T}{2}}^{0} e^{-j2\pi ft} dt + A \int_{0}^{\frac{T}{2}} e^{-j2\pi ft} dt$$

The terms are evaluated seperately:

$$-A \int_{\frac{T}{2}}^{0} e^{-j2\pi ft} dt = \frac{-jA}{2\pi f} \left\{ 1 - \cos(\pi fT) - j\sin(\pi fT) \right\}$$

$$A \int_{0}^{\frac{T}{2}} e^{-j2\pi ft} dt = \frac{-jA}{2\pi f} \left\{ 1 - \cos(\pi fT) + j\sin(\pi fT) \right\}$$

$$\frac{-2A}{T} \int_{\frac{T}{2}}^{\frac{T}{2}} te^{-j2\pi ft} dt = \frac{-jA}{2\pi f} \left\{ \cos(\pi fT) - \frac{\sin(\pi fT)}{\pi fT} \right\}$$

And added to get the result:

$$G(f) = \frac{jA}{2\pi f}\left\{\frac{\sin(\pi fT)}{\pi fT} - 1\right\}$$

Conversion from the Fourier Integral to the Fourier Series requires division by the period of the waveform, T. Since the function is now discrete and the harmonics are multiples of the fundamental frequency, the $\sin(\pi fT)$ term reduces to zero, and the function reduces to:

$$G(f_k) = \frac{-jA}{2\pi f_k T}$$

It can be seen that the result is imaginary and odd, which is as expected for an input function which is real and odd. In order to obtain the RMS power spectrum, the magnitude of the function is computed and multiplied by 2 to account for the negative frequency components. The results are converted to RMS values, and to a dB scale with the relevant reference value. (2×10^{-5} Pa in the case of sound pressure levels).

Thus, in the case of a cylinder pressure spectrum, the levels of the harmonics f_k are given by:

$$|G(f_k)| = 20 \log \left\{\frac{\sqrt{2}\,A}{2 \times 10^{-5}\ \pi f_k T}\right\} \longrightarrow$$

APPENDIX E

FOURIER SERIES EXPANSION OF AN EXPONENTIALLY DECAYING SINE WAVE

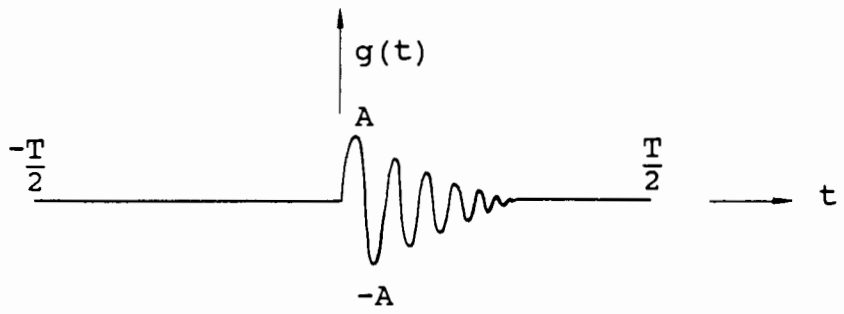

$$g(t) = e^{\frac{-t}{k}} A\sin(2\pi Ft) \qquad \text{where} \quad F = \text{frequency of the sine wave}$$
$$k = \text{modulus of decay}$$

The expression for the Fourier Integral Transform is:

$$G(f) = \int_0^{\frac{T}{2}} e^{\frac{-t}{k}} A\sin(2\pi Ft) e^{-j2\pi ft} dt$$

$$= \frac{A}{2j}\int_0^{\frac{T}{2}} \left\{ e^{j2\pi Ft} - e^{-j2\pi ft} \right\} e^{\frac{-t}{k}} e^{-j2\pi ft} dt$$

The derivation may be simplified by evaluating at f = F:

$$\therefore G(F) = \frac{A}{2j}\int_0^{\frac{T}{2}} e^{\frac{-t}{k}} dt - \frac{A}{2j}\int_0^{\frac{T}{2}} e^{-(j4\pi F + \frac{1}{k})t} dt$$

The terms in this expression are evaluated seperately:

$$\frac{A}{2j}\int_0^{\frac{T}{2}} e^{\frac{-t}{k}} dt = \frac{-Ak}{2j}\left\{ e^{\frac{-T}{2k}} - 1 \right\}$$

$$= \frac{Ak}{2j} \qquad (1)$$

since, for realistic values of k, $e^{\frac{-T}{2k}} \ll 1$.

$$\frac{-A}{2j}\int_0^{\frac{T}{2}} e^{-(j4\pi F + \frac{1}{k})t}\,dt = \frac{-Ak}{8\pi Fk - 2j}\left\{e^{-j2\pi FT}e^{\frac{-T}{2k}} - 1\right\}$$

$$= \frac{Ak}{8\pi Fk - 2j} \qquad (2)$$

since, $e^{-j2\pi FT} = \pm 1$ because FT is an integer if F is a harmonic of the fundamental.

The solution is obtained by adding equations (1) and (2):

$$G(F) = \frac{Ak}{2j} + \frac{Ak}{8\pi Fk - 2j}$$

$$= \frac{2Ak^2\pi F(1 - j4\pi Fk)}{1 + 16\pi^2F^2k^2}$$

The expression for the magnitude can be derived:

$$|G(F)| = \frac{2A\pi Fk^2}{\sqrt{1 + 16\pi^2F^2k^2}}$$

But, for large values of F, $16\pi^2F^2k^2 \gg 1$,

$$\therefore |G(F)| \simeq \frac{Ak}{2}$$

Conversion to a Fourier series (i.e division by T), RMS values, and a dB scale with a reference value of 2×10^{-5} (as for sound pressure levels) yields:

$$|G(F)| \simeq 20 \log \left\{\frac{\sqrt{2}\ Ak}{4 \times 10^{-5}\ T}\right\} \longrightarrow$$

APPENDIX F

NISSAN L28 ENGINE TEST RESULTS

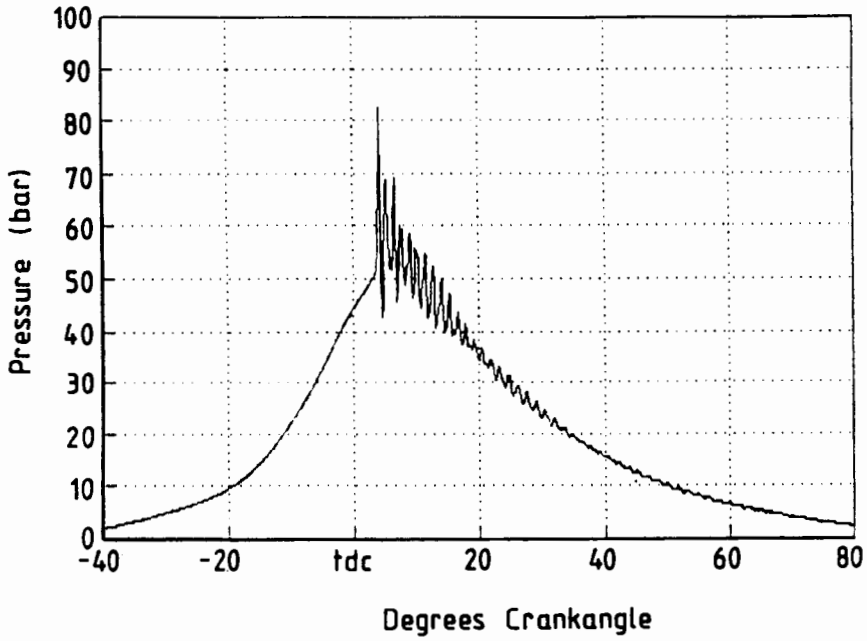

Figure F.1a Cylinder pressure diagram.

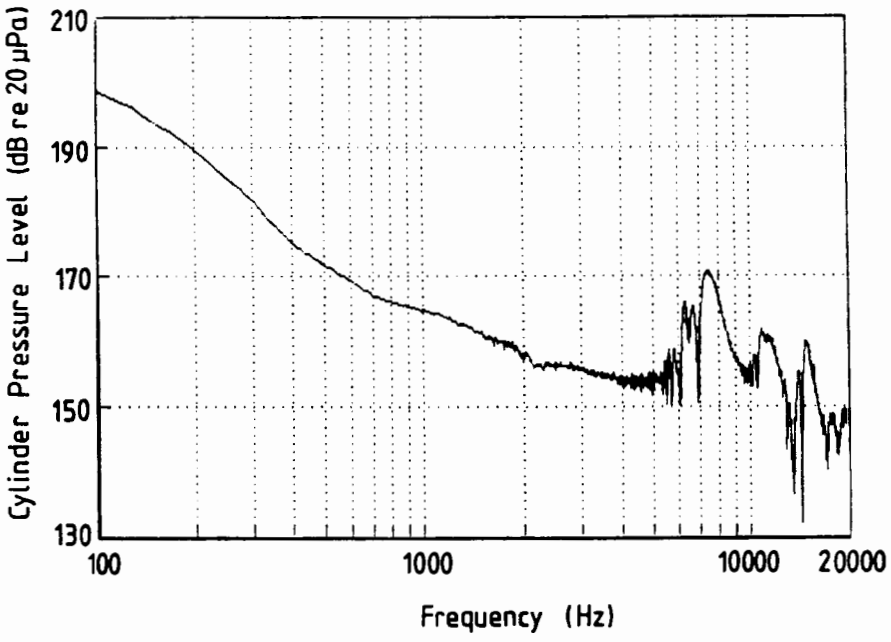

Figure F.1b Cylinder pressure spectrum.

Engine	:	Nissan L28
Engine Speed	:	1500 rpm
Spark Timing	:	20° BTDC
Fuel	:	93 RON gasoline

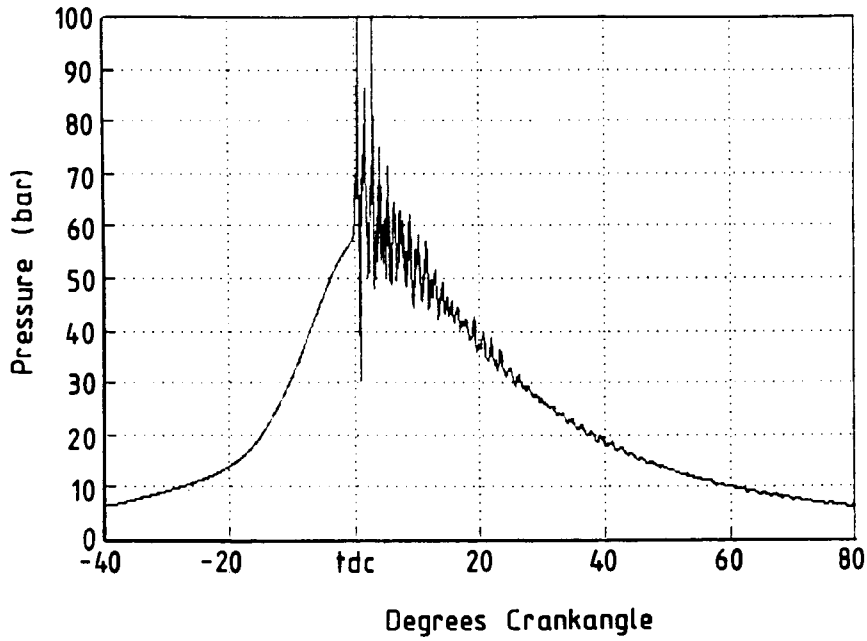

Figure F.2a Cylinder pressure diagram.

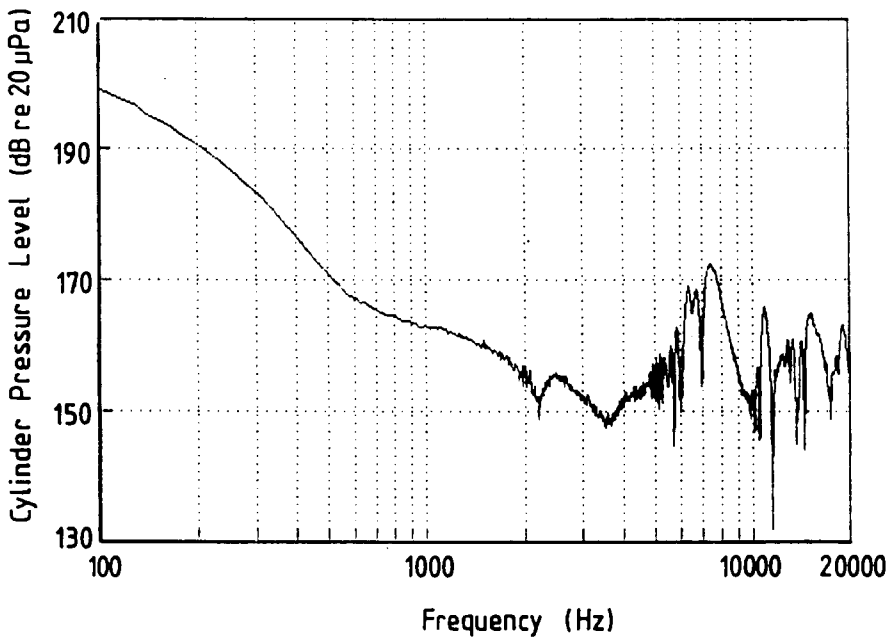

Figure F.2b Cylinder pressure spectrum.

Engine	:	Nissan L28
Engine Speed	:	1500 rpm
Spark Timing	:	20° BTDC
Fuel	:	93 RON gasoline

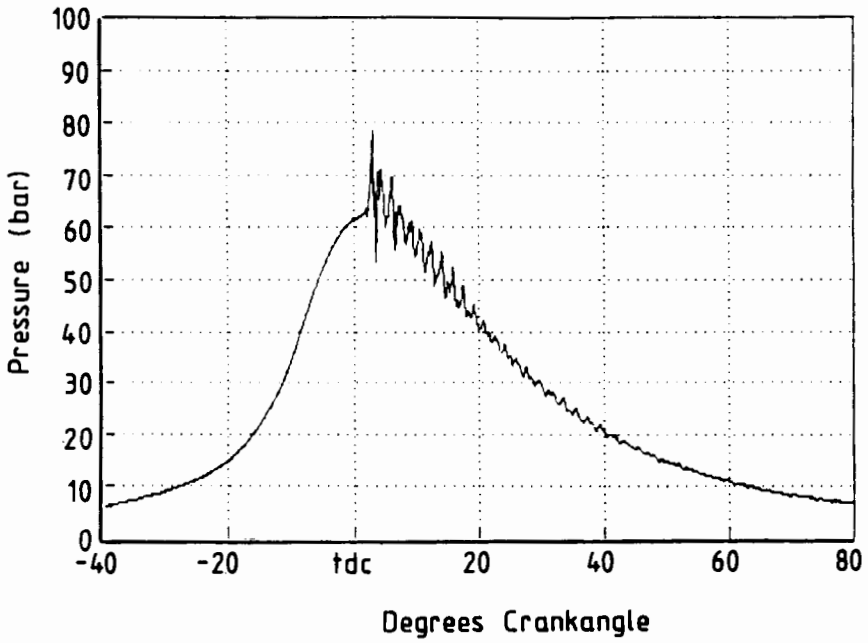

Figure F.3a Cylinder pressure diagram.

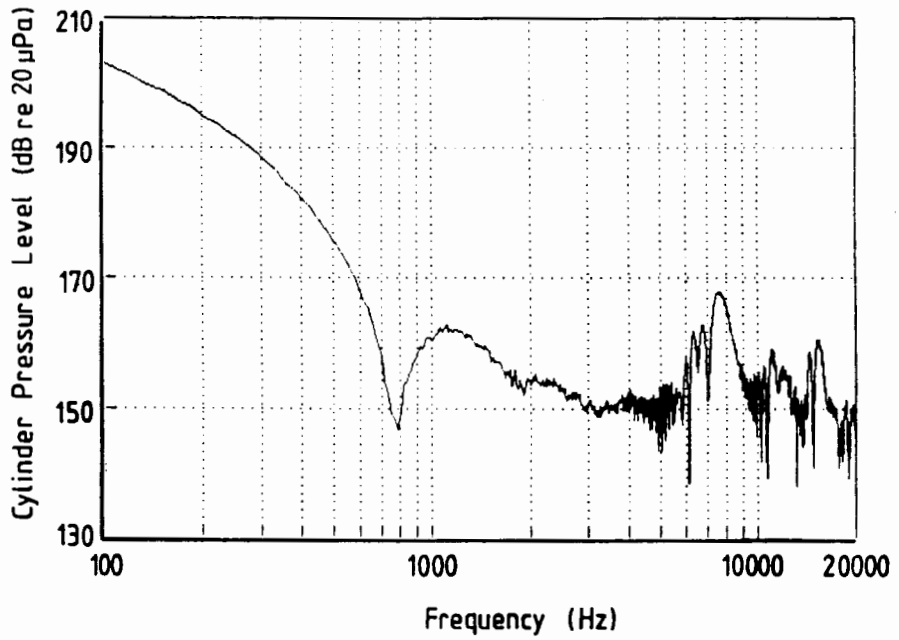

Figure F.3b Cylinder pressure spectrum.

Engine	:	Nissan L28
Engine Speed	:	2000 rpm
Spark Timing	:	20° BTDC
Fuel	:	93 RON gasoline

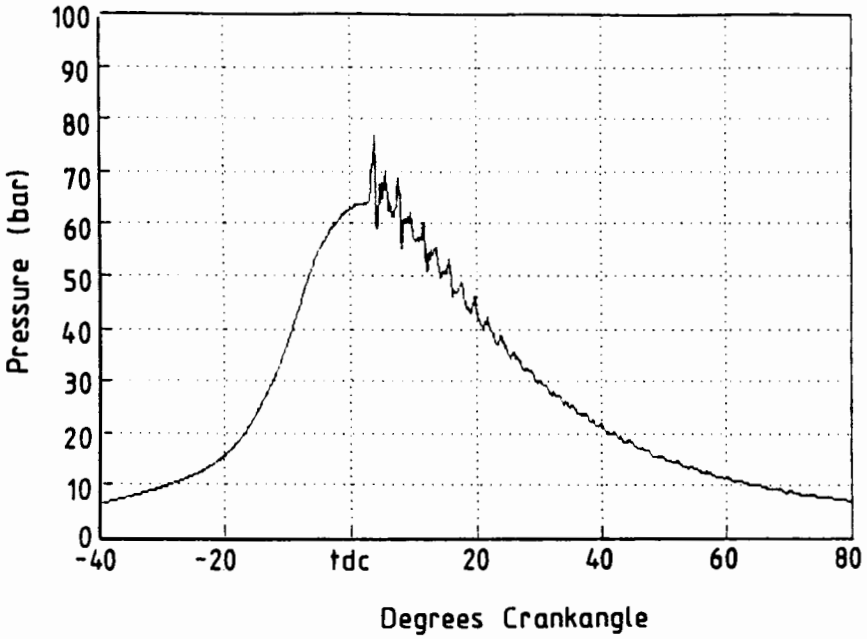

Figure F.4a Cylinder pressure diagram.

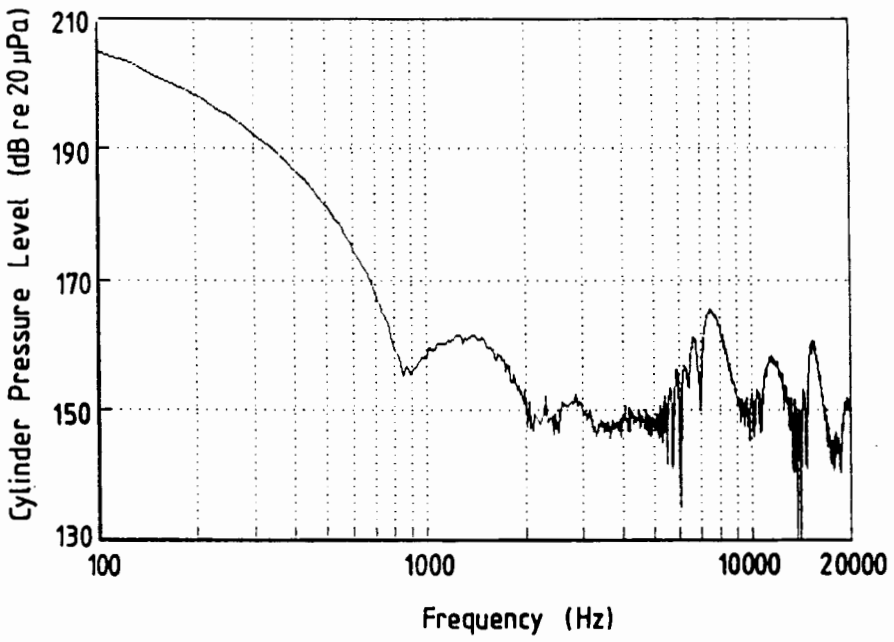

Figure F.4b Cylinder pressure spectrum.

Engine	:	Nissan L28
Engine Speed	:	2500 rpm
Spark Timing	:	20° BTDC
Fuel	:	93 RON gasoline

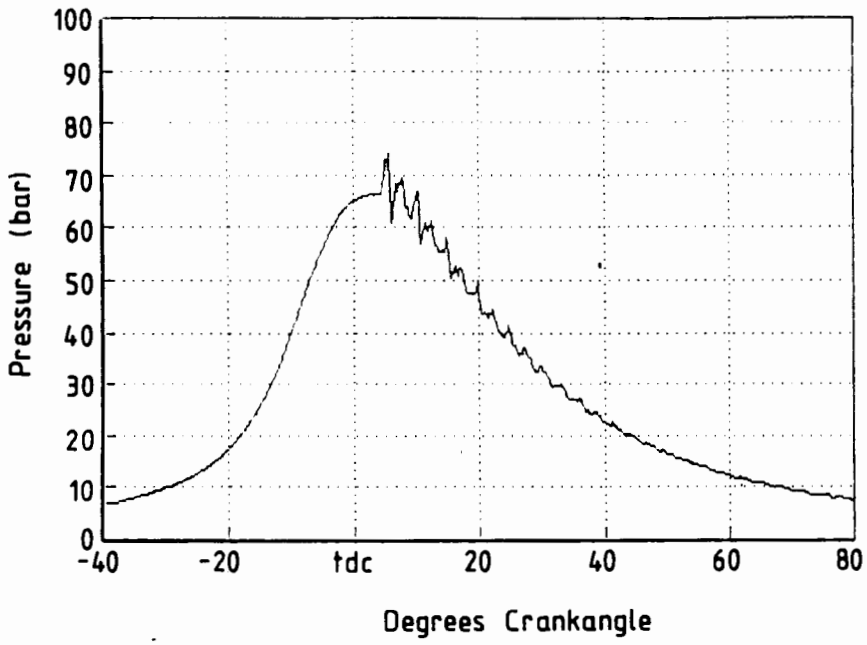

Figure F.5a Cylinder pressure diagram.

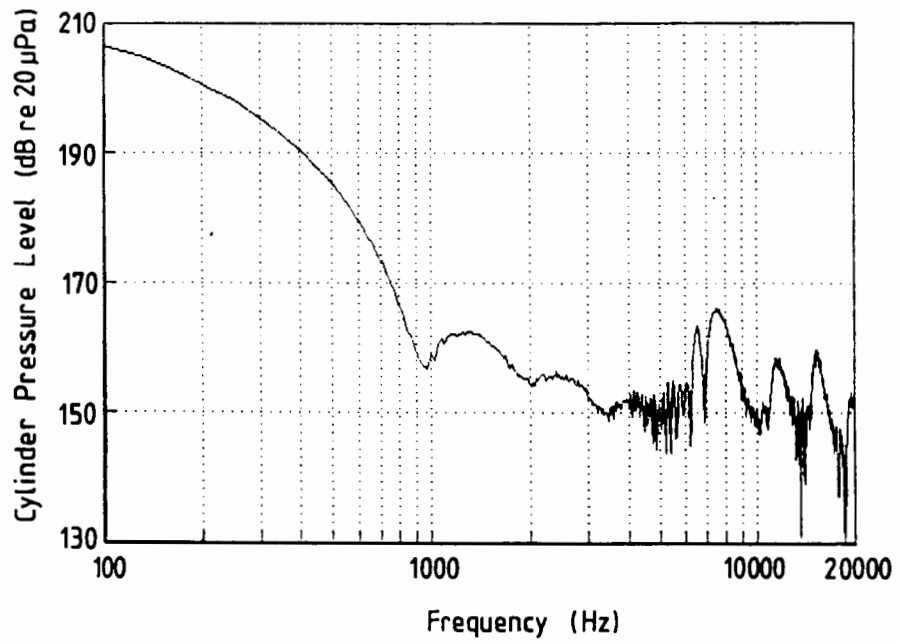

Figure F.5b Cylinder pressure spectrum.

Engine	:	Nissan L28
Engine Speed	:	3000 rpm
Spark Timing	:	20° BTDC
Fuel	:	93 RON gasoline

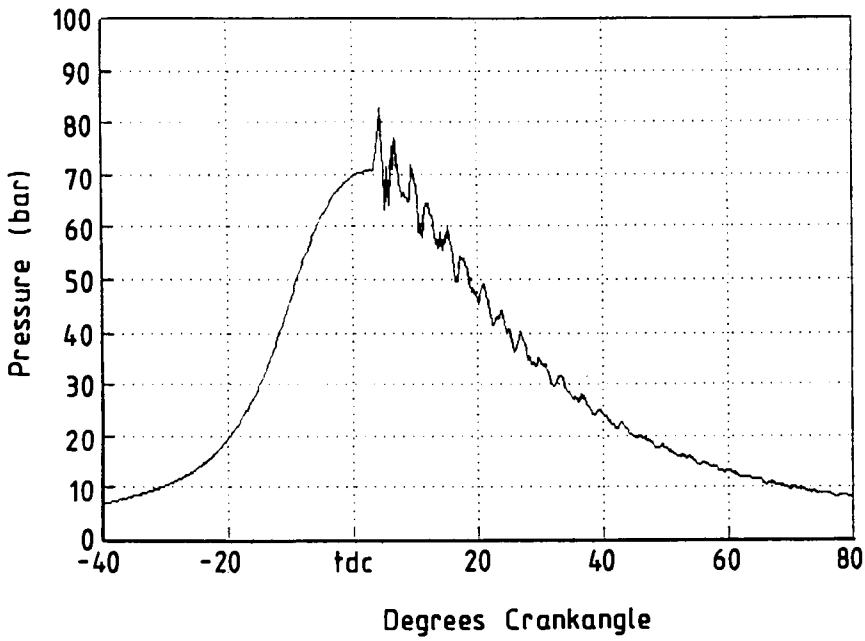

Figure F.6a Cylinder pressure diagram.

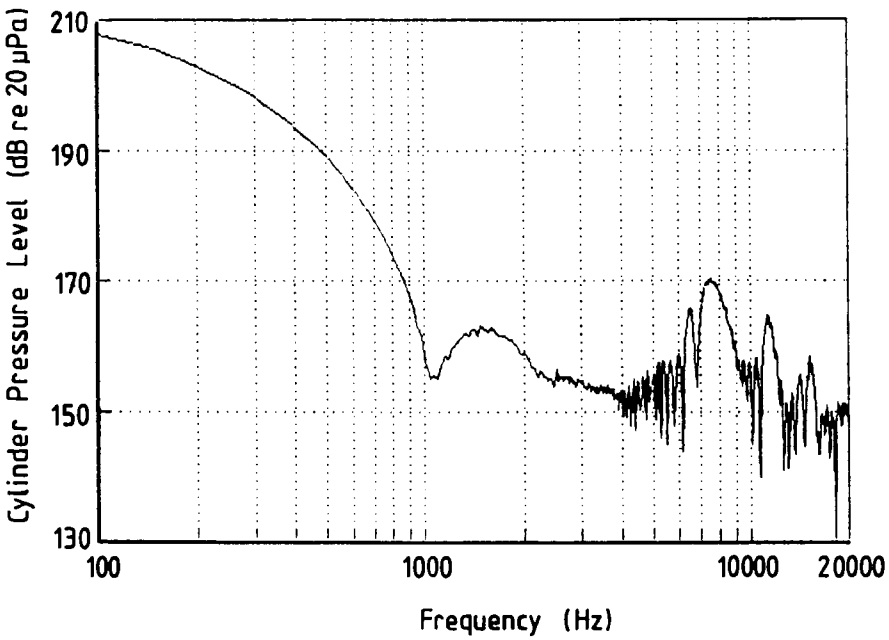

Figure F.6b Cylinder pressure spectrum.

Engine	:	Nissan L28
Engine Speed	:	3500 rpm
Spark Timing	:	20° BTDC
Fuel	:	93 RON gasoline

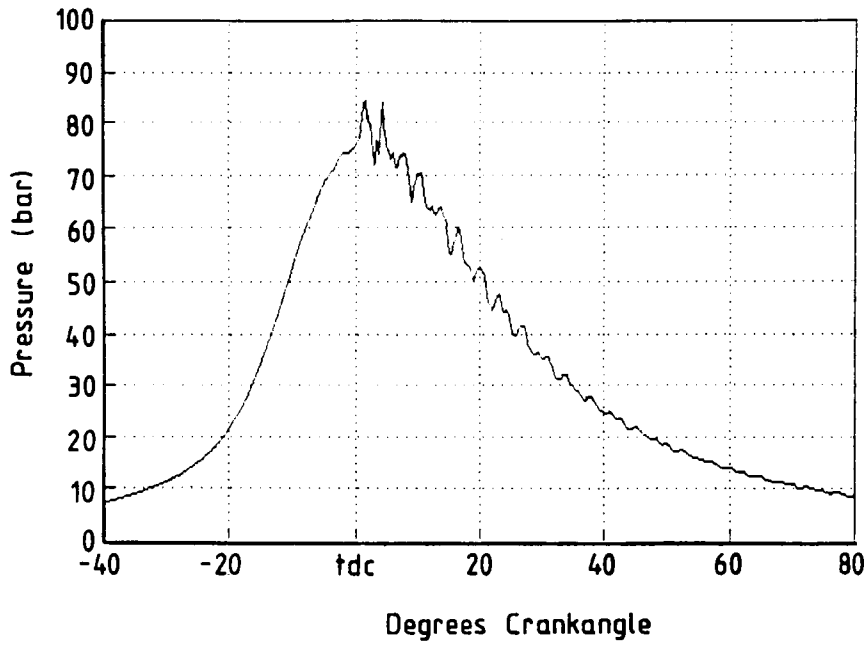

Figure F.7a Cylinder pressure diagram.

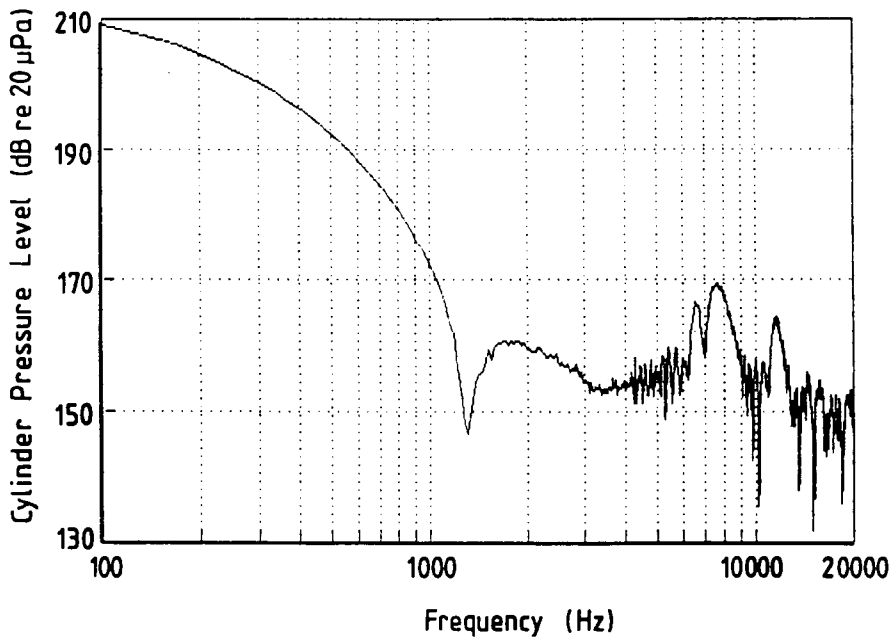

Figure F.7b Cylinder pressure spectrum.

Engine	:	Nissan L28
Engine Speed	:	4000 rpm
Spark Timing	:	20° BTDC
Fuel	:	93 RON gasoline

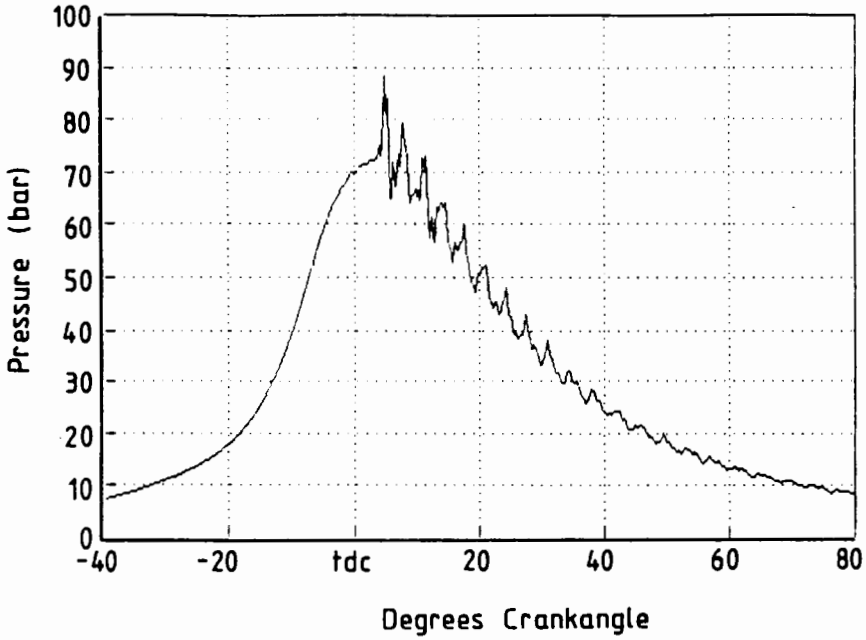

Figure F.8a Cylinder pressure diagram.

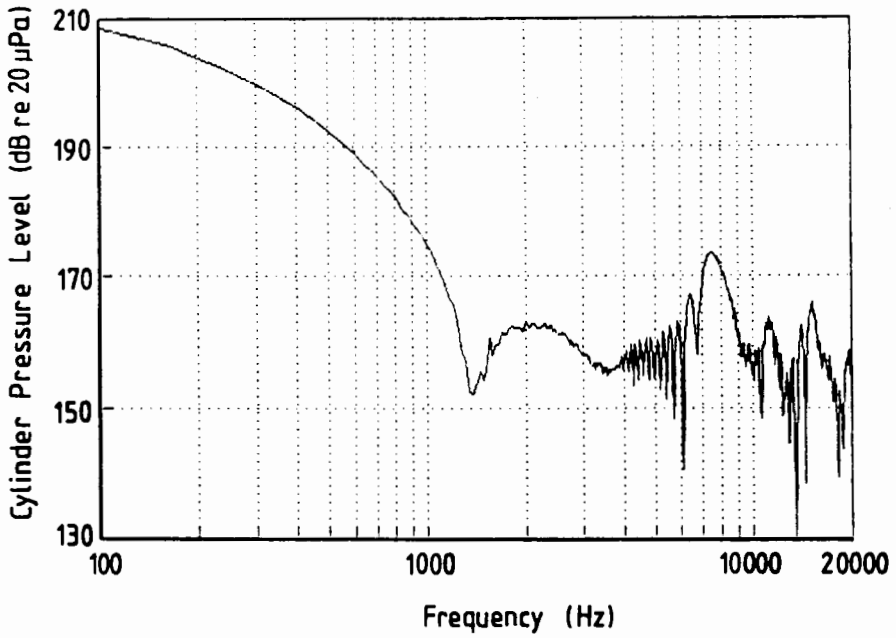

Figure F.8b Cylinder pressure spectrum.

Engine	:	Nissan L28
Engine Speed	:	4000 rpm
Spark Timing	:	20° BTDC
Fuel	:	93 RON gasoline

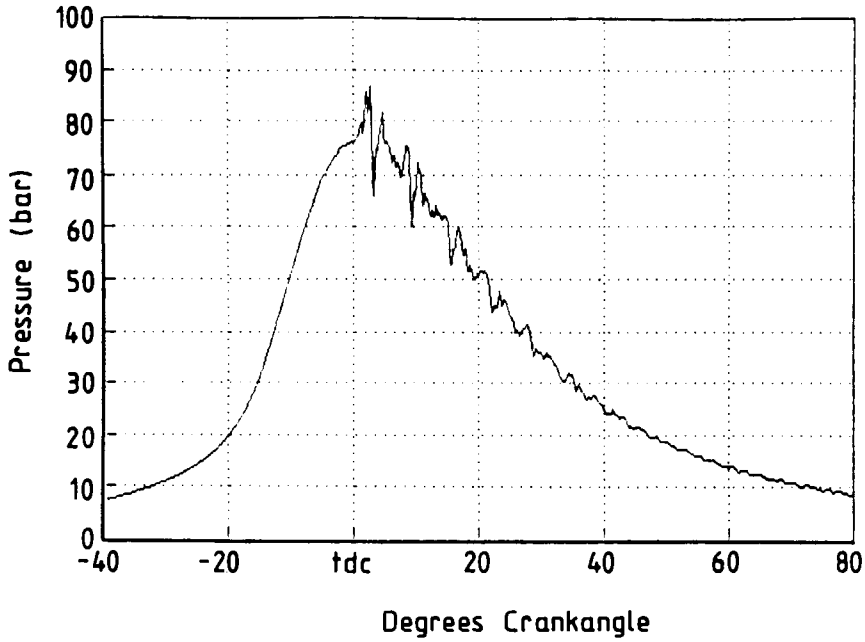

Figure F.9a Cylinder pressure diagram.

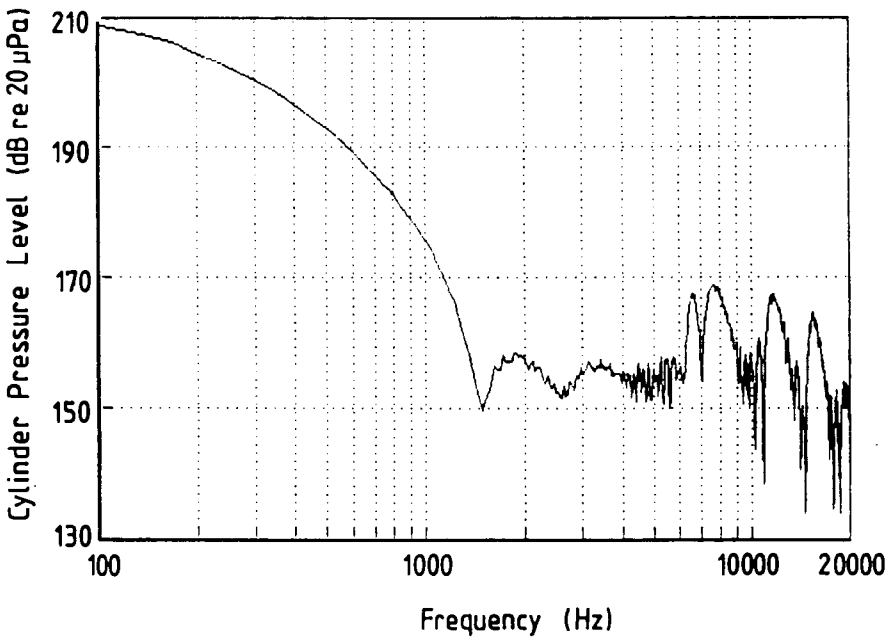

Figure F.9b Cylinder pressure spectrum.

Engine	:	Nissan L28
Engine Speed	:	4000 rpm
Spark Timing	:	20° BTDC
Fuel	:	93 RON gasoline

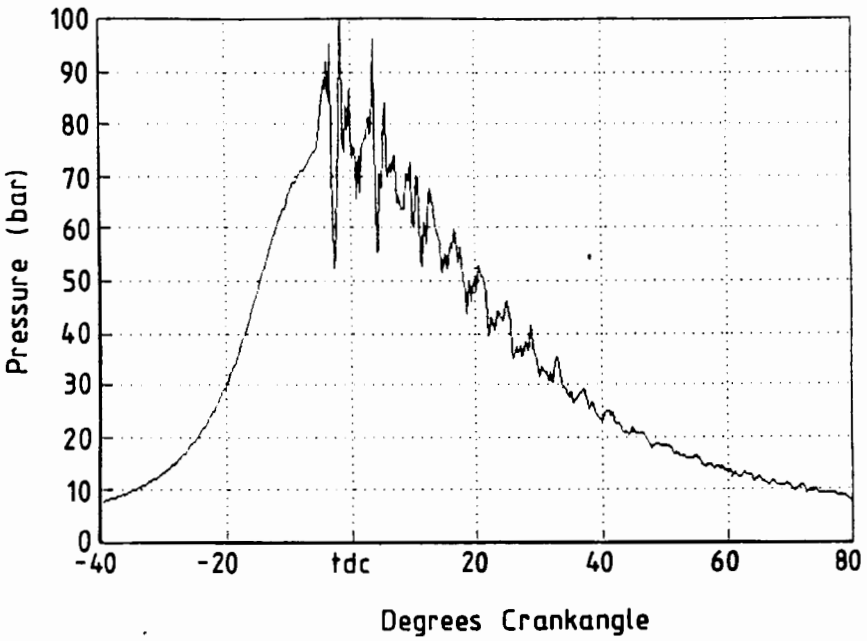

Figure F.10a Cylinder pressure diagram.

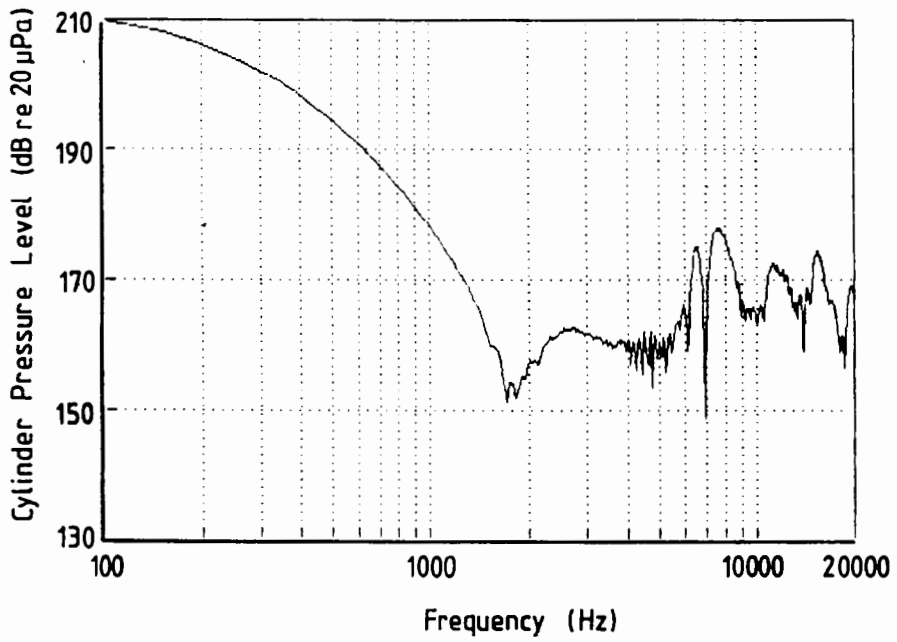

Figure F.10b Cylinder pressure spectrum.

Engine	:	Nissan L28
Engine Speed	:	4500 rpm
Spark Timing	:	20° BTDC
Fuel	:	93 RON gasoline

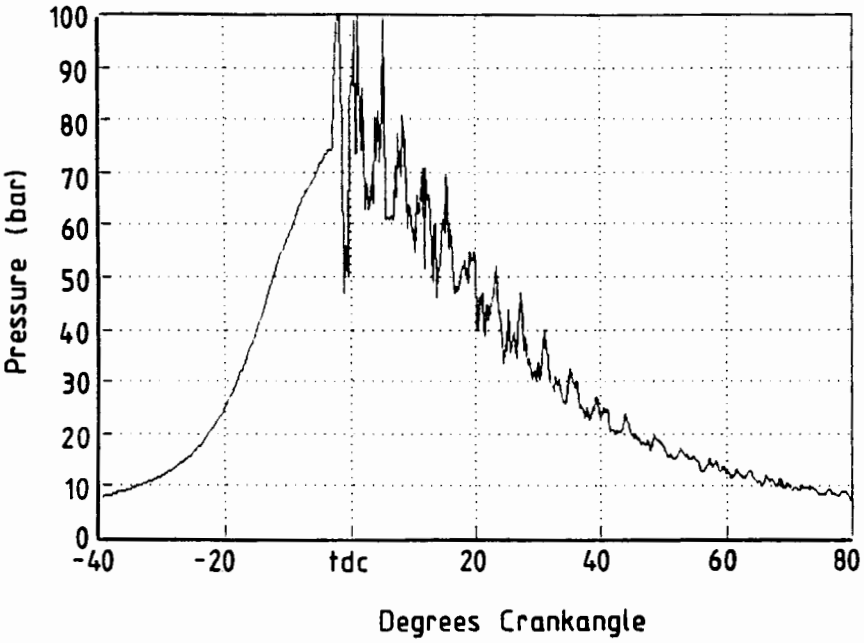

Figure F.11a Cylinder pressure diagram.

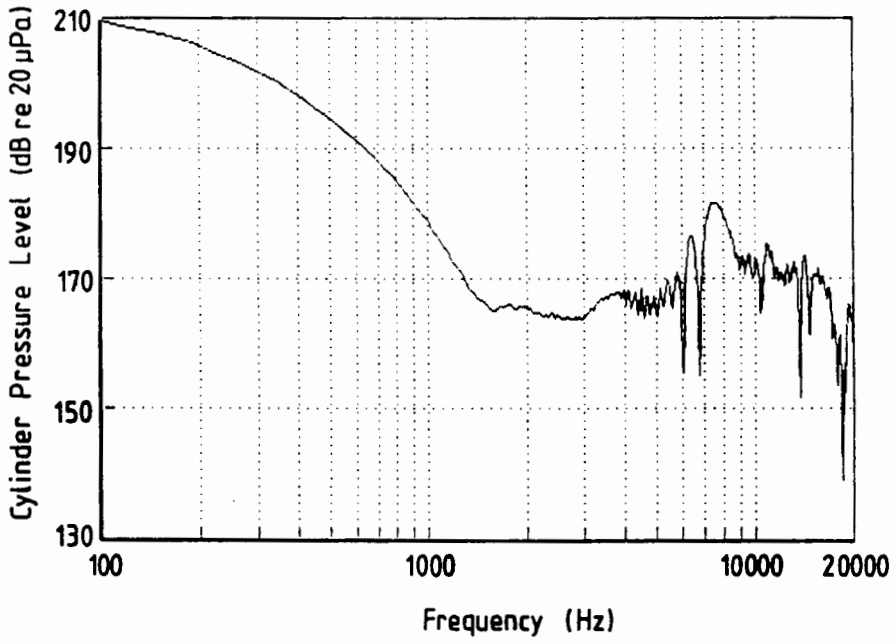

Figure F.11b Cylinder pressure spectrum.

Engine	:	Nissan L28
Engine Speed	:	4500 rpm
Spark Timing	:	20° BTDC
Fuel	:	93 RON gasoline

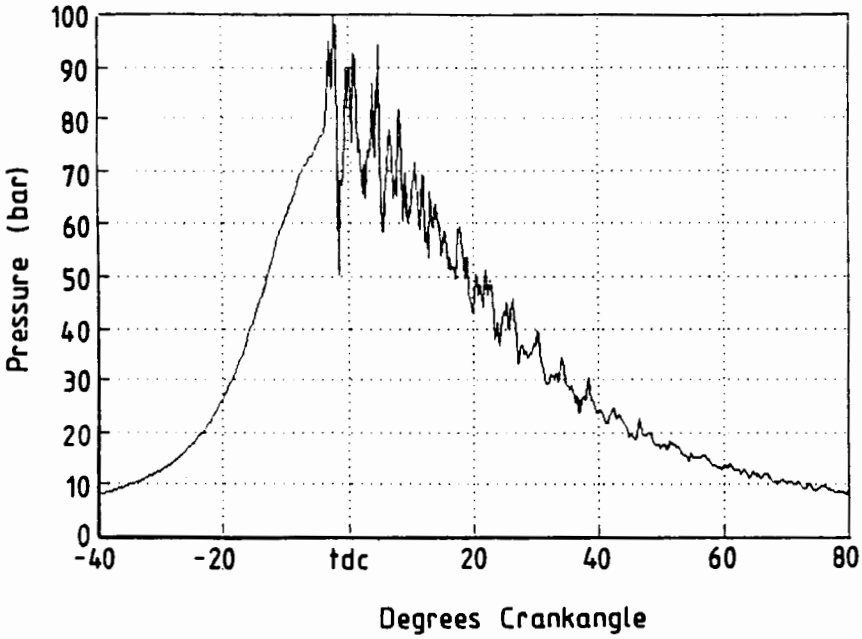

Figure F.12a Cylinder pressure diagram.

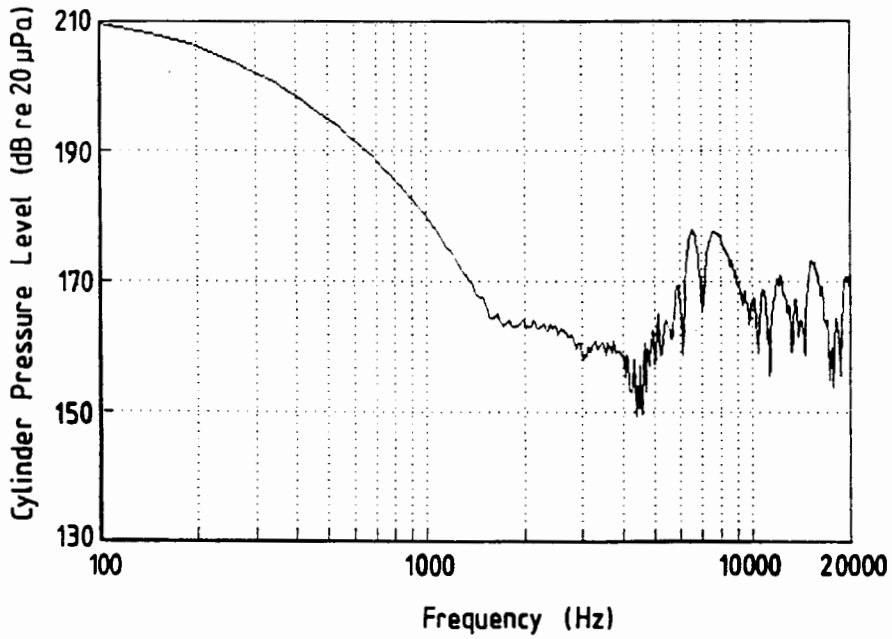

Figure F.12b Cylinder pressure spectrum.

Engine	:	Nissan L28
Engine Speed	:	4500 rpm
Spark Timing	:	20° BTDC
Fuel	:	93 RON gasoline

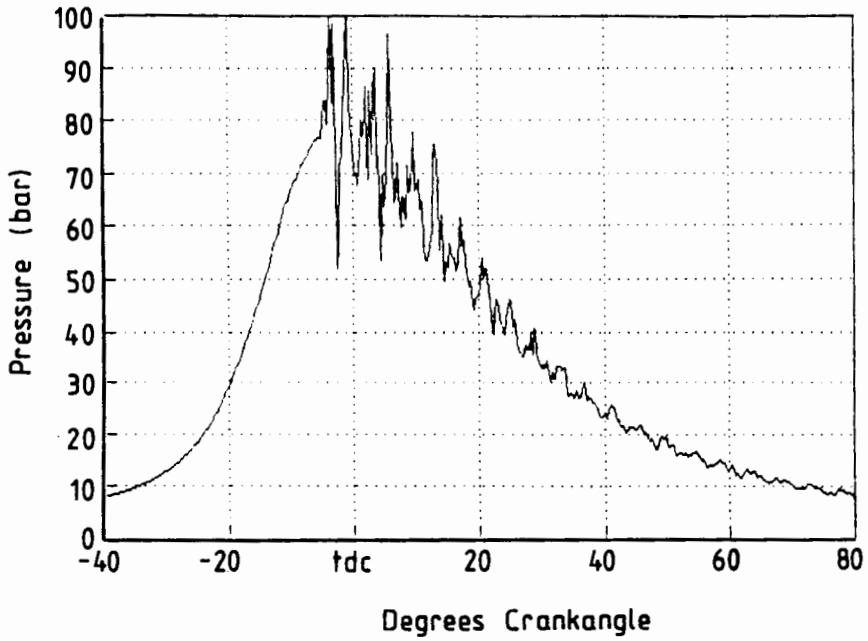

Figure F.13a Cylinder pressure diagram.

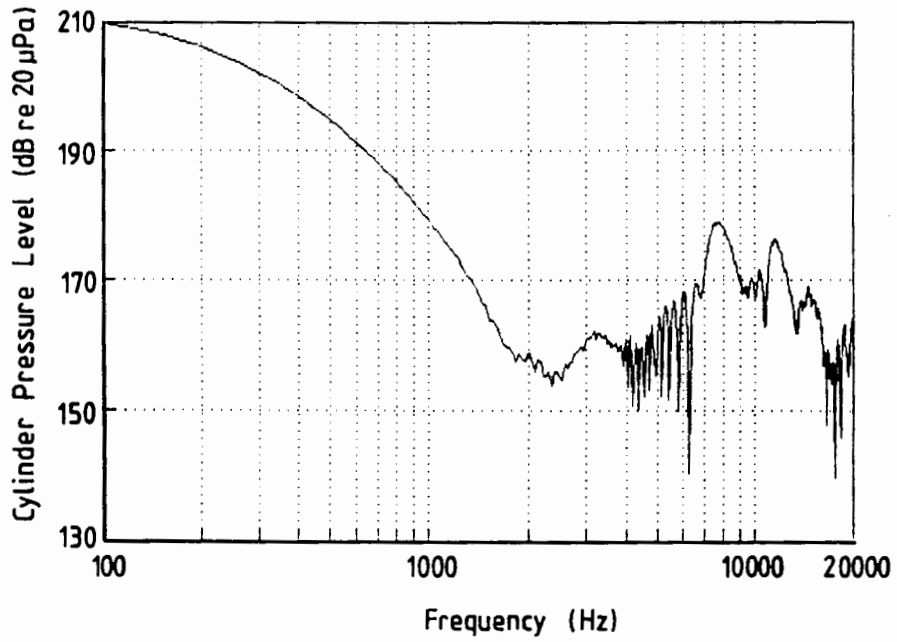

Figure F.13b Cylinder pressure spectrum.

Engine	:	Nissan L28
Engine Speed	:	4500 rpm
Spark Timing	:	20° BTDC
Fuel	:	93 RON gasoline

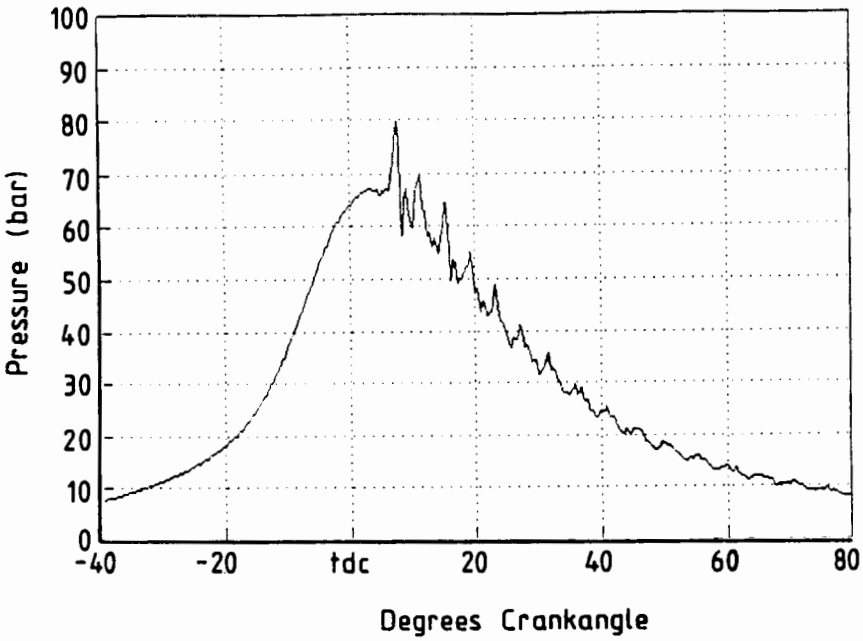

Figure F.14a Cylinder pressure diagram.

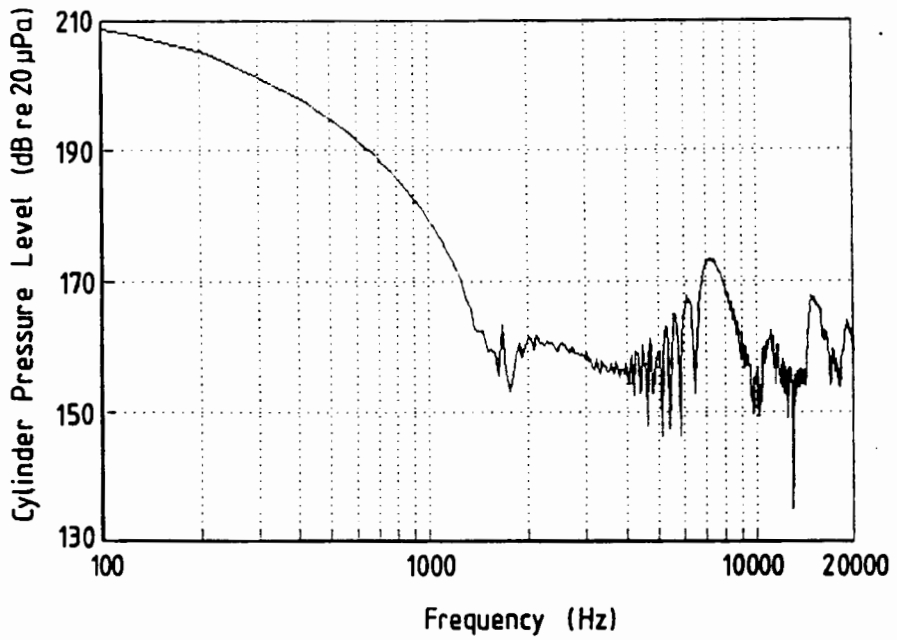

Figure F.14b Cylinder pressure spectrum.

Engine	:	Nissan L28
Engine Speed	:	5000 rpm
Spark Timing	:	20° BTDC
Fuel	:	93 RON gasoline

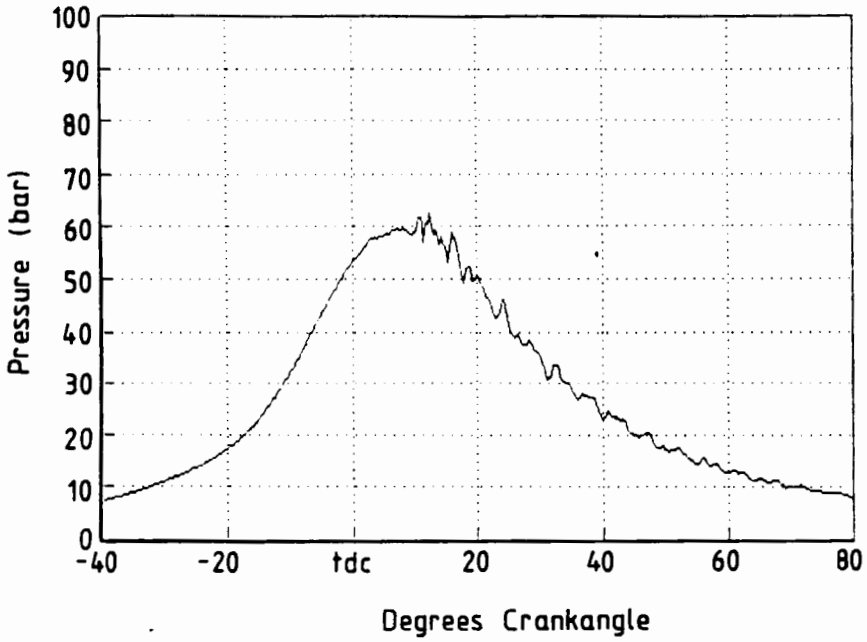

Figure F.15a Cylinder pressure diagram.

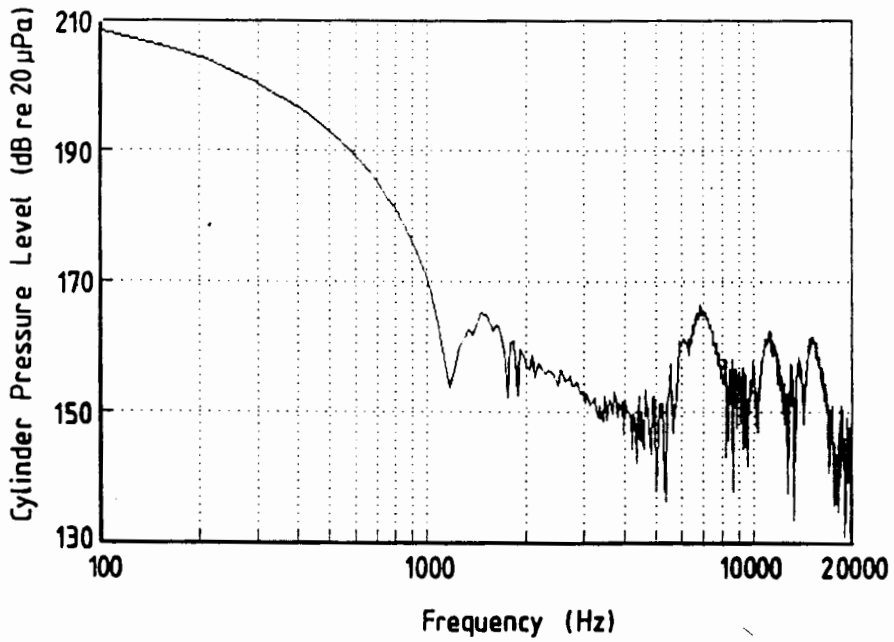

Figure F.15b Cylinder pressure spectrum.

Engine	:	Nissan L28
Engine Speed	:	5000 rpm
Spark Timing	:	20° BTDC
Fuel	:	93 RON gasoline

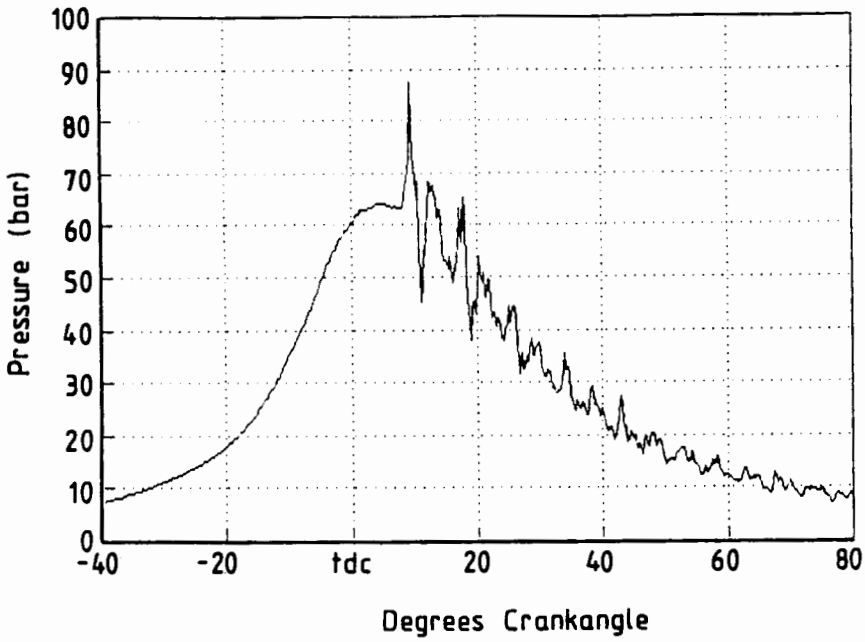

Figure F.16a Cylinder pressure diagram.

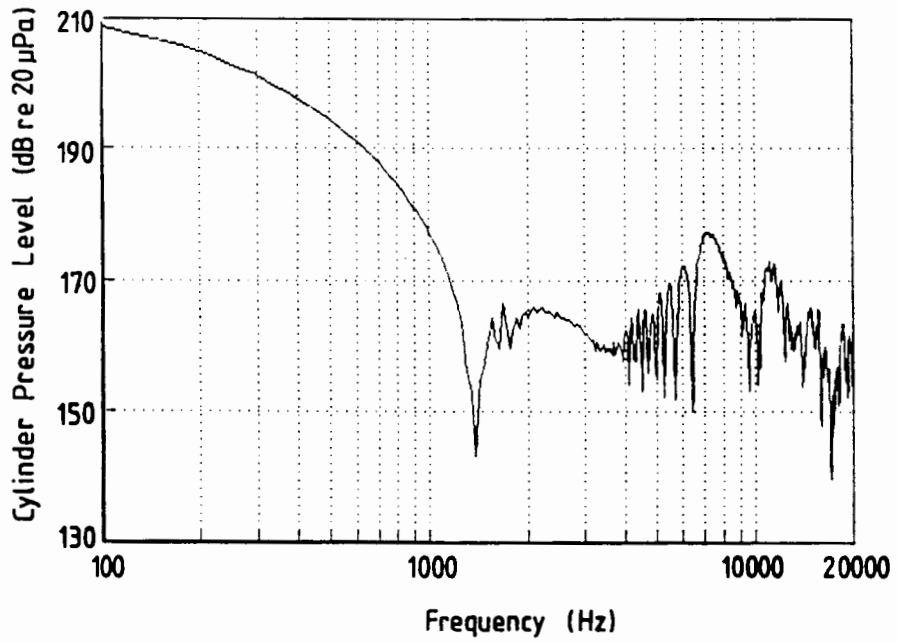

Figure F.16b Cylinder pressure spectrum.

Engine	:	Nissan L28
Engine Speed	:	5000 rpm
Spark Timing	:	20° BTDC
Fuel	:	93 RON gasoline

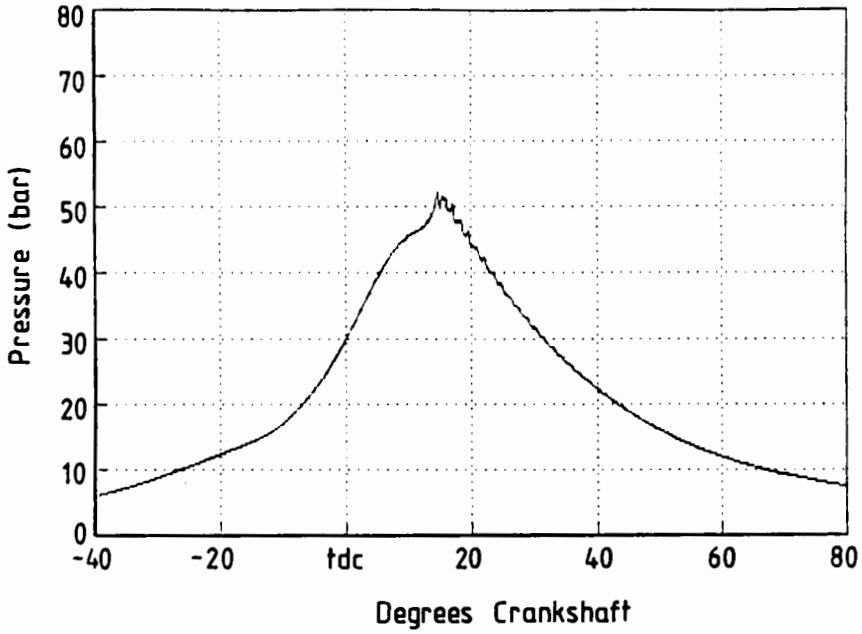

Figure F.17a Cylinder pressure diagram.

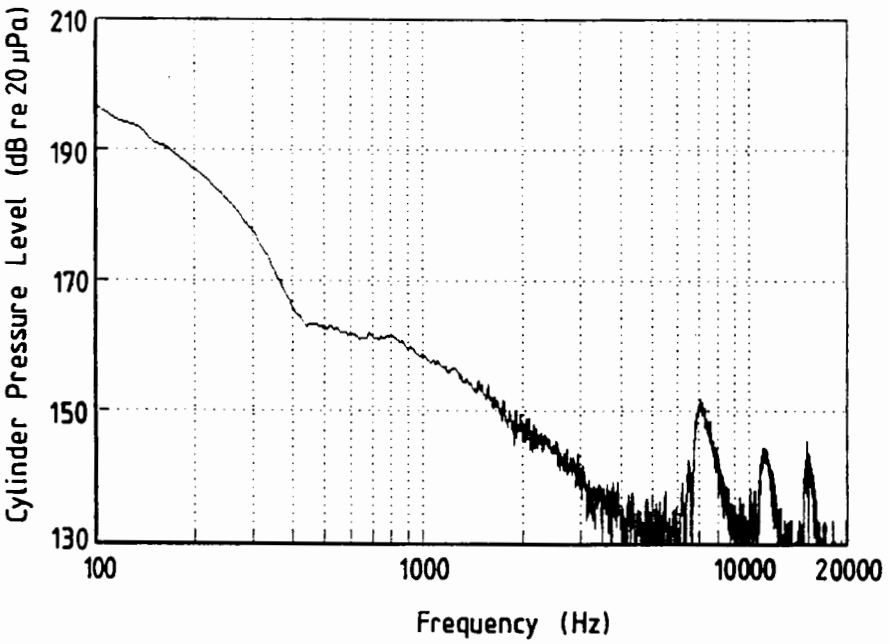

Figure F.17b Cylinder pressure spectrum.

Engine	:	Nissan L28
Engine Speed	:	1500 rpm
Spark Timing	:	10° BTDC
Fuel	:	93 RON gasoline

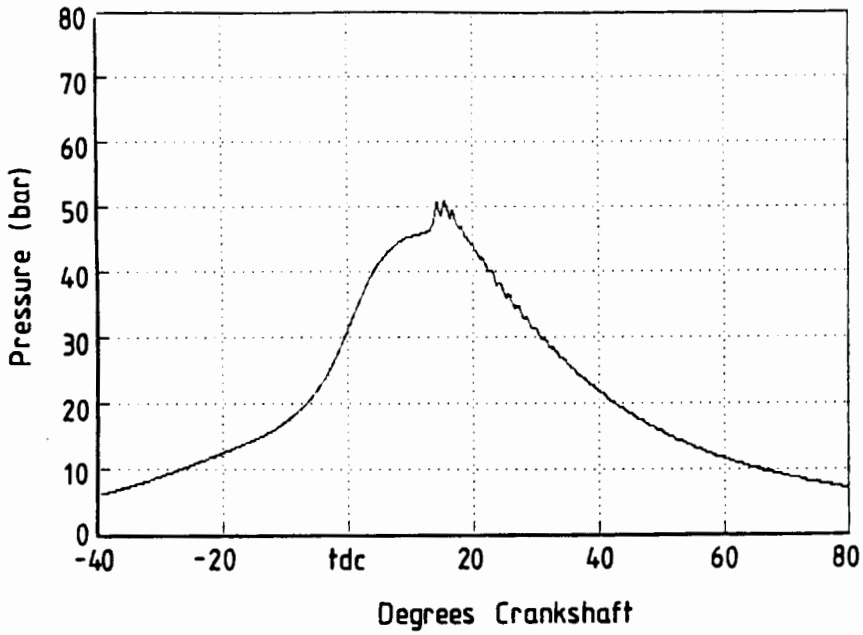

Figure F.18a Cylinder pressure diagram.

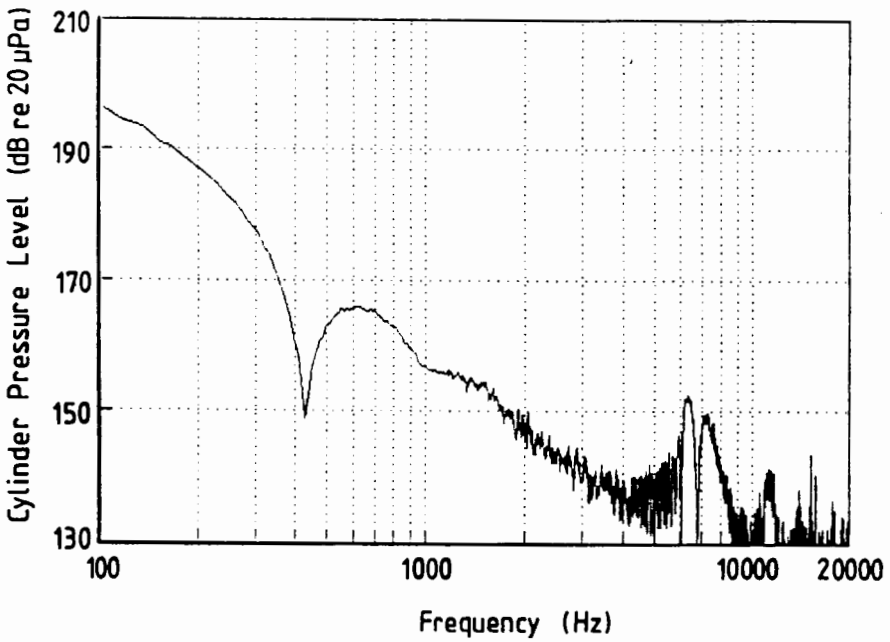

Figure F.18b Cylinder pressure spectrum.

Engine	:	Nissan L28
Engine Speed	:	1500 rpm
Spark Timing	:	10° BTDC
Fuel	:	93 RON gasoline

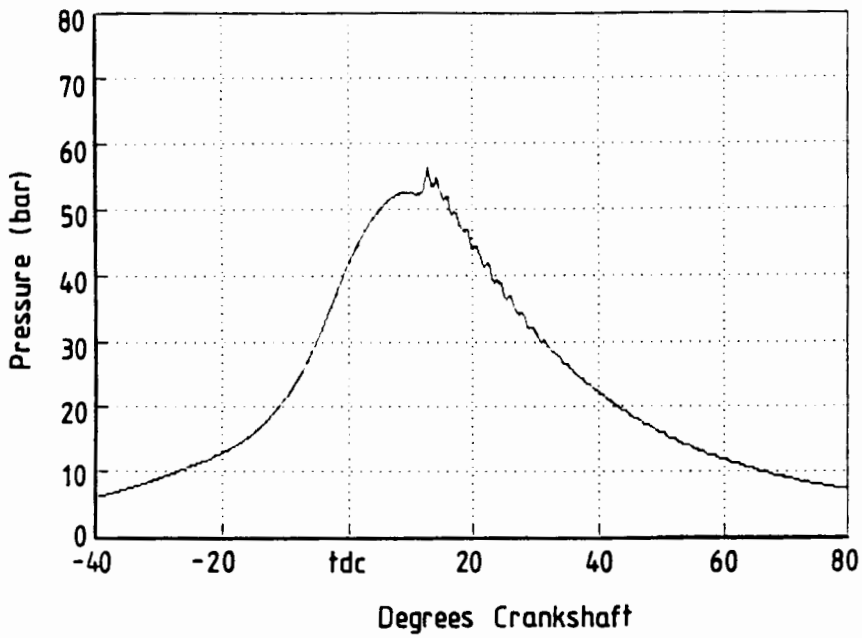

Figure F.19a Cylinder pressure diagram.

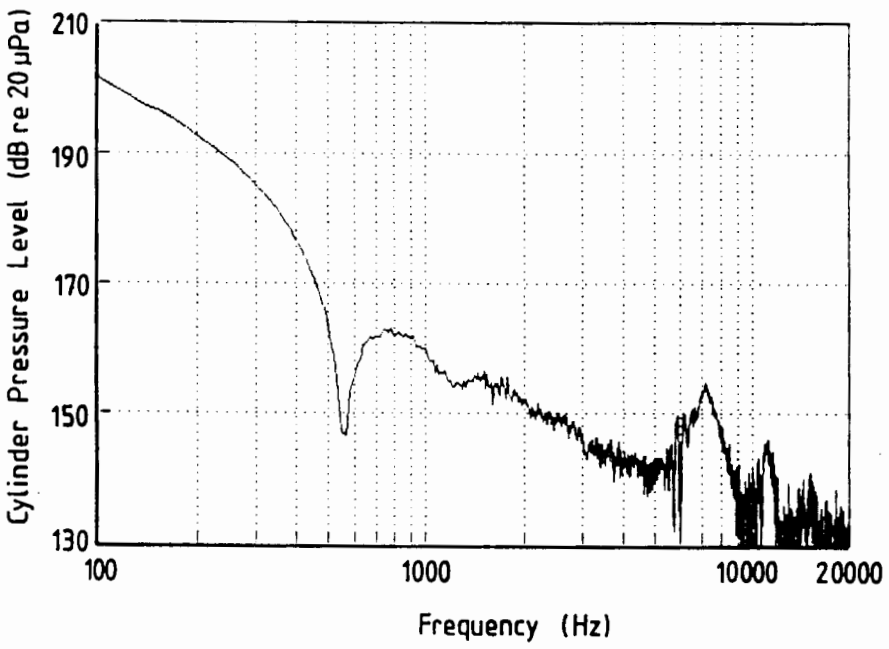

Figure F.19b Cylinder pressure spectrum.

Engine	:	Nissan L28
Engine Speed	:	2000 rpm
Spark Timing	:	10° BTDC
Fuel	:	93 RON gasoline

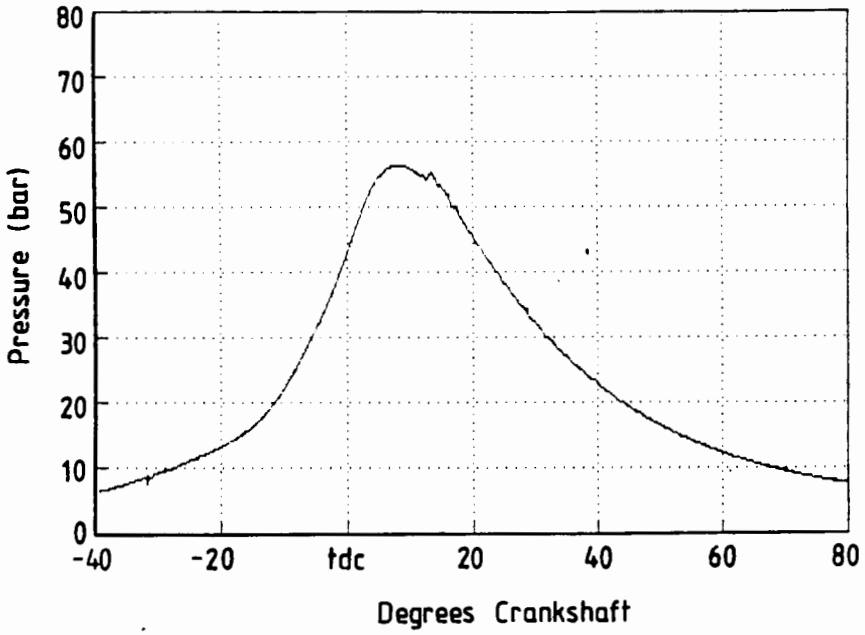

Figure F.20a Cylinder pressure diagram.

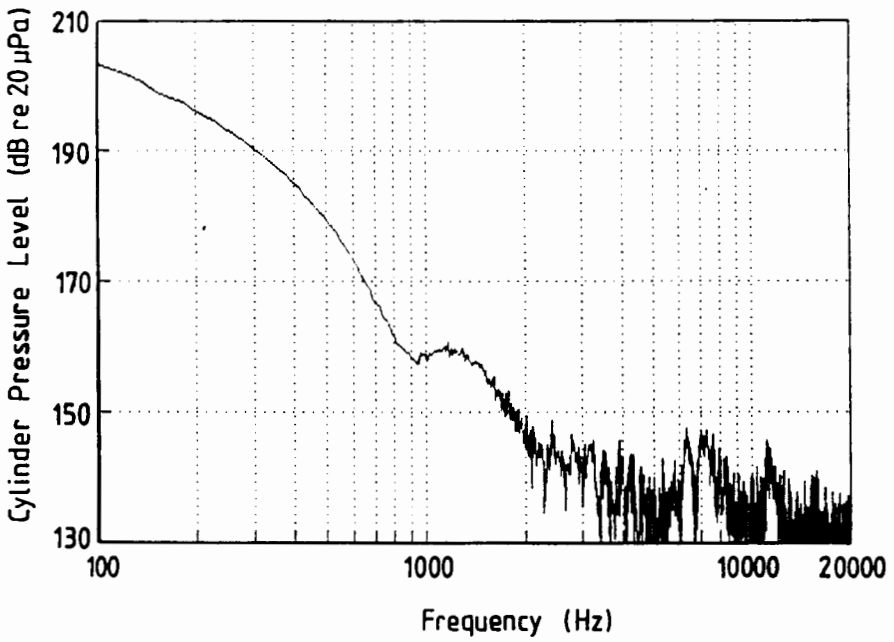

Figure F.20b Cylinder pressure spectrum.

Engine	:	Nissan L28
Engine Speed	:	2500 rpm
Spark Timing	:	10° BTDC
Fuel	:	93 RON gasoline

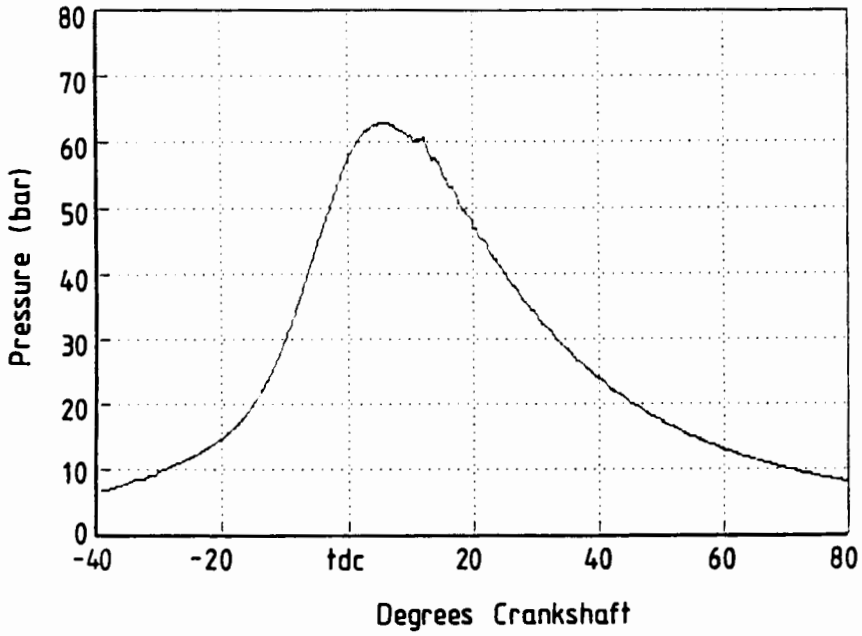

Figure F.21a Cylinder pressure diagram.

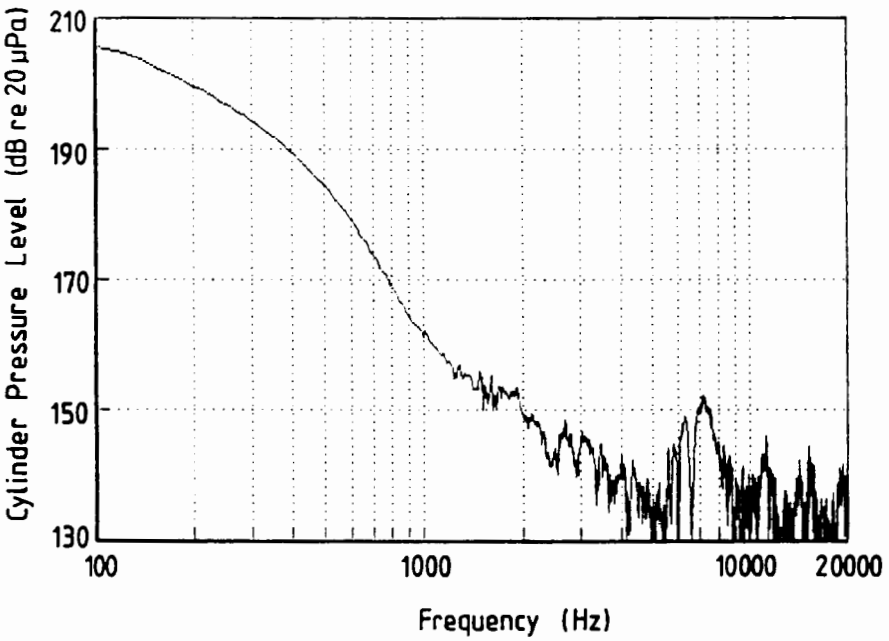

Figure F.21b Cylinder pressure spectrum.

Engine	:	Nissan L28
Engine Speed	:	3000 rpm
Spark Timing	:	10° BTDC
Fuel	:	93 RON gasoline

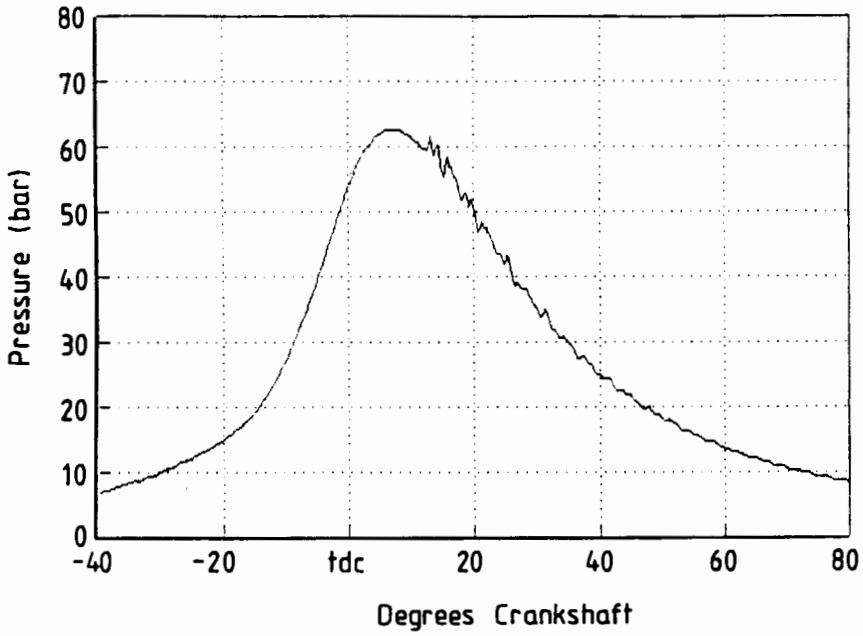

Figure F.22a Cylinder pressure diagram.

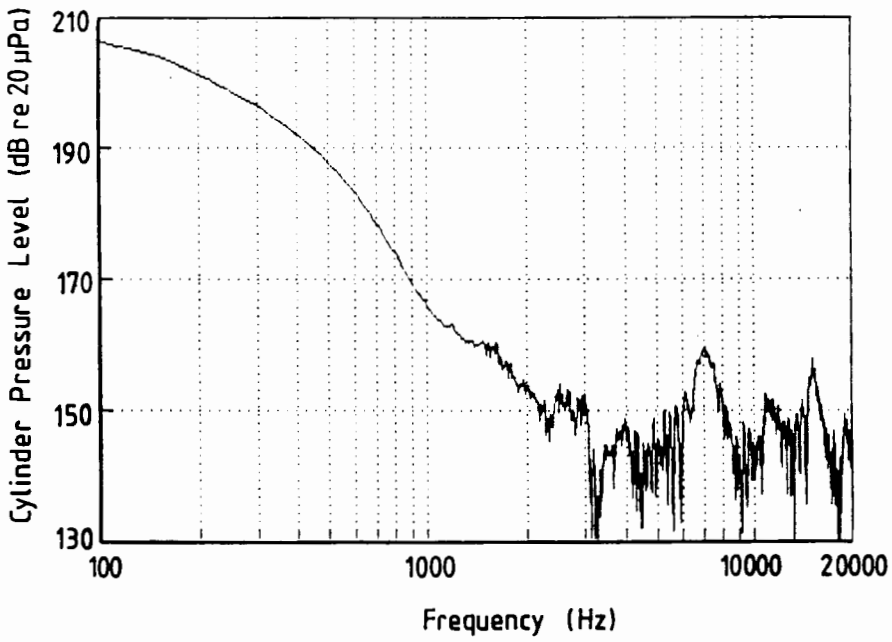

Figure F.22b Cylinder pressure spectrum.

Engine	:	Nissan L28
Engine Speed	:	3500 rpm
Spark Timing	:	10° BTDC
Fuel	:	93 RON gasoline

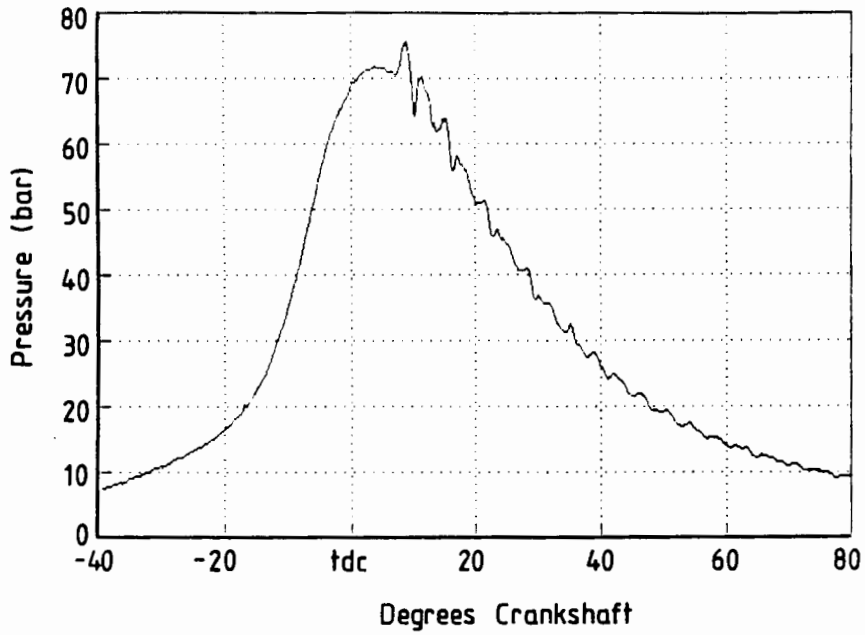

Figure F.23a Cylinder pressure diagram.

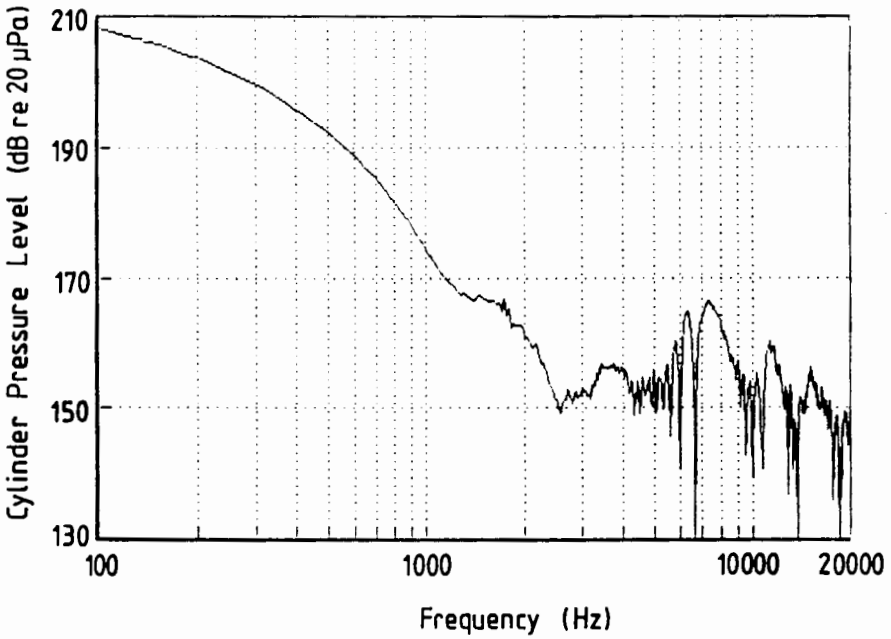

Figure F.23b Cylinder pressure spectrum.

Engine	:	Nissan L28
Engine Speed	:	4000 rpm
Spark Timing	:	10° BTDC
Fuel	:	93 RON gasoline

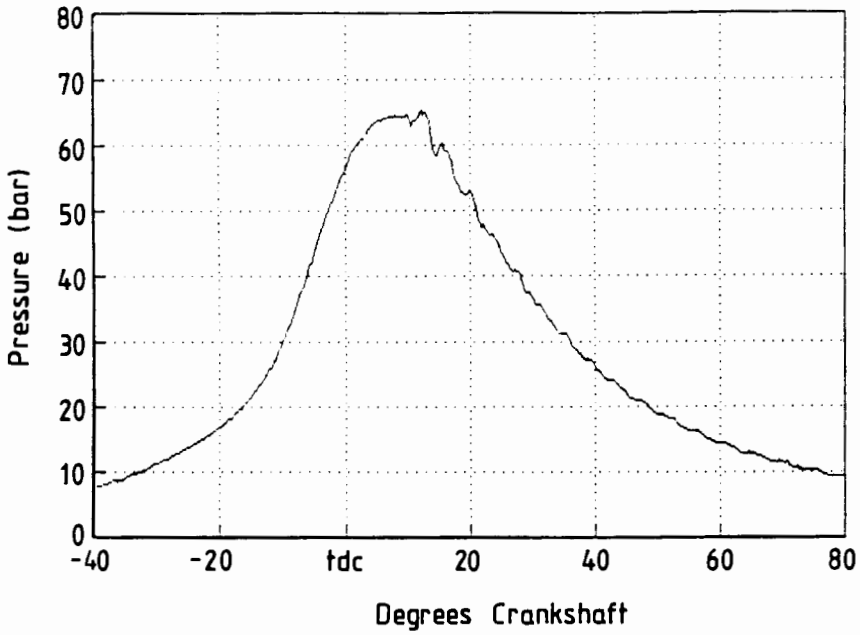

Figure F.24a Cylinder pressure diagram.

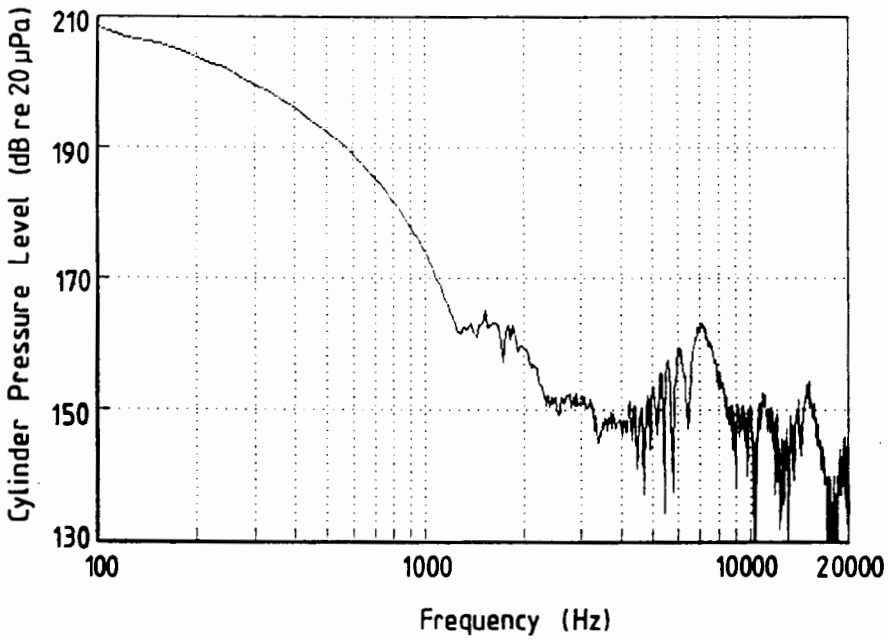

Figure F.24b Cylinder pressure spectrum.

Engine	:	Nissan L28
Engine Speed	:	4500 rpm
Spark Timing	:	10° BTDC
Fuel	:	93 RON gasoline

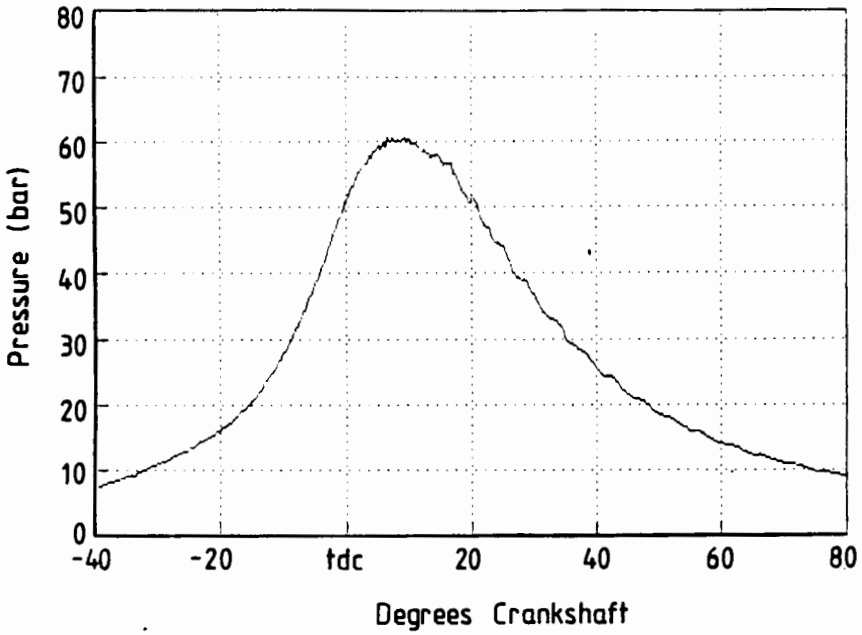

Figure F.25a Cylinder pressure diagram.

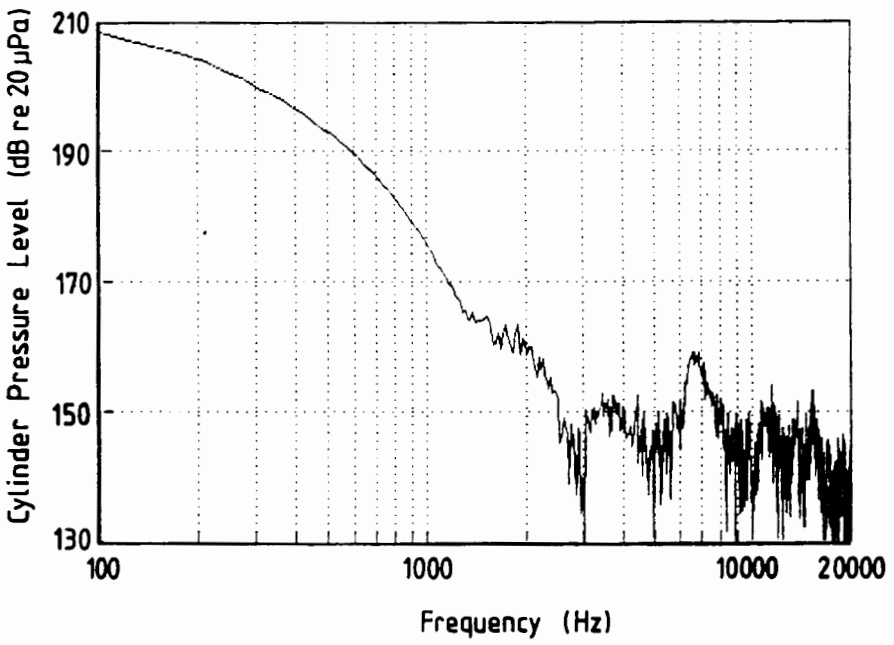

Figure F.25b Cylinder pressure spectrum.

Engine	:	Nissan L28
Engine Speed	:	5000 rpm
Spark Timing	:	10° BTDC
Fuel	:	93 RON gasoline

APPENDIX G

VOLKSWAGEN 1800 ENGINE TEST RESULTS

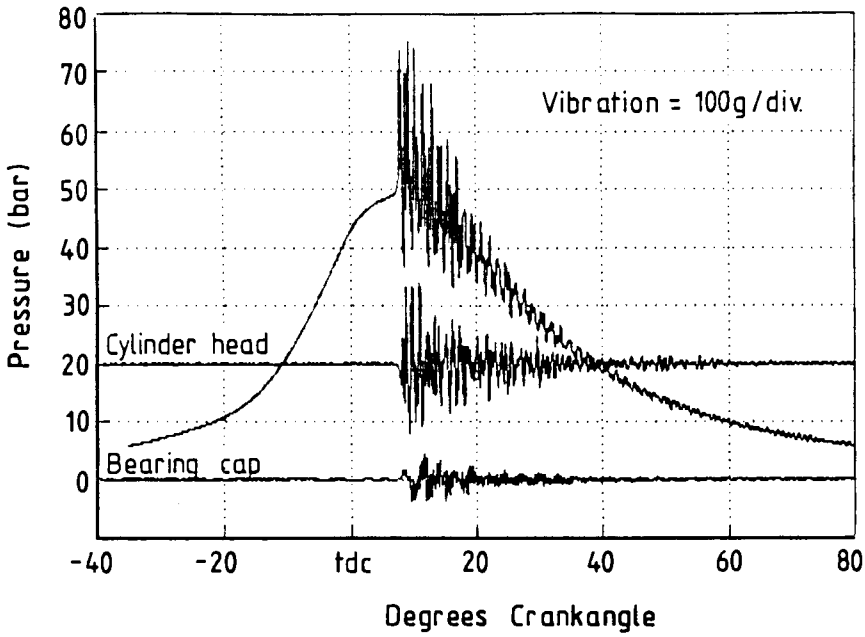

Figure G.1a Cylinder pressure diagram.

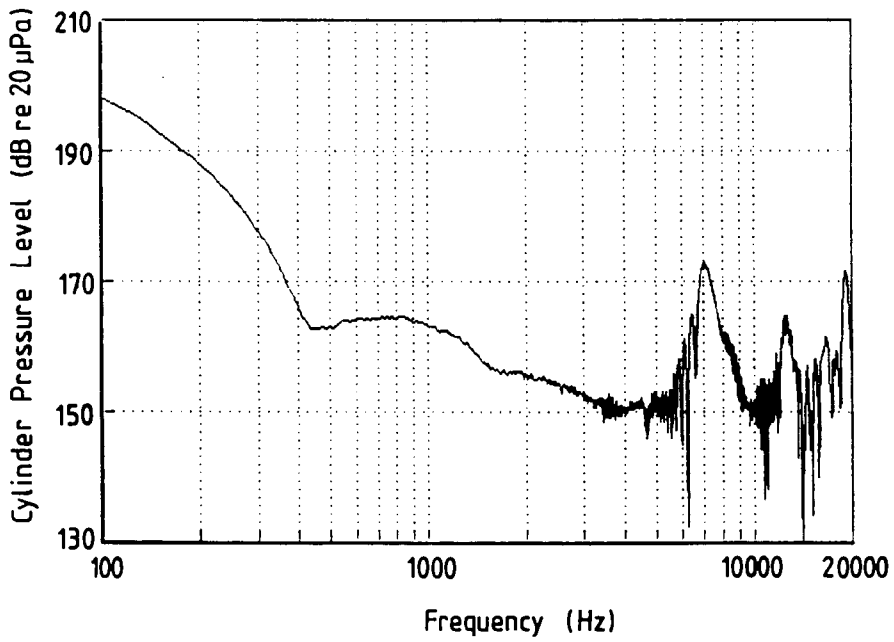

Figure G.1b Cylinder pressure spectrum.

Engine	:	Volkswagen 1800
Engine Speed	:	1500 rpm
Spark Timing	:	26° BTDC
Fuel	:	93 RON gasoline

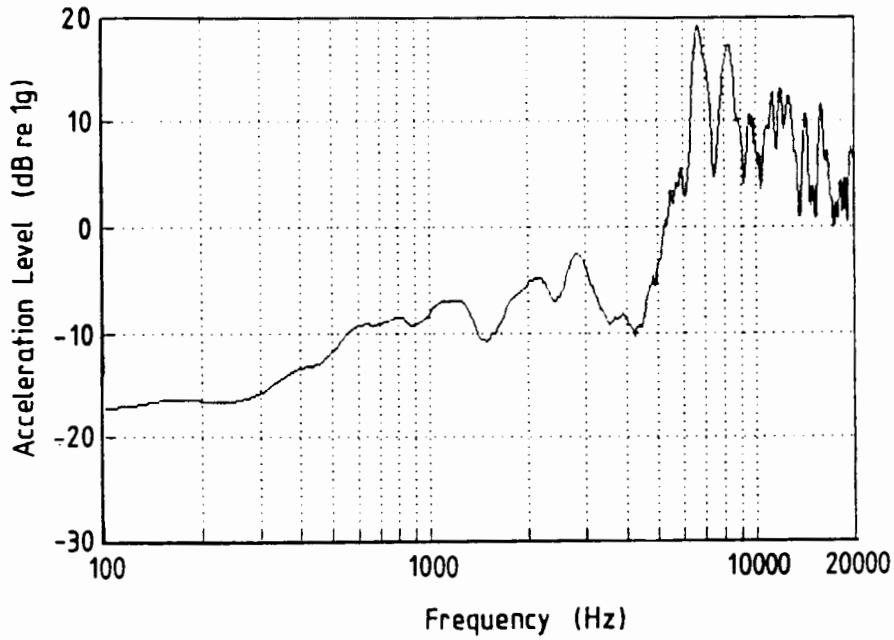

Figure G.1c Cylinder head vibration spectrum.

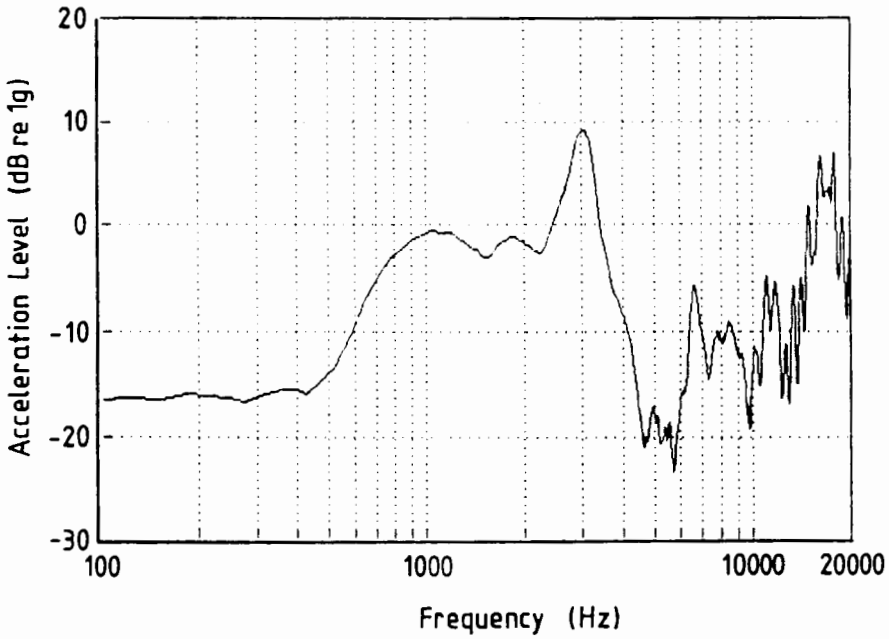

Figure G.1d Main bearing cap vibration spectrum.

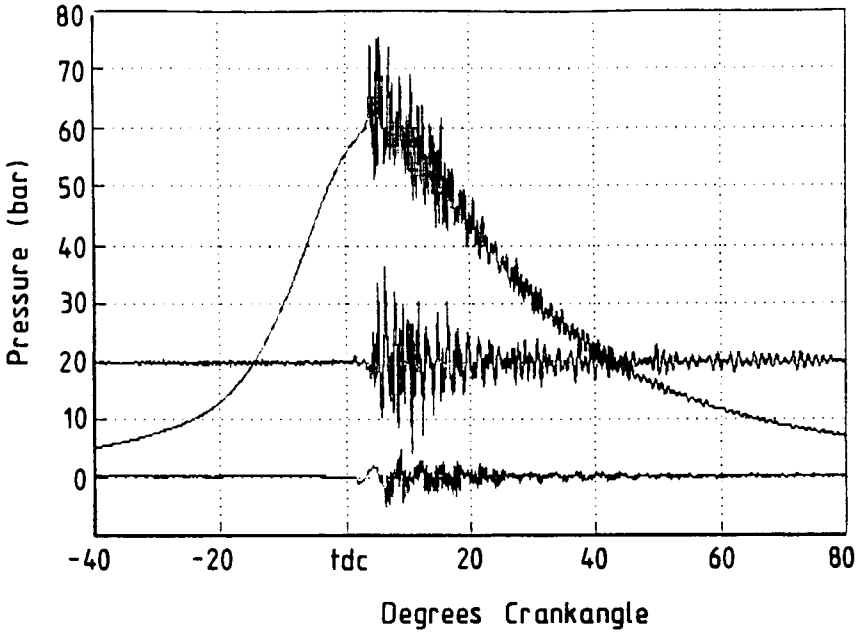

Figure G.2a Cylinder pressure diagram.

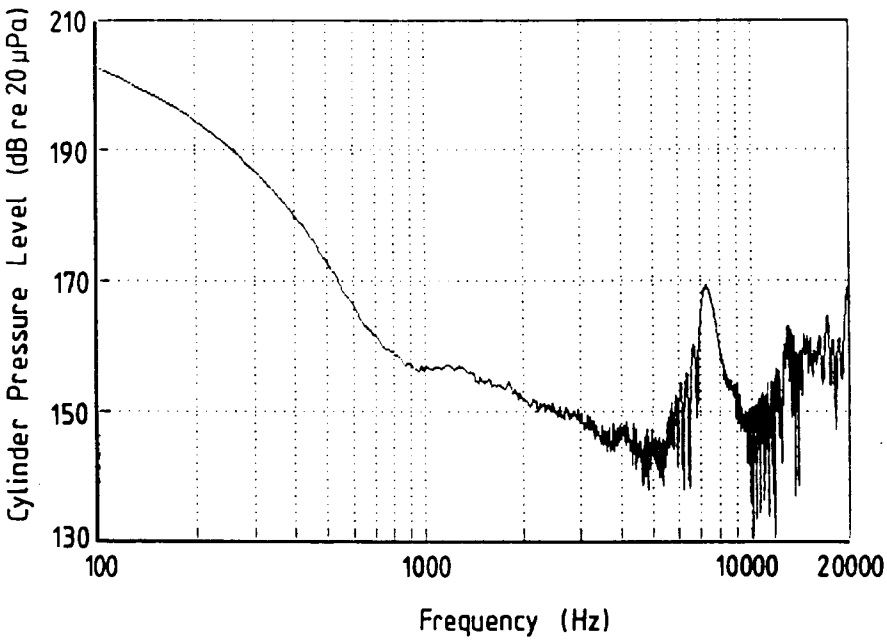

Figure G.2b Cylinder pressure spectrum.

Engine	:	Volkswagen 1800
Engine Speed	:	2000 rpm
Spark Timing	:	26° BTDC
Fuel	:	93 RON gasoline

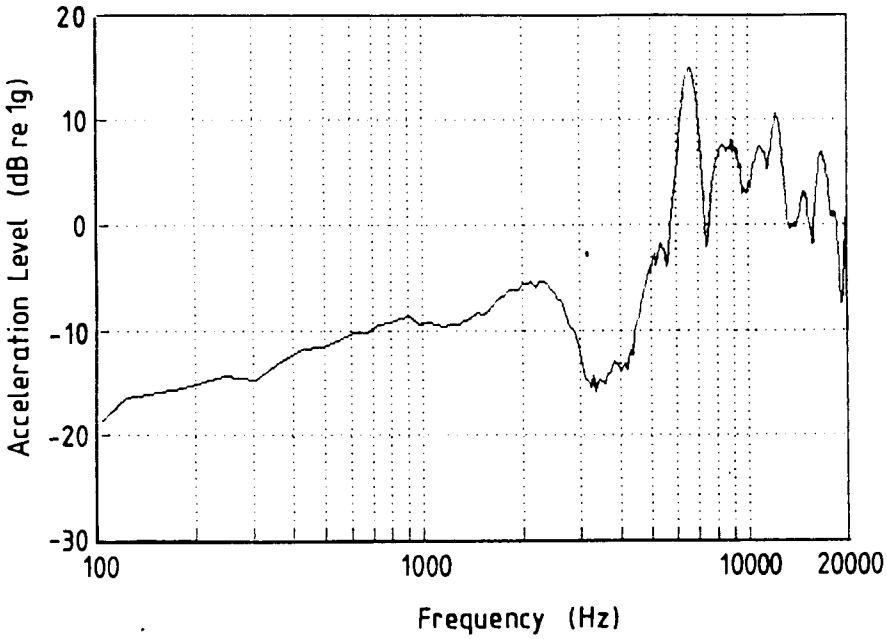

Figure G.2c Cylinder head vibration spectrum.

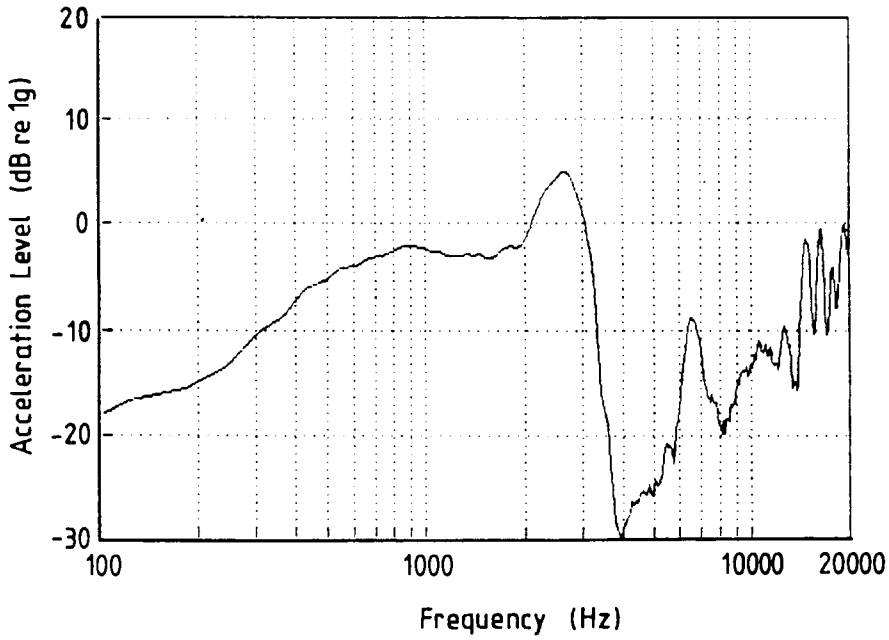

Figure G.2d Main bearing cap vibration spectrum.

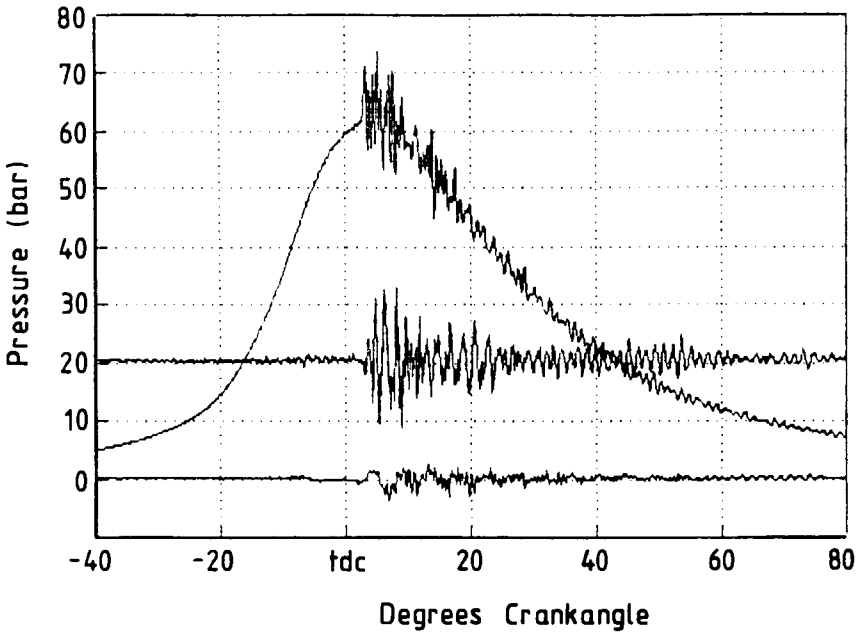

Figure G.3a Cylinder pressure diagram.

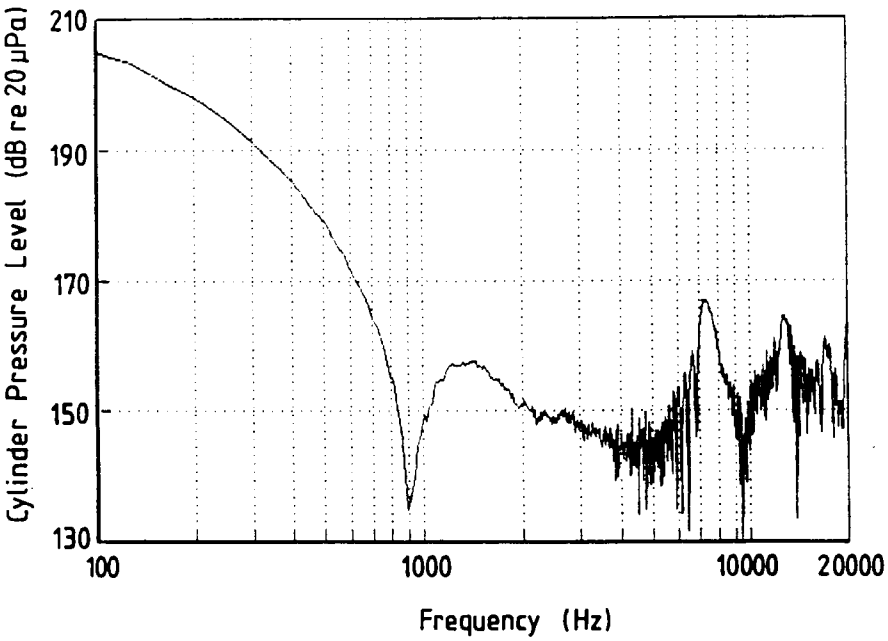

Figure G.3b Cylinder pressure spectrum.

Engine	:	Volkswagen 1800
Engine Speed	:	2500 rpm
Spark Timing	:	26° BTDC
Fuel	:	93 RON gasoline

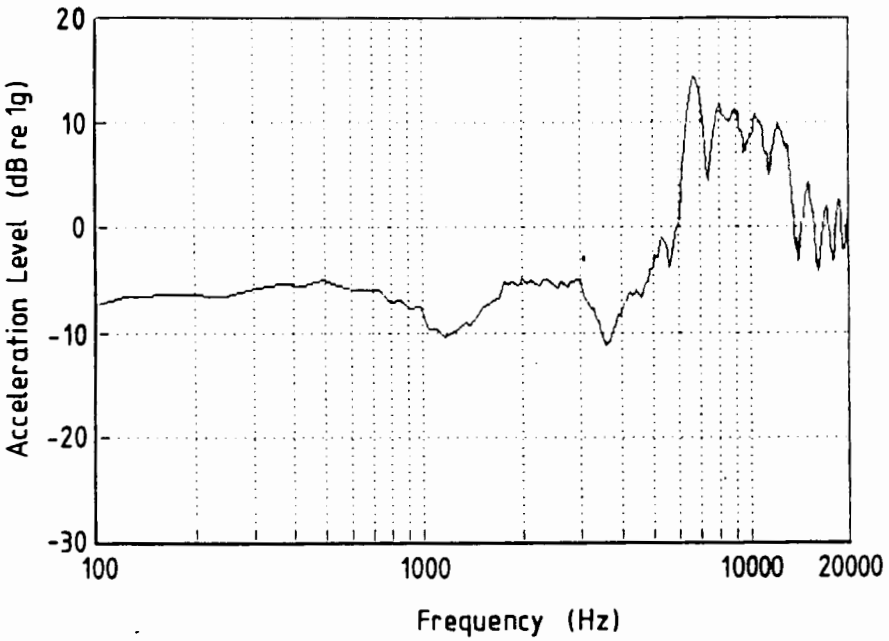

Figure G.3c Cylinder head vibration spectrum.

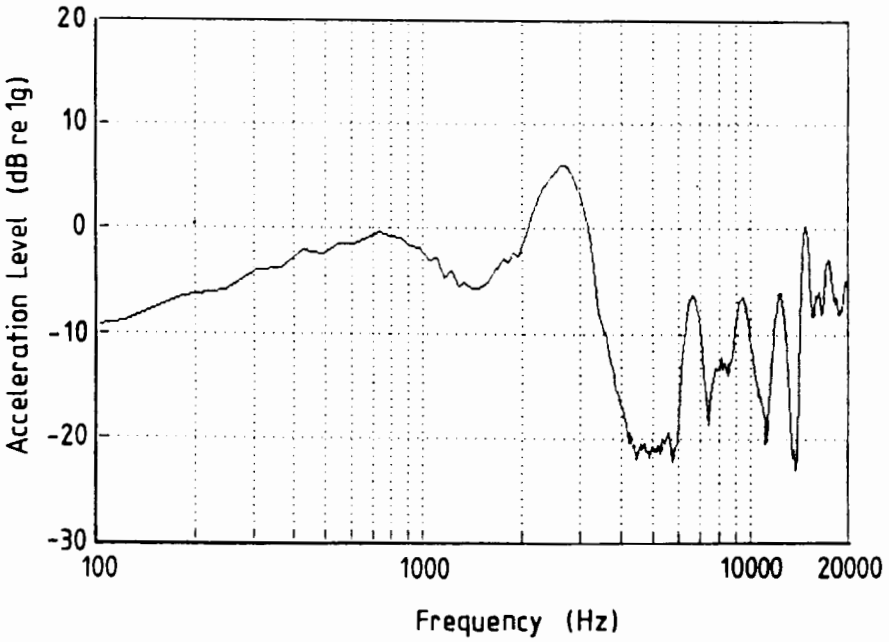

Figure G.3d Main bearing cap vibration spectrum.

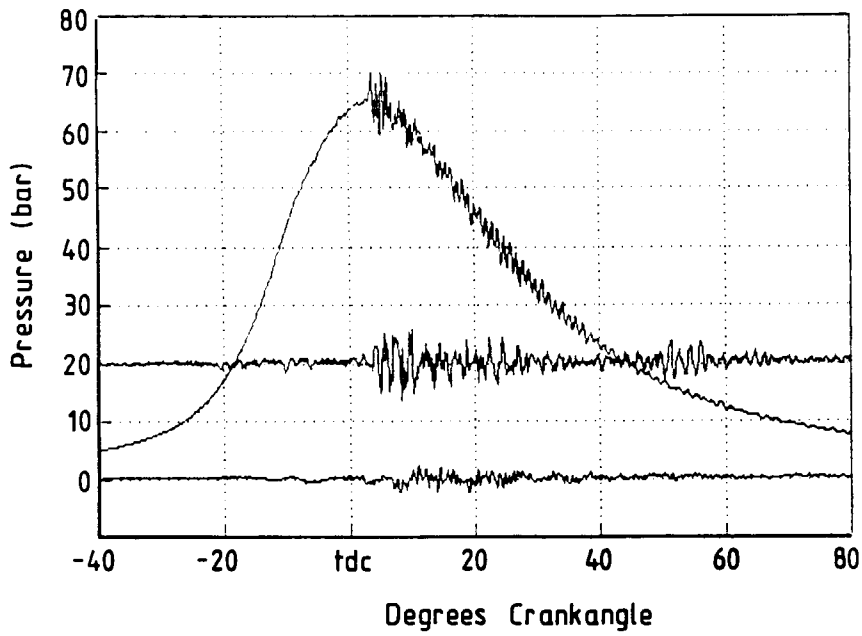

Figure G.4a Cylinder pressure diagram.

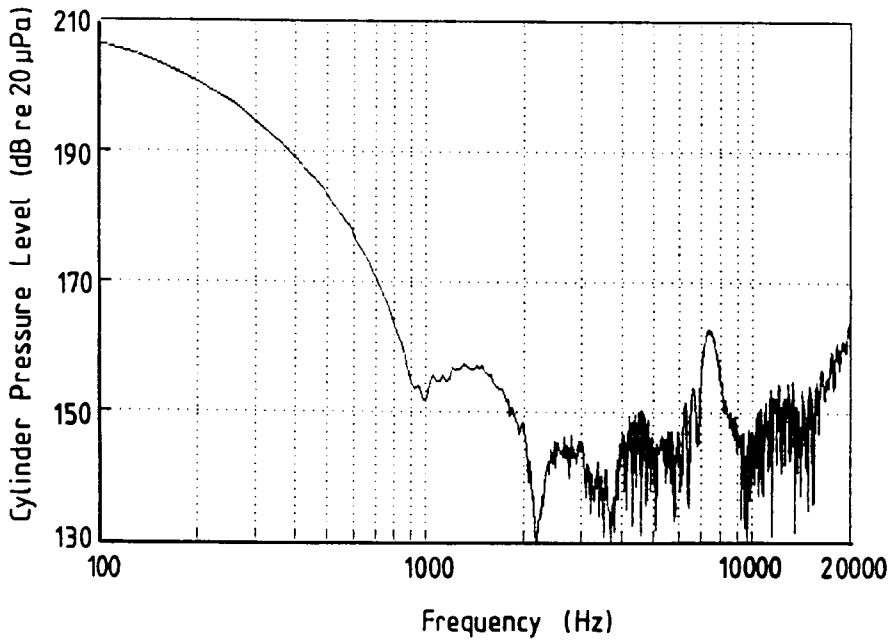

Figure G.4b Cylinder pressure spectrum.

Engine	:	Volkswagen 1800
Engine Speed	:	3000 rpm
Spark Timing	:	26° BTDC
Fuel	:	93 RON gasoline

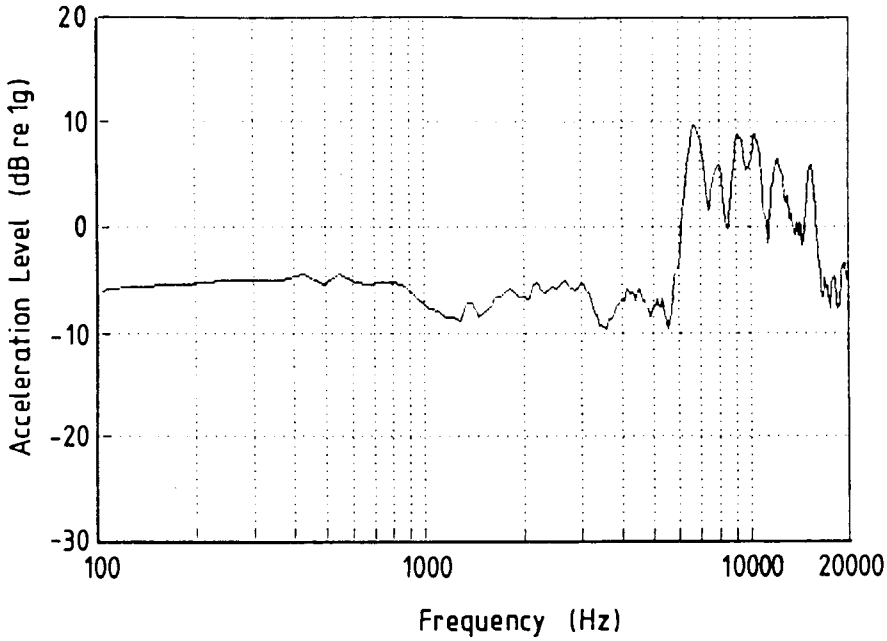

Figure G.4c Cylinder head vibration spectrum.

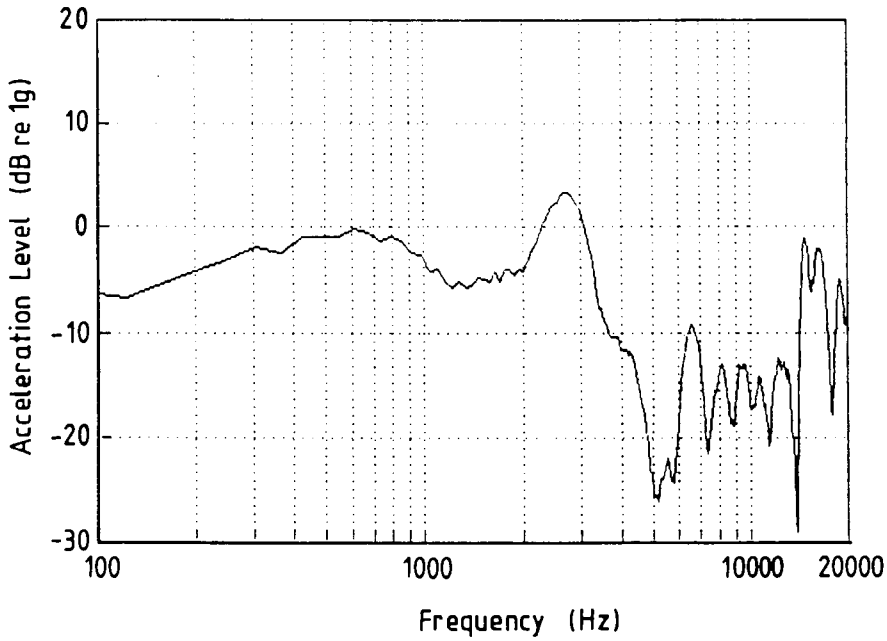

Figure G.4d Main bearing cap vibration spectrum.

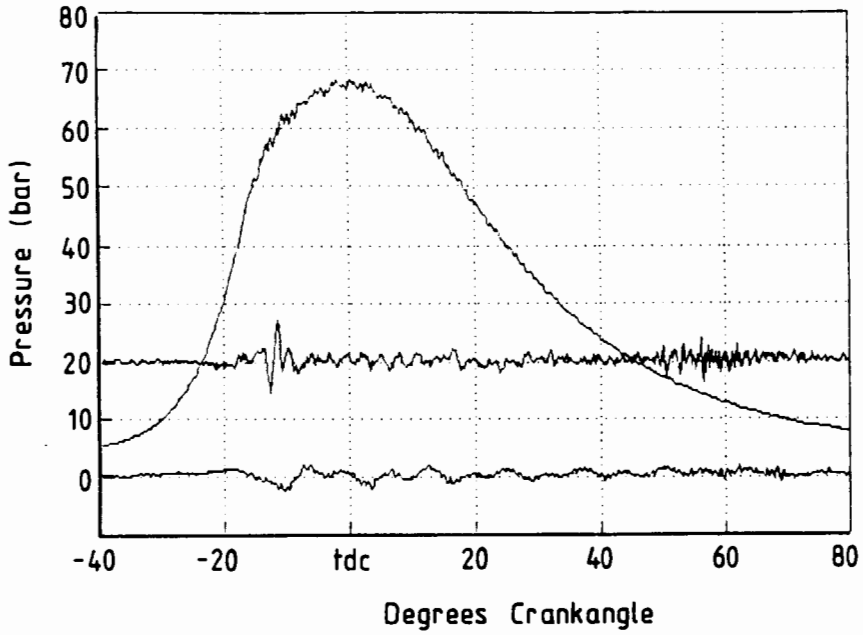

Figure G.5a Cylinder pressure diagram.

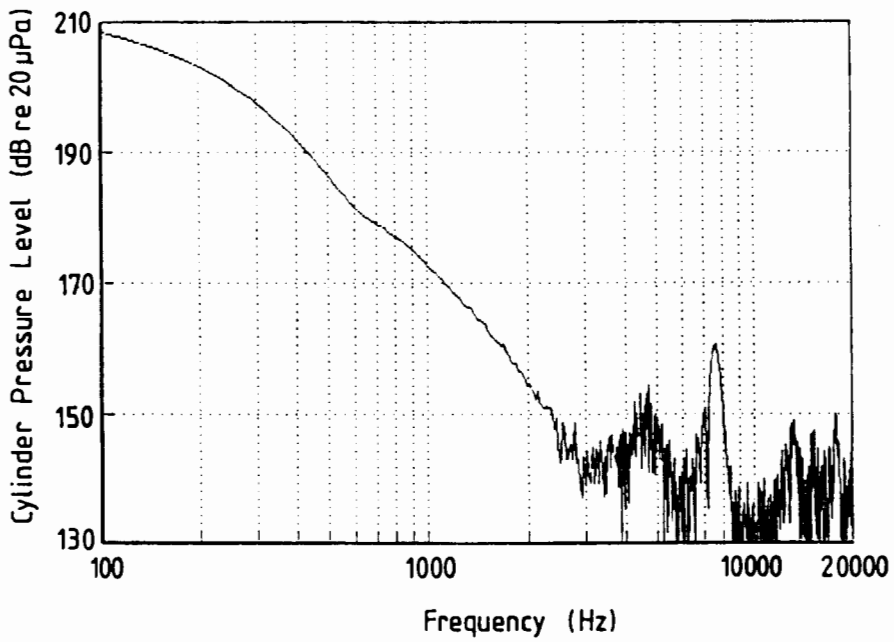

Figure G.5b Cylinder pressure spectrum.

Engine	:	Volkswagen 1800
Engine Speed	:	3500 rpm
Spark Timing	:	26° BTDC
Fuel	:	93 RON gasoline

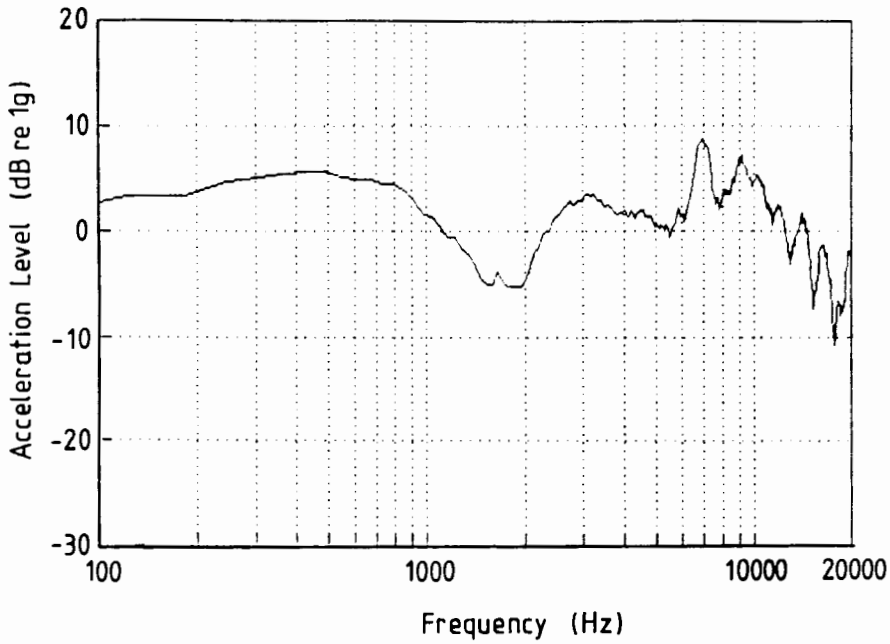

Figure G.5c Cylinder head vibration spectrum.

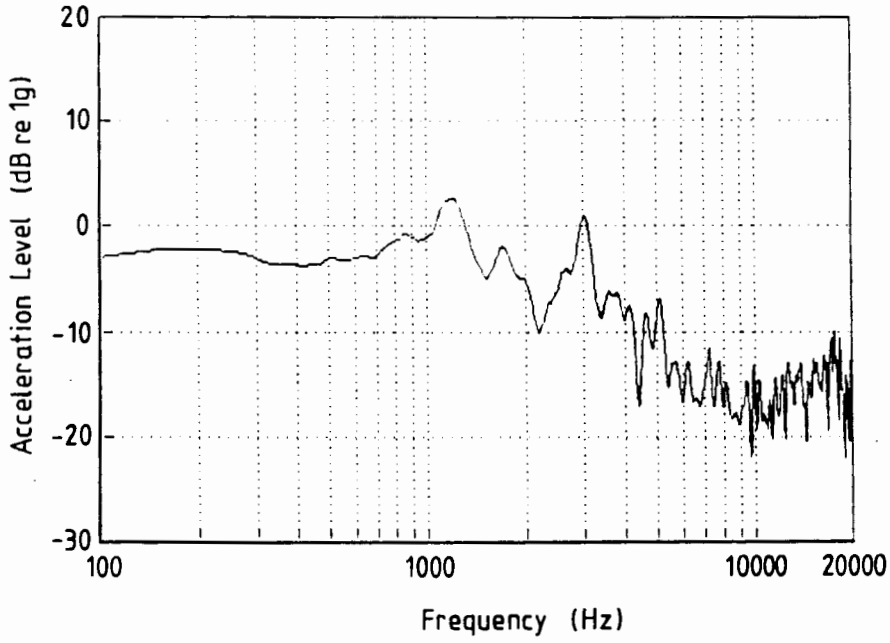

Figure G.5d Main bearing cap vibration spectrum.

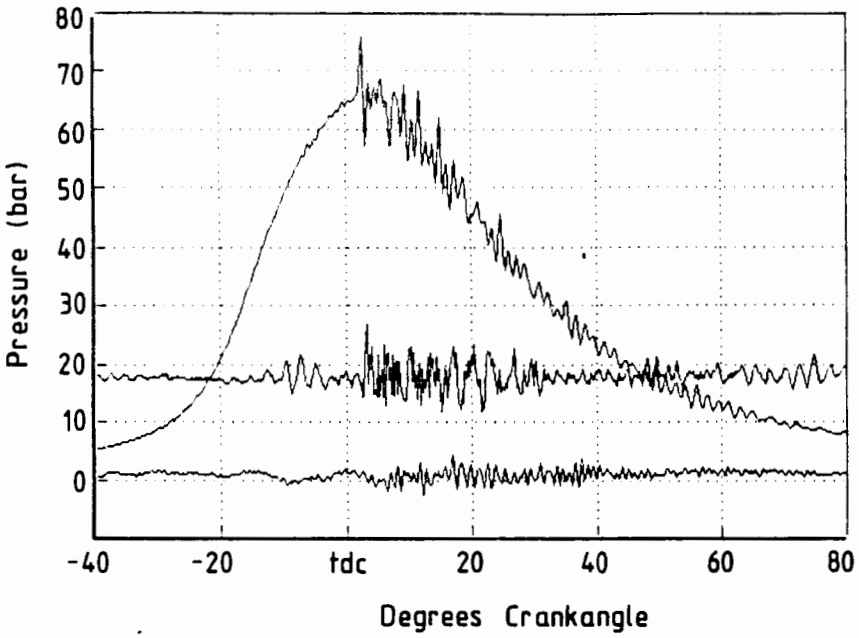

Figure G.6a Cylinder pressure diagram.

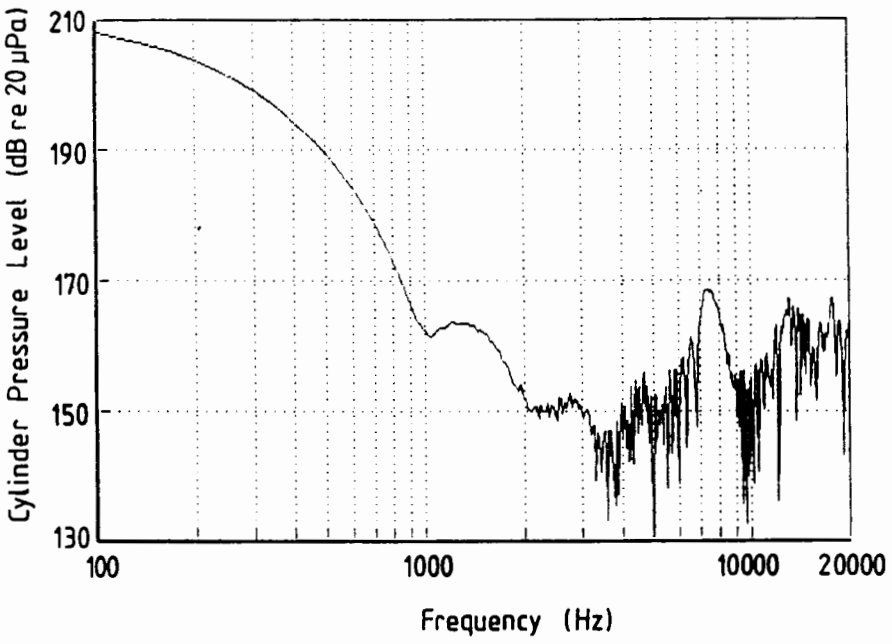

Figure G.6b Cylinder pressure spectrum.

Engine	:	Volkswagen 1800
Engine Speed	:	4000 rpm
Spark Timing	:	26° BTDC
Fuel	:	93 RON gasoline

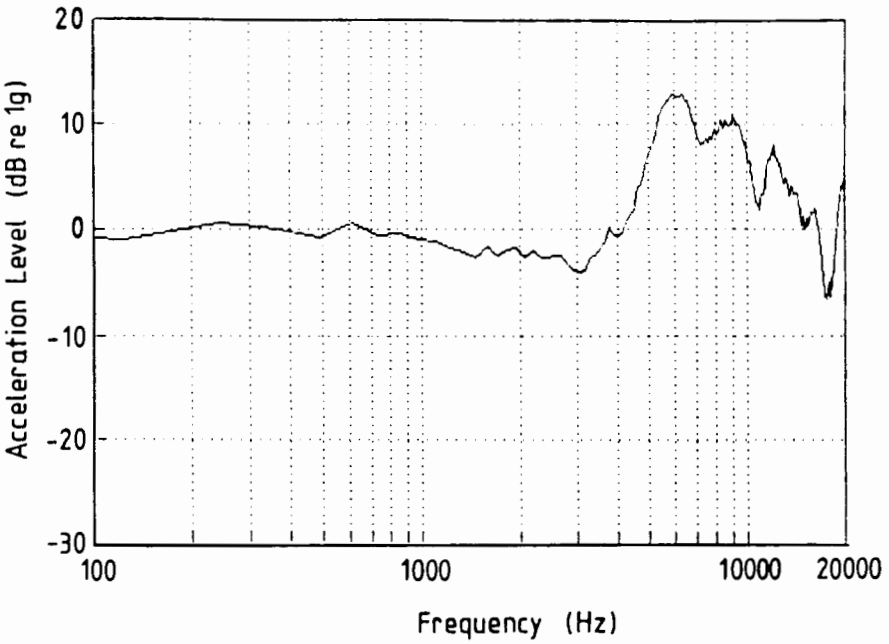

Figure G.6c Cylinder head vibration spectrum.

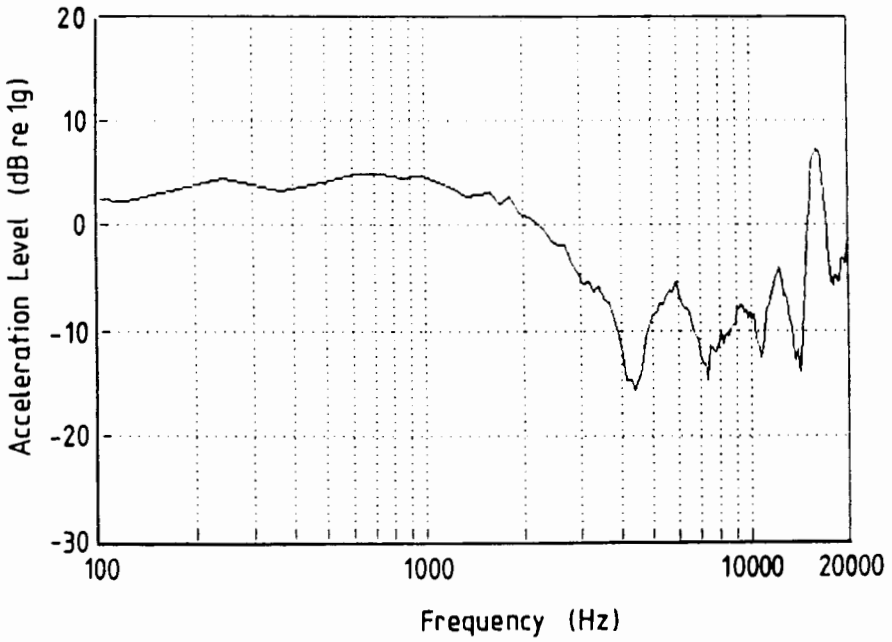

Figure G.6d Main bearing cap vibration spectrum.

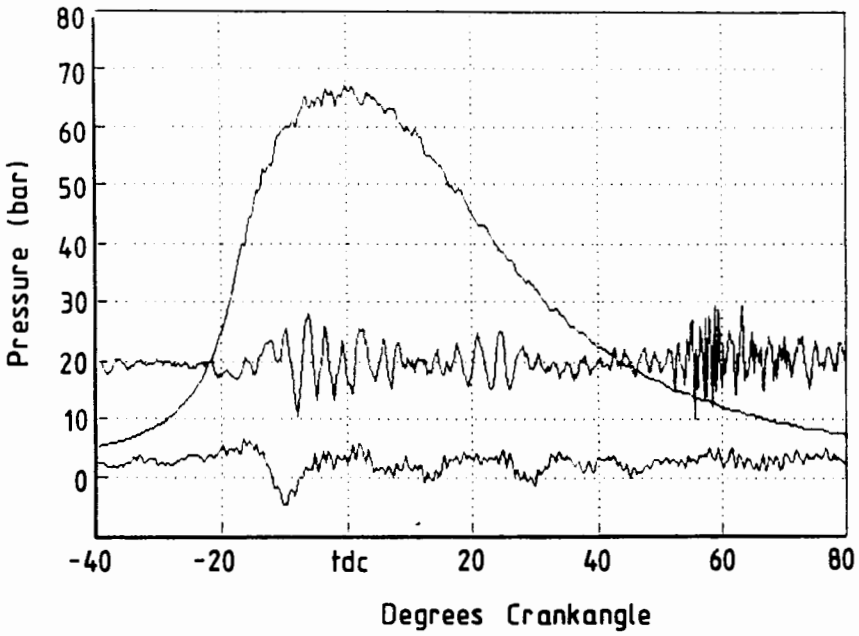

Figure G.7a Cylinder pressure diagram.

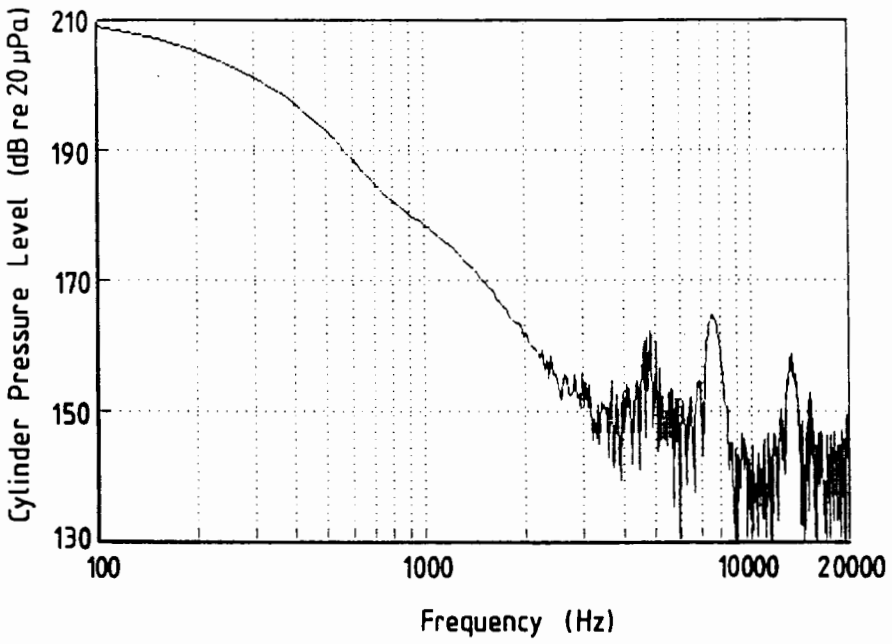

Figure G.7b Cylinder pressure spectrum.

Engine	:	Volkswagen 1800
Engine Speed	:	4500 rpm
Spark Timing	:	26° BTDC
Fuel	:	93 RON gasoline

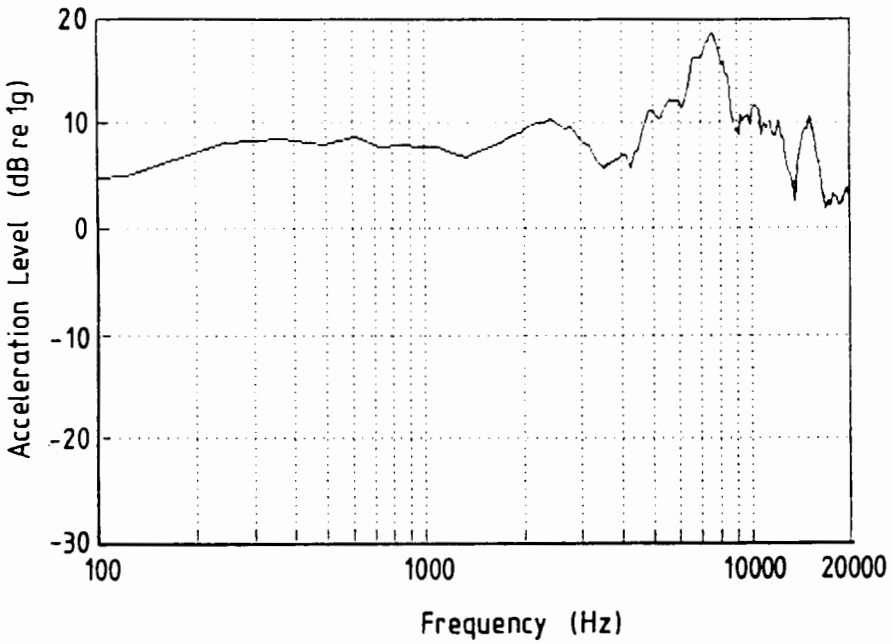

Figure G.7c Cylinder head vibration spectrum.

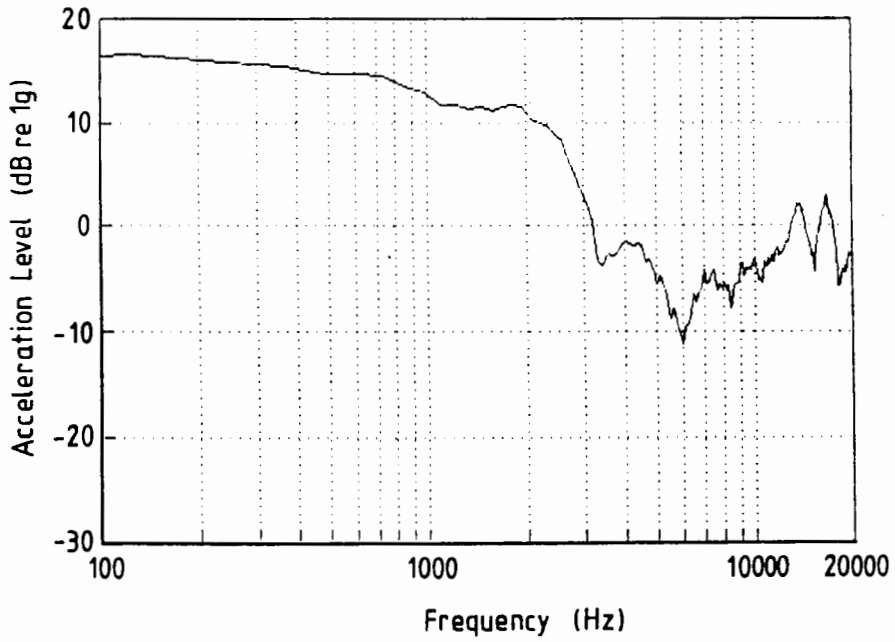

Figure G.7d Main bearing cap vibration spectrum.

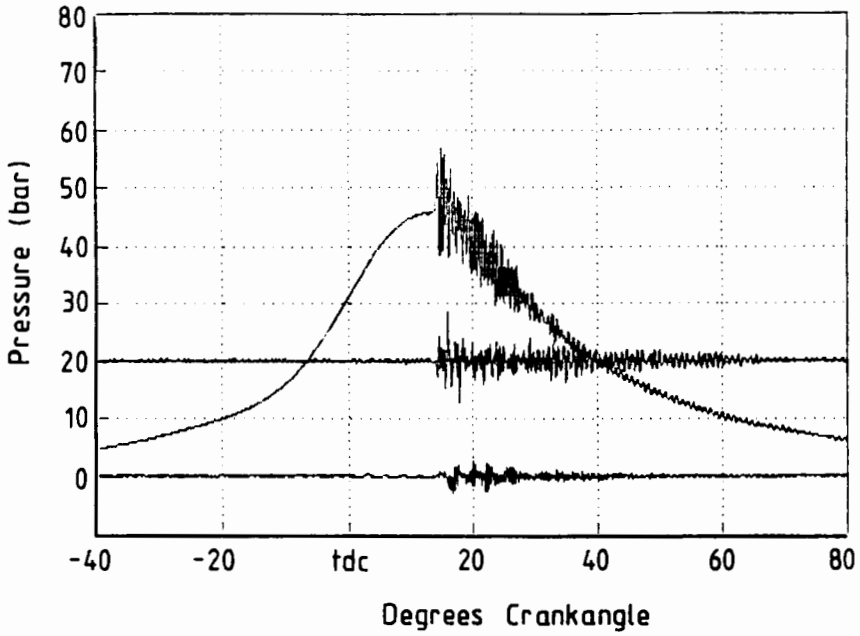

Figure G.8a Cylinder pressure diagram.

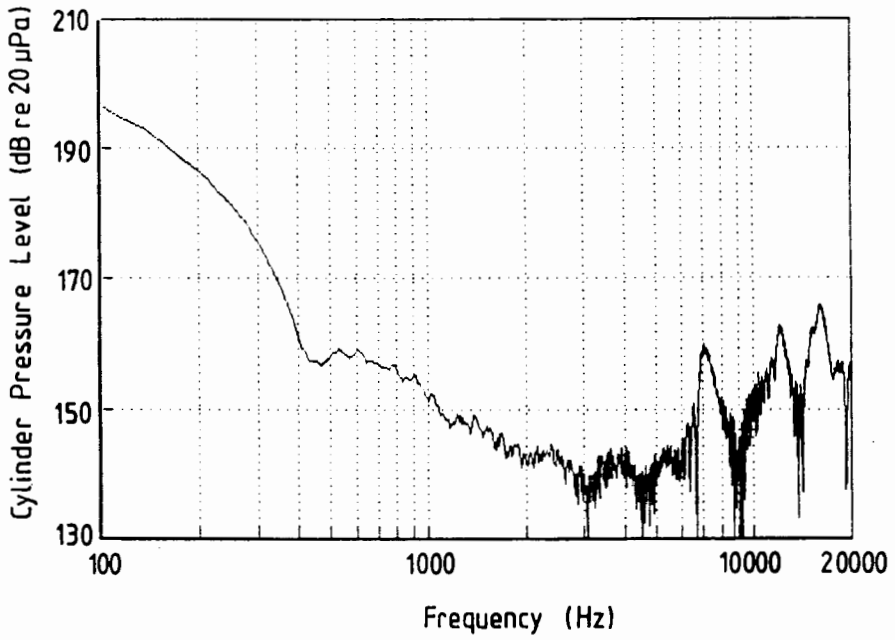

Figure G.8b Cylinder pressure spectrum.

Engine	:	Volkswagen 1800
Engine Speed	:	1500 rpm
Spark Timing	:	16° BTDC
Fuel	:	93 RON gasoline

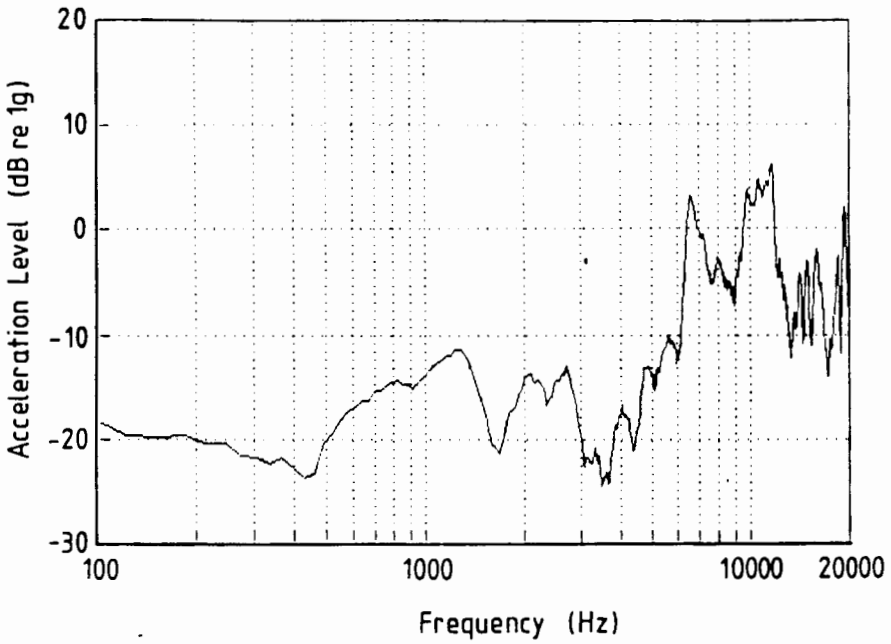

Figure G.8c Cylinder head vibration spectrum.

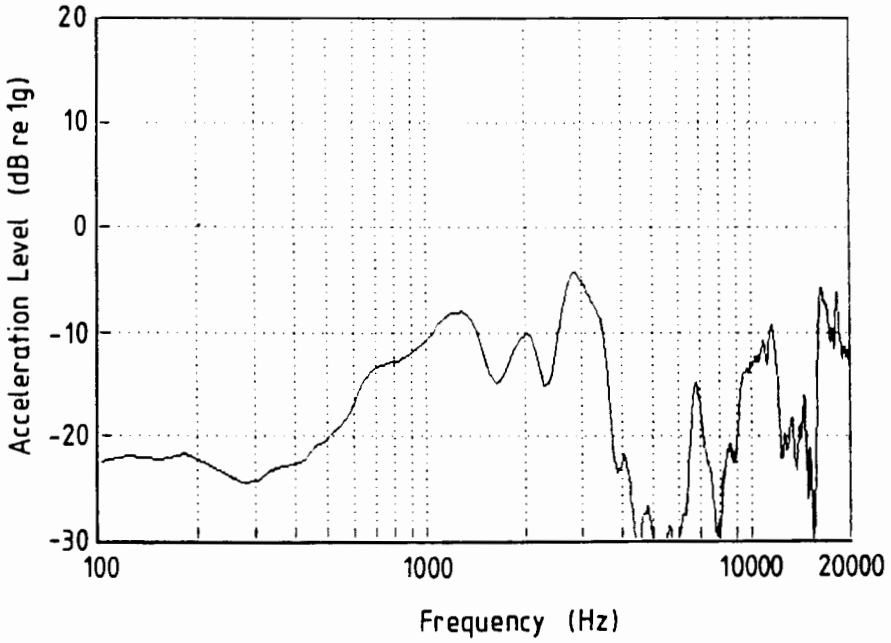

Figure G.8d Main bearing cap vibration spectrum.

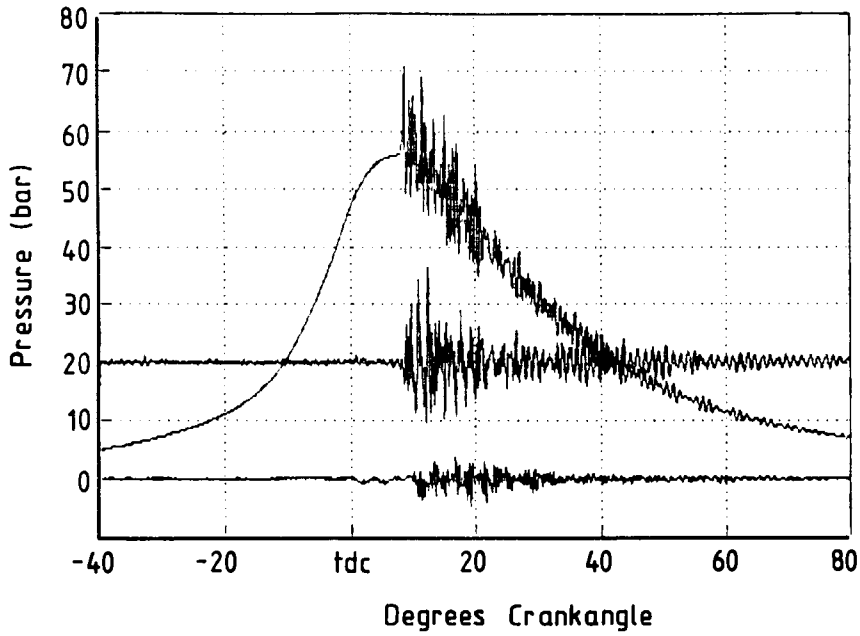

Figure G.9a Cylinder pressure diagram.

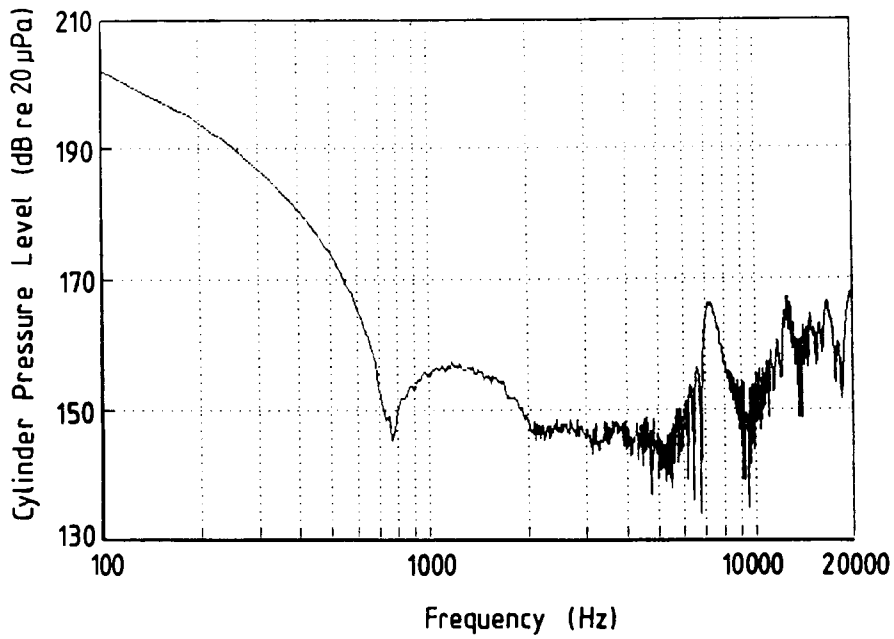

Figure G.9b Cylinder pressure spectrum.

Engine	:	Volkswagen 1800
Engine Speed	:	2000 rpm
Spark Timing	:	16° BTDC
Fuel	:	93 RON gasoline

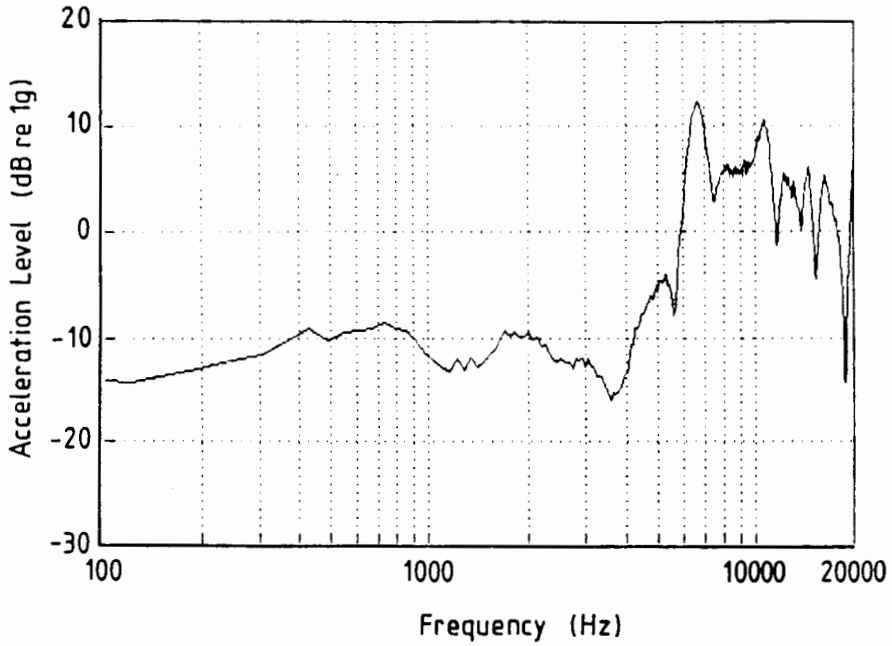

Figure G.9c Cylinder head vibration spectrum.

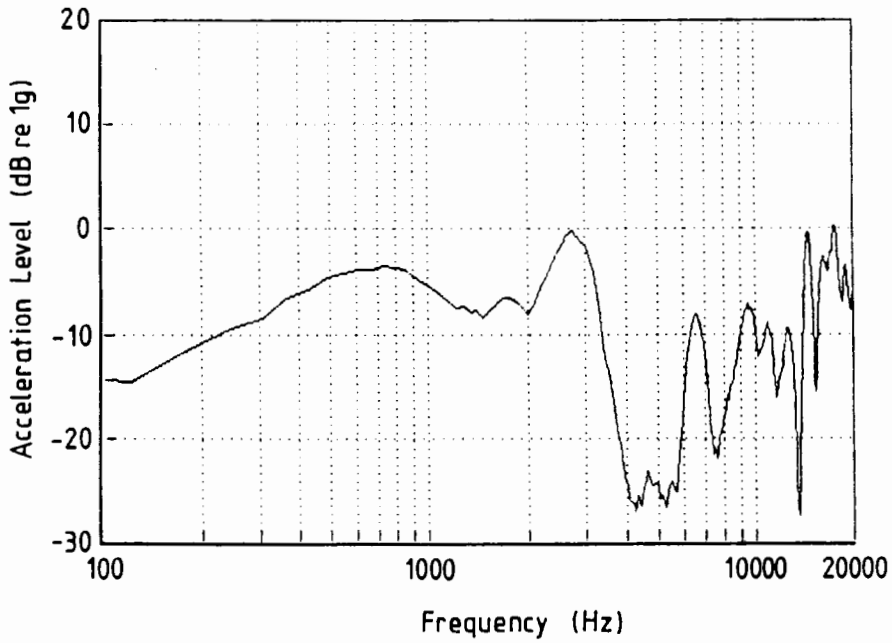

Figure G.9d Main bearing cap vibration spectrum.

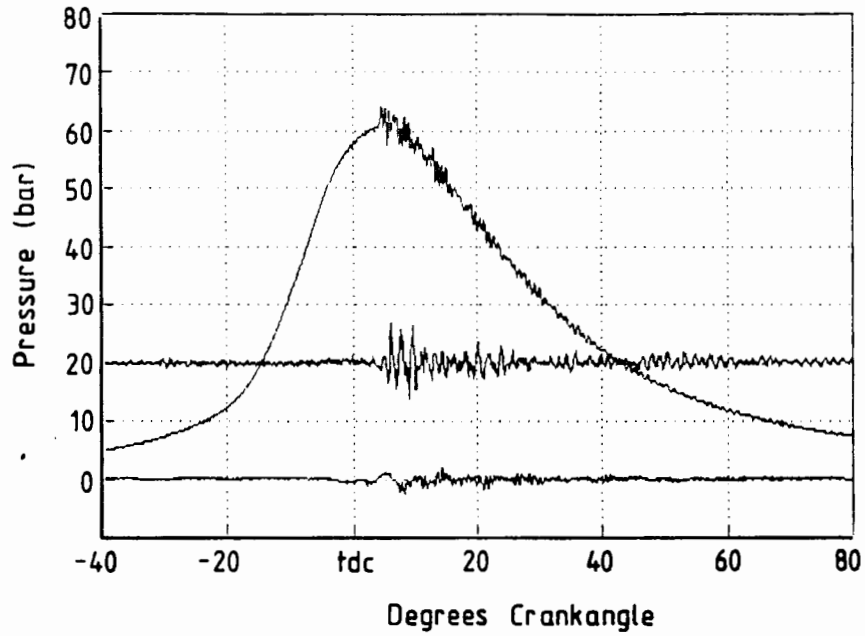

Figure G.10a Cylinder pressure diagram.

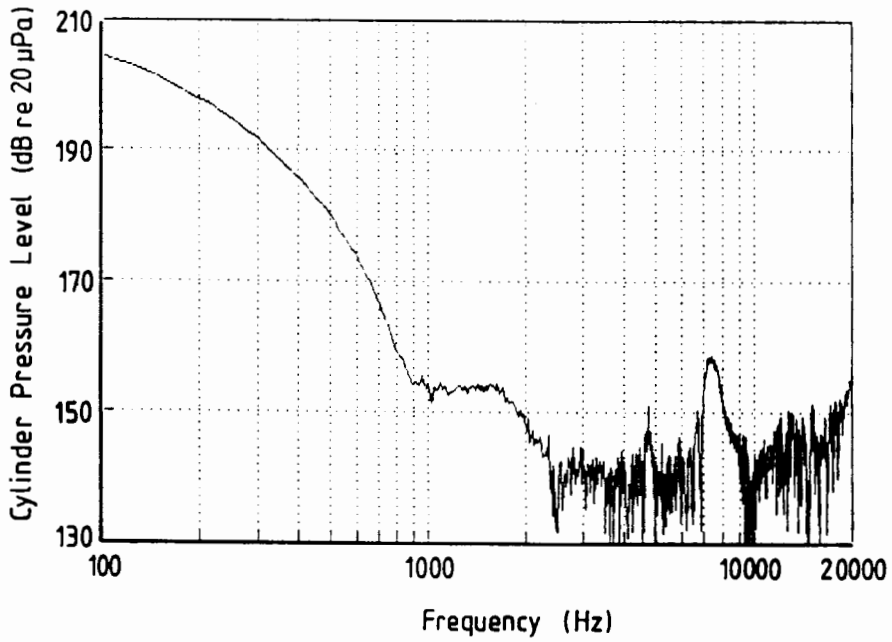

Figure G.10b Cylinder pressure spectrum.

Engine	:	Volkswagen 1800
Engine Speed	:	2500 rpm
Spark Timing	:	16° BTDC
Fuel	:	93 RON gasoline

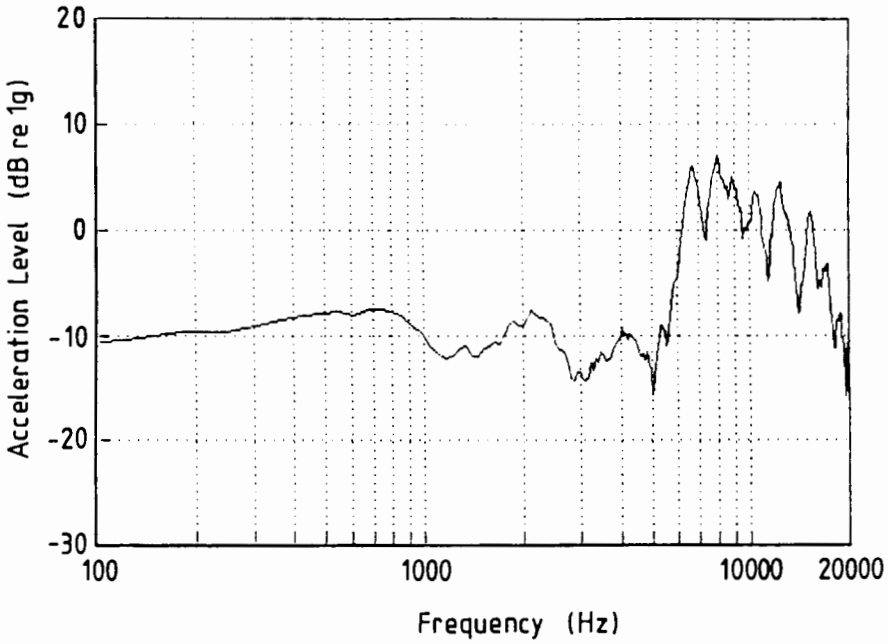

Figure G.10c Cylinder head vibration spectrum.

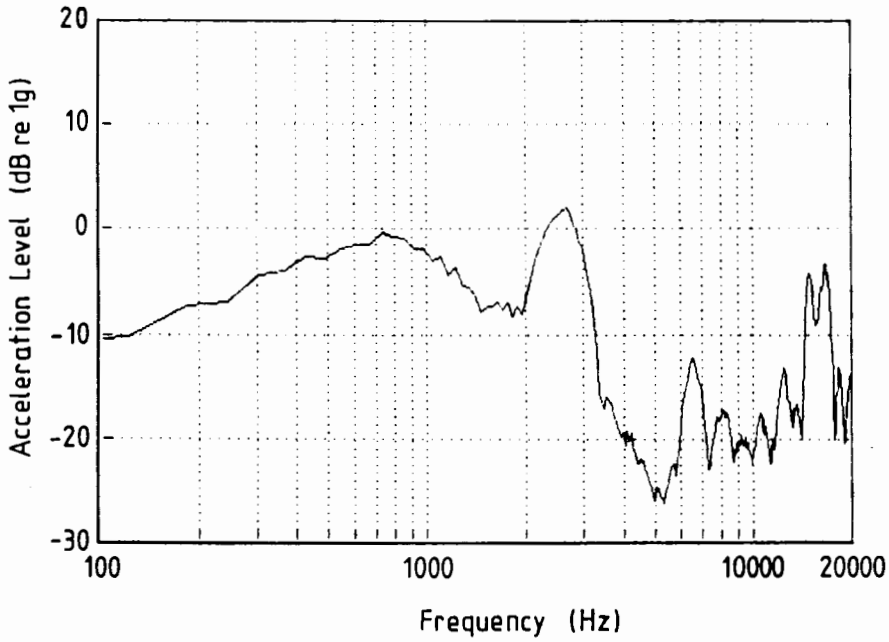

Figure G.10d Main bearing cap vibration spectrum.

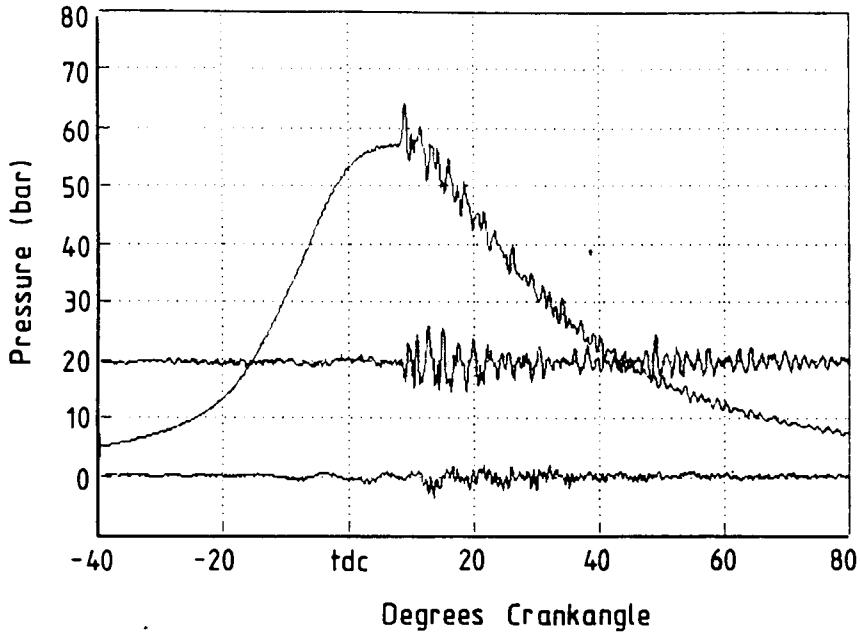

Figure G.11a Cylinder pressure diagram.

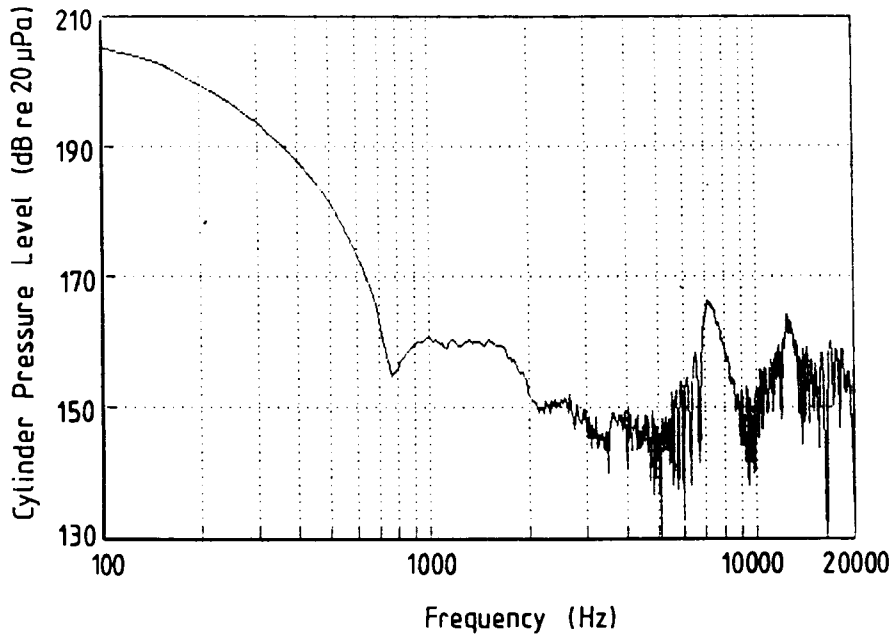

Figure G.11b Cylinder pressure spectrum.

Engine	:	Volkswagen 1800
Engine Speed	:	3000 rpm
Spark Timing	:	16° BTDC
Fuel	:	93 RON gasoline

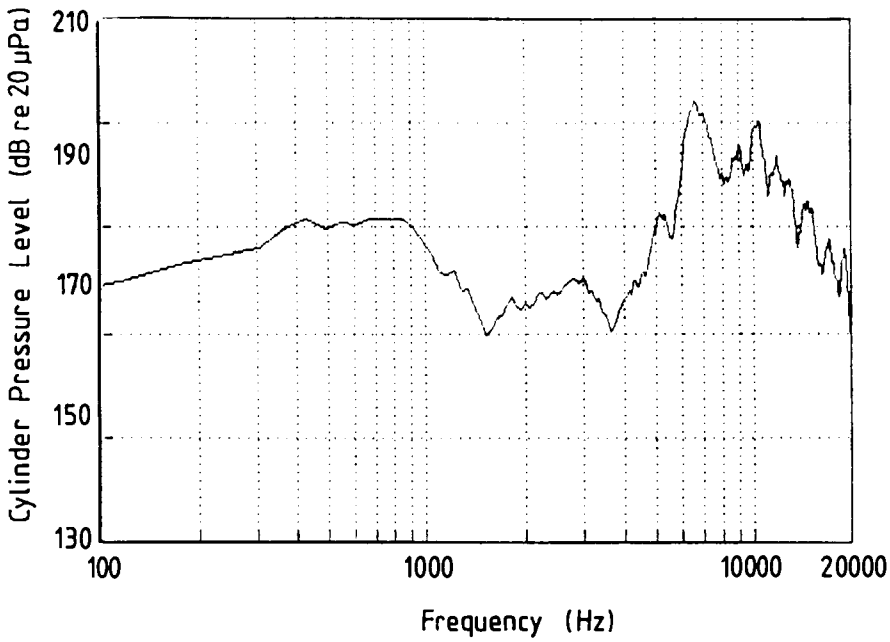

Figure G.11c Cylinder head vibration spectrum.

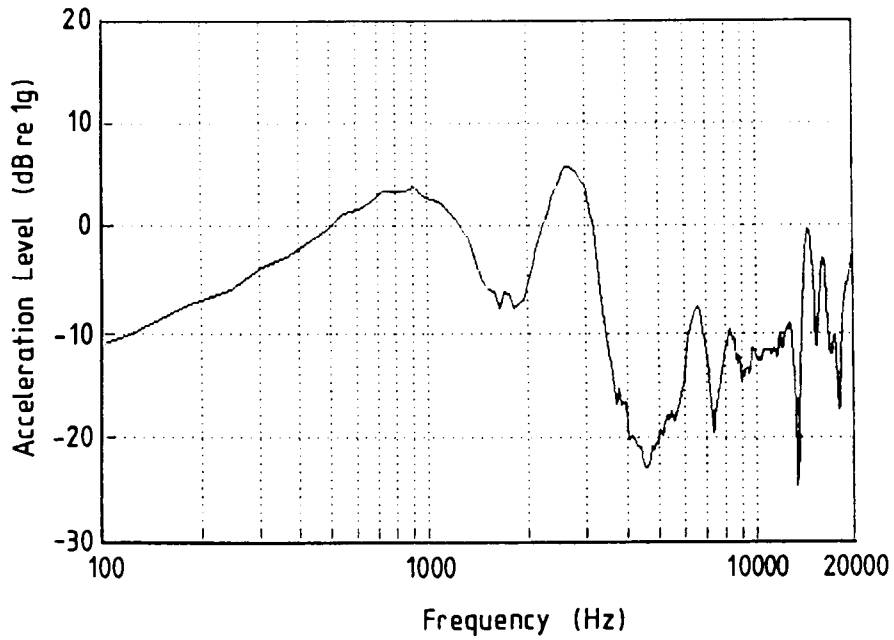

Figure G.11d Main bearing cap vibration spectrum.

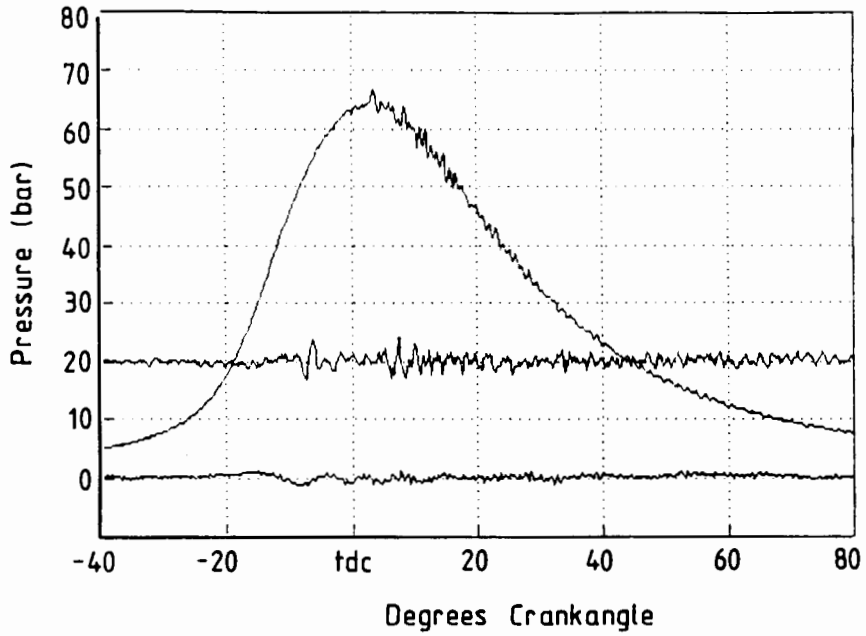

Figure G.12a Cylinder pressure diagram.

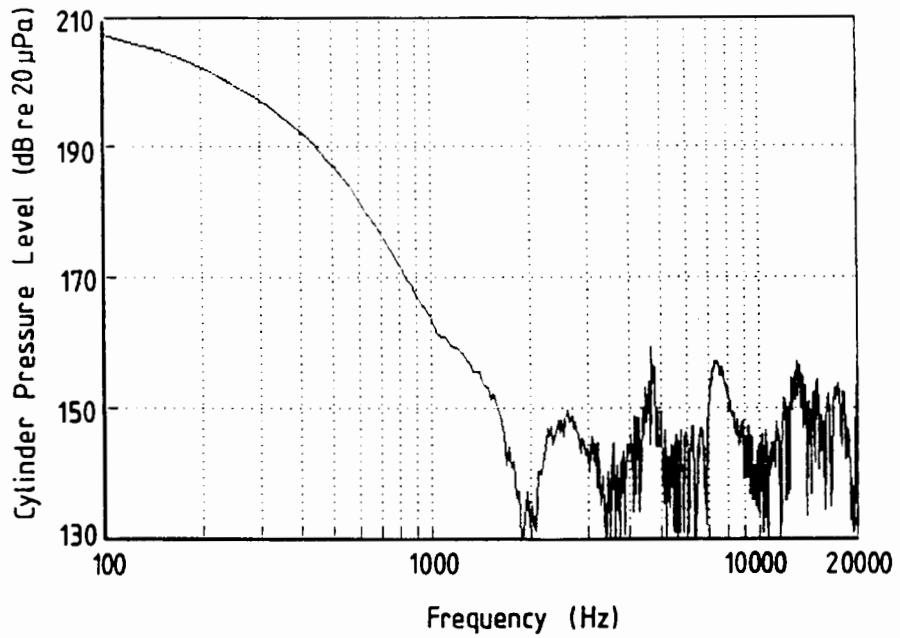

Figure G.12b Cylinder pressure spectrum.

Engine	:	Volkswagen 1800
Engine Speed	:	3500 rpm
Spark Timing	:	16° BTDC
Fuel	:	93 RON gasoline

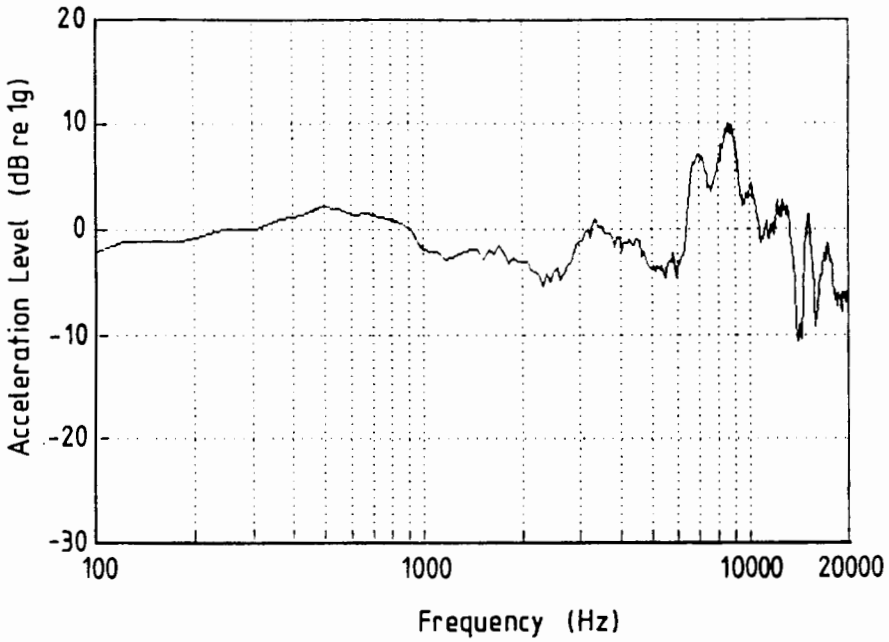

Figure G.12c Cylinder head vibration spectrum.

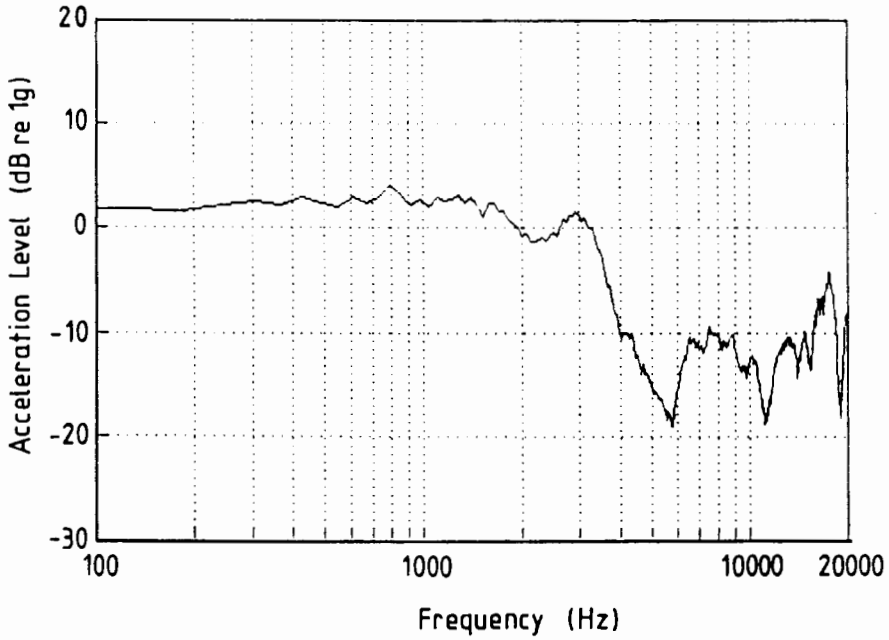

Figure G.12d Main bearing cap vibration spectrum.

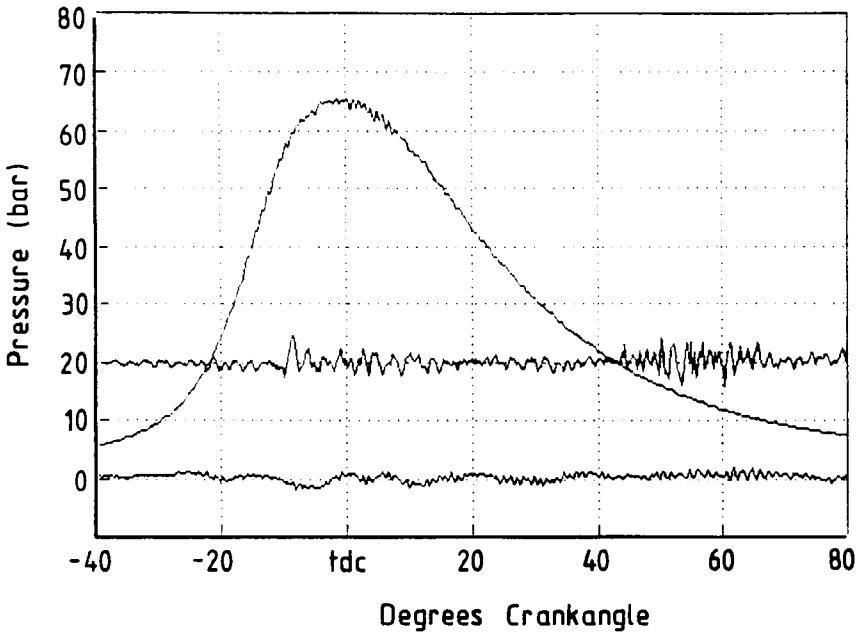

Figure G.13a Cylinder pressure diagram.

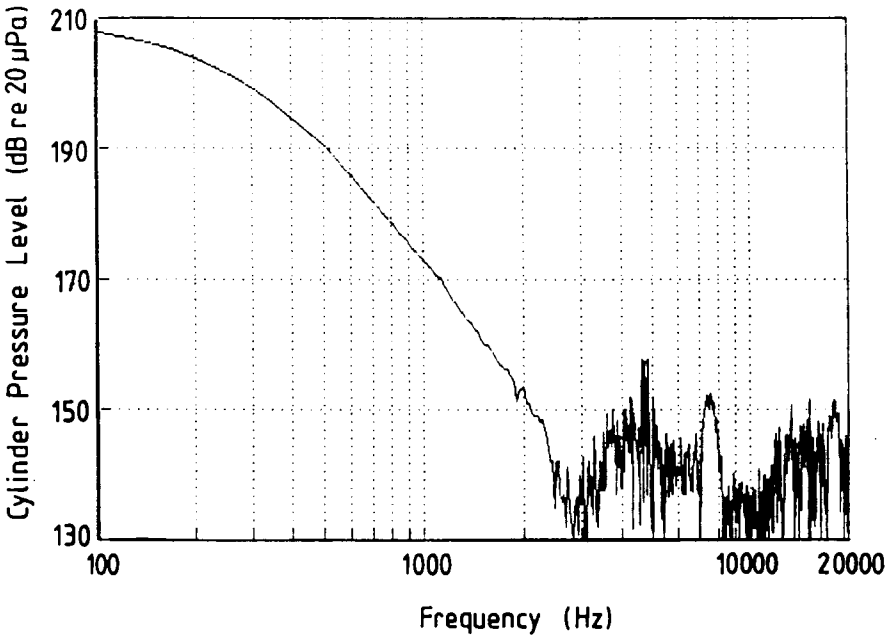

Figure G.13b Cylinder pressure spectrum.

Engine	:	Volkswagen 1800
Engine Speed	:	4000 rpm
Spark Timing	:	16° BTDC
Fuel	:	93 RON gasoline

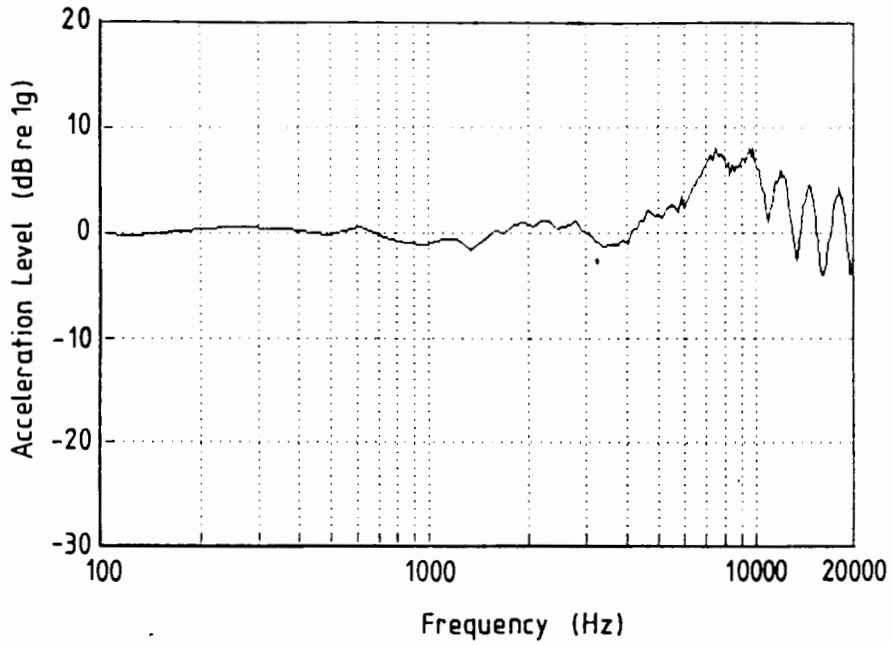

Figure G.13c Cylinder head vibration spectrum.

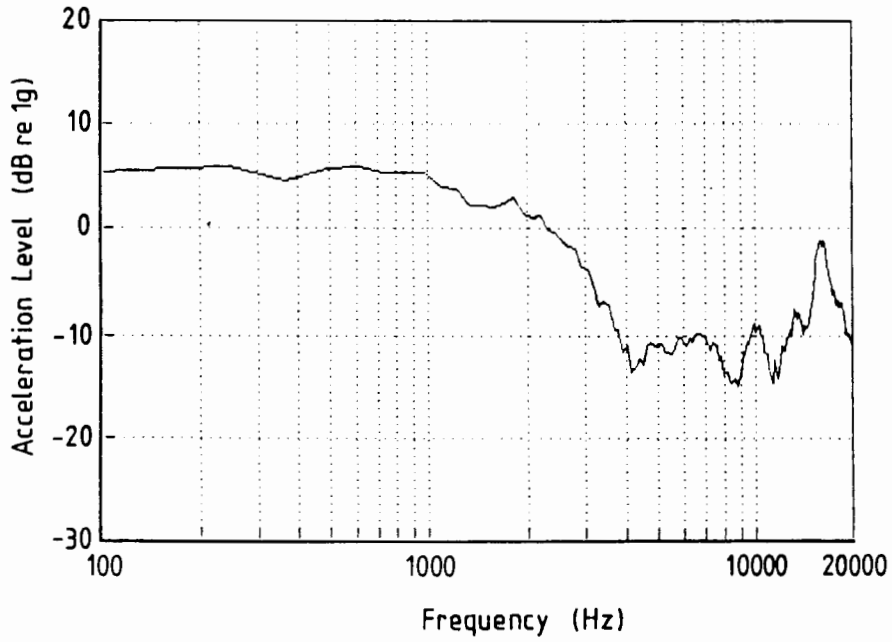

Figure G.13d Main bearing cap vibration spectrum.

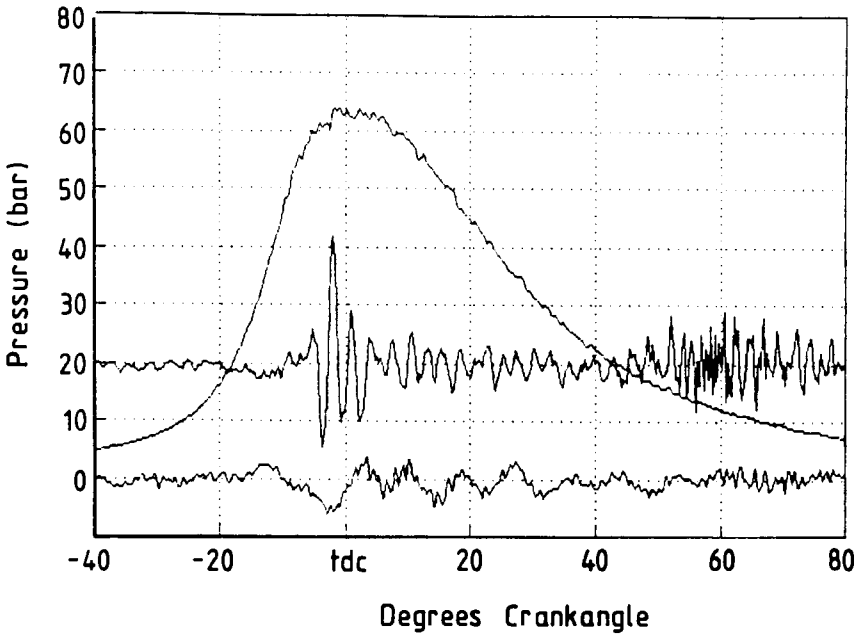

Figure G.14a Cylinder pressure diagram.

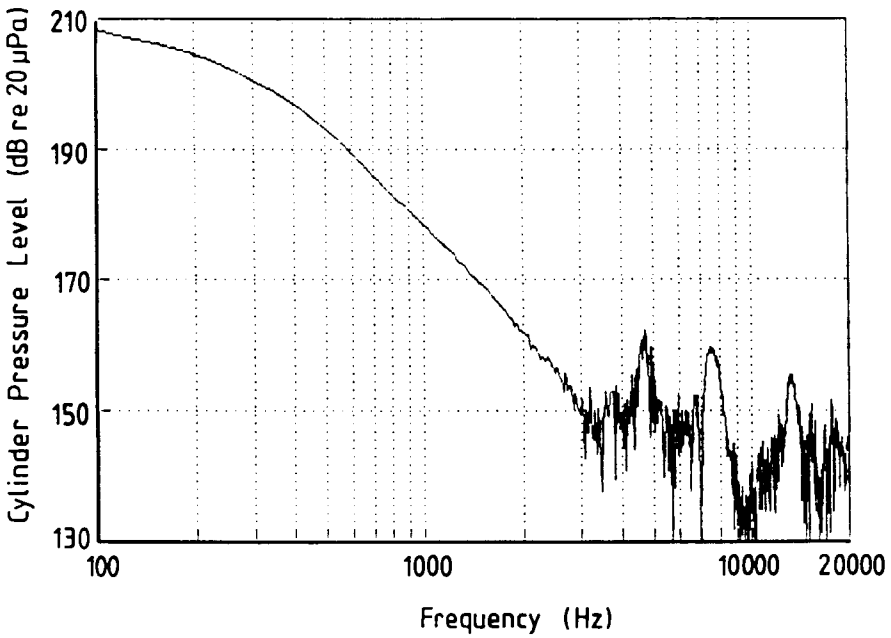

Figure G.14b Cylinder pressure spectrum.

Engine	:	Volkswagen 1800
Engine Speed	:	4500 rpm
Spark Timing	:	16° BTDC
Fuel	:	93 RON gasoline

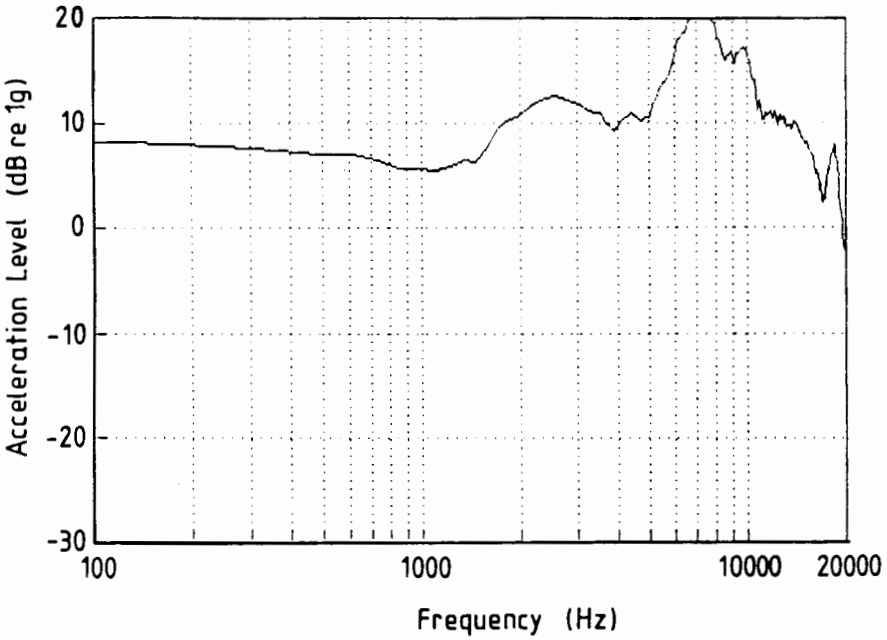

Figure G.14c Cylinder head vibration spectrum.

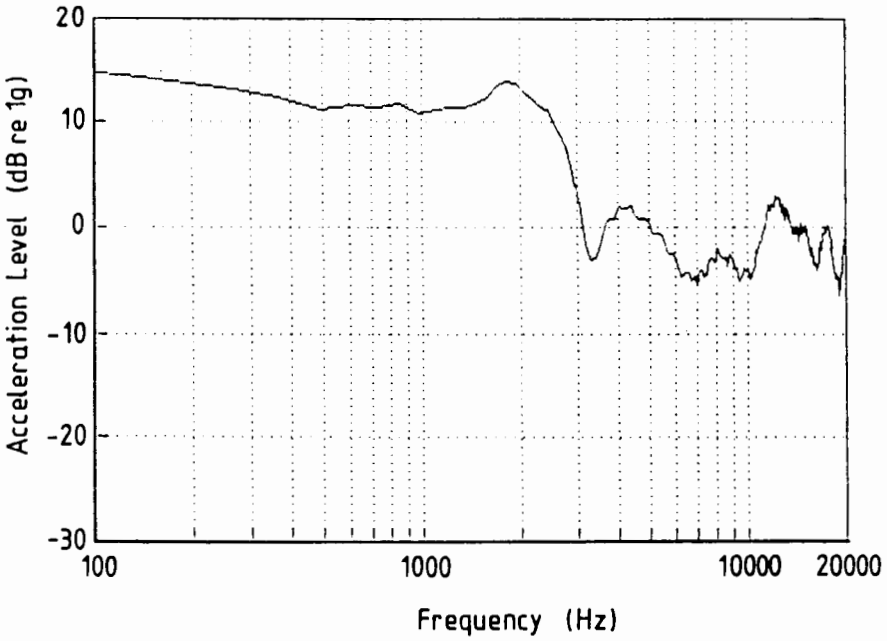

Figure G.14d Main bearing cap vibration spectrum.